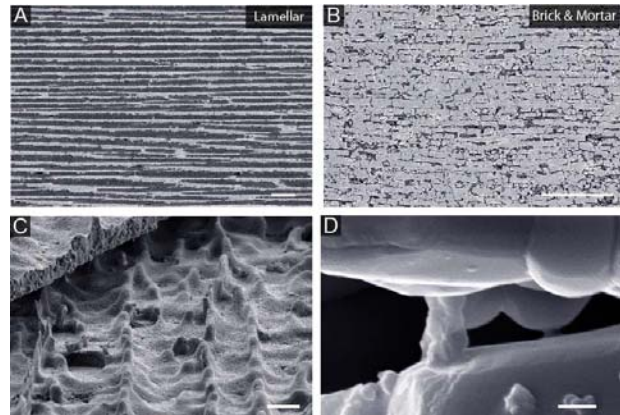
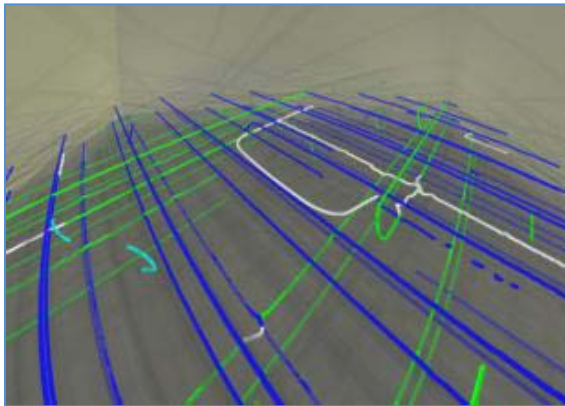


Mechanical Behavior and Radiation Effects 2010 Contractors' Meeting

*September 28 - October 1, 2010
Rockville Hilton, Rockville, MD*



U.S. DEPARTMENT OF
ENERGY

Office of
Science

Materials Sciences and Engineering Division
Office of Basic Energy Sciences

Cover

Top Left: Typical dislocations structures observed in multilayer interfaces using Multiscale Dislocation Dynamics Plasticity (Zbib et al, Washington State University)

Top Right: Al_2O_3 /PMMA lamellar composites fabricated using freeze casting of ceramic suspensions followed by polymer infiltration (the lighter phase is the ceramic; the dark phase is the polymer). (Ritchie et al, Lawrence Berkeley National Laboratory)

Bottom: SEM with OIM overlay information and color coded plane traces for slip bands (**prism**, **basal**, **<c+a>** and **T1 twinning**) in a deformed commercial purity Ti sample (Boehlert et al, Michigan State University)

Foreword

This volume comprises the scientific content of the 2010 Mechanical Behavior and Radiation Effects Contractors' Meeting sponsored by the Division of Materials Science and Engineering (DMS&E) in the Office of Basic Energy Sciences (BES) of the U. S. Department of Energy (DOE). The meeting, held on Sept. 28 – Oct. 1 at the Rockville Hilton, Rockville, MD, is the third Contractors' Meeting on this topic and is one among a series of research theme-based Contractors' Meetings being held by DMS&E. The meeting's focus is on research in mechanical behavior and radiation effects of materials, and it also features research that cuts across several other BES core research program areas and Energy Frontier Research Centers where appropriate and relevant.

The studies of mechanical behavior and radiation effects have a long and important history with respect to the generation, transmission, utilization and conservation of energy. It is a tribute to the researchers that they have continued to move the field forward into a number of important areas, as can be seen by the diversity of projects being presented at this meeting.

The purpose of the Mechanical Behavior and Radiation Effects Contractors' Meeting is to bring together researchers funded by DMS&E in this important area of research on a periodic basis (approximately every three years) in order to facilitate the exchange of new results and research highlights, to nucleate new ideas and collaborations among the participants, and to identify needs of the research community. The meeting will also help DMS&E in assessing the state of the program, identifying new research directions and recognizing programmatic needs.

I would like to express my sincere thanks to all of the attendees, especially the invited speakers, for their active participation and sharing their ideas and new research results. I would also like to express my sincere gratitude to Ms Teresa Crockett in DMS&E, and Joreé O'Neal of the Oak Ridge Institute of Science and Education (ORISE) for their dedicated and outstanding work in taking care of all the logistical aspects of the meeting.

John Vetrano
Program Manager
Mechanical Behavior and Radiation Effects
Division of Materials Sciences and Engineering
Office of Basic Energy Sciences
U.S. Department of Energy

Table of Contents

Table of Contents

Foreword	i
Table of Contents	ii
Agenda.....	vi
Poster Session I.....	ix
Poster Session II	x
Keynote Speakers	
Center for Materials Science for Nuclear Fuel	
Todd Allen.....	1
EFRC title: Center for Materials at Irradiation and Mechanical Extremes	
Michael Nastasi, Amit Misra	2
The Modeling and Simulation Energy Innovation Hub: Consortium for Advanced Simulation of Light water reactors (CASL)	
Alex R. Larzelere.....	5
Energy Frontier Center for Defect Physics in Structural Materials (CDP)	
G. Malcolm Stocks	9
University Grant Projects	
High-Temperature Grain Growth and Swift Heavy Ion Irradiation Damage in CeO₂ as a UO₂ Surrogate	
Todd Allen, John Moore, Jian Gan, Anter El-Azab	11
Structure/Property Relationships in High Strength Nanostructured FeNiMnAl Alloys	
Ian Baker	15
Materials for Extreme Irradiation Environments	
Pascal Bellon, Robert Averback, Shen Dillon, William King, Dallas Trinkle	19
Characterization and Modeling of Deformation Induced Damage in Titanium Alloys	
Carl J. Boehlert, Thomas R. Bieler, Martin A. Crimp, Hongmei Li, James Seal	23
Deformation and Failure Mechanisms of Shape Memory Alloys	
Samantha Daly	27
Molecular-Reinforced Hybrid Glass Films with Superior ThermoMechanical Properties	
Reinhold H. Dauskardt , Mark Oliver and Taek-Soo Kim	31

Mechanical Properties and Microstructural Evolution in Al-Li-Sc-Yb Alloys Containing Multi-Shell Nanosize Precipitates David C. Dunand, David N. Seidman, Christopher Wolverton	35
The Closure Problem in Density-Based Modeling of Dislocation Dynamics Anter El-Azab	39
Particle-Induced Modificaton Of Complex Ceramics: Response of Materials to Extreme Conditions Rodney C. Ewing, J. Lian, L.-M. Wang	43
Program Title: Stress-coupled Grain Boundary Migration Kevin J. Hemker	47
Plasticity in ultra-fine grained materials Marisol Koslowski	51
SISGR: Micro-mechanisms and Multiscale Modeling of Cyclic Plastic Deformation of Magnesium Single Crystals Qizhen Li, Yanyao Jiang	55
Understanding microplasticity processes related to fatigue damage using high energy x-rays and a crystal-based modeling formulation Matthew P. Miller, Paul R. Dawson, Ulrich Lienert and James C. Williams	59
Mechanisms and Modeling of High Output Shape Memory Alloys Prof. Michael J. Mills and Prof. Peter M. Anderson	63
The Inverse Magnetoplastic Effect of Magnetic Shape-Memory Alloys Peter Müllner	67
Roles of nanoclusters in shear banding and plastic deformation of bulk metallic glasses T.G. Nieh	71
Mechanical Properties of Materials with Nanometer Scale Microstructures William D. Nix	75
Understanding the Role of High-Angle Grain Boundaries in Failure of Thin Film Materials Yu Qiao	79
The Coupling Between Interfacial Charge and Mechanical Deformation at High Temperatures in Ceramics Rishi Raj	83
Controlling Transformations for Desirable Mechanical Response Ivar Reimanis and Cristian Ciobanu	87
NanoMechanics: Elastidity and Friction in Nano-Objects Elisa Riedo	91
Using Artificial Microstructures to Understand Microstructure Property Relationship-Toughening Mechanisms in Metallic Glass Jan Schroer	95

Deformed Materials: Towards a theory of materials Morphology Dynamics James P. Sethna	96
Understanding and Controlling Toughening Mechanisms in Nanotube Reinforced Ceramic Coatings Brian W. Sheldon and William A. Curtin	100
Shape memory in nanoscale metallic alloys Alejandro Strachan.....	101
Radiation effects in nanocrystalline ceramics: Multi-scale model and experiment Izabela Szlufarska	105
Electrical, mechanical and thermal properties of single molecules Nongjian (NJ) Tao	109
Chemomechanics of Far-From-Equilibrium Interfaces (COFFEI) Harry L. Tuller, Craig Carter, Yet Ming Chiang, Yang Shao-Horn, Krystyn Van Vliet, Bilge Yildiz, Sidney Yip	113
Combined Atomistic And Mesoscopic Study Of Deformation Of Body-Centered-Cubic Transition Metals: Effects Of Alloying And Magnetism V. Vitek	117
Nanostructure Patterning Under Energetic Particle Beam Irradiation Lumin Wang, Wei Lu.....	121
Localized Deformation and Intergranular Fracture of Irradiated Alloys under Extreme Environmental Conditions Gary S. Was, Ian M. Robertson, Diana Farkas.....	125
Investigating Deformation and Failure Mechanisms in Nanoscale Multilayer Metallic Composites H. M. Zbib, D. F. Bahr	129
Laboratory Projects	
Mechanical Properties of Materials:Nature-Inspired Ultrahigh Toughness, Lightweight Structural Materials Robert O. Ritchie and Antoni P. Tomsia	133
Radiation Damage Effects In Ceramics And Non-Metals Kurt E. Sickafus	137
Deformation Physics of Ultra-fine Scale Materials Amit Misra	141
Statistical multi-scale study of twinning in HCP Mg & Zr C.N. Tomé, I.J. Beyerlein, J. Wang, R. McCabe.....	145
SISGR: Evolution of Grain Boundary Networks in Extreme Radiation Environments Mukul Kumar, James Belak, Joel Bernier, Vasily Bulatov, Thomas Lagrange, Bryan Reed and, Ming Tang	149

Multiscale Mechanical Properties and Alloy Design E. P. George, H. Bei, J. R. Morris, G. M. Pharr	153
Stability of Nanoclusters in Metal Matrices under Extreme Environments Michael K. Miller, Chong Long Fu, Xun-Li Wang and Michael J. Mills.....	157
Interfacial Charge Transfer and the Radiation Response of Nano-Dispersed Ceramics Ram Devanathan, Fei Gao, Weilin Jiang, Rick Williford, Matt Olszta and Gregory J Exarhos	161
Exploring the Radiation Damage Resistance of Nanoscale Interfaces Richard Kurtz.....	165
Crack-Tip Mechanisms During Environmental Degradation Stephen M. Bruemmer, Kevin M. Rosso, Matthew Olszta, Chongmin Wang, Donald R. Baer, Gary S. Was and David N. Seidman	169
Nanomechanics and Nanometallurgy of Boundaries B.L. Boyce, B.G. Clark, S.M Foiles, K.M. Hattar, E.A. Holm, J.A. Knapp.....	173
Author Index.....	177
Participant List.....	179

Agenda

Agenda

U.S. Department of Energy
Office of Basic Energy Sciences
Mechanical Behavior and Radiation Effects
2010 Contractor's Meeting
September 28 – October 1, 2010

Tuesday, September 28, 2010

4:00 – 7:00 pm	Registration
7:00 – 7:15 pm	John Vetrano: Welcome
7:15 – 7:45 pm	Alex R. Larzelere, Hub – DOE Office of Nuclear Energy <i>The Modeling and Simulation Energy Innovation Hub Consortium for Advanced Simulation of Light water reactors (CASL)</i>
7:45 – 8:05 pm	Michael Nastasi (Presented by Amit Misra), EFRC - Los Alamos National Laboratory Center for Materials at Irradiation and Mechanical Extremes
8:05 – 8:25 pm	Todd Allen, EFRC - Idaho National Laboratory <i>Center for Materials Science for Nuclear Fuel</i>
8:25 – 8:45 pm	G. Malcolm Stocks, Oak Ridge National Laboratory <i>Energy Frontier Center for Defect Physics in Structural Materials (CDP)</i>

Wednesday, September 29, 2010

7:30 – 8:30 am	*****Breakfast*****
8:30 – 9:00 am	Linda Horton: News from the Office of Basic Energy Sciences
9:00 – 9:30 am	Izabela Szlufarska, University of Wisconsin – Madison <i>Radiation effects in nanocrystalline ceramics: Multi-scale model and experiment</i>
9:30 – 10:00 am	Kurt E. Sickafus, Los Alamos National Laboratory <i>Low Temperature Ion irradiation Damage Effects in Complex Titanates</i>
10:00 – 10:30 am	*****Break*****
10:30 – 11:00 am	Ram Devanathan, Pacific Northwest National Laboratory <i>Interfacial Charge Transfer and the Radiation Response of Nano-Dispersed Ceramics</i>
11:00 – 11:30 am	Mukul Kumar, Lawrence Livermore National Laboratory <i>SISGR: Evolution of Grain Boundary Networks in Extreme Radiation Environments</i>
11:30 – 12:00 pm	B.L. Boyce, Sandia National Laboratory <i>Nanomechanics and Nanometallurgy of Boundaries</i>
12:00 – 1:15 pm	*****Working Lunch*****
1:15 – 1:30 pm	John Vetrano: Core Research Area Information <i>Mechanical Properties of Materials with Nanometer Scale Microstructures</i> <u>Chair:</u> William D. Nix, Stanford University
1:30 – 2:00 pm	Pascal Bellon, University of Illinois <i>Materials for Extreme Irradiation Environments</i>
2:00 – 2:30 pm	Michael K. Miller, Oak Ridge National Laboratory <i>Stability of Nanoclusters in Metal Matrices under Extreme Environments</i>

2:30 – 3:00 pm David C. Dunand, Northwestern University
Mechanical Properties and Microstructural Evolution in Al-Li-Sc-Yb Alloys Containing Multi-Shell Nanosize Precipitates

3:00 – 3:30 pm *****Break*****

3:30 – 4:00 pm Harry L. Tuller, Massachusetts Institute of Technology
Chemomechanics of Far-From-Equilibrium Interfaces (COFFEI)

4:00 – 4:30 Reinhold H. Dauskardt, Stanford University
Molecular-Reinforced Hybrid Glass Films with Superior ThermoMechanical Properties

4:30 – 5:00 pm Poster Intro

5:00 – 7:00 pm *****Working Dinner*****

7:00 – 9:00 pm Poster Session I -- Plaza I Room

Thursday, September 30, 2010

7:30 – 8:30 am *****Breakfast*****

8:30 – 9:00 am Nongjian (NJ) Tao, Arizona State University
Electrical, mechanical and thermal properties of single molecules

9:00 – 9:30 am Yu Qiao, University of California, San Diego
Understanding the Role of High-Angle Grain Boundaries in Failure of Thin Film Materials

9:30 – 10:00 am E. P. George, Oak Ridge National Laboratory
Multiscale Mechanical Properties and Alloy Design

10:00 – 10:30 am *****Break*****

10:30 – 11:00 am Robert O. Ritchie, Lawrence Berkley National Laboratory
Mechanical Properties of Materials:Nature-Inspired Ultrahigh Toughness, Lightweight Structural Materials

11:00 – 11:30 am Brian W. Sheldon, Brown University
Understanding and Controlling Toughening Mechanisms in Nanotube Reinforced Ceramic Coatings

11:30 – 12:00 pm Rishi Raj, University of Colorado at Boulder
The Coupling Between Interfacial Charge and Mechanical Deformation at High Temperatures in Ceramics

12:00 – 1:30 pm *****Working Lunch*****

Combined Atomistic And Mesoscopic Study Of Deformation Of Body-Centered-Cubic Transition Metals: Effects Of Alloying And Magnetism
Chair: V. Vitek, University of Pennsylvania

1:30 – 2:00 pm Qizhen Li, University of Nevada, Reno
SISGR: Micro-mechanisms and Multiscale Modeling of Cyclic Plastic Deformation of Magnesium Single Crystals

2:00 – 2:30 pm Carl J. Boehlert, Michigan State University
Characterization and Modeling of Deformation Induced Damage in Titanium Alloys

2:30 – 3:00 pm C.N. Tomé, Los Alamos National Laboratory
Statistical multi-scale study of twinning in HCP Mg & Zr

3:00 – 3:30 pm *****Break*****

3:30 – 4:00 pm James P. Sethna Cornell University
Deformed Materials: Towards a theory of materials Morphology Dynamics

4:00 – 4:30 pm Anter El-Azab, Florida State University
The Closure Problem in Density-Based Modeling of Dislocation Dynamics

4:30 – 5:00 pm Poster Intro

5:00 – 7:00 pm *****Working Dinner*****

7:00 – 9:00 pm Poster Session II -- Plaza I Room

Friday, October 1, 2010

7:30 – 8:30 am *****Breakfast*****
8:30 – 9:00 am Samantha Daly, University of Michigan
Deformation and Failure Mechanisms of Shape Memory Alloys
9:00 – 9:30 am Michael J. Mills, Ohio State University
Mechanisms and Modeling of High Output Shape Memory Alloys
9:30 – 10:00 am Alejandro Strachan, Purdue University
Shape Memory In Nanoscale Metallic Alloys
10:00 – 10:30 am *****Break*****
10:30 – 11:00 am Elisa Riedo, Georgia Tech
NanoMechanics: Elasticity and Friction in Nano-Objects
11:00 – 11:30 am Amit Misra, Los Alamos National Laboratory
Deformation Physics of Ultra-fine Scale Materials
11:30 – 12:00 pm *Wrap Up*

Poster Session I
Plaza I Room
Wednesday, September 29, 2010

- P-1-1 **Todd Allen, EFRC** - Idaho National Laboratory
Center for Materials Science for Nuclear Fuel
- P-1-2 **Pascal Bellon**, University of Illinois
Materials for Extreme Irradiation Environments
- P-1-3 **Stephen M. Bruemmer**, Pacific Northwest National Laboratory
Crack-Tip Mechanisms During Environmental Degradation
- P-1-4 **Rodney C. Ewing, (Presented by Maik Lang)**, University of Michigan
Particle-Induced Modification Of Complex Ceramics: Response of Materials to Extreme Conditions
- P-1-5 **Mukul Kumar**, Lawrence Livermore National Laboratory
SISGR: Evolution of Grain Boundary Networks in Extreme Radiation Environments
- P-1-6 **Richard Kurtz**, Pacific Northwest National Laboratory
Exploring the Radiation Damage Resistance of Nanoscale Interfaces
- P-1-7 **Frances Marshall**, Idaho National Laboratory
Advanced Test Reactor User Facility
- P-1-8 **Matthew P. Miller**, Cornell University
Understanding microplasticity processes related to fatigue damage using high energy x-rays and a crystal-based modeling formulation
- P-1-9 **Michael K. Miller**, Oak Ridge National Laboratory
Stability of Nanoclusters in Metal Matrices under Extreme Environments
- P-1-10 **Amit Misra**, Los Alamos National Laboratory
Deformation Physics of Ultra-fine Scale Materials
- P-1-11 **William D. Nix**, Stanford University
Mechanical Properties of Materials with Nanometer Scale Microstructures
- P-1-12 **Michael Nastasi, (Presented by Blas Uberuaga)**, Los Alamos National Laboratory
Damage production and evolution near grain boundaries in Cu
- P-1-13 **G. Malcolm Stocks**, Oak Ridge National Laboratory
Energy Frontier Center for Defect Physics in Structural Materials (CDP)
- P-1-14 **Izabela Szlufarska**, University of Wisconsin – Madison
Radiation effects in nanocrystalline ceramics: Multi-scale model and experiment
- P-1-15 **Harry L. Tuller**, Massachusetts Institute of Technology
Chemomechanics of Far-From-Equilibrium Interfaces (COFFEI)
- P-1-16 **V. Vitek**, University of Pennsylvania
Combined Atomistic And Mesoscopic Study Of Deformation Of Body-Centered-Cubic Transition Metals: Effects Of Alloying And Magnetism
- P-1-17 **Lumin Wang, (Presented by Ian Robertson)**, University of Michigan Nanostructure Patterning
Under Energetic Particle Beam Irradiation
- P-1-18 **Gary S. Was, (Presented by H.M. Zbib and D.F. Bahr)**, University of Michigan
Localized Deformation and Intergranular Fracture of Irradiated Alloys under Extreme Environmental Conditions
- P-1-19 **H. M. Zbib**, Washington State University
Investigating Deformation and Failure Mechanisms in Nanoscale Multilayer Metallic Composites

Poster Session II
Plaza I Room
Thursday, September 30, 2010

- P-2-1 **Ian Baker**, Dartmouth College
Structure/Property Relationships in High Strength Nanostructured FeNiMnAl Alloys
- P-2-2 **Carl J. Boehlert**, Michigan State University
Characterization and Modeling of Deformation Induced Damage in Titanium Alloys
- P-2-3 **B.L. Boyce**, Sandia National Laboratory
Nanomechanics and Nanometallurgy of Boundaries
- P-2-4 **E. P. George, (Presented by George Pharr)**, Oak Ridge National Laboratory
Multiscale Mechanical Properties and Alloy Design
- P-2-5 **Kevin J. Hemker**, Johns Hopkins University
Program Title: Stress-coupled Grain Boundary Migration
- P-2-6 **Marisol Koslowski**, Purdue University
Plasticity in ultra-fine grained materials
- P-2-7 **Richard LeSar**, Iowa State University, Ames,
Mechanical Behavior and Defects in Solids
- P-2-8 **Qizhen Li**, University of Nevada, Reno
SISGR: Micro-mechanisms and Multiscale Modeling of Cyclic Plastic Deformation of Magnesium Single Crystals
- P-2-9 **Peter Müllner**, Boise State University
The Inverse Magnetoplastic Effect of Magnetic Shape-Memory Alloys
- P-2-10 **T.G. Nieh**, University of Tennessee, Knoxville
Roles of nanoclusters in shear banding and plastic deformation of bulk metallic glasses
- P-2-11 **Ivar Reimanis**, Colorado School of Mines
Controlling Transformations for Desirable Mechanical Response
- P-2-12 **Jan Schroers**, Yale University
Using Artificial Microstructures to Understand Microstructure Property Relationship-Toughening Mechanisms in Metallic Glass
- P-2-13 **Brian W. Sheldon**, Brown University
Understanding and Controlling Toughening Mechanisms in Nanotube Reinforced Ceramic Coatings
- P-2-14 **Kurt E. Sickafus, (Presented by Blas Uberuaga)**, Los Alamos National Laboratory
Radioparagenesis: The formation of novel compounds and crystalline structures via radioactive decay
- P-2-15 **C.N. Tomé**, Los Alamos National Laboratory
Statistical multi-scale study of twinning in HCP Mg & Zr

Keynote Speakers

Center for Materials Science for Nuclear Fuel
Dr. Todd Allen
Interim Director

The goal of the *Center for Materials Science for Nuclear Fuel (CMSNF)* is to develop a predictive multi-scale modeling framework that captures how defect generation and evolution and microstructure changes under irradiation lead to the degradation of fission-reactor fuel properties. Degradation of the thermo-mechanical behavior results from the cumulative, intricately coupled effects of fission-damage processes, high temperatures and high thermal gradients. Yet, apart from large empirical databases, a fundamental predictive science basis that connects “structure” across the relevant length and time scales with fuel behavior does not currently exist. To elucidate the underlying point-defect and microstructural mechanisms controlling this degradation behavior, the *CMSNF* will develop a predictive computational framework based upon the non-linear dynamical theory of driven material systems and combining multi-scale models of defect and microstructure physics with complementary experimentation, on commensurate length scales. This unique combination of theory, computation and experiments will capture the complex interplay between the fission-induced defects and emerging microstructure with pre-existing grain structure, thus enabling the prediction of the impact of microstructure evolution on thermal transport in UO_2 . The availability of the new ATR National User Facility at INL not only gives the Center a distinct local dimension but also provides the unique capability of tying all of the experimental investigations to a true fission environment. Indeed, the ultimate target of the Center’s research is to provide basic science understanding that supports the development of an in-pile measurement capability to monitor degradation of critical components of the fuel assembly.

EFRC title: Center for Materials at Irradiation and Mechanical Extremes

<http://cmime.lanl.gov/>

Director: Michael Nastasi <nasty@lanl.gov>

Co-Director: Amit Misra <amisra@lanl.gov>

Lead Institution: Los Alamos National Laboratory

Mission Statement: To understand, at the atomic scale, the behavior of materials subject to extreme radiation doses and mechanical stress in order to synthesize new materials that can tolerate such conditions.

Our EFRC addresses two of the five BESAC grand challenges: *How do we design and perfect atom and energy-efficient syntheses of revolutionary new forms of matter with tailored properties? and How do we characterize and control matter away-especially very far away-from equilibrium?* In responding to these grand challenges our center will focus on *Materials at Irradiation and Mechanical Extremes*. This Center recognizes that the challenge to developing materials with radically extended performance limits at irradiation and mechanical extremes will require designing and perfecting atom- and energy- efficient synthesis of revolutionary new materials that maintain their desired properties while being driven very far from equilibrium. We have developed a set of common issues that will drive our science focus and serve as the unifying foundation of this center. These scientific issues include: 1) Absorption and recombination of point and line defects at interface; 2) Morphological and chemical stability of interfaces; 3) Interface-driven mechanical response. By addressing these issues we will develop a fundamental understanding of how atomic structure and energetics of interfaces contribute to defect and damage evolution in materials, and use this information to design nanostructured materials with tailored response at irradiation and mechanical extremes.

In the pursuit of the grand challenge and science issues outlined above, we have developed specific hypotheses for each science issue. These defining hypotheses are listed below.

Scientific issue #1: *Absorption and recombination of point and line defects at interfaces*

Hypotheses:

- 1) The atomic structure of the interface controls the absorption, emission, storage and annihilation of defects at the interface.
- 2) Misfit dislocation intersections with other misfit dislocations and with disconnections are the most favorable sites for point defect absorption and delocalization.
- 3) The lower the elastic strain energy penalty associated with defect absorption, the more likely it is that point defect delocalization by interface reconstruction can take place.
- 4) The ability of an interface to absorb dislocations is determined by its shear strength and the areal density of preferred sites for nucleation of interface glide dislocations.

Scientific issue #2: *Morphological and chemical stability of interfaces*

Hypotheses:

- 5) Interface structures with high sink strengths or enhanced abilities to act as defect sources will be morphologically stable at extremes of temperature, irradiation and mechanical deformation.
- 6) Interface energy controls interface stability; high-energy interfaces are less likely to be morphologically stable.
- 7) The saturation limit for defect absorption at interfaces for a given type of defect (e.g., helium atom, solute segregant, vacancy, interstitial, dislocation) is determined by the interface structure. Above the defect solubility limit, interfaces exhibit chemical instabilities such as defect clustering, gas bubbles, precipitates, disordering or amorphization.

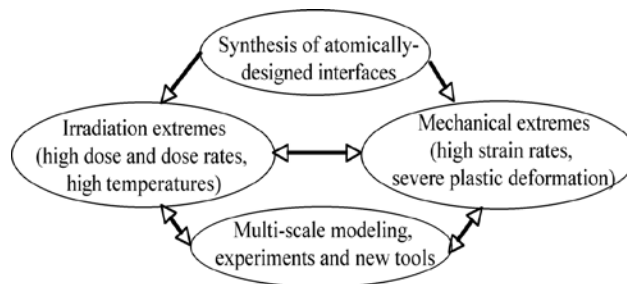
Scientific issue #3: *Interface-driven mechanical response*

Hypothesis:

- 8) The cohesive strength/mechanical damage evolution behavior for a given interface structure may change at high dose or high strain rates.

Using the above hypotheses, we are developing **quantitative figures-of-merit** for the defect sink strength of interfaces. These figures-of-merit will allow us to use a focused approach where model systems containing interfaces with high and low values of predicted sink strengths can be experimentally tested and the results used to refine the models.

The hypotheses driven research proposed in this center, naturally has two focus areas (thrusts) dealing with the *role of interfaces* in: 1) *extreme irradiation environments*; and 2) *mechanical extremes*. Synergy is enhanced through the development of new computational and characterization methods, and synthesis of common model systems. Materials are synthesized via physical vapor deposition methods, solidification processing, and severe plastic deformation. Common theory, modeling, and simulation tools and methods include *ab initio*, molecular dynamics (MD) and accelerated MD (AMD), kinetic Monte Carlo (KMC), and rate theory calculations. New tools will be developed for extending our abilities to carry out multi-length and multi-time scale studies. This will include the development of a parallel off-lattice KMC, a hybrid MD/AMD/KMC method, and ultra-fast laser characterization of defects in oxides. The development of these methods will allow, for the first time, direct coupling of experimental measurements and computer simulations at comparable length and time scales. The integrated structure of the center is shown schematically in the figure below.



The irradiation extremes thrust has two teams, one focused on metallic systems (Mike Demkowicz, MIT, team leader) and another on oxides (Blas Uberuaga, LANL, team leader). The mechanical thrust has two teams, one on severe plastic deformation (Irene Beyerlein, LANL, team leader) and another on high strain rate deformation (Tim Germann, LANL, team leader). The key personnel are listed below.

Center for Materials at Irradiation and Mechanical Extremes	
Los Alamos National Laboratory	M. Nastasi (Director) , A. Misra, G.T. Gray, S.A. Maloy, B.P. Uberuaga, C. P. Stanek, I.J. Beyerlein, N. A. Mara, T.C. Germann, E.K. Cerreta, A.F. Voter, S.M. Valone, S. Luo, Q. Jia, D.A. Yarotski, Y.Q. Wang, R.M. Dickerson, P. O. Dickerson, A. Caro
University of Illinois-Urbana Champaign	R.S Averbach, P. Bellon
MIT	Michael J. Demkowicz
Carnegie Mellon University	A.D. Rollett

Abstract

The Modeling and Simulation Energy Innovation Hub Consortium for Advanced Simulation of Light water reactors (CASL)

**Alex R. Larzelere, Director Advanced Modeling and Simulation Office (AMSO) Office of
Nuclear Energy, U.S. Department of Energy**

ENERGY INNOVATION HUBS

In the spring of 2009, Secretary of Energy Steven Chu introduced the concept of Energy Innovation Hubs. His idea was based on his experience as the Director of Lawrence Berkeley National Laboratory and in particular his experience with the Joint Bio-Energy Institute. In his testimony to the House and Senate Energy and Water Appropriations Sub-committees he said:

A few years ago, I changed the course of my scientific work to focus on solving our energy and climate challenges. I did so because of the great national and global urgency of this issue – but also because, as a scientist, I remain optimistic that science can offer us better solutions than we can imagine today. But those solutions won't come easily; they will only come if we harness the creativity and ingenuity and intellectual horsepower of our best scientists in the right way.

Having dedicated the last several years of my work to solving the energy challenge, I'm convinced that launching Energy Innovation Hubs is a critical next step in this effort. Bringing together the best scientists from different disciplines in collaborative efforts is our best hope of achieving priority goals such as making solar energy cost competitive with fossil fuels, or developing new building designs that use dramatically less energy, or developing an economical battery that will take your car 300 miles without recharging.

These are the breakthroughs we need – and the Energy Innovation Hubs will help us achieve them. I saw the power of truly collaborative science like this firsthand during my time at Bell Laboratories. I believe that to solve the energy problem, the Department of Energy must strive to be the modern version of Bell Labs in energy research, and that is what these Hubs will do. They will essentially be little “Bell Labses.”

The scientific collaboration the Hubs will foster will be unique and indispensable, and must be backed by a meaningful and sustained investment. These investments will pay for themselves many times over, ensuring American leadership and American competitiveness when it comes to the green energy jobs of tomorrow.

CONSORTIUM FOR ADVANCED SIMULATION OF LIGHT WATER REACTORS (CASL)

On May 28, 2010, after the completing Funding Opportunity Announcement competitive process, a selection was announced for the NE Modeling and simulation Energy Innovation Hub. The following is a high level summary of the scope of the Hub:

The Consortium for Advanced Simulation of Light Water Reactors (CASL) brings together an exceptionally capable team that will apply existing modeling and simulation (M&S) capabilities and develop advanced capabilities to create a usable environment for predictive simulation of light water reactors (LWRs). This environment designated the Virtual Reactor (VR), will:

- Enable the use of leadership-class computing for engineering design and analysis to achieve reactor power uprates, life extensions, and higher fuel burnup.
- Promote an enhanced scientific basis and understanding by replacing empirically based design and analysis tools with predictive capabilities.
- Develop a highly integrated multiphysics M&S environment for engineering analysis through increased fidelity methods [e.g., neutron transport and computational fluid dynamics (CFD) rather than diffusion theory and subchannel methods].
- Incorporate UQ as a basis for developing priorities and supporting application of the VR tools for predictive simulation.

CASL will further educate today's reactor engineers in the use of advanced M&S through direct engagement in CASL activities and develop the next generation of engineers through curricula at partner universities and engage the nuclear regulator (NRC) to obtain guidance and direction on the use and deployment of the CASL VR tools to support licensing applications.

CASL will focus on a set of challenge problems that encompass the key phenomena limiting the performance of PWRs [Pressurized Water Reactors], with the expectation that much of the capability developed will be applicable to other types of reactors. Broadly, CASL's mission is to develop and apply M&S capabilities to address three critical areas of performance for nuclear power plants (NPPs):

¹ Chu, Steven, Testimony to House and Senate Appropriations Energy and Water Subcommittees, June 3, 2009

- Capital and operating costs per unit energy, which can be reduced by enabling power uprates and lifetime extension for existing NPPs and by increasing the rated powers and lifetimes of new Generation III+ NPPs;
- Nuclear waste volume generated, which can be reduced by enabling higher fuel burnups; and
- Nuclear safety, which can be enhanced by enabling high-fidelity predictive capability for component performance through failure.

CASL will connect fundamental research and technology development through an integrated partnership of government, academia, and industry that extends across the nuclear energy enterprise. The CASL partner institutions possess the interdisciplinary expertise necessary to apply existing M&S capabilities to real-world reactor design issues and to develop new system focused capabilities that will provide the foundation for advances in nuclear energy technology.

CASL's organization and management plan have been designed to promote collaboration and synergy among the partner institutions, taking advantage of the breadth and depth of their expertise and capitalizing on their shared focus on delivering solutions.²

CASL PROJECT ORGANIZATION

CASL has been organized into five technical focus areas (FAs) to perform the necessary work ranging from basic science, model development, and software engineering, to applications:

Advanced Modeling Applications (AMA) – The primary interface of the CASL VR with the applications related to existing physical reactors, the challenge problems, and full-scale validation. In addition, AMA will provide the necessary direction to the VR development by developing the set of functional requirements, prioritizing the modeling needs, and performing assessments of capability.

Virtual Reactor Integration (VRI) – Develops the CASL VR tools integrating the models, methods, and data developed by other FAs within a software framework. VRI will collaborate with AMA to deliver usable tools for performing the analyses, guided by the functional requirements developed by AMA.

² Consortium for Advanced Simulation of LWRs, A Project Summary, pg 1.

Models and Numerical Methods (MNM) – Advances existing and develops new fundamental modeling capabilities for nuclear analysis and associated integration with solver environments utilizing large-scale parallel systems. The primary mission of MNM is to deliver radiation transport and T-H components that meet the rigorous physical model and numerical algorithm requirements of the VR. MNM will collaborate closely with MPO for sub-grid material and chemistry models and will connect to VRI for integration and development of the CASL VR.

Materials Performance and Optimization (MPO) – Develops improved materials performance models for fuels, cladding, and structural materials to provide better prediction of fuel and material failure. The science work performed by MPO will provide the means to reduce the fuel forms.

Validation and Uncertainty Quantification (VUQ) – The quantification of uncertainties and associated validation of the VR models and integrated system are essential to the application of modeling and simulation to reactor applications. Improvements in the determination of operating and safety margins will directly contribute to the ability to uprate reactors and extend their lifetimes. The methods proposed under VUQ will significantly advance the state of the art of nuclear analysis and support the transition from integral experiments to the integration of small scale separate-effect experiments.

In addition to these focus areas, CASL implements a management strategy distinguished by collaboration, central leadership, and multidisciplinary teams executing a single milestone-driven plan, and integrated codependent projects. The CASL streamlined management structure includes collocation at CASL, use of technology to achieve multidisciplinary collaboration, face-to-face meetings, and a Virtual Office, Community, and Computing (VOCC) project that integrates both the latest and emerging technologies to build an extended “virtual one roof.” CASL has a strong management philosophy, and with significant input provided by independent scientific and industry councils.

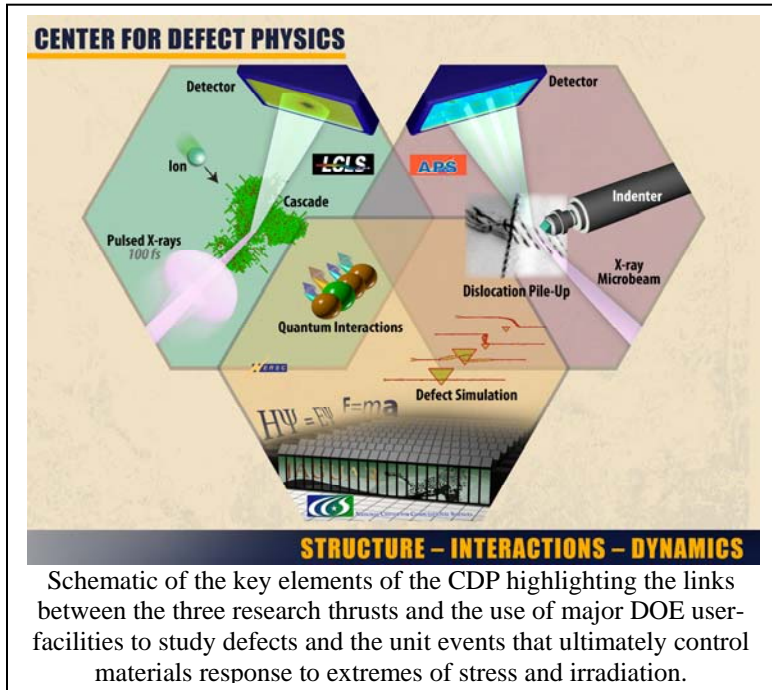
Integration of all the CASL milestones and FAs will lead to the development of a state-of-the-art pellet-to-plant VR simulation environment, with high-resolution representation of a physical reactor on the computational platforms of today and the future, creating distinct technological innovation and paving the way for a nuclear power industrial revolution.³

³ Ibid, pg 5-6.

Energy Frontier Center for Defect Physics in Structural Materials (CDP)
EFRC Director: G. Malcolm Stocks
Lead Institution: Oak Ridge National Laboratory

Mission Statement: To provide a fundamental understanding of materials' defects, defect interactions, and defect dynamics, thereby enabling atomistic control and manipulation of defects and the charting of new pathways to the development of improved materials – materials with ultra-high strength, toughness, and radiation resistance.

The “Energy Frontier Center for Defect Physics in Structural Materials (CDP), focuses on providing the fundamental knowledge to allow atomistic control and manipulation of defects, defect interactions, and defect dynamics – the very defect properties that currently limit the performance and lifetime of materials. Underpinning the CDP is the realization that we are on the verge of a new era of *quantitative measurement* and *direct quantum simulation* of the dramatic impact of defects on bulk structural materials. Furthermore, that the new era can be realized by utilizing innovative experimental techniques and major national facilities, such as the Advanced Photon Source (APS) and the Linac Coherent Light Source (LCLS), and by advancing the frontiers of first principles simulations using the, soon to be PFlop/s computing power available at the National Center for Computational Science (NCCS) and the National Energy Research Scientific Computing Center (NERSC).



ational Science (NCCS) and the National Energy Research Scientific Computing Center (NERSC).

The overarching goal of the CDP is to bring a radically new level of rigor and insight to the discussion of defect structure, interactions, and dynamics in metals and alloys – rigor born of quantitative experimental studies of defect evolution at the level of unit defect events and insight born of highly accurate calculations and simulations of properties that are based on a full quantum description of the underlying electronic interactions. The Center focuses on three interrelated research thrusts (RT) areas:

RT1: *Fundamental Physics of Defect Formation and Evolution during Irradiation:* Research in this thrust addresses one of the most fundamental and challenging issues in radiation damage through direct measurement of the dynamics of atomic displacement cascades. The underlying science of the formation and evolution of energetic-ion induced atomic displacement cascades as unit events will be probed for the first time using ultra-high resolution time-resolved x-ray diffuse scattering measurements. Measurements ranging from the sub-picosecond generation through millisecond range evolution of cascades will exploit the ultra-high brilliance of femtosecond x-ray pulses that will be produced by the LCLS. Together with complementary damage accumulation investigations

and the development of first-principles-based molecular dynamics techniques in RT3, a multi-pronged approach will be directed toward a full understanding of the generation, accumulation, and the potential for mitigating radiation damage in structural materials.

RT2: *Fundamental Physics of Defect Interactions during Deformation*: Research in this thrust addresses fundamental and longstanding issues associated with achieving a quantitative understanding of the local stresses near single dislocations, their aggregates, and the stress-driven interactions of dislocations with microstructural features (e.g. grain-boundary pile-ups). Recently developed submicron-resolution 3D x-ray microscopy at the APS will be used for groundbreaking non-destructive measurements of the local stresses and the indenter-driven motion and interactions of single dislocations as fundamental unit events of deformation in bulk and micro-pillar metals and alloys. Complementary investigations of the local stresses that drive dislocation motion and interactions with irradiation-induced defects will be performed in connection with RT1, and all measurements will be performed in close synergy with top-down and first-principles-based theory and simulations in RT3.

RT3: *Quantum Theory of Defects and Interactions*: Research in this thrust will overcome limitations of DFT molecular dynamics with respect to accuracy, system size, and simulation time by advancing the underlying theory and the software implementation of the theory on high performance computers. Consistent with the experimental challenge of quantifying the unit events of defect formation, evolution, and deformation, the modeling task will develop high fidelity models treating spin and ion dynamics on an equal footing and addressing system sizes and time scales commensurate with experiments in RT1 and RT2. Using comparisons with essentially exact quantum Monte Carlo calculations for magnetic systems to ensure accuracy as new DFT functions are developed, intelligent use of the raw computing power of the NCCS and NERSC facilities will be supplemented by classical ion-spin dynamics and diffusive atom density MD to go beyond the state of the art, e.g. in the inclusion of spin degrees of freedom.

Center for Defect Physics (CDP)	
Oak Ridge National Laboratory	G. Malcolm Stocks (Director) , Hongbin Bei, Easo George, Gene Ice, Ben Larson, Jamie Morris, Don Nicholson, Yury Osetskiy, Rad Radhakrishnan, Fernando Reboredo, Roger Stoller, Jon Tischler
University of Illinois	Jon Dantzig, Ian Robertson, Duane Johnson, Jeongnim Kim
Ohio State University	Mike Mills
Brown University	Sharvan Kumar
Lawrence Livermore National Laboratory	Randy Hood
University of California Berkeley	Andy Minor
Carnegie Mellon University	Yang Wang
University of Tennessee	George Pharr, Yanfei Gao

Contact: G. Malcolm Stocks;
 Corporate Fellow, Group Leader, Center Director
 e-mail address: stocksgm@ornl.gov
 telephone number: (865) 574-5163
 web site: <http://cdp.ornl.gov>

University Grant Projects

High-Temperature Grain Growth and Swift Heavy Ion Irradiation Damage in CeO₂ as a UO₂ Surrogate

Todd Allen, University of Wisconsin, Madison & Idaho National Laboratory
John Moore, Colorado School of Mines
Jian Gan, Idaho National Laboratory
Anter El-Azab, Florida State University

Energy Frontier Research Center for Materials Science of Nuclear Fuel

Idaho National Laboratory
Contact: Todd Allen (allen@enr.wisc.edu)

Program Scope

We present the initial results of an investigation focusing on understanding the high-temperature grain growth and the swift heavy-ion irradiation damage in CeO₂. This investigation is a part of the microstructure science effort of the Energy Frontier Research Center for Materials Science of Nuclear Fuel (<http://www.inl.gov/efrc>). The mission of the center is to achieve a first-principles based understanding of the impact of the defects and microstructure on thermal transport in irradiated UO₂ (with CeO₂ as a surrogate oxide). The center's research thus integrates the physics of thermal transport in crystalline solids with microstructure evolution in irradiated oxides. The microstructure science effort aims at understanding the thermal and irradiation driven microstructure evolution in the oxide systems of interest. As such, we present a combined experimental/theoretical investigation of the thermally-driven grain growth in polycrystalline bulk and thin film CeO₂, as well as initial results of swift-ion irradiation damage in this material. Grain growth is achieved by annealing CeO₂ samples at high temperature, and the results are intended to validate a phase field model for grain growth and porosity evolution, a building block for a more generalized phase field theory for the irradiated materials.

Recent Progress

Grain Growth in CeO₂

The goal of this work is to develop a phase field model for grain growth in UO₂ (and surrogate CeO₂) under thermal and irradiation conditions, and to provide experimental validation of this phase field model. As a first step, the model is now under testing for thermally-driven grain growth in polycrystalline bulk and thin-film based samples.

Grain Growth Experiments for Bulk CeO₂ (Allen and coworkers): Polycrystalline bulk CeO₂ samples (Alpha Aesar, 99.9%) were mechanically polished to mirror finished and then thermally etched at 1400°C for 30 minutes. Figure 1(a) shows the microstructure of the etched as-received CeO₂ sample. The samples were then annealed at temperatures in the range 1400°C to 1600°C for 5, 10 and 15 hours. Figure 1(b) shows the microstructure of the CeO₂ sample annealed at

1600°C for 10h, where a significant grain growth was observed in this annealed sample compared to as-received ones. The average grain size was determined using the Planimetric procedure per ASTM standard E112. The average grain size determined for the as-received CeO₂ and the one annealed at 1600°C for 10h were 4.69 μm and 15.53 μm, respectively.

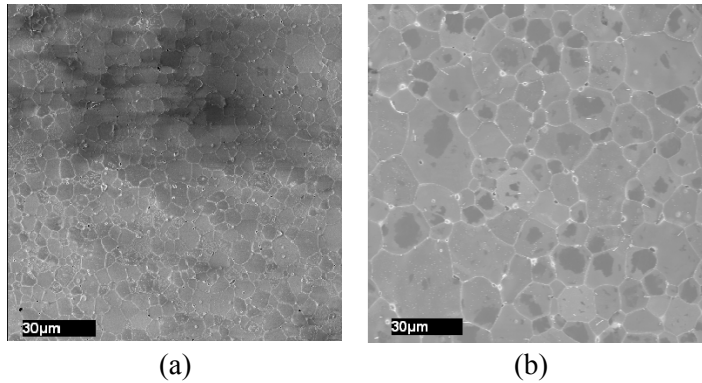


Figure 1. (a) As-received polycrystalline CeO₂ after thermal etching at 1400°C for 30 minutes, and (b) CeO₂ annealed at 1600°C for 10 h.

CeO₂ Thin-Film Samples (Moore and coworkers): CeO₂ thin film

samples were deposited on silicon wafer substrates in argon-oxygen atmosphere using pulsed unbalanced magnetron sputtering (P-UBMS) from a pure Ce target (99.99%) with a substrate heating capability system. Before being placed into the chamber for deposition, all substrates were ultrasonically cleaned in acetone, ethanol, and deionized water for 10, 15, and 10 min, respectively. Substrates were further cleaned in the deposition chamber by ion bombardment using bias voltage of -350 V under Ar atmosphere of 8.8 Pa (65 mTorr) for 30 min. After depositions of the samples, the CeO₂ thin film samples were post-annealed at different temperature (room temperature to 700°C) in oxygen atmosphere in the chamber. This process was achieved in a rapid thermal annealing (RTA) process allowing a high heating rate (50°C /s) and short duration temperature plateaus.

Figure 2 shows the cross-section SEM photomicrographs of the CeO₂ thin films on silicon wafer substrate. The CeO₂ thin films exhibit a dense columnar grain structure. A significant grain growth accompanied by a dense structure was observed with an increase in annealing temperature after deposition. The columnar size of CeO₂ films increased from a range of 100 to 500 nm to a range of 800 to 1500 nm as annealing temperature increased from room temperature to 700°C.

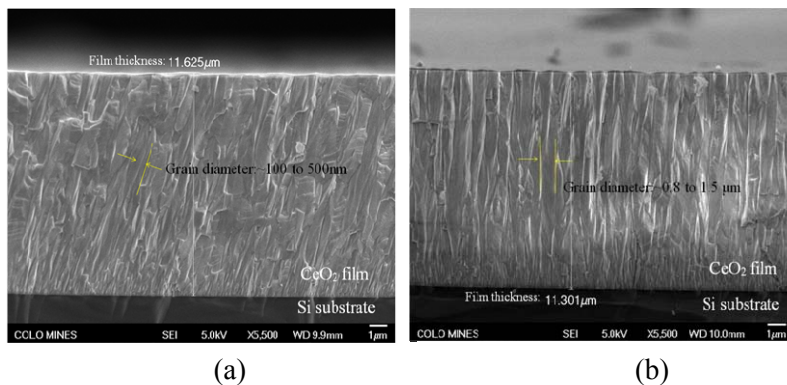


Figure 2. Scanning electron photomicrographs of cross-section of (a) as-deposited and (b) post-annealed CeO₂ thin films at 700°C for 5 minutes.

Phase Field Modeling of Grain Growth (El-Azab and coworkers): A novel phase field model is applied to understand the thermally driven grain growth in CeO₂. This model was initially developed to study the sintering of oxide thermal barrier coating systems. In this model, the polycrystalline material (with porosity) is modeled by two phase field variables, the conserved order parameter (density) and a set of non-conserved order parameters representing the grains. The system free energy formulation in terms of these order parameters leads to one Cahn-Hilliard equation for the density and a set of Allen-Cahn type equations for the order parameters:

$$\text{(C-H Eq.) } \frac{\partial \rho}{\partial t} = \nabla \cdot \left(M \nabla \frac{\delta F}{\delta \rho} \right) \quad \text{(A-C Eqs.) } \frac{\partial \eta_\alpha}{\partial t} = -L \frac{\delta F}{\delta \eta_\alpha},$$

with F , ρ , η_α being the free energy, density and phase field variables, respectively. These

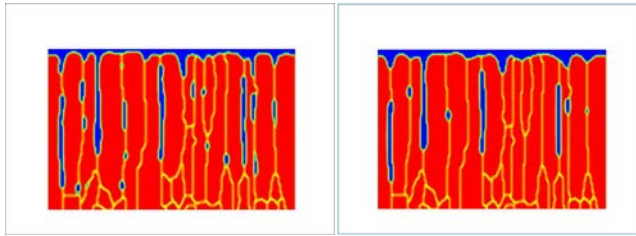


Figure 3. Preliminary testing of the phase field model on a thermal barrier coating system with columnar grain structure similar to CeO₂ films shown in Figure 2.

equations are integrated to yield the evolution of porosity and grain boundary network in the system. Figure 3 illustrates a typical application of the model to columnar grain structure. In the case of CeO₂, the model will be validated by applying it to polycrystalline and film samples, where the pre-annealed microstructure will be used as initial condition and the final result will be compared with the annealed microstructure.

Irradiation of CeO₂ by Swift Heavy Ion: Preliminary Results

Polycrystalline bulk CeO₂ samples were irradiated by ~300 and ~1000 MeV Au ions to fluences in the range 5×10^{10} to 5×10^{12} cm⁻² at room temperature in the irradiation facility GSI in Germany. The irradiated samples have been characterized using conventional tools such as lab x-ray diffraction, scanning electron microscopy, transmission electron microscopy, and Raman spectroscopy. Figures 4 and 5 show initial TEM and XRD

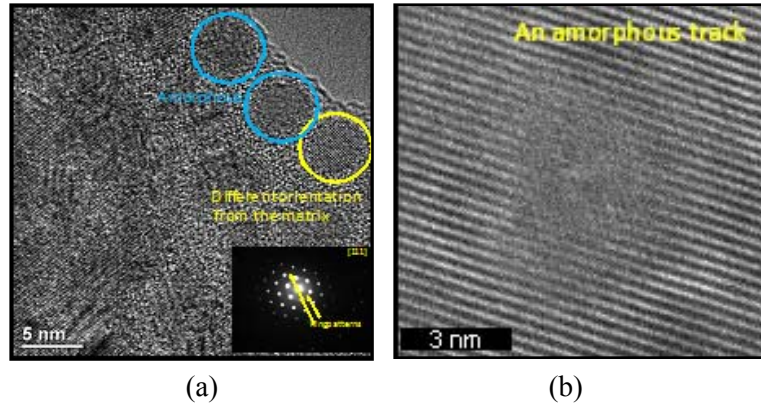


Figure 4. HR-TEM Characterization of swift heavy ion irradiated CeO₂ showing severe lattice disorder. (a) amorphous and recrystallized ion track areas, (b) an enlarged amorphous region.

results for irradiated CeO₂, respectively. Both single ion track and overlapped track were

observed using TEM. The tracks have an average diameter of about 5 nm. Some tracks show amorphous structure, while others show completely different orientation to the matrix (recrystallized regions), indicating recrystallization may occur at room temperature. The XRD analysis suggests that the lattice parameter of CeO_2 decreased after irradiation.

Future Plans

CeO_2 thin film samples will be annealed using RTA with much higher temperatures in a range from room temperature to 1000°C . The crystallinity of the annealed samples also will be characterized by x-ray diffraction (XRD, PHILIPS, X'pert-MPD) using $\text{CuK}\alpha$ radiation. X-ray photoelectron spectroscopy (XPS, PHI XPS System, 5600LS) using a monochromatic Al source will be also performed to determine the contents of Ce and O and to observe the bonding status of the annealed CeO_2 samples. A MTS nano-indenter equipped with Berkovich diamond indenter will be used to perform depth sensing nanoindentation testing on the annealed CeO_2 films and to obtain mechanical values of nanohardness and Young's modulus with a Poisson's ratio of 0.25.

The phase field model will be applied to the polycrystalline and thin film samples. Typical micrographs will be digitized to provide the initial microstructure, and the phase field simulations will be used to track the evolution of the grain structure, which will then be compared with annealed microstructure. The simulations will give insight into the relative importance of bulk, grain boundary and surface diffusion in the overall grain structure evolution.

The polycrystalline bulk CeO_2 samples and P-UBMS-sputtered CeO_2 thin films will be irradiated using 2.6 MeV proton beam at various temperatures from 500°C to 800°C . In-situ irradiation will also be performed using the IVEM-TANDEM facility located at Argonne National Lab to study the fission product damage including bubble formation and fission gas evolution. The swift heavy ion irradiated CeO_2 will also be irradiated in-situ to study the radiation and temperature effect on the track evolution. Phase field modeling will be applied to understand the damage and microstructure evolution in CeO_2 under irradiation.

Acknowledgment

This work was supported by the US Department of Energy, Office of Basic Energy Sciences as part of an Energy Frontier Research Center.

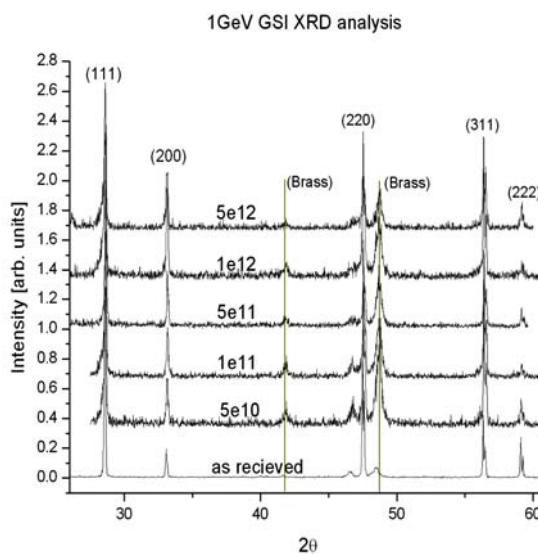


Figure 5. XRD analysis of swift heavy ion irradiated CeO_2 .

Structure/Property Relationships in High Strength Nanostructured FeNiMnAl Alloys

P.I.: Ian Baker

Thayer School of Engineering, Dartmouth College, Hanover, NH 03755

Ian.Baker@Dartmouth.edu

Student: Xiaolan Wu

Program Scope

The objective of this research is to understand the microstructural evolution and deformation mechanisms that control the strength of a range of nanostructured, very high strength FeNiMnAl alloys as a function of temperature and strain rate. The work involves:

1. Preparing a series of FeNiMnAl alloys by arc-melting, and then ageing them for various times at different temperatures.
2. Characterizing the resulting microstructures using an array of state-of-the-art techniques and instruments, both at Dartmouth and at the Oak Ridge National Laboratory (ORNL), including: X-ray diffractometry (XRD), scanning electron microscopy (SEM), transmission electron microscopy (TEM) with convergent beam electron diffraction (CBED) and energy dispersive X-ray spectroscopy (EDS), local electrode atom probe (LEAP) and high-temperature X-ray diffractometry in collaboration with Dr. M. K. Miller, Dr. K. More and Dr. A. Payzant through the Shared Research Equipment (SHaRE) program.
3. Measuring the strength of the as-cast and aged alloys as a function of temperature and strain rate by performing both hardness tests and compression tests.
4. Determining the deformation mechanism of the as-cast and aged alloys for a variety of temperatures and strain rates using slip line analysis via SEM; and dislocation analysis via both *post-mortem* TEM and *in-situ* TEM studies.

Accomplishments

Overview

In this period, a series of FeNiMnAl alloys of slightly different compositions (~5 at. % difference, see in Table 1) were arc-melted, and then aged. XRD, TEM and LEAP were used to characterize the resulting microstructures and analyze the phases present. Hardness measurements were performed on both the as-cast and aged alloys. Table 1 provides a summary of the compositions examined, phases present, phase widths and hardness values of the as-cast FeNiMnAl alloys.

As shown in Table 1, those FeNiMnAl alloys can be divided into three categories based on the phases present: b.c.c./B2 (ordered b.c.c.), f.c.c./B2, and B2/L₂₁ (L₂₁ is a further ordering of the B2 structure). The b.c.c./B2/L₂₁ microstructures may have formed by spinodal decomposition, but the f.c.c./B2 alloys clearly did not. The latter alloys had significantly lower hardness values.

Table 1. Compositions, phases, phase widths and hardness values of as-cast FeNiMnAl.

Composition (at. %)				Phases Present	Phase Widths (nm)	Hardness (HV)
Fe	Ni	Mn	Al			
30	20	20	30	B2-/L2 ₁	~10	514 ± 7
25	25	20	30	B2-/L2 ₁	~5	524 ± 13
30	20	30	20	f.c.c./B2	~65	454 ± 6
25	25	30	20	f.c.c./B2	~85	413 ± 10
30	20	35	15	f.c.c./B2	f.c.c. ~500; B2-ordered ~200	310 ± 15
30	20	25	25	b.c.c./B2	~50	504 ± 8
35	15	25	25	b.c.c./B2	~10	543 ± 17

One of the alloys, Fe₃₀Ni₂₀Mn₂₀Al₃₀, a B2/L2₁ two-phase alloy, was studied in greater detail. *In-situ* heating in the TEM was used to study the effect of the temperature on the microstructure. Compression tests of this alloy in both the as-cast condition and after various heat treatments were performed at different temperatures and strain rates.

Phase Analysis

As-cast Fe₃₀Ni₂₀Mn₂₀Al₃₀ showed mottled contrast in bright field (BF) TEM images, see Figure 1(a), while LEAP observation of the as-cast alloy showed a very fine structure with phase widths of ~5 nm, see Figure 2. Annealing at 823 K for 30 min produced only a modest increase in phase width to ~10 nm, see Figure 1(b), and for 72 h to ~20 nm, see Figure 1(c). CBED patterns from the phases in the aged microstructures showed that the alloys consist of L2₁ and B2 phases in a cube-on-cube relationship, see Figure 3. TEM-based EDS showed that the L2₁-ordered phase was enriched in Ni and Al, while the B2-ordered phase was enriched in Fe and Mn, a feature confirmed by LEAP observations. Table 2 shows approximate compositions of the phases. The compositions of the phases changed little upon ageing. Interestingly, TEM *in-situ* heating of as-cast Fe₃₀Ni₂₀Mn₂₀Al₃₀ showed that the L2₁ phase started to disorder to B2-order at ~723 K and that only two B2 phases were present at ~773 K.

Mechanical Properties

The hardness of Fe₃₀Ni₂₀Mn₂₀Al₃₀ showed a small increase of 5~6% for short time ageing (10 min) at 823 K, but little subsequent change for longer anneals, see Figure 4, indicating that the strength had no direct relationship with the phase size, which increases with annealing time. Compression tests performed at temperatures up to 873 K at a strain rate of $5 \times 10^{-4} \text{ s}^{-1}$ showed a brittle-to-ductile transition and a large drop in yield strength at ~773 K, coincident with the L2₁/B2 order/disorder temperature, see Figure 5.

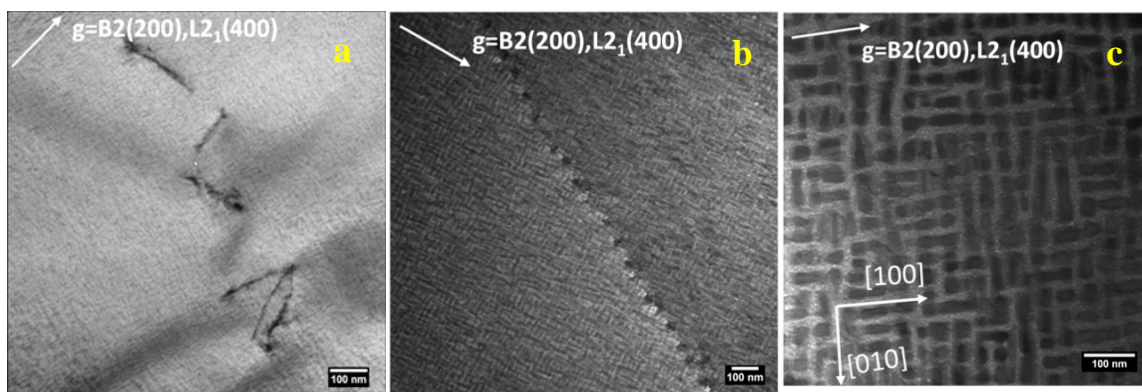


Figure 1. BF TEM images of $Fe_{30}Ni_{20}Mn_{20}Al_{30}$: (a) as-cast, (b) after a 30 min anneal at 823 K, and (c) after a 72 h anneal at 823 K.

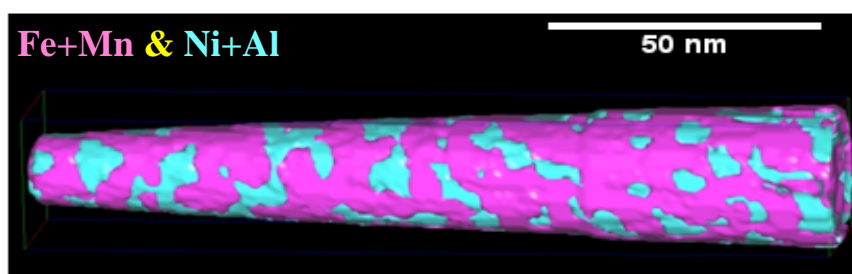


Figure 2. LEAP isoconcentration surfaces of as-cast $Fe_{30}Ni_{20}Mn_{20}Al_{30}$. The mauve phase contains $Fe + Mn > 50$ at.%, while the blue phase contains $Ni + Al > 50$ at.%.

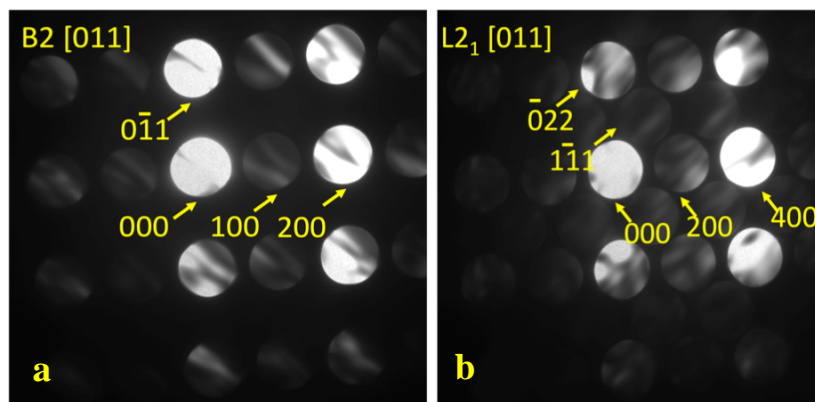


Figure 3. CBED patterns from (a) B2 and (b) L_{21} phases in $Fe_{30}Ni_{20}Mn_{20}Al_{30}$ after 72 h anneal at 823 K showing cube-on-cube relationship between the phases.

Table 2. Compositions (at. %) of the phases in $Fe_{30}Ni_{20}Mn_{20}Al_{30}$ as determined from three EDS measurements on TEM thin foils.

Phase	Fe	Ni	Mn	Al
Alloy	30	20	20	30
B2-ordered	32 ± 1	23 ± 1	21 ± 2	24 ± 2
L_{21} -ordered	15 ± 1	39 ± 2	12 ± 1	34 ± 1

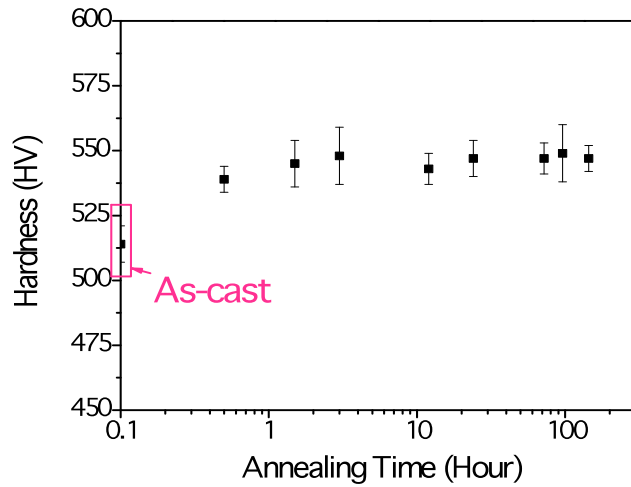


Figure 4. Hardness versus ageing time at 823 K for $Fe_{30}Ni_{20}Mn_{20}Al_{30}$.

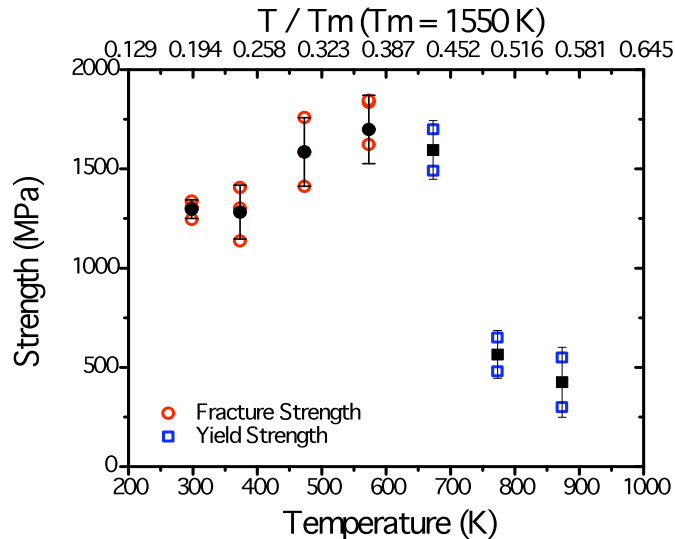


Figure 5. Strength versus temperature for $Fe_{30}Ni_{20}Mn_{20}Al_{30}$.

Future Plans

Future plans are to use both *post-mortem* TEM and *in-situ* TEM to perform dislocation analyses and determine the deformation mechanisms of the as-cast and aged alloys for a variety of temperatures and strain rates.

Publications

- “Microstructural Evolution of spinodally formed $Fe_{35}Ni_{15}Mn_{25}Al_{25}$ ”, I. Baker *et al.*, *Intermetallics* **17** (2009) 886-893.
- “An Overview of the Microstructures of High-strength Two-phase Near-equi-atomic FeNiMnAl Alloys”, I. Baker *et al.*, in preparation.
- “The Effect of Processing on the Microstructure and Mechanical Properties of $Fe_{35}Ni_{15}Mn_{25}Al_{25}$ ”, X. Wu *et al.*, in preparation.

Materials for Extreme Irradiation Environments

Pascal Bellon, Robert Averback, Shen Dillon, William King, Dallas Trinkle

Frederick Seitz Materials Research Laboratory, University of Illinois
104 S. Goodwin Av. Urbana, IL 61801

Phone: (217) 265-0284, e-mail: bellon@illinois.edu

Program Scope

A common roadblock in the development of future, high-efficiency, energy-generation technologies is the lack of materials that could function safely and economically in the envisioned harsh and aggressive in-service environments. This materials challenge is a daunting one, as the envisioned in-service conditions represent major departures from current systems, pushing materials into a domain that is largely unexplored. In particular, future nuclear energy reactors will subject materials to high levels of irradiation damage over prolonged periods of times and at very high temperatures.

We are developing in this program a new approach to design materials, which are intrinsically resistant to irradiation and other extreme conditions by utilizing nanostructuring and self-organization in highly nonequilibrium systems. While we focus on nuclear applications, we expect that the scientific advancements achieved in this program will have broad based significance for materials needs in a number of other extreme environments.

Recent Progress

A generic property of nonequilibrium materials is that they can self-organize into patterns. In order to understand and utilize these reactions, one needs to identify the control parameters that can trigger patterning, the threshold values of these parameters for which patterning takes place, and the characteristics of the patterns that develop, i.e., their nature, their morphology, and their length scales. In the present research, we have focused on patterning of composition in alloys subjected to irradiation. We have confirmed experimentally on a series of Cu-base alloys that, in moderately immiscible alloy systems, such as Cu-Ag, Cu-Co, Cu-Fe, irradiation under appropriate conditions can induce compositional patterning, and that its characteristics are in very good agreement with the model introduced by Enrique and Bellon in 2000 [1]. In this model, compositional patterning results from the dynamical competition between the forced mixing induced by irradiation and phase separation promoted by thermodynamics, as illustrated in Fig. 1. A key condition for patterning to occur is that the average ballistic relocation distance, R , exceeds a threshold value, which is typically one to two nearest neighbor distances. We have also observed experimentally that, when the ion type and flux are kept constant, patterning occurs only in a narrow temperature range. Indeed, at low irradiation temperature, the forced mixing dominates and the forcing intensity γ , defined as the ratio of the forced mixing jump frequency and the thermally activated atomic mobility under irradiation (see Fig. 1) takes large values. This large forcing intensity leads to the stabilization of a nonequilibrium solid solution. As the irradiation temperature is increased, thermally activated diffusion becomes more and more significant, and the forcing intensity increases continuously. Fig. 1 illustrates the fact that, in the above model, when the forcing intensity drops below a threshold value, compositional patterning is no longer a stable steady state under irradiation, and continuous phase coarsening is predicted. This is indeed what we found experimentally in Cu-Ag, Cu-Co, and Cu-Fe [2, 3].

We have directly imaged irradiation-induced self-organized nanostructures by transmission electron microscopy and by atom probe tomography (APT) [3] (see Fig. 2 for Cu-Fe). While the observation of compositional patterning in Cu-Fe for the conditions given in Fig. 3 is consistent with the model predictions, APT reveals unexpected features in these nanoscale structures. In particular, the composition of the Fe-rich regions is far from being pure Fe, as one would anticipate from the very low equilibrium

solubility of Cu in Fe at 250C. In fact most of these zones have a maximum Fe concentration between 60% and 80%. Second, interfaces are very diffuse; they extend over several nanometers. It is noteworthy that these two features are also observed in the nanoscale ODS steels, which are also processed by a highly nonequilibrium route, ball-milling and extrusion [4]. These two techniques lead to severe plastic deformation of the microstructure, and can also stabilize self-organized nanostructures [5]. These similarities suggest that large nonequilibrium solubilities and diffuse interfaces may be intrinsic to self-organized nonequilibrium nanostructures, be it stabilized by irradiation or by plastic deformation.

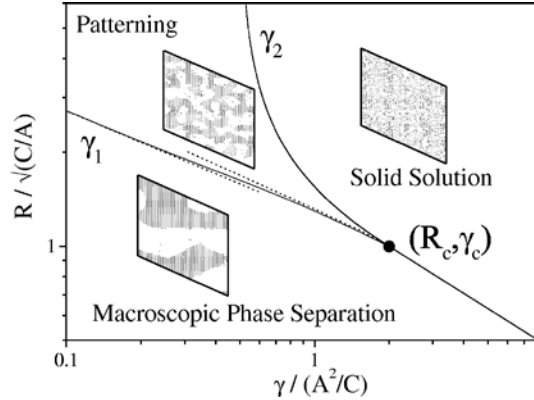


Fig. 1. Analytical dynamical phase diagram yielding the most stable steady-state of a phase separating $A_{50}B_{50}$ alloy as a function of the average forced relocation distance R and γ , the ballistic jump frequency normalized by thermally activated atomic mobility. Insets are (111) sections of 3D kinetic Monte-Carlo results; the lateral size of the section is 17 nm From ref. [1].

Another important finding obtained from our experimental studies in Cu-based, binary alloy systems is that the maximum temperature of self-organization, i.e., the boundary γ_1 in Fig. 1, is largely controlled by the solute thermal diffusion coefficient in Cu (see Fig. 3). This maximum temperature ranges from 175°C for Cu-Ag, to 350C for Cu -Co. We expect that further reductions in the solute diffusion coefficient would shift γ_1 to even high temperatures, and indeed this is observed in Fig. 3.

In the case of Cu-Mo, Cu-W, and possibly also Cu-Nb, the strong immiscibility of the alloys leads to a new and different type of self-organization. We first note that these systems are immiscible even in the liquid state, and atomic mixing in the thermal spike can no longer be considered ballistic since these alloy components do not randomize in the liquid. Ballistic mixing due to energetic recoil events, $E > 20$ eV, still occurs, but mixing by this mechanism is rather inefficient

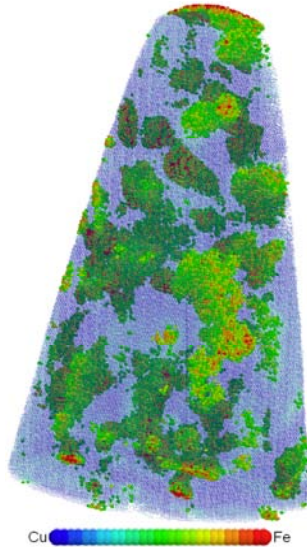


Fig. 2. Compositional patterning in $Cu_{90}Fe_{10}$ irradiated with 1.8 MeV Kr at 250°C to 3×10^{16} ions/cm². Composition map from atom probe tomography. Diameter of base ≈ 150 nm [3].

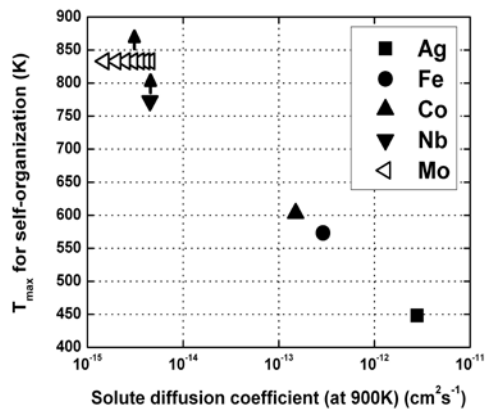


Fig. 3. Maximum temperature for irradiation-induced self-organization in Cu-base binary alloy systems as a function of solute diffusion coefficient (evaluated at 900K) [3]. Arrows for Nb and Mo indicate that T_{max} is higher, but not yet observed.

[6]. We have found that these systems have very interesting properties for applications of extreme radiation environments. Fig. 4 shows the precipitate sizes in $\text{Cu}_{90}\text{Mo}_{10}$ and $\text{Cu}_{90}\text{W}_{10}$ alloys as a function of irradiation temperature or annealing temperature [7]. The microstructures of these two alloys are seen to be remarkably stable. Notice that coarsening does not occur until annealing temperatures exceed 650°C ($0.68T_m$) and 900°C ($0.86T_m$) in $\text{Cu}_{90}\text{Mo}_{10}$ and $\text{Cu}_{90}\text{W}_{10}$, respectively.

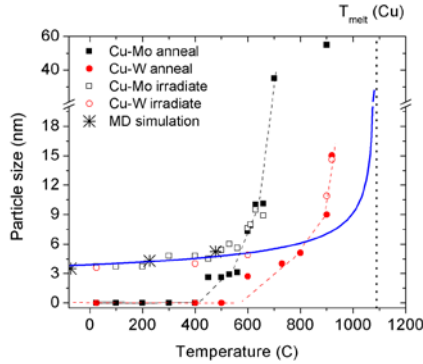


Fig. 4. Precipitate size versus temperature during thermal annealing or irradiation at high temperature in Cu-Mo and Cu-W alloys. Blue solid line is a fit to Eq. 1. From ref. [9].

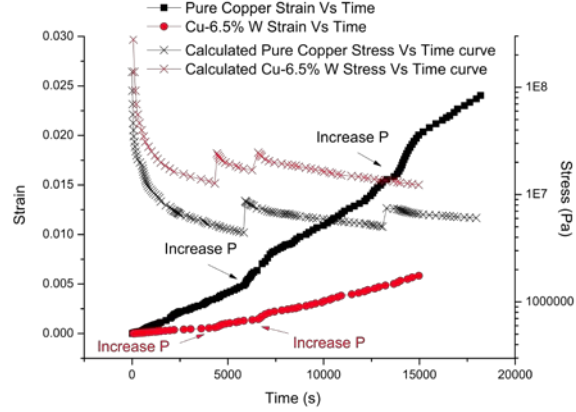


Fig. 5. In-situ strain and stress in nanocrystalline Cu (■) and Cu-6.5%W (●) as a function of irradiation time during 1.8 MeV Kr irradiation at 473 K (dose rate = 10^{-3} dpa/s) during creep using a bulge test on free-standing thin films. The pressure, initially 1kPa, was increased to 2 kPa and 3 kPa at times indicated by arrows.

In addition to possible grain growth, a second potential drawback of employing nanocrystalline materials for high temperature applications is poor creep resistance. Although we are just beginning to investigate creep properties in our new materials, we see in Fig. 5, already, that the creep resistance in the Cu-W alloy during 1.8 MeV Kr ion irradiation is far superior to that in pure nanocrystalline Cu. Moreover, the grain size was stable in the alloy sample, whereas in increased to nearly the thickness of the film, 300 nm, in the pure Cu. We believe that these *in situ* creep measurements are the first using heavy ion irradiation.

Future Plans

Our Cluster will investigate the fundamental processes controlling the formation of new, self-organized, nanostructured materials, their long-term structural and dimensional stability, and the relationships between the nanoscale features and the macroscopic properties. The research will combine irradiation experiments, *in situ* and *ex situ* characterization of microstructure and mechanical properties, and atomistic simulations and continuum modeling.

We will focus our work on model systems such as Cu-W-X, since we have established that nanostructured Cu-W alloys are structurally stable during irradiation at very high temperatures to very high doses. Ni and Fe matrices will also be investigated to determine whether the results on Cu alloys are general and can be extended to other materials. In these cases nanoinclusions such as TiB_2 or oxide dispersoids will be employed to provide microstructural stability. Ternary and quaternary additions will be selected, e.g., Cu-W-Nb, Cu-W-Co, Ni- TiB_2 -Cr, to create core/shell nanoprecipitates that we anticipate will provide dimensional and creep stability under irradiation. Phase field modeling will be employed to explore the generic materials and irradiation parameters conducive to the stabilization of these new nanostructures, while atomistic kinetic simulations will be used to simulate the evolution of specific alloy systems. New computational methods based on first-principles density-functional theory calculations will be developed to elucidate the energetic and kinetic interactions of solute elements and precipitates with grain boundaries and dislocations. Experiments will be performed to guide the theoretical developments and to provide validation. Nanoscale characterization will be achieved by combining atom probe

tomography and transmission electron microscopy tomography. We will measure the strength and creep response of self-organized alloys during ion irradiation by *in situ* and post-irradiation experiments, using microcantilevers for compression tests on micropillars, and laser deflection for bulge tests on thin films.

References

1. Enrique, R.A. and P. Bellon, Physical Review Letters, 2000. **84**(13).
2. Krasnochtchekov, P., R.S. Averback, and P. Bellon, Physical Review B - 2005. **72**(17): p. 1-12.
3. Chee, S.W., et al., Acta Materialia, 2010. **58**(12): p. 4088-4099.
4. Pareige, P., et al., Journal of Nuclear Materials, 2007. **360**(2): p. 136-142.
5. Bellon, P. and R.S. Averback, Physical Review Letters, 1995. **74**(10): p. 1819-1822.
6. Averback, R.S. and T.D. de la Rubia, *Solid State Physics, Vol 51*. 1998. p. 281-402.
7. Vo, N.Q., et al., Scripta Materialia, 2010. **in press**.

Publications of DOE sponsored research

- Chan, W.L., Y. Ashkenazy, and R.S. Averback, "Anisotropic diffusion of point defects under a biaxial stress field – dependences on crystal orientation", *J. Appl. Phys.*, **104**, 023502 (2008).
- Chan, W.L., K. Zhou, V. Nhon, Y. Ashkenazy, D.G. Cahill, and R.S. Averback, "Stress induced in platinum thin films by low energy ion irradiation", *Phys. Rev. B*, **77**, 205405 (2008).
- Vo, N.Q., R.S. Averback, P. Bellon, S. Odunuga, and A. Caro, "Quantitative description of plastic deformation in nanocrystalline Cu: Dislocation glide versus grain boundary sliding", *Phys. Rev. B*, **77**, 134108 (2008).
- Vo, N.Q., R.S. Averback, P. Bellon, and A. Caro, "Limits of Hardness at the Nanoscale: Molecular dynamics simulations", *Phys. Rev. B (Rapid Communications)*, **78**, 241402 (2008).
- Vo, N.Q., R.S. Averback, P. Bellon, and A. Caro, "Yield strength in nanocrystalline Cu during high strain rate deformation", *Scripta Materialia*, **61**, 76 (2009).
- Vo, N.Q., S. Odunuga, R.S. Averback, and P. Bellon, "Forced chemical mixing in immiscible alloys during severe plastic deformation at elevated temperatures", *Acta Materialia*, **57**, 3012 (2009).
- Averback, R.S. and P. Bellon, "Fundamental concepts in ion beam processing", chapter for *Materials Science with Ion Beams*, Ed. H. Bernas, Springer, 1-28 (2010)
- Bellon, P., "Phase Field Modeling", chapter for handbook series on *Comprehensive Nuclear Materials*, Ed. In chief R. Konings, Springer, in press.
- Bellon, P., "Precipitate and microstructural stability in alloys subjected to sustained irradiation", chapter for *Materials Science with Ion Beams*, Ed. H. Bernas, Springer, 29-52 (2010).
- Chee, S., B. Stumphy, N. Vo, R.S. Averback, and P. Bellon, "Dynamic self-organization in Cu alloys under ion irradiation", *Acta. Materialia*, **58**, 4088 (2010).
- Huang, M., D. Schwen, and R.S. Averback, "Molecular dynamic simulation of fission fragment induced thermal spikes in UO₂: sputtering and bubble re-resolution", *J. Nucl. Mater.*, **399**, 175 (2010).
- Schwen, D. and R.S. Averback, "Intragranular Xe bubble population evolution in UO₂: A first passage Monte Carlo simulation approach", *J. Nucl. Mater.*, **402**, 116 (2010).
- N. Vo, S. Chee, D. Schwen, X. Zhang, P. Bellon, and R.S. Averback, "Microstructural stability of nanostructured Cu alloys during high-temperature irradiation", *Scripta. Materialia*, in press.

Characterization and Modeling of Deformation Induced Damage in Titanium Alloys

Carl J. Boehlert, Thomas R. Bieler, Martin A. Crimp, Hongmei Li, James Seal

Michigan State University

DOE award #113920

The ability to characterize heterogeneous deformation in titanium is important, as it will lead to mechanistic understanding that will support model development that can predict material performance in polycrystals. By understanding how heterogeneous deformation occurs at the mesoscale, it will then be possible to develop understanding of damage nucleation mechanisms that will allow optimal material processing strategies to be developed. This will enable materials that are more resistant to developing performance-limiting damage. Building on fundamental prior research on commercially pure titanium (CP Ti), we are examining how heterogeneous deformation differs in titanium alloys in order to identify the mechanistic and microstructural features that are most likely to cause damage nucleation. This paper compares and contrasts heterogeneous deformation in CP Ti and a near- α alloy, Ti-5Al-2.5Sn (wt.%).

Experiments

Prior work on CP Ti was accomplished on 4-point bend specimens deformed to strains from 1 to 15% [1-4]. These specimens were characterized using a large range of experimental methods to quantitatively characterize heterogeneous strain, including electron microscopy using both secondary (topographic) and backscattered electron imaging (which can reveal regions of dislocation activity). Coupled with orientation imaging microscopy (OIMTM), slip system and orientation gradients were identified. Additionally, atomic force microscopy was used to accurately measure surface topography, which combined with orientation information from OIM, can be used to determine the amount of shear on activated slip systems. These values of shear can be directly compared with computational models of the same microstructural region examined using crystal plasticity-based finite element (CPFE) simulations. In addition, 3-D x-ray microscopy (using beam line 35ID-E at the Advanced Photon Source) observations have revealed details of dislocation slip interactions influenced by grain boundaries beneath the surface. These observations have been compared with OIM near surface observations [3].

The forged Ti-5Al-2.5Sn alloy was received with grain sizes between 50 and 100 micron, making it suitable for examining heterogeneous deformation as outlined above (heat treatments have been designed for Ti-3Al-2.5V, Ti-6Al-4V, Ti-6Al-2Sn-4Zr-2Mo alloys to obtain larger grain sizes than the as-received state for future studies). Tensile and four point bend specimens have been fabricated and results from a particular in-situ deformation experiment on a Ti-5Al-2.5Sn alloy are presented here. This tensile experiment was interrupted 4 times while straining to about 15% and SEM images were taken. OIM measurements were taken prior to and after deformation to characterize the polycrystalline orientations. This information, combined with the SEM images of the surface slip traces, allowed for accurate identification of the activated slip systems and calculation of the Schmid factors.

Crystal plasticity finite element (CPFE) models were built to replicate experimentally characterized patches of 10-20 grains of the CP Ti microstructure [1-3]. The mesh was projected into quasi-3-D space so that grain boundaries were perpendicular to the surface. The mesh was surrounded by rim elements that roughly simulate the effects of surrounding microstructure. The model was deformed so that the perimeter rim elements displaced to an amount that matched the nominal strain imposed on the experimental specimen.

Heterogeneous deformation in commercial purity titanium

The deformation patterns in CP Ti in Figure 1 were observed with (a) SEM observation coupled with OIM, (b) atomic force microscopy measurements converted into shear, and the same microstructure was (c) modeled using CPFE [1]. The specimen was cut so that the bending tensile axis was 45° from the centroid of the strong basal plane peak (with 8 x random texture), which results in high Schmid factors for basal slip. Despite this, slip trace analysis indicated that the strain was predominantly due to prism slip (Figure 1(a)); weak evidence for basal and (2nd order) pyramidal <c+a> slip are in faint plane traces best observed with higher-magnification images. In grains where basal or <c+a> slip was observed, the amount of shear was small, around 20-30% of the shear in grains where prism slip was favored. AFM analysis indicated that the strain was heterogeneously distributed, with shears on active slip systems varying from near-0 to about 0.07 in a specimen nominally deformed to about 1.5% strain. Mechanical twinning occurred in some grains with hard orientations, where neither basal or prism slip was favored (e.g. grain 2 in Figure 1(b)). Mechanical twinning was often stimulated by prism slip in a neighboring grain (e.g. grain 1). Basal slip was occasionally observed (grains 5 and 10), and <c+a> slip was observed in grain 10.

In this CP Ti specimen, about 6% of the grains exhibited mechanical twins, but about 40% of the grains had orientations that would favor twin formation, implying that twin nucleation is difficult. Most of the twins were “T1” extension (tensile) twins, which have a shear of 0.17. “T2” twins, which have a shear of 0.67, were also observed in a few grains (~0.25%). In general, only one type of slip/twinning system was observed in most grains. Sometimes two deformation traces were observed, but they were in different parts of the same grain. Multiple slip systems were evident only within a few microns of grain boundaries, and in many cases, this was related to heterogeneous strain accommodation by slip transfer across the grain boundary.

In CP Ti, three kinds of damage nucleation were observed as shown in Figure 2: (a) Grain boundary microcracks at small strains associated with complex multiple twin activity including the rarer T2 twins. (b) At larger strains, grain boundary sliding/mode II fracture was commonly observed. (c) Mode I crack opening associated with a grain boundary with heavy T1 twinning activity.

The CPFEM simulation shown in Figure 1(c) shows that the slip activity within a given grain is predicted at the correct magnitudes. Nevertheless, the model fails to capture the spatial distribution of strains within a given grain, and along grain boundary regions. This may result from the fact that slip resistance at grain boundaries is not modeled, and the mesh does not simulate grain boundary inclinations or underlying grain orientations present in the actual microstructure.

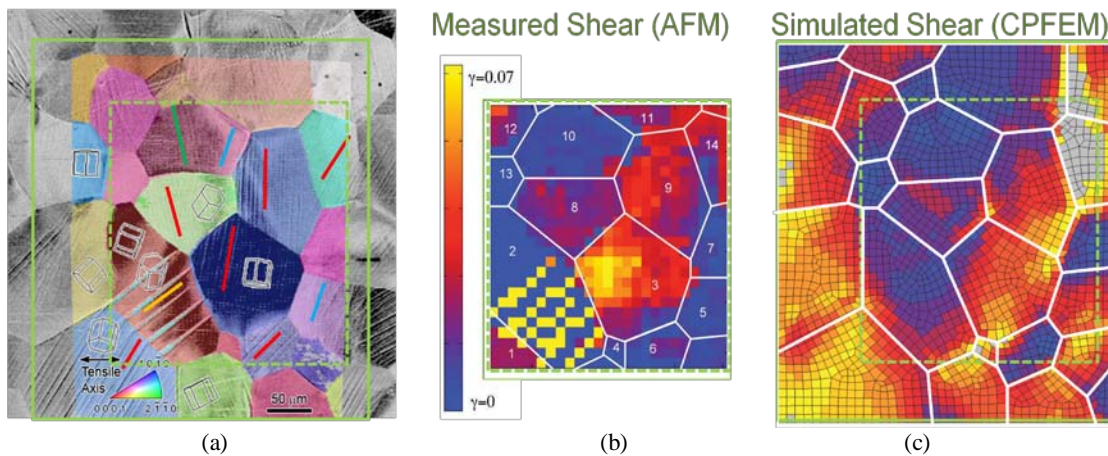


Figure 1 (a) SEM with OIM overlay information and color coded plane traces for slip bands (prism, basal, $\langle c+a \rangle$ and T1 twinning), (b) shears on observed slip and twinning systems measured using atomic force microscopy, (c) simulated deformation in a CPFEM model using a phenomenological hardening constitutive model. The simulation captures the magnitude and types of shears correctly, but not the spatial arrangement of shears within a grain or along grain boundaries.

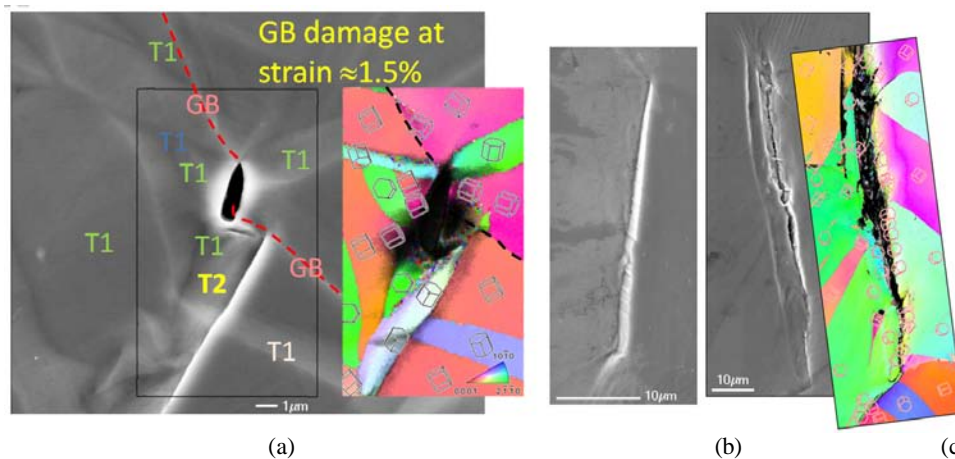


Figure 2 (a) Heterogeneous strain in CP Ti is accentuated at grain boundaries facilitating damage nucleation such as this microcrack observed after $\approx 1.5\%$ strain, where many mechanical twins (T1, T2) interacted with a grain boundary (GB). (b) Ledge development after about 15% strain in CP Ti related to grain boundary sliding or mode II cracking, and (c) mode I crack opening related to intense T1 twinning on both sides of the boundary.

Heterogeneous deformation in Ti-5Al-2.5Sn

A BSE SEM image of a microstructural patch containing approximately 100 grains of a Ti-5Al-2.5Sn specimen after it was deformed in RT tension to a strain of about 15% (prior to failure) is shown in Figure 3. The microstructure consists of large α grains with some scattered β (bright phase) that is often found in a grain boundaries. The corresponding load displacement curve shows stress-relaxation at locations where the deformation was stopped to take SEM images (none took place during elastic loading, where the first arrow is shown). Unlike CP Ti, no evidence of crack nucleation observed in the alloy, even after large strains [5,6]. The deformed microstructure differs considerably from CP Ti in several ways. First, no mechanical twinning was observed anywhere on the specimen. In contrast to CP Ti, basal slip is activated as much as prism slip as shown in the histogram in Figure 4, despite the fact that basal slip was more favored by the texture in the CP Ti. This result is consistent with prior work showing that the c/a ratio is higher in Ti alloys, which favors the activation of basal slip [7-8]. An implication of the greater activity of basal slip is that deformation is more likely to be homogeneous in alloys, consistent with smaller crystal rotations in the alloy as compared to CP Ti (Figure 5). In addition to the more homogeneous deformation in the alloy, slip bands that cross one another were commonly observed. This observation is in contrast to the deformation behavior of CP Ti, where intersecting slip systems were rarely observed. This suggests that accommodation of heterogeneous deformation in polycrystalline arrays occurs more readily in this alloy and suggests that damage nucleation at grain boundaries should be less likely.

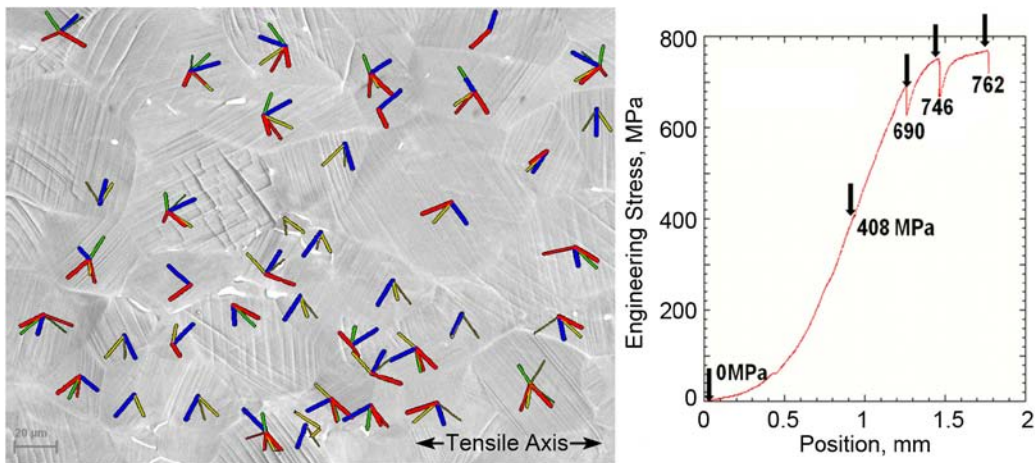


Figure 3 (a) BSE SEM image of a RT tensile deformed Ti-5Al-2.5Sn specimen which exhibited basal (blue) and prism (red), but no pyramidal a (green) or pyramidal $\langle c+a \rangle$ (gold) slip traces for systems with high Schmid factors.. The corresponding stress vs displacement plot shows arrows (b) the test was interrupted for SEM imaging.

In addition to the manner in which alloying additions affect the deformation of the α phase, formation of the β phase also plays a role in the heterogeneous deformation of the alloy. In CP Ti, analysis of the slip system geometry at the grain boundary showed that observed slip transfer occurred when the slip plane and slip direction on either side of the boundary were similar. One example of this was twin nucleation stimulated by prism slip in a neighboring grain [3]. For Ti-5Al-2.5Sn, the grain boundaries slip transfer statistics for the area in Figure 3 are shown in Figure 6, where 23% of the grain boundaries showed evidence for slip transfer. 25% of α - α grain boundaries showed correlated slip from one grain to the other. 15% of boundaries with intergranular β showed slip transfer from α to β , but very few instances of slip transfer from α to α through the grain boundary β were observed. This suggests that the soft bcc grain boundary β mitigates strain concentrations associated with dislocation pileups at grain boundaries, and may act to mitigate damage nucleation.

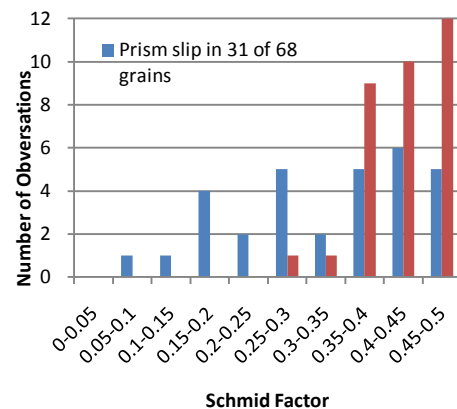


Figure 4 Basal slip is more strongly correlated with high Schmid factors than prism slip.

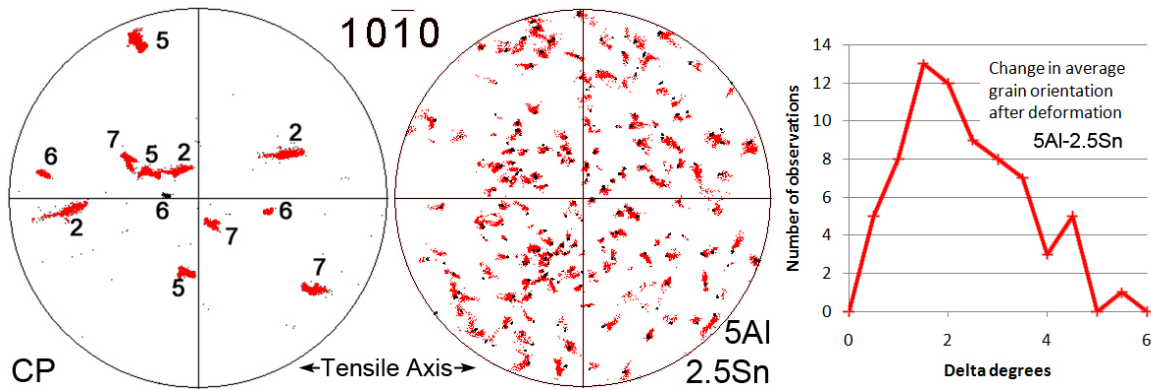


Figure 5 Comparison of (10-11) discrete pole figures for several deformed CP Ti grains [2], and all the grains in the Ti-5Al-2.5Sn region in Figure 3. Black dots represent undeformed grains, and red is deformed. There are smaller rotations in the alloy than in the CP Ti, which had half as much strain.

Summary and future work

Understanding the nature of heterogeneous deformation in CP Ti and Ti alloys is critical for predicting material performance. Alloying clearly modifies the nature of slip, but more critically, it also enables multiple slip system activation that leads to more homogeneous slip within grains that facilitates strain accommodation at grain boundaries. This may result in lower stress concentrations at grain boundaries, and reduced propensity for grain boundary crack nucleation.

In the coming year, we will model characterized microstructure patches using the CPFEE approach used for CP Ti, to examine the effect of this modified slip behavior on strain heterogeneity in CP Ti and Ti alloys. In our collaboration with colleagues at the Max-Planck-Institut für Eisenforschung, we will use new approaches to model slip heterogeneity in CPFEE microstructures using dislocation-density based models that have features that force planar non-local slip to be propagated across distances larger than one element. This should provide improved simulation of local strains, and additional schemes to introduce slip transmission and slip resistance across grain boundaries. We will extend our experimental characterization to additional alloys as indicated above, and conduct 3-D x-ray microscopy to measure grain orientations beneath the surface. We also plan to do more focused analysis of dislocation-grain/phase boundary interactions in local volumes.

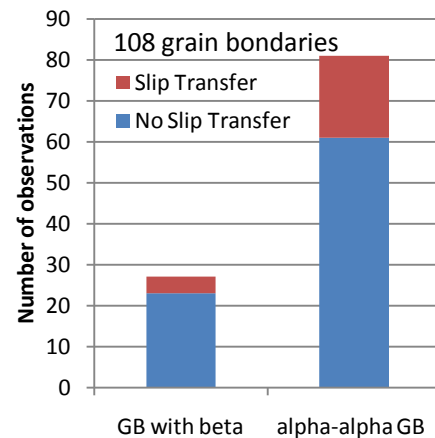


Figure 6 Slip transfer occurs in about 23% of boundaries in Figure 3, and less occurs across β than α boundaries.

References

1. Quantitative AFM characterization and crystal plasticity finite element modeling of heterogeneous deformation in commercial purity titanium, Y. Yang, L. Wang, T. R. Bieler, P. Eisenlohr, M. A. Crimp *Metall. Mater. Trans. A*, in press.
2. Experimental characterization and crystal plasticity modeling of heterogeneous deformation in polycrystalline α -Ti, L. Wang, R. Barabash, Y. Yang, T.R. Bieler, M.A. Crimp, P. Eisenlohr, W. Liu, . G.E. Ice, *Metall Mater. Trans. A*, in press.
3. Twin Nucleation by Slip Transfer across Grain Boundaries in Commercial Purity Titanium, L. Wang, Y. Yang, P. Eisenlohr, T.R. Bieler, M.A. Crimp, and D.E. Mason, *Metall Mater Trans. A* 41A(2) (2010) 421-30.
4. Nucleation of paired twins at grain boundaries in titanium, L. Wang, P. Eisenlohr, Y. Yang, T.R. Bieler, M.A. Crimp, *Scripta Materialia* (2010), doi: 10.1016/j.scriptamat.2010.06.027.
5. Deformation behavior of HCP Ti-Al alloy single crystals, J.C. Williams, R.G. Braggerly, N.E. Paton. *Metallurgical and Materials Transactions A*, vol. 33A, pp. 837-850, March 2002.
6. A study of active deformation systems in titanium alloys: dependence on alloy composition and correlation with deformation texture, S. Zaefferer. *Materials Science and Engineering*, vol. A344, pp. 20-30, 2003.
7. Phase diagrams of the titanium-aluminum, titanium-chromium-iron, and titanium-oxygen alloy systems, R.R. Van Thyne, E.S. Bumps, H.D. Kessler, M. Hansen, WADC Technical Report 52-15, 1952.
8. D. Buckley and R. Johnson, NASA Tech. Note, TN-D-3235, 1966, as discussed in: The formation of low friction wear-resistant surfaces on titanium by iron plating, D.G. Teer, and F.B. Salem, *Thin Solid Films*, 45 (1977) 583-89.

Deformation and Failure Mechanisms of Shape Memory Alloys (DOE Grant DE-SC0003996, 4/15/2010-4/15/2015)

Principal Investigator: Assistant Professor Samantha Daly (samdaly@umich.edu)
Department of Mechanical Engineering
2350 Hayward Street
The University of Michigan, Ann Arbor, Michigan 41809

Program Scope

We are exploring the fundamental mechanics that drive the deformation and failure of shape memory alloys (SMAs). SMAs are difficult materials to characterize because of the complex solid-to-solid phase transformations that give rise to their unique properties, including shape memory and superelasticity. These phase transformations occur across multiple length scales and result in a large hysteresis loop, which allows these materials to store or dissipate substantial amounts of energy. Our current efforts focus on new methodologies that will provide the first quantitative, full-field characterizations of phase transformation across multiple length scales. We are working on utilizing new combinations of microscopy, diffraction, digital image correlation, and customized testing equipment (ultrasonic testing, miniaturized testing) to study phase transformation processes at a wide range of length scales, including very small length scales with fields of view on the order of tens of microns.

We have chosen to examine Nickel-Titanium as a representative shape memory alloy. In addition to being the most widely used SMA, it is also a very good example of the fact that nearly all materials are dependent on multi-scale interactions. We aim to have the lessons that we are learning from these experiments be representative of, and applicable to, a wide class of materials. Here, atomic interactions, sub-granular transformation, intra-granular interactions, localized strain banding, and macroscopic behavior are all closely linked. We expect that the quantitative information from our experiments will be especially useful to the numerous theoretical and computational studies of shape memory alloys that are currently underway. In addition, the new experimental methodologies that we are developing are applicable to a wide range of future investigations into the mechanics of strain localization. Finally, these experiments investigate the change in the underlying mechanisms of phase transformation at small length scales (as well as experiments probing macroscopic thermo-mechanical behavior), with specific attention to the damping behavior and stability of these alloys.

Recent Progress

Fatigue & Fracture

We have made substantial progress towards understanding the low-cycle fatigue behavior of stress-induced martensitic phase transformation. These experiments are on going; we are currently focusing on the effect of strain rate, texture, and hard cycling. The rich local thermo-mechanical interactions that underlie transformation are being

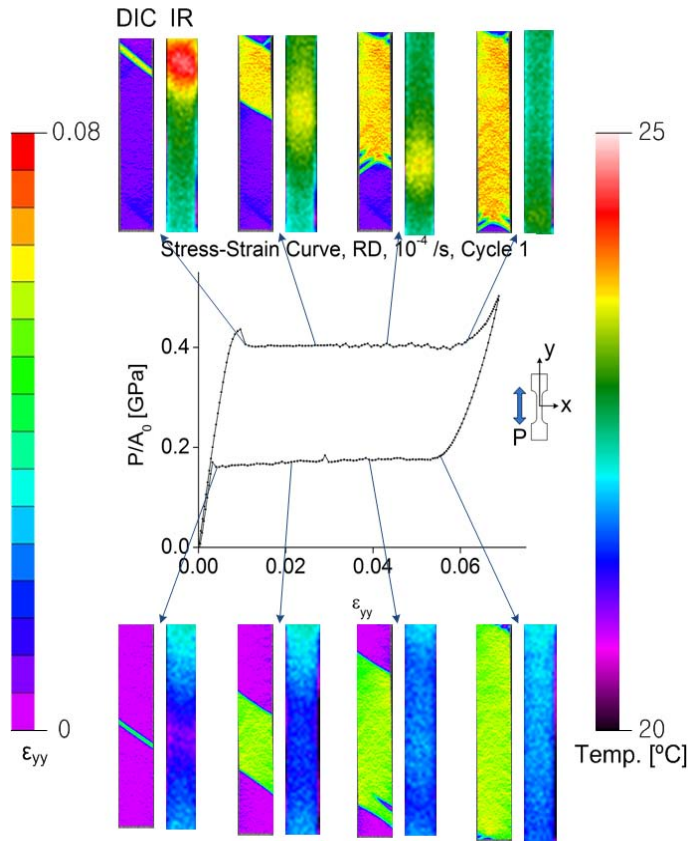


Figure 1: A recent experiment to track martensitic phase transformation in a SMA using combined Digital Image Correlation (strain measurements) and IR imaging (thermal measurements). Each full-field, simultaneous strain and thermal measurement of the gage section corresponds to a point on the stress-strain curve.

extent of transformation, and to also explore the characteristics of the phase fronts and the evolution of phase volume fraction. We have found and quantified, for the first time, a remarkable amount of strain memory in the martensite phase, that forms in the wake of the phase transformation front. This means that the accommodated strain in the martensite will remain stable during loading, even as the existing phase front propagates. Interestingly, we are also finding evidence of a remarkably strong strain memory in the martensite that persists from cycle to cycle. We are able to quantify this strain memory to a sub-micron degree of accuracy. This memory indicates that the local elastic stress fields in the martensite are driven by a dislocation structure and martensitic nuclei that largely stabilize during the first loading cycle.

We are also working on an experimental setup to examine the behavior of SMAs under very high-cycle fatigue. Currently, we are building a setup utilizing a 20 kHz ultrasonic fatigue tester and micro-strain tracking in order to examine the strain at the level of the microstructure during high-cycle, low-load fatigue of these alloys. The system is nearing completion and is currently being refined for experiments beginning

examined through the use of three-dimensional Digital Image Correlation (strain fields) and infrared imaging (thermal fields). Digital Image Correlation, or DIC, is an *in situ* method that measures displacements (and thus Lagrangian strain) on the surface of an object by tracking and correlating a random pattern on the sample surface. This non-contact approach to material characterization is somewhat analogous to putting tens of thousands of contiguous strain gages over the entire specimen surface, except that by using digital image correlation we can calculate the full-field strain as a “snapshot” in time and with much higher resolution than through the use of strain gages (which are locally averaged).

A representative experiment is shown in Figure 1. We are able to quantify the complex local interactions between the released or absorbed latent heat and the

in Fall 2010. Experiments will also begin in Fall 2010 utilizing two high-speed cameras (Photron SA-1s) to map mixed-mode fracture behavior in SMAs.

Small-Scale Behavior

In order to examine the small-scale phase transformation behavior, we need to combine the Digital Image Correlation (DIC) technique with Scanning Electron Microscopy, a technique we refer to as SEM-DIC. This is substantially harder than applying DIC to track macroscopic strains (length scales of $>mm$), because of two main reasons: (1) the need to apply a random, isotropic pattern of “tracking markers” for SEM-DIC where the markers are now very small, approximately 1-50 nanometers in size; and (2) the complex spatial and temporal distortion corrections that need to be applied to the SEM images prior to calculating displacements through the DIC algorithm (this is due to the fact that SEM is a rastering method, and thus each pixel is captured at a different point in time. Electron beam drift is also an issue). Over the past 4 months, we have made good progress of both of these issues.

Very little is currently known about small-scale patterning for SEM-DIC measurements, so we are performing an on-going study to systematically examine the feasibility of a variety of patterning methods. We have succeeded in creating viable patterns through the use of chemical vapor thin film rearrangement, template patterning methods, focused ion beam patterning, e-beam lithography, and nanoparticle patterning, where we find that the choice of optimal method depends on the length scale under consideration. We have also succeeded in coding the first portion of the temporal correction codes needed to adjust the SEM images prior to strain calculations. An example of this correction is shown in Figure 2. Spatial correction codes (less complicated than temporal codes) are currently underway.

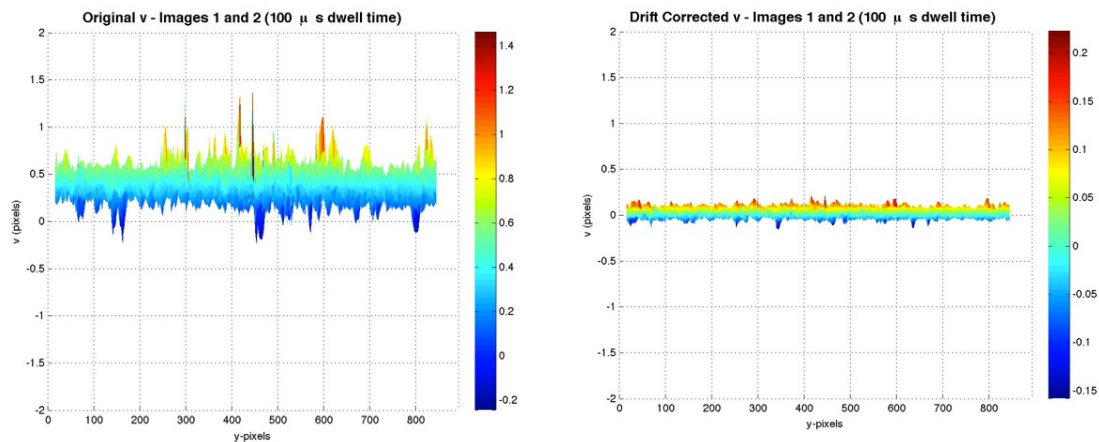


Figure 2: Initial temporal (drift) correction of the vertical component of strain (v) in an image captured by SEM. Note that prior to correction (left image), error in the v component is quite large with a mean of approximately 0.5 pixel. After the 1st stage of correction accounting for temporal drift (right image), error magnitude is now significantly smaller, and is correctly centered around 0 pixel.

Future Plans

We will continue to study the thermo-mechanical response of shape memory alloys, and the effects of length scale on the mechanics of phase transformation.

1. *Thermo-Mechanical Response*: Our aim here is to obtain the first quantitative measurements of the complex local thermo-mechanical interactions that occur during phase transformation. Our preliminary experiments have been successful (see Figure 1), but we still have much to accomplish. We are particularly interested in the influence of strain rate and texture, and the effect that loading and material parameters have on the cycling response. A comprehensive suite of experiments has been started, and there is a substantial amount of work that needs to be done in this regard. These experiments will also include an examination of phase transformation characteristics during both low-cycle and high-cycle fatigue. We have also begun to examine the deformation and failure of SMAs under structural loads, including bending and combined tension-torsion.
2. *Fracture*: Fracture work will begin in Fall 2010. As a first step, this will necessitate the construction of an experimental setup capable of measuring and quantifying phase transformation during fracture events. One aim is to examine the contribution of phase transformation towards shielding the crack tip under Mode I, II, and mixed-mode fracture. The dependence of crack behavior on microstructural variations will also be investigated.
3. *Micromechanics of Phase Transformation/ Small-Scale Studies*: Work will continue on the small-scale patterning and distortion correction codes needed for deformation tracking in the SEM. When this portion of work is complete, we will use the SEM-DIC methodology to obtain the first full-field maps of strain inhomogeneity inside of and across grains of SMAs under thermo-mechanical loading, as well as pre- and post-microstructures of the specimen using EBSD. The information will provide insights into, and validation benchmarks for, the microstructural evolution (particularly intergranular interactions) that are central to constitutive theories of phase transformation. We envision characterizing a local cluster of grains – including stress-strain behavior, energy absorption, and degree of martensitic transformation – and also knowing the displacement boundary conditions from the intragranular constraints on the outer edges of this cluster. A main aim of these experiments is to yield a wealth of new information on the effect of microstructure, relative grain size, and boundary conditions on the ability of these alloys to store/dissipate energy on the small scale, and to provide experimental knowledge that can be directly tied into current theoretical and numerical modeling.

Recent Publications (April 2010-current)

1. K. Kim, S. Daly. Martensite Strain Memory in the Shape Memory Alloy Nickel-Titanium under Mechanical Cycling. *Invited: Submitted to Experimental Mechanics, Special Issue on Advanced Imaging Methods (preprint available)*.

Molecular-Reinforced Hybrid Glass Films with Superior ThermoMechanical Properties

Reinhold H. Dauskardt (PI), Mark Oliver and Taek-Soo Kim (PhD Students)

Department of Materials Science and Engineering
Stanford University

Email: dauskardt@stanford.edu

Motivation

Hybrid glass films are processed from small organosilane precursors and exhibit unique electro-optical properties while maintaining excellent thermal stability to above 400°C. The resulting organosilicate network contains organic and inorganic silicate molecular components. As shown in Fig. 1, applications include antireflective coatings for photovoltaics, microelectronic interlayer dielectrics, optical waveguides, and high-performance coupling layers in laminates. Nanoporous forms of hybrid films are often desirable for size-selective membranes, biosensors, microfluidic structures, and membranes in fuel cell and photovoltaic technologies. Current applications of hybrids are limited only by their inherently mechanical fragile nature which remains a fundamental challenge for their integration and application.

Mechanical properties of hybrid glasses are controlled by the molecular structure and connectivity of the molecular precursors and how they form an extended molecular network. Their inherently fragile nature derives from the inorganic glass component and the incorporation of *univalent* (terminal) organic carbon groups which dramatically reduce network connectivity. In nanoporous hybrids, the nature and connectivity of the nanometer-scale pore distribution introduces further nanostructural variables. Remarkably little understanding exists of how these variables govern even such basic mechanical properties as elastic stiffness and cohesive fracture.

Program Scope

Realizing advanced hybrid glasses that exhibit outstanding mechanical properties will require precise engineering of the glass structure at a level not presently possible with existing understating of how chemical and network structure govern mechanical behavior. Toward that goal, we are developing combined synthetic, molecular and mechanical characterization capabilities, together with computational tools to generate highly accurate molecular models of a broad range of hybrid glasses and make quantitative predictions about both their elastic and fracture properties. The hybrids represent a rich area for future fundamental materials discovery with significant technological impact.

Recent Progress

We have developed the capability to create highly accurate molecular models of dense and nanoporous hybrids from a variety of precursors (Fig. 2). With these models, we can accurately predict the elastic properties of hybrids as well as predict their fracture properties by using a novel model of cohesive fracture. Development of these computational tools required thorough comparison with experimental data of synthesized hybrid materials. Two ethane-bridged glasses, Et-OCS and Et-OCS(Me) (Fig. 2a) were synthesized and fully characterized to provide experimental data sets for the calibration and validation of the models. Having established predictive accuracy,

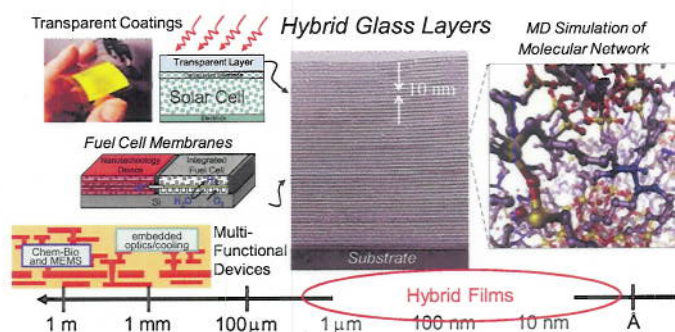


Fig. 1: Hybrid glass films have application in a wide range of nanoscience and energy technologies including flexible electronics, photovoltaics, fuel cell membranes and multi-functional devices. Mechanical properties and their relationship to molecular and nanopore structure are poorly understood but critical for integration and application.

we have begun to guide experimental efforts through predictions and discoveries made using these models.

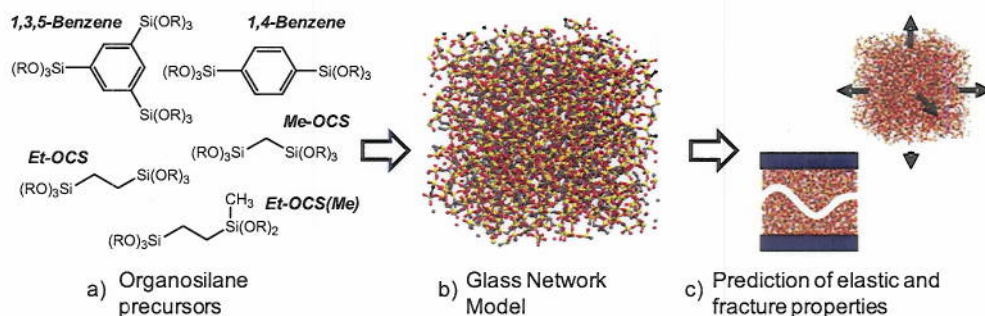


Fig. 2: Molecular models of hybrid glass networks can be generated from a wide range of molecular precursors. With these glass networks models, the elastic and fracture properties can be simulated.

Model glasses are created using isothermal-isobaric (NPT) molecular dynamics based simulated annealing with a newly developed interatomic potential. The accuracy of the model structures has been established through rigorous comparison with experimental data. The bond lengths, bond angles, and atom coordination numbers have been confirmed to be consistent with known values. Additionally, models can be generated to have realistic distributions of the various Si bonding states. As an example, the distribution of Si T groups and condensation degree, q , for Et-OCS measured experimentally with ^{29}Si NMR can be adequately simulated, as shown in Table 1. T_0 , T_1 , T_2 , and T_3 groups are silicon atoms in the glass connected to zero, one, two, or three other silicon atoms, respectively, via a Si-O-Si bond. Our model structures represent the most accurate molecular models of hybrid glasses generated to date.

Table 1: T-group distribution and condensation degree, q , for real and model Et-OCS

	T_0	T_1	T_2	T_3	q
Synthesized Et-OCS (NMR)	0	.041	.463	.495	0.818
Model Et-OCS	.004	.069	.401	.526	0.816

The elastic properties of the model glasses were simulated using molecular dynamics. The predicted modulus values for Et-OCS and Et-OCS(Me) glasses having the same condensation degree as the synthesized glasses, are in good agreement with experimental data, as shown in Table 2. Having quantitative predictive capabilities, we investigated the scaling of the bulk modulus with the network connectivity by generating Et-OCS and Et-OCS(Me) models with different connectivities (Fig. 3). The Si-X-Si connectivity, p (where X = O or C-C) is equal to the fraction of bridging Si-X-Si bonds per silicon atom that are present compared to fully connected SiO_2 . These results demonstrate the importance of network connectivity to hybrid material reliability and provide a simple scaling law.

Table 2: Experimental and Predicted Young's Modulus of Et-OCS and Et-OCS(Me)

	Et-OCS ($q = 0.818$)	Et-OCS(Me) ($q = 0.820$)
E_{SAWS}	19.5 GPa	7.5 GPa
MD Model	19.8 GPa	9.1 GPa

To guide the development new hybrid glasses, we have generated a variety of model glasses from different precursors, keeping the connectivity constant (a very difficult task experimentally). The simulated elastic moduli are plotted against the simulated densities in Fig. 4. All the bridged precursors fall along a universal modulus-density trend except for 1,3,5-Benzene, suggesting that using 1,3,5-Benzene as a precursor may result in materials with exceptional mechanical properties. This result

demonstrates the ability of these models to identify new potential network stiffening strategies as well as fundamental scaling relationships that are difficult to establish experimentally.

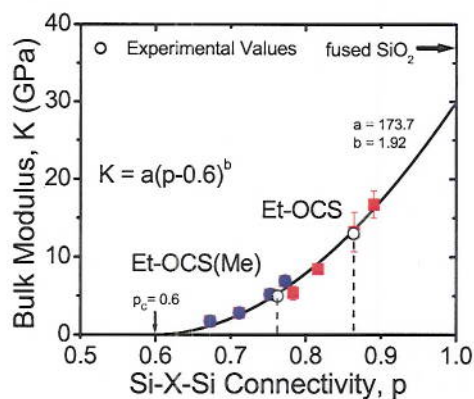


Fig. 3: Experimental measurements and model predictions of bulk modulus, K , as a function of Si-X-Si connectivity, p .

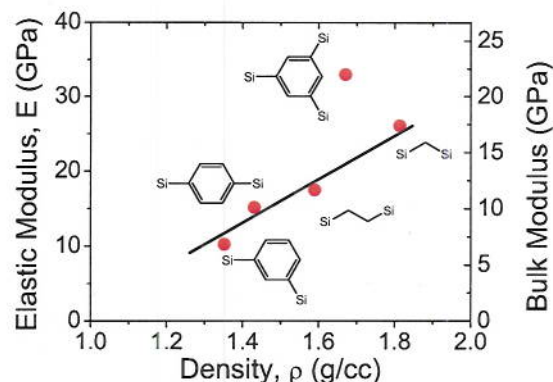


Fig. 4: Simulated stiffness versus density for hybrid glasses with various basic structural units. All models had a connectivity of 0.85.

Another critically important material property for reliable integration is cohesive fracture energy, G_c , which quantifies a materials resistance to cracking. We have developed a novel fracture model using the minimum cut principle of graph theory that predicts the complex three-dimensional cohesive fracture path at the atomic scale and provides both the number and type of bonds broken. We have used this minimum-cut fracture model to predict the fracture surface bond density (bonds/nm²) of Et-OCS and Et-OCS(Me) as a function of Si-X-Si connectivity, p (Fig. 5a). The model predicts a linear scaling of the area density of bonds broken during fracture with Si-X-Si connectivity, p , that goes through zero at $p = 0.55$. Given the brittle nature of the materials, their fracture energy, G_c , can be well approximated as the product of the area density of atomic bonds broken during fracture and the average energy required to break each bond:

$$G_c \left[\frac{\text{energy}}{\text{area}} \right] = \frac{\text{bonds}}{\text{area}} \frac{\text{energy}}{\text{bond}}$$

Thus the fracture energy, G_c , should also be proportional to $(p-0.55)$. Fig. 5b shows fracture energy values for various brittle hybrids plotted against the Si-X-Si connectivity calculated from the various reported measures of connectivity. The measured values for Et-OCS and Et-OCS(Me) are also plotted. All the fracture energy values from these four independent studies are proportional to $(p-0.55)$, falling along a very similar trend when plotted against Si-X-Si connectivity. This demonstrates that the minimum cut fracture model provides a powerful new tool for predicting fracture properties of hybrid materials. The computational tools developed thus far represent a significant advance in our ability to investigate the molecular origins of hybrid material mechanical behavior and to design new mechanically robust hybrids that are of critical importance to a range of emerging technology areas.

Future Plans

Our research will continue to focus on new classes of molecularly-reinforced hybrid glass films that overcome the mechanically-fragile limitations of existing non-reinforced hybrids. We will continue to develop new thin-film metrologies to characterize bond rupture kinetics and cohesive fracture in reactive chemical and UV photon environments where there is a paucity of experimental data and an almost

complete lack of fundamental understanding. We will be interested in the synergistic effects of the reactive chemical and UV photon environments. The effects of UV photons with energies in the solar spectrum on molecular bond rupture kinetics and resulting cohesive cracking processes are of specific interest since hybrid films have application in emerging solar energy technologies.

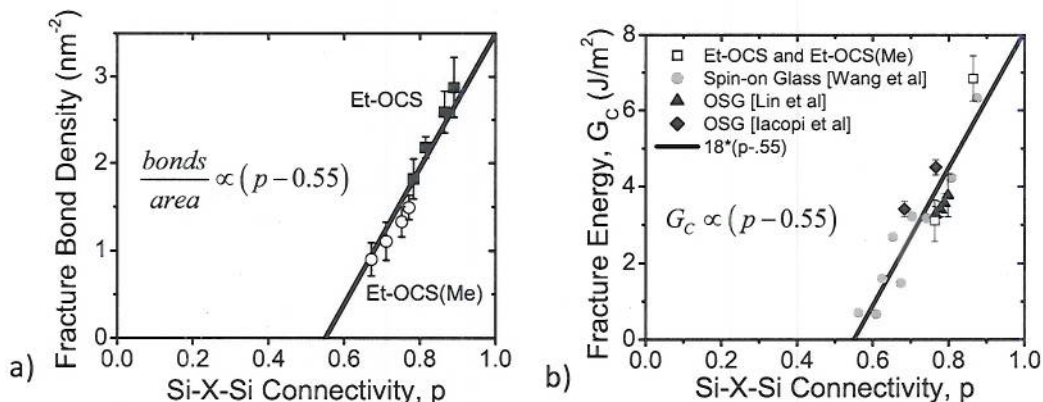


Fig. 5: The dependence of a) fracture surface bond density in bonds/ nm² for Et-OCS and Et-OCS(Me) and b) fracture energy, on Si-X-Si connectivity, p.

DoE Program Publications

1. MS Oliver, Dubois G, Sherwood M, Gage DM, Dauskardt RH, "Molecular origins of the mechanical behavior of hybrid glasses", **Advanced Functional Materials** vol. 20 (2010) p. 2884
2. MS Oliver, Dubois G, Dauskardt RH, "Molecular Design of Ultra-Low-k Hybrid Glasses", **Proceeding of the IEEE International Interconnect Technology Conference**, June 7-9 2010
3. T. Kim and R. H. Dauskardt, "Molecular Mobility under Nanometer Scale Confinement," **Nano Letters**, 10(5), 1955-1959, 2010.
4. T. Kim and R. H. Dauskardt, "Integration Challenges of Nanoporous Low Dielectric Constant Materials," **IEEE Transactions on Device and Materials Reliability**, 9(4), 509-515, 2009.
5. T. Kim, D. Chumakov, E. Zschech, and R. H. Dauskardt, "Tailoring UV cure depth profiles for optimal mechanical properties of organosilicate thin films," **Applied Physics Letters**, 95, 071902, 2009.
6. T. Kim, T. Konno, and R. H. Dauskardt, "Surfactant-Controlled Damage Evolution during Chemical Mechanical Planarization of Nanoporous Films," **Acta Materialia**, 57, 4687-4696, 2009.
7. T. Kim, K. Mackie, Q. Zhong, M. Peterson, T. Konno, and R. H. Dauskardt, "Surfactant Mobility in Nanoporous Glass," **Nano Letters**, 9(6), 2427-2432, 2009.
8. T. Kim, N. Tsuji, K. Matsushita, N. Kobayashi, D. Chumakov, H. Geisler, E. Zschech, and R. H. Dauskardt, "Tuning depth profiles of organosilicate films with ultraviolet curing," **J App Phy**, 104, 074113, 2008.
9. T. Kim, N. Tsuji, N. Kemeling, K. Matsushita, D. Chumakov, H. Geisler, E. Zschech, and R. H. Dauskardt, "Depth dependence of ultraviolet curing of organosilicate low-k thin films," **J App Phy**, 103, 064108, 2008.
10. T. Kim, N. Tsuji, J. van der Hilst, K. Matsushita N. Kobayashi, D. Chumakov, H. Geisler, E. Zschech and R. H. Dauskardt, "Tuning Depth Profiles of Low-k Dielectrics with UV Curing," **Advanced Metallization Conference Proceedings**, 337-340, San Diego, CA, 2008.
11. T. Kim, T. Konno, T. Yamanaka, and R. H. Dauskardt, "Quantitative Roadmap for Optimizing CMP of Ultra-Low-k Dielectrics," **2008 IEEE Int Interconnect Tech Conf Proc**, Burlingame, CA, 2008.
12. T. Kim, T. Konno, T. Yamanaka, and R. H. Dauskardt, "Optimizing CMP for Ultra-Low-k Dielectrics," **13th International Chemical Mechanical Planarization Conference for ULSI Multilevel Interconnection**, Fremont, CA, 2008.

Mechanical Properties and Microstructural Evolution in Al-Li-Sc-Yb Alloys Containing Multi-Shell Nanosize Precipitates

Prof. David C. Dunand (dunand@northwestern.edu), Prof. David N. Seidman, Prof. Christopher Wolverton
Department of Materials Science & Engineering, Northwestern University, Evanston IL 60208

1. Program Scope or Definition

Development - based on theoretical principles and modeling – of nanosize precipitates with atomic-level control of composition and size within Al alloys to provide resistance to coarsening and creep up to 400 °C.

2. Recent Progress

Microstructural Investigations and Ambient-Temperature Microhardness

Core-shell nanoscale precipitates in Al-0.06 at.% Sc microalloyed with Tb, Ho, Tm or Lu [1]

The age-hardening response at 300 °C of Al-0.06Sc-0.02RE (with RE = Tb, Ho, Tm or Lu; all concentrations hereafter are in at.%), was found to be similar to that of binary Al-0.08Sc (at.%), except that a shorter incubation period for hardening is observed, which is associated with nanoscale RE-rich $Al_3(RE_{1-x}Sc_x)$ precipitates. Peak-age hardening occurs after 24 h, and is associated with a high number density of nanoscale Sc-rich $Al_3(Sc_{1-x}RE_x)$ precipitates. Analysis by three-dimensional local-electrode atom-probe tomography shows that the REs partition to the core of the precipitates, and that x increases with increasing atomic number. None of the REs studied was found to be superior to Yb as an addition to Al-Sc alloys, which affects an early increase in microhardness, produces a high number density of precipitates, and exhibits a high degree of Sc-replacement.

The effect of Li additions on precipitation-strengthened Al-Sc-Si and Al-Sc-Si-Yb alloys [2]

Four alloys: Al-0.12 Sc-0.013 Si, Al-2.9 Li-0.11 Sc-0.018 Si, Al-0.042 Sc-0.013 Si-0.0088 Yb, and Al-5.53 Li-0.048 Sc-0.013 Si-0.0092 Yb, were aged at 325 °C to produce strengthening $L1_2$ -structured α' - $Al_3(Sc,Li)$ and α' - $Al_3(Sc,Li,Yb)$ precipitates. The Li-containing alloys reach greater peak Vickers microhardness values than their Li-free counterparts; and in the case of Al-0.12 Sc-0.013 Si, an addition of Li increases the overaging time by a factor of four (Fig. 1a). Furthermore, for alloys in the peak-aged state, the addition of Li causes the following changes in the precipitates: the number density is increased, the mean radius is decreased, and the volume fraction is increased. These changes result from an increase in the driving force for nucleation due to Li, and also a decrease in the interfacial free energy. This produces the unexpected

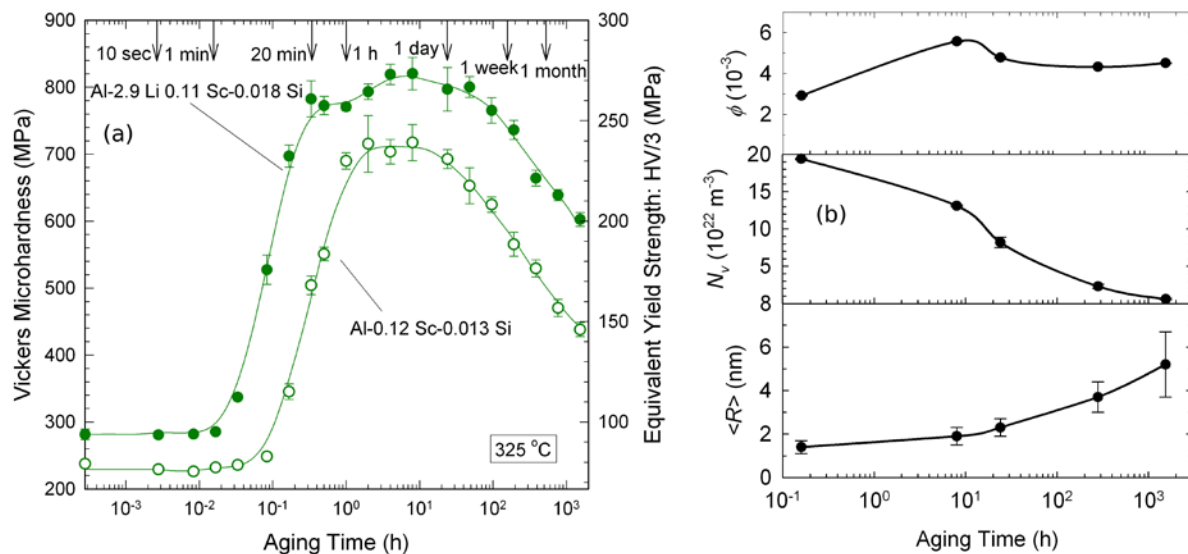


Figure 1. (a) Vickers microhardness vs. aging time for Al-0.12 Sc-0.013 Si and Al-2.9 Li-0.11 Sc-0.018 Si; and (b) the volume fraction (ϕ), number density (N_v), and average radius ($\langle R \rangle$) of precipitates vs. aging time for Al-2.9 Li-0.11 Sc-0.018 Si, aged isothermally at 325 °C.

result that addition of Li (which diffuses faster than Sc) to a binary Al-Sc alloy causes a decrease in the rate of precipitate coarsening. As a result of a decreasing amount of Li incorporation in the α' -Al₃(Sc,Li) precipitates with aging time, their volume fraction reaches a maximum value at peak-age, and then decreases during overaging (Fig. 1b).

Chemistry and structure of core/double-shell nanoscale precipitates in Al-6.5Li-0.07Sc-0.02Yb (at.%) [3]

An Al-6.3Li-0.07Sc-0.02Yb alloy was subjected to a double-aging treatment to create nanoscale precipitates, which were studied by atom-probe tomography and transmission electron microscopy. This builds on our previous work on a double-aged Al-Li-Sc alloy [4], which also exhibited core-shell precipitates. A first aging step at 325 °C leads to a doubling of microhardness as result of the formation of coherent L1₂-structured precipitates with an Al₃Yb-rich core and an Al₃Sc-rich shell. The core and shell both contain a large concentration of Li, which substitutes for up to 50 % of the Sc or Yb atoms. These core/single-shell precipitates provide excellent resistance to overaging at 325 °C. Subsequent aging at 170 °C increases the microhardness by an additional 30%, through precipitation of a metastable δ' -Al₃Li second shell on the core/single-shell precipitates (Fig. 2), thereby forming a chemically and structurally complex core/double-shell structure. More complex multiple-core/double shell precipitate structures have also been observed [5].

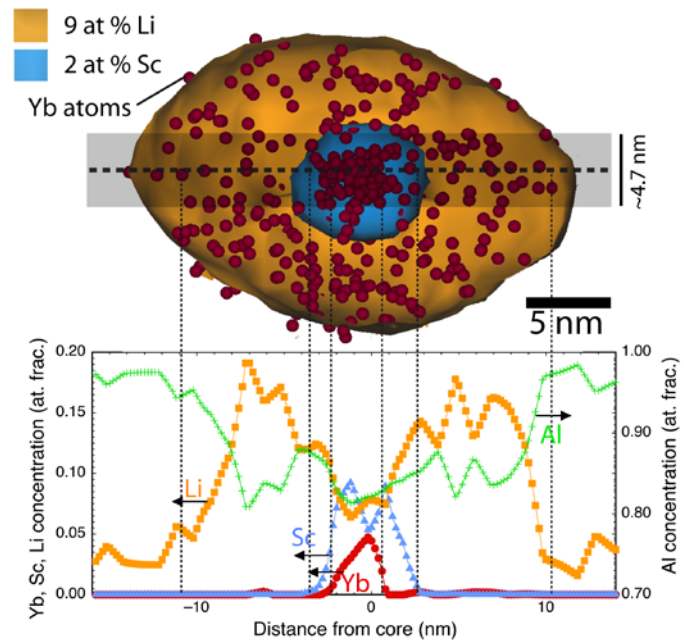


Figure 2. A core/double-shell precipitate observed via atom probe tomography, for aging at 325 °C for 8 h, followed by 2 weeks at 170 °C.

High-Temperature Mechanical Properties: Creep of Al-Sc, Al-Li-Sc, and Al-Li-Sc-Yb Alloys [6]

Three alloys: Al-0.12Sc, Al-2.9Li-0.11Sc, and Al-5.53Li-0.048Sc-0.0092Yb, were aged at 325 °C, producing precipitation-strengthened, creep-resistant alloys (see above section). The aged alloys were crept at 300 °C in compression, yielding minimum steady-state strain rates from 10⁻⁹s⁻¹ to 10⁻⁴s⁻¹. The alloys exhibit high apparent stress exponents in the range 13.8 – 33.0, which are indicative of threshold stress behavior; threshold stresses are measured ranging from 7.9 MPa – 20.0 MPa. The normalized threshold stresses are expected to increase with precipitate size and lattice parameter mismatch due to elastic strains induced in the matrix, and their interactions with dislocations. The measured creep properties of the alloys will be accompanied by microstructural investigations of the crept alloys (see Future Plans).

Dislocation Dynamics Modeling of Complex Microstructures

We have completed modifications of an existing code (written by V. Mohles [7]) to study the strengthening of Al-Li-Sc-RE alloys with complex precipitate morphologies. This code was designed to simulate dislocation interactions with precipitates to determine the critical resolved shear stress (CRSS). The code originally only supported simulations of single-phase spherical precipitates having a prescribed size and spatial distribution.

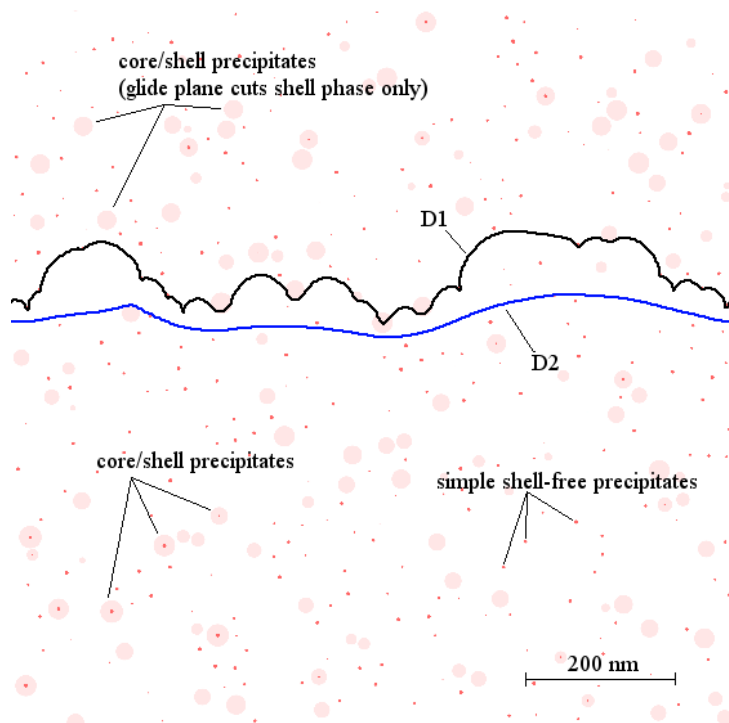


Figure 3. An obstacle field using experimentally-observed atom-probe datasets containing complex core/shell precipitates in a double-aged Al-Li-Sc-Yb alloy. Two dislocations (D1 and D2) are traversing the obstacle field under an applied stress.

The following modifications were made to extend the model:

- large experimental obstacle fields may be imported using atom-probe tomography-measured datasets
- complex core-shell precipitates can be simulated (Fig. 3)
- a stress field for lattice-parameter mismatch of core-shell precipitates having different lattice constants has been derived and implemented in the simulation code
- a stress field for modulus mismatch between the precipitates and the matrix has been derived and implemented in the simulation code

We are in the midst of applying the extended model to a wide variety of precipitate obstacle fields (see Future Plans).

First-Principles Calculations of Al-Li-Sc System Properties [8]

We utilized first-principles density functional calculations to study the nucleation and stability of $L1_2$ -ordered precipitates in Al-rich Al-Sc-Li alloys. We find the following results: (1) The coherency strains to form coherent interfaces between Al_3Sc/Al , Al_3Li/Al , and Al_3Sc/Al_3Li are relatively small, due to the small atomic size mismatches in these systems; (2) the Al_3Li and Al_3Sc phases may be off-stoichiometric due to a non-zero solubility of the other solute elements. Sc atoms from the α -Al-solid solution, substitute on the Li sublattice-sites of the Al_3Sc phase, while Li substitutes on the Sc sites of Al_3Li ; (3) the solubilities of Sc and Li in Al alloys, calculated from first-principles, are in good agreement with experimental results, and in the case of Sc, agree well with prior first-principles results; (4) we calculated the interfacial energies for Al/Al_3Sc , Al/Al_3Li , and Al_3Sc/Al_3Li for (100), (110), and (111) interfaces, and the value of the Al/Al_3Sc interfacial energy is much larger than those of the Al/Al_3Li , and Al_3Sc/Al_3Li structures; (5) Combining the bulk and interfacial energies yields the nucleation barriers and critical radii for Al_3Sc and Al_3Li precipitates; and (6) if the Li concentration in the alloy is sufficient, $Al_3Li(L1_2)$ will wet Al_3Sc , decreasing the interfacial energy of the system and leading to stable core/shell precipitates.

First-Principles Calculations of Al-Rare Earth Compounds [9]

We utilized first-principles density functional calculations to study the phase stability, magnetic properties, and the solubility of aluminum rare-earth (RE) compounds. Standard potentials correctly predict all the stable phases of Al-RE compounds and frozen potentials are also in good agreement with experiments, except $Al_3Yb.cP4$. The contributions of RE magnetic properties to the relevant formation energies are crucial to predict the correct ground Al_3RE structures. RE solubilities in Al were calculated, including the vibration entropy, and our calculated results are in very good agreement with experimentally measured values.

3. Future Plans

Elevated Temperature Mechanical Properties: Creep-Microstructure Correlations [10]

The creep properties measured for the three alloys studied (see Recent Progress) indicate threshold-stress behavior, due to elastic interactions between dislocations and coherent, misfitting precipitates. The magnitude of the elastic interactions scales with precipitate size. Hence, a complete understanding of the role of the precipitates in imparting creep resistance necessitates measurement of the precipitate sizes, which evolved during the early stages of creep testing. TEM will be used to verify that coherency misfit strains are indeed found in the matrix surrounding the precipitates, and LEAP will be used to acquire accurate size distribution information for the crept alloys. To add further insight into these results, we plan to extend the dislocation dynamics model discussed above to investigate the possibility that threshold stresses are due to departure-side attractive interactions between dislocations and precipitates during climb.

Dislocation Dynamics Modeling [11]

Development of the simulation (described above) is complete. The program is currently being evaluated by comparing the measured strength increment to the simulated strength increment in alloys for which microhardness and precipitate structure have been experimentally determined. A variety of alloys was selected to obtain a broad range of strengths, including aging states for which both precipitate shearing and Orowan looping is expected. This includes core-shell precipitates in the Al-Li-Sc system, with shear-resistant Al_3Li cores and easily shearable Al_3Li shells. Once validated, the simulation may be used with simulated precipitate fields to find optimal conditions for maximum strengthening in Al-Li-Sc alloys, which will depend on alloy composition (volume fraction) and the distribution of the strengthening phases.

First-Principles Calculations of Al-alloys with Li, Sc, Zr, and Rare Earth Additions

We are systematically studying the solubility of the substitution elements of Sc, Li and all rare-earth elements, in aluminum by first-principles calculations [12], leading to the following preliminary conclusions:

- The solubility of metastable $\text{L1}_2 \text{Al}_3\text{Li}$ was calculated and is in good agreement with experimental results.
- The calculated solubility of RE decreases significantly as the RE atomic number increases.
- The vibration entropy makes a significant contribution to the solubility of RE in Al

We are also studying the nucleation and precipitation of core-shell ordered structures in Al-Sc-Zr-Er alloys by both experimental 3D APT and first principles calculations [13]. These results will reveal the possible mechanism of the nucleation and precipitation process of such structures during aging. We establish several theoretical models based on the experimental observations and bulk thermodynamics (both static total energies and vibrational free energies) and interfacial energies by first-principles calculations.

4. Publications from program

- [1] Krug ME, Werber A, Dunand DC, Seidman DN. *Acta Materialia* 2010;58:134.
- [2] Krug ME, Seidman DN, Dunand DC. To be submitted to *Acta Materialia* 2010.
- [3] Monachon C, Krug ME, Dunand DC, Seidman DN. *Acta Mater* 2010; Sumbitted.
- [4] Krug ME, Dunand DC, Seidman DN. *Applied Physics Letters* 2008;92.
- [5] Monachon C, Dunand DC, Seidman DN. *SMALL* 2010;Accepted Manuscript.
- [6] Krug ME, Dunand DC, Seidman DN. To be submitted to *Scripta Materialia* 2010.
- [7] Mohles V. *Phil. Mag. A* 2001;81:971.
- [8] Mao Z, Chen W, Seidman DN, Wolverton C. To be submitted to *Acta Materialia* 2010
- [9] Mao Z, Seidman DN, Wolverton C. To be submitted to *Acta Materialia* 2010
- [10] Krug ME, Dunand DC, Seidman DN. To be submitted to *Scripta Materialia* 2010.
- [11] Krug ME, Dunand DC, Seidman DN. In Progress 2011.
- [12] Mao Z, Seidman DN, Wolverton C. To be submitted to *Scripta Materialia* 2011
- [13] Mao Z, Booth-Morrison C, Seidman DN, Wolverton C. To be submitted to *Scripta Mater.* 2011

The Closure Problem in Density-Based Modeling of Dislocation Dynamics

Anter EL-AZAB

400 Dirac Science Library, Department of Scientific Computing, Florida State University,
Tallahassee, FL 32306, E-mail address: aelazab@fsu.edu

Program Scope

This research is performed as a part of a project entitled “Statistical Mechanics Modeling of Mesoscale Deformation of Metals,” which aims to develop a statistical modeling framework of dislocation dynamics in crystals. The research focuses on modeling the statistical properties of dislocation ensembles and incorporating the resulting models into a kinetic description of dislocations. This approach is thus called “density-based modeling of dislocation dynamics.” In density-based models of dislocations, the space and time evolution of a dislocation population is described in terms of a set of kinetic equations, the completion of which requires dealing with a closure problem similar to that of classical kinetic theories of particle systems. Here, we tackle this problem by modeling the statistics of dynamical dislocation systems and associated internal elastic fields. We thus present the modeling results for the spatial statistics of dislocations, the statistics of dislocation velocity and resolved shear stress, and the temporal statistics of cross slip and short range reactions in deforming crystals. The statistics of the velocity and resolved shear stress are required for the development of a density-based dislocation mobility law for use in the kinetic equations. The spatial statistics is required for modeling the dislocation correlations, and the temporal statistics is needed for fixing the source terms in the kinetic equations for the dislocation density evolution. The method of dislocation dynamics simulation, along with the appropriate theoretical formalisms of statistics, has been used to conduct numerical simulation of all relevant statistical measures.

Recent Progress

Spatial Statistics of Dislocations—Modeling the spatial statistics and dislocation correlations has been performed using the mathematics of stochastic fiber process in conjunction with the method of dislocation dynamics simulation [1]. It has been found that, in Cu and Mo crystals, the radial dislocation correlation exhibits an oscillatory behavior before reaching an uncorrelated regime at several microns. It has been also found that the correlations of dislocations of the same Burgers vector is much higher (about an order of magnitude stronger) than the

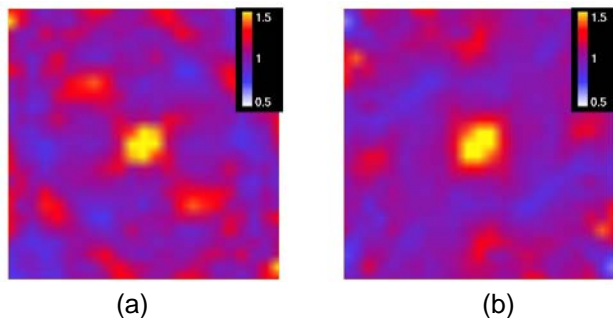


Figure 1. Anisotropy of 3D correlation in Cu at (a) 1% and (b) 1.3% strain. Linear dimension of the figures is 7.5 microns.

correlation between dislocations of different Burgers vectors. In addition, the 3D correlation of dislocations was found to be highly anisotropic in space. Figure 1 shows sample realization of the 3D correlation in a Cu single crystal at strains of 1% and 1.3%. It is clear that the correlation peaks along certain crystallographic directions and that the correlation values at the peaks are strongly dependent on the strain.

The anisotropic and long-range nature of the dislocation correlation poses a challenge in solving the kinetic equations for the density evolution of dislocations.

Temporal Statistics of Cross Slip and Junction Reactions—Cross slip and junction reactions are important processes in the deformation of FCC crystals because they are directly related to hardening and dislocation density increase. A time series analysis has been used to model the temporal statistics of cross slip and junction reactions in dislocation dynamics. The objective of this analysis is to model the coarse graining time scale of dislocation dynamics, and to demonstrate how this time can be used to determine the source terms associated with cross slip and junction reactions in the kinetic theory of dislocations. The analysis includes the collection of time series data for cross slip and junction reaction events using the method of dislocation dynamics simulation, stationarization of the time series and computing the correlation time [2].

Figure 2 (a) shows a typical time series (blue curve) for the junction density on slip system $[110](1\bar{1}1)$ in a Cu crystal deforming under $[100]$ loading at strain rate of 25s^{-1} . The red curve in Figure 2 (a) is the stationarized time series for junction reactions. Using the stationarized series, the correlation time has been computed for both cross slip and dislocation reactions (junction formation and annihilation reactions) for all slip systems in deforming copper. The results are summarized in Figure 2 (b).

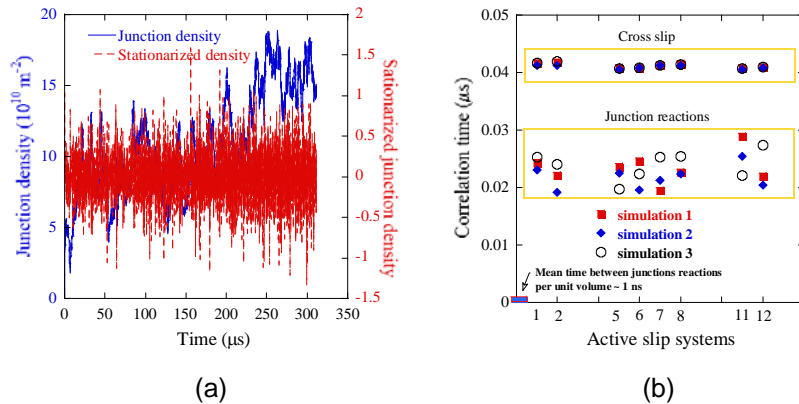


Figure 2. (a) A time series of the junction density for a slip system in a deforming Cu crystal. (b) Correlation time for cross slip and junction reactions for active slip systems in Cu deformed under $[100]$ type loading.

It has been found that, the cross slip correlation time is larger than the junction reaction correlation time, and that the latter is approximately the same as the correlation time for dislocation annihilation reactions. The coarse graining time scale, which is a fundamental characteristic time of dislocation dynamics, is thus taken to be the cross slip correlation time. This time scale was then used to perform time-averaging of the cross slip and junction reaction rates and compute the corresponding rate parameters in the kinetic equations.

Statistics of Internal Stress of Dislocations—A detailed study of the statistics of internal stress in deformed crystals has been completed. The ultimate objective of this study is to obtain

statistically averaged dislocation velocity law for use in the continuum (statistical) theory of dislocations. Such law can be obtained by connecting three levels of statistics: the statistical distribution of internal stress in the crystal (this includes the resolved shear stress), the resolved shear stress statistics at dislocation segments (a subset of crystal points), and the velocity statistics of dislocation. The mean velocity of the dislocations, which is directly connected to the resolved stress on segments, is now possible to relate to the mean resolved shear stress in the crystal by simply correlating the statistics

of the latter on segments and at the crystal level. This step has not been accomplished yet. The internal stress field at the crystal level, which is estimated from crystal mechanics computations, will thus link the kinetic equations to crystal mechanics via the stress-velocity law. A probability density function and pair correlation function of stress are important in this regard. A sample correlation result for the resolved shear stress is shown in Figure 3. It is clearly shown that the stress correlations are long ranged and that they are highly anisotropic. These properties are dictated by the correlation of the underlying dislocation structure. As part of the internal stress analysis, we were able to find the analytical connection between the stress correlation and the dislocation correlation. More results can be found in [3].

Statistics of Internal Elastic Fields—In an effort to compare the modeling results with experimental data on internal elastic field, we are performing a detailed analysis of the internal geometric fields of dynamical dislocation systems; namely, the lattice rotation, elastic strain and dislocation density tensor are being analyzed. This work is performed jointly with ORNL. The lattice rotation and elastic strain have been computed by solving a complex elastic boundary value problem of many-dislocation systems. The dislocation density tensor itself can be computed from these fields or from the dislocation structure directly. At this point, we use the method of dislocation dynamics simulation to obtain the internal elastic fields and the dislocation density tensor. In the near future, these same quantities will be obtained using the statistical theory of dislocations.

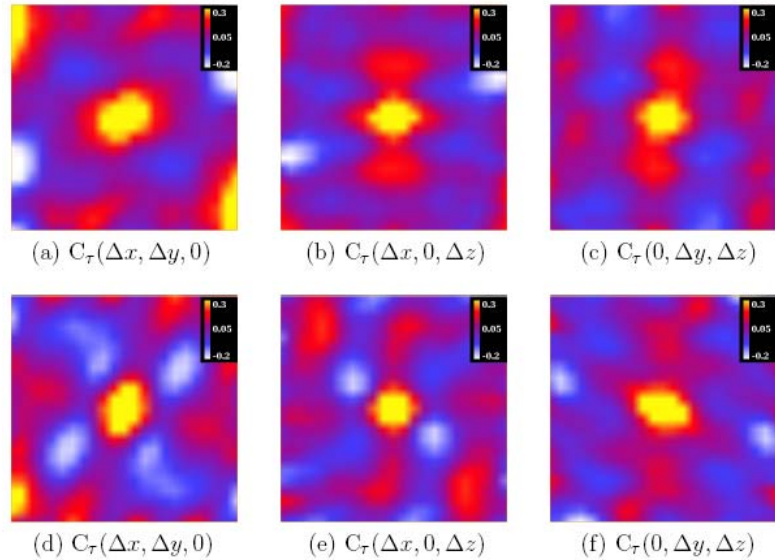


Figure 3. Sample result for the resolved shear stress correlation in 3D in a copper crystal. The top row shows the sections of the correlation at strain 0.25% and the bottom row shows the same at strain 1.13%.

Preliminary results show that, for a Cu, the probability density functions of all internal elastic fields are nearly symmetric, with zero mean values for the elastic strain and the dislocation density tensor components and non-trivial mean for the lattice rotation. The radial pair correlation function of the dislocation density tensor and lattice orientation showed slow decay followed by slight oscillatory behavior with correlation and anti-correlation regimes. Preliminary comparison of simulation results with X-ray measurements showed good agreement for the dislocation density tensor. The results are currently being refined.

Future Plans

The statistical analysis of dislocations and their internal fields, which has been performed under this project, enables us to close the kinetic equations governing the space and time evolution of dislocation systems in deforming crystals. This task will be accomplished by establishing closure models based on the statistical analysis discussed earlier. The dislocation kinetic equations can then be solved in conjunction with crystal mechanics to understand hardening and dislocation patterning in deforming crystals starting from the properties of dislocations and their interactions. We are now casting the dislocation correlations, density-based mobility law, and the rates of cross slip and junction reactions in analytical forms. We are also establishing a coupled finite-element scheme to solve the kinetic equations and crystal mechanics concurrently. Preliminary results will be obtained in the near future, and comparison with experimental data for uniform compression and indentation of single crystal copper are under planning.

Acknowledgment

This work was supported by the U.S. DOE Office of Basic Energy Sciences, Division of Materials Science and Engineering through contract number DE-FG02-08ER46494 at Florida State University (*Program Manager: Dr. John S. Vetrano*).

References

1. Jie Deng and Anter El-Azab, Mathematical and computational modeling of correlations in dislocation dynamics, *Modelling and Simulation in Materials Science and Engineering*, 17 (2009) 075010:1-31.
2. Jie Deng and Anter El-Azab, Temporal statistics and coarse graining of dislocation ensembles, *Philosophical Magazine*, 90 (2010) 3651–3678.
3. Anter El-Azab and Jie Deng, Statistics of internal stress of dynamical dislocation ensembles in deforming crystals, submitted to *Journal of the Mechanics and Physics of Solids*, 2010.

GRANT #DE-FG02-97ER45656

PARTICLE-INDUCED MODIFICATION of COMPLEX CERAMICS: Response of Materials to Extreme Conditions

Rodney C. Ewing^{1,2,3} (Principal Investigator: rodewing@umich.edu)
J. Lian⁴ (Co-Investigator); L.-M. Wang^{2,3} (Co-Investigator)

¹Geological Sciences; ²Materials Science & Engineering
³Nuclear Engineering & Radiological Sciences
University of Michigan

1100 N. University Avenue
Ann Arbor, Michigan 48109

⁴Mechanical, Aerospace & Nuclear Engineering
Rensselaer Polytechnic Institute
Troy, NY 12180

Program Scope:

We have established a new method for attaining extreme conditions in materials. The combination of pressure, temperature and ion beams has been recently achieved by injecting relativistic heavy projectiles through the diamond anvil of a diamond-anvil cell into the heated and pressurized sample. These projectiles exhibit exceptional properties because they deposit their kinetic energy within an exceedingly short interaction time (fs) into nanometer-sized sample volumes. This high density of energy transferred to the electrons along the ion path leads to intense electronic excitation, a confined plasma-like state that screens the Coulomb field and decreases rapidly away from the ion trajectory. Through electron-phonon coupling, the excited electrons transfer their energy to target atoms by exceeding the average binding energy (few eV/atom), which leads to local melting with an accompanying shock wave to the surrounding material. These collective processes, which occur over pico- to nano-second time frames, drive the local atomic structure far from equilibrium, resulting in rapid phase transition pathways through equilibrium and nonequilibrium states that trigger complex structural modifications within a cylindrical zone of diameter ~10 nm, the so-called ion track.

Combining such energy depositions simultaneously with extremes in pressure and temperature adds complexity and provides unique access to an extended pressure-temperature space, which is difficult to access by other means. This opens up a unique opportunity for a new physical regime that allows us to address exciting questions:

- *How do solids respond to the simultaneous exposure of several extremes, such as pressure, temperature, and very large energy deposition?*
- *Can these ion-matter interactions be used to create new phases that exist only at extreme pressures and temperatures?*

- *Can nano-scale manipulations by swift heavy ions be used to tune the thermodynamic properties of unstable high-pressure phases, which leads to their stabilization upon pressure release?*
- *How are pressure-temperature phase boundaries affected by high-energy irradiations?*

Recent Progress:

The principal scientific accomplishment of the past three years has been to develop the methodology for swift heavy ion (10s of GeV) irradiations in combination with high-pressure (< 100 GPa) experiments. This has involved, not only developing the irradiation techniques, but the extensive use of synchrotron sources (NSLS, CHESS, APS and ALS) to investigate *in situ* phase transformations at high pressures. We have perfected procedures that allow us to reclaim DAC samples for examination by HRTEM. We have also applied a combination of quantum mechanical calculations (DFT) and Monte Carlo simulations to understand the response of materials at the nanoscale (see for example, the recent paper in the *Journal of Materials Research*, 2010, that describes and simulates the internal structure of individual tracks created by swift heavy ions).

Because much of the recent work is entirely new, we have been invited to write review articles for the *Journal of Synchrotron Radiation* (2009) and *Nuclear Instruments and Methods in Physics Research B* (2010). In addition, important breakthroughs in the research program have appeared in *Physical Review Letters* (2008, 2010) and *Nature Materials* (2009). The first *PRL* paper (2008) identified the remarkable parallel between radiation-induced and pressure-induced disordering. Both processes are controlled by the energetics of the disordering process, and this was confirmed by DFT calculations. The second *PRL* paper (2010) described a new technique for determining the degree of disordering during *in situ* high-pressure experiments. Finally, the *Nature Materials* paper illustrated, for the first time, how one can use irradiation at high pressure to manipulate a material and stabilize previously unquenchable high-pressure phases.

Maik Lang received the Alvin Van Valkenburg Award, which recognizes a young scientist who has made seminal contributions to high-pressure science.

Future Plans:

The objective of this research program is to develop a fundamental understanding of materials behavior under extreme environments of intense irradiation fields, high temperatures and high pressures. We will investigate irradiation-induced phase transformations utilizing a wide spectrum of radiation sources and nano-scale analytical techniques. We will specifically focus on the effects of high-temperature and high-pressure on radiation-induced structural transformations: crystalline → crystalline; crystalline → amorphous; amorphous → amorphous. The simple model structures will be mainly oxides: SiO₂, ZrO₂, CeO₂, HfO₂, TiO₂, SnO₂, GeO₂, as well as AlPO₄ and their composites.

The new research builds on the foundation of experimental results that were established during the previous years; however, the next efforts will utilize new experimental and

computational techniques to establish a more fundamental understanding of the response in *simple, model systems* to radiation effects over a range of temperatures and pressures.

Although most of our previous work has focused on the order-disorder and amorphization of complex structure-types, in the future, we will focus on simple oxides with multiple structure types. The hallmark of our work will continue to be that of careful systematic studies of different structure-types combined with detailed characterization as a function of the type of damage and dose over a range of temperatures, pressures and fluences.

References: (Note, not all of the BES-supported papers are listed, due to limited space)

2008

- A. Abdelouas, S. Utsunomiya, T. Suzuki, B. Grambow, T. Advocat, F. Bart, and R.C. Ewing (2008) Effects of ionizing irradiation on hollandite structure-type: $\text{BaCs}_{0.28}\text{Al}_{1.46}\text{Fe}_{0.84}\text{Ti}_{5.72}\text{O}_{16}$. *American Mineralogist*, vol. 93, 241-247.
- F.X. Zhang, M. Lang, U. Becker, R.C. Ewing and J. Lian (2008) High pressure phase transitions and compressibilities of $\text{Er}_2\text{Zr}_2\text{O}_7$ and $\text{Ho}_2\text{Zr}_2\text{O}_7$. *Applied Physics Letters*, vol. 92, 011909 (3 pages).
- F.X. Zhang, J.W. Wang, J. Lian, M.K. Lang, U. Becker and R.C. Ewing (2008) Phase stability and pressure dependence of defect formation in $\text{Gd}_2\text{Ti}_2\text{O}_7$ and $\text{Gd}_2\text{Zr}_2\text{O}_7$ pyrochlore. *Physical Review Letters*, vol. 100(4), 045503, 4 pages.
- Maik Lang, Fuxiang Zhang, Jie Lian, Christina Trautmann, Reinhard Neumann, and R. C. Ewing (2008) Irradiation-induced stabilization of zircon (ZrSiO_4) at high pressure. *Earth and Planetary Science Letters*, vol. 269, 291-295.
- Z.J. Chen, H.Y. Xiao, Y.T. Zu, L.M. Wang, F. Gao, J. Lian and R.C. Ewing (2008) Structural and bonding properties of stannate pyrochlores: a density functional theory investigation. *Computational Materials Science*, vol. 42, 653-658.
- F.X. Zhang, M. Lang, R.C. Ewing, J. Lian, Z.W. Wang, J. Hu and L.A. Boatner (2008) Pressure-induced zircon-type to scheelite-type phase transition in YbPO_4 and LuPO_4 . *Journal of Solid State Chemistry*, 181, 2633-2638.
- F.X. Zhang, M. Lang, J.W. Wang, U. Becker and R.C. Ewing (2008) Structural phase transitions of cubic Gd_2O_3 at high pressures. *Physical Review B*, 78, 064114 (9 pages).

2009

- M. Lang, F.X Zhang, R.C. Ewing, J. Lian, C. Trautmann, and Z. Wang (2009) Structural modifications of $\text{GdZr}_{2-x}\text{Ti}_x\text{O}_7$ pyrochlore induced by swift heavy ions: Disorder and amorphization. *Journal of Materials Research*, 24, 1322-1334.
- Jie Lian, L.M. Wang, Kai Sun and Rodney C. Ewing (2009) In situ TEM of radiation effects in complex ceramics. *Microscopy Research and Techniques*, vol. 72, 165-181.
- F.X. Zhang, V. Pointeau, L.C. Shuller, D.M. Reaman, M. Lang, Zhenxian Liu, Jingzhu Hu, W.R. Panero, U. Becker, C. Poinssot and R.C. Ewing (2009) Structural transitions and electron transfer in coffinite, USiO_4 , at high pressure. *American Mineralogist*, vol. 94, 916-920.
- Jiaming Zhang, Maik Lang, Jie Lian, Jie Liu, Christina Trautmann, S. Della-Negra, Marcel Toulemonde and Rodney C. Ewing (2009) Liquid-like phase formation in $\text{Gd}_2\text{Zr}_2\text{O}_7$ by extremely ionizing irradiation. *Journal of Applied Physics*, vol. 105, 113510 (5 pages)

- Jie Lian, Jiaming Zhang, Fereydoon Namavar, Y.W. Zhang, F.Y. Lu, H. Haider, K. Garvin, W.J. Weber and Rodney C. Ewing (2009) Ion beam-induced amorphous-to-tetragonal phase transformation and grain growth of nanocrystalline zirconia. NanoTechnology, 20, 245303.
- Maik Lang, Jie Lian, Jiaming Zhang, Fuxiang Zhang, William J. Weber, Christina Trautmann, and Rodney C. Ewing (2009) Single-ion tracks in $Gd_2Zr_{2-x}Ti_xO_7$ pyrochlore irradiated with swift heavy ions. Physical Review B, vol. 79, article number 224105.
- J. Lian, V. Pointeau, J.M. Zhang, F.X. Zhang, M.K. Lang, F.Y. Lu, and R.C. Ewing (2009) Response of synthetic coffinite to energetic ion beam irradiation. Journal of Nuclear Materials, vol. 393, 481-486.
- Jiaming Zhang, Jie Lian, Antonio F. Fuentes, Fuxiang Zhang, Maik Lang, Fengyuan Lu and Rodney C. Ewing (2009) Enhanced radiation resistance of nanocrystalline pyrochlore $Gd_2(Ti_{0.65}Zr_{0.35})_2O_7$. Applied Physics Letters, vol. 94, article number 243110 (3 pages).
- Fuxiang Zhang, Maik Lang, Rodney C. Ewing, Jie Lian and Zhongwu Wang (2009) High-pressure response of zirconia nanoparticles with an alumina shell. Journal of Physical Chemistry - C, vol. 113, 14658-14662.
- Maik Lang, Fuxiang Zhang, Jiaming Zhang, Jianwei Wang, Beatrice Schuster, Christina Trautmann, Reinhard Neumann, Udo Becker and Rodney C. Ewing (2009) Nanoscale manipulation of the properties of solids at high pressure with relativistic heavy ions. Nature Materials, vol. 8, 793-797, DOI: 10.1038/NMAT2528.
- Maik Lang, F.X. Zhang, Jie Lian, Christina Trautmann, Reinhard Neumann, and R.C. Ewing (2009) Combined high-pressure and heavy-ion irradiation: A novel approach. Journal of Synchrotron Radiation, vol. 16, 773-777.
- F.X. Zhang, J.W. Wang, M. Lang, J.M. Zhang and R.C. Ewing (2009) High-pressure phase transitions of $ScPO_4$ and YPO_4 . Physical Review B, vol. 80, 184114 (7 pages).

2010

- Maik Lang, Fuxiang Zhang, Jiaming Zhang, Jianwei Wang, Jie Lian, William J. Weber, Beatrice Schuster, Christina Trautmann, R. Neumann and Rodney C. Ewing (**in press**) Review of $A_2B_2O_7$ pyrochlore response to irradiation and pressure. Nuclear Instruments and Methods in Physics Research B. [Note, includes partial support from EFRC (DE-SC0001089)].
- F.X. Zhang, J. Lian, J.M. Zhang, K.J. Moreno, A.F. Fuentes, Zhongwu Wang, and R.C. Ewing (2010) Increased stability of nanocrystals of $Gd_2(Ti_{0.65}Zr_{0.35})_2O_7$ pyrochlore at high pressure. Journal of Alloys and Compounds, vol. 494 pp. 34-39.
- T.S. Livshits, A.A. Lizin, J. Zhang and R.C. Ewing (2010) Amorphization of REE-aluminate garnets by ion irradiation and decay of Cm-244 admixture. Geology of Ore Deposits. 52 267-278.
- J. Zhang, M. Lang, R.C. Ewing, R. Devanathan, W.J. Weber, M. Toulemonde (2010) Nanoscale phase-transitions under extreme conditions within an ion track. Journal of Materials Research, vol. 25, 1344-1351 [cover]. [Note, includes partial support from EFRC (DE-SC0001089)].
- F.X. Zhang, M. Lang, R.C. Ewing and Zhenxian Liu (2010) Pressure-induced disordering and anomalous lattice expansion in $La_2Zr_2O_7$ pyrochlore. Physical Review Letters, vol. 105, 015503.
- Ming Zhang, Ekhard K.H. Salje and Rodney C. Ewing (**in press**) OH species, U ions and CO/CO_2 in thermally annealed metamict zircon ($ZrSiO_4$). American Mineralogist.
- H.Y. Xiao, F.X. Zhang, Fei Gao, M. Lang, Rodney C Ewing, W.J. Weber (**in press**) Zirconate pyrochlores under high pressure. Physical Chemistry Chemical Physics.

DOE Award #: DE-FG02-07ER46437

Program Title: Stress-coupled Grain Boundary Migration

PI: Kevin J. Hemker

Department of Mechanical Engineering, Johns Hopkins University
3400 N. Charles St., Baltimore, MD 21218; hemker@jhu.edu

Report Date: August 27, 2010; period covered: August 15, 2007 – August 15, 2010

Program scope:

Stress-coupled grain boundary migration has recently been manifest in observations of stress-assisted room temperature grain growth in nanocrystalline metals. Of particular interest to this study are micro-tensile experiments involving nanocrystalline Al thin films that highlight the fact that the mechanical behavior of these films is not only different that bulk materials but dynamic as well. These observations of stress-assisted grain growth in these nanocrystalline thin films cannot be described by traditional grain growth driving forces and appears to be a direct experimental observation of stress-coupled grain boundary motion. In additional to providing a unique avenue for studying stress-coupled boundary motion, the experiments to be conducted in this study will help lay the foundation for understanding and modeling the dynamic mechanical response of nanocrystalline materials.

Observations of stress-assisted grain growth, accompanied by enhanced plasticity, also offer intriguing prospects for increased fracture toughness. Nanocrystalline metals are generally stronger but also much less ductile than their microcrystalline counterparts and fracture toughness is emerging as a key consideration in their use. In situ TEM observations of our nanocrystalline Al thin films have revealed that grain growth occurs predominantly at crack tips and appears to be highly effective at crack-tip blunting. If properly understood and exploited, stress-assisted grain growth, at crack tips where stress concentrations are highest, may naturally lead to crack tip blunting and increased fracture toughness. Thus, the motivation for the proposed work is actually three-fold: (i) to experimentally characterize stress-coupled boundary migration, (ii) to provide a foundation for describing the dynamic nature of nanocrystalline metals, and (iii) to explore the possibility of increasing the fracture toughness of nanocrystalline materials through self-selected grain growth and crack tip blunting.

Description of accomplishments:

We have written a perspective on mechanical annealing [1] and expanded our experimental studies to elucidate the fundamental mechanisms associated with stress-coupled grain boundary migration as manifest in the observation of stress-assisted room temperature grain growth in nanocrystalline metals. Evidence in support of the recently proposed theory of stress-coupled boundary migration, which although widely accepted for low-angle grain boundaries has been largely overlooked with regard to high-angle grain boundaries, has been forthcoming. In situ TEM observations of anomalously fast grain growth that precedes dislocation activity have been

linked to stress-coupled grain boundary motion [2]. The development of surface relief, terraces with dimensions of the grain size as shown in Fig. 1, attest to the presence of shear displacements that accompany grain growth [3]. Variations in grain growth associated with the deposition background pressures have been used to highlight the role of impurities in pinning grain boundaries and preventing grain growth [4]. Recent results from MEMS-inspired micro-tensile experiments, which incorporate geometric features (stress concentrators) to experimentally quantify the effect of stress state (deviatoric vs. hydrostatic) on grain growth, point to the importance of shear stresses in promoting grain growth [5].

One of the earliest reports of stress driven boundary migration was for the motion of low-angle tilt boundaries in hexagonal-close-packed (hcp) zinc. We are exploring the existence of stress-coupled GB migration in various materials and crystal structures. Nanocrystalline Pt thin films exhibit very high strengths, limited ductility and clear evidence of grain growth [6]. The fact that grain growth is realized in Pt at room temperature is especially important because 25°C represents a homologous temperature of 0.14 for Pt as compared to 0.32 for Al. Thus, the observation of grain growth in Pt confirms our previous finding that grain boundary migration is stress-coupled and not thermally driven. Vapor deposition of bcc metals as ductile, stress-free thin films has proven to be very challenging. Parallel studies involving vapor deposited Mg thin films have, however, provide preliminary evidence of grain growth in an hcp metal.

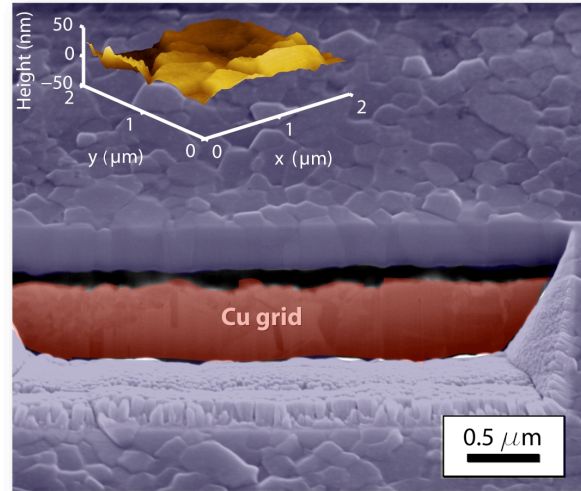


Fig. 1: SEM and AFM (insert) micrographs of a nanocrystalline-Al thin film that has undergone RT grain growth. The as-deposited film was smooth but the surface topography of the deformed sample is terraced and suggestive of stress-coupled grain boundary migration.

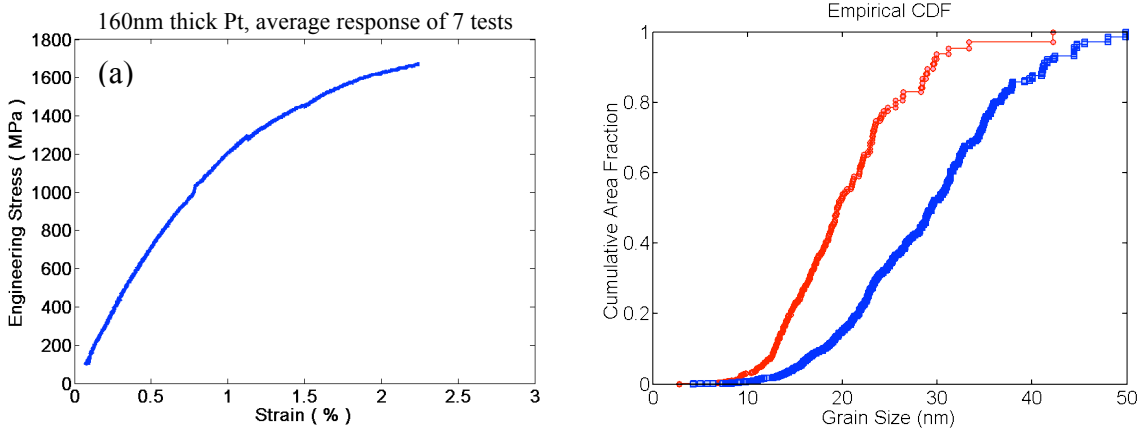


Fig. 2: (a) Mechanical behavior of 160nm thick Pt and (b) cumulative grain size distribution plot comparing as-deposited Pt to stressed Pt.

It is challenging to obtain a detailed understanding of stress coupled GB migration using nanocrystalline materials as they contain numerous overlapping grains of random orientation. Such a microstructure makes it difficult to accurately orient neighboring grains and track the motion of the boundary between them. We are collaborating with Minor and colleagues at NCEM to fabricate bi- and tri-crystalline films of Al and Au. The bi- and tri-crystalline films are polycrystalline and have columnar grains with a variety of grain boundary character but only two or three variants of crystallographic orientation. ‘Restricting’ the microstructure in this manner will greatly facilitate our ability to load the films in tension and detect specifically how different boundaries respond to the applied stress. This will require in situ mapping of grain orientations to determine and track GB characters in the films during the application of stress. One option that we are developing with Schuster and colleagues at the Army Research Laboratory is the use of SEM-based electron back-scattered detection (EBSD). A second option that we are pursuing with Legros and colleagues at CEMES Toulouse is the use of automated orientation detection and mapping methods now available for TEM. With the combination of these two techniques, we are now positioned to combine orientation mapping with mechanical testing and to make direct in situ observations relating applied stress to GB migration.

Planned activities for the coming year:

The main focus of the upcoming year is two fold. The first will be to complete the work on the Pt and Mg nanocrystalline thin films to provide insight on the influence of crystal structure on stress-coupled GB migration. The second will be to conduct experiments with the bi- and tri-crystalline films to explore the effect of grain boundary character on stress-coupled GB migration. These films have known, well-defined microstructures. Therefore, if these special films are loaded in tension, it should be possible to directly observe which boundaries (straight, curved, high/low angle misorientation, etc...) couple to the applied stress and move. The fabrication of thin film micro-tensile specimens is being conducted through collaborations with Professor Minor and his group at NCEM, who have demonstrated the ability to produce both Au and Al bi-crystalline films. Post mortem EBSD measurements and observations will allow us to identify and characterize the salient GB characteristics, but we will also conduct micro- and meso-scale in situ experiments by mechanically loading the films inside the electron microscope. Both SEM and TEM experiments are planned. The GB migration will be tracked using both visual observations from standard electron images as well as changes in grain/microstructural maps produced by orientation imaging microscopy such as electron backscattered detection (EBSD). These micro- and meso-scale observations will provide meaningful complements to the high-resolution in situ observations that are underway at NCEM.

List of papers related to this work:

1. KJ Hemker, WD Nix, Nanoscale Deformation: Seeing is believing, *Nature Materials*, **7** (2008) 97-98.
2. Marc Legros, D.S. Gianola, K.J. Hemker, In-situ observations of fast grain boundary motion in stressed nanocrystalline aluminum films, *Acta Materialia*, in press (2008).
3. DS Gianola, C Eberl, X Cheng, and KJ Hemker, Stress-Driven Surface Topography Evolution in Nanocrystalline Al Thin Films, *Advanced Materials*, **20** (2008) 303-308.

4. DS Gianola, BG Mendis, XM Cheng, KJ Hemker, “Grain size stabilization by impurities and effect on stress-coupled grain growth in nanocrystalline Al thin films”, *Materials Science and Engineering: A*, **483-484** (2008) 637-640.
5. TJ Rupert, DS Gianola, Y Gan, KJ Hemker, Experimental observations of stress-driven grain boundary migration, *Science*, **326** (2009) 1686-90.
6. JA Sharon, LC Su, FB Prinz, KJ Hemker, Stress Driven Grain Growth in Nanocrystalline Pt Thin Films, *Scripta Materialia*, (in press).

List of personnel supported by this project:

1. Professor Kevin J. Hemker, PI, partial support.
2. Mr. John A. Sharon, PhD. student, full support.
3. Dr. Marc Legros, visiting scientist, CEMES, Toulouse, France, 2 months support.
4. Mr. Timothy Rupert, M.S. student, no financial support.

Plasticity in ultra-fine grained materials
DE-FG02-07ER46398

Marisol Koslowski
School of Mechanical Engineering, Purdue University
585 Purdue Mall, West Lafayette, IN 47906
marisol@purdue.edu

Program Scope

Our goal is to develop a predictive continuum plasticity model to address the evolution of dislocations in confined geometries and their interaction with interfaces. This model constitutes an important step towards the integration of the *microstructural evolution* into continuum mechanical modeling for crystalline materials in general.

Recent Progress. Progress under the DE-FG02-07ER46398 grant can be summarized as follows:

1. We apply a phase field model of dislocations to model the deformation close to hard interfaces that act as a rigid constraint. This boundary condition for the dislocation field has been also widely used to model grain boundaries. The simulations show size effects in excellent agreement with experimental results and predict the formation of dislocation pile ups of opposite sign at the interfaces. Yield stress depends on the size of the sample and also on the density of obstacles that arrest the motion of dislocations. These findings were presented at the 2009 ASME meeting in Lake Buena Vista, FL., November 2009 and published in the Proceedings of ASME 2009.
2. We calculated the length scales parameters introduced in gradient theories of plasticity in closed form with phase-field dislocation based theory of plasticity. The similarity of the governing equations in both models for the evolution of plastic deformation of a constrained thin film makes it possible to identify parameters of the gradient plasticity theory with the dislocation based model. A one to one identification is not possible given that gradient plasticity does not account for individual dislocations. However, by comparing the mean plastic deformation across the film thickness we find that the length scale parameter introduced in the gradient plasticity theory depends on the geometry as well as materials constants. These findings resulted in a manuscript published in the *Journal of Mechanics and Physics of Solids* [4].

3. We developed a continuum crystal plasticity model that accounts for the effect of hard interfaces in the evolution of the dislocation density. The model integrates the dislocation density microstructure obtained from our dislocation dynamics model into a **continuum crystal plasticity theory** in a finite element code. Dislocations pile up in these interfaces leading

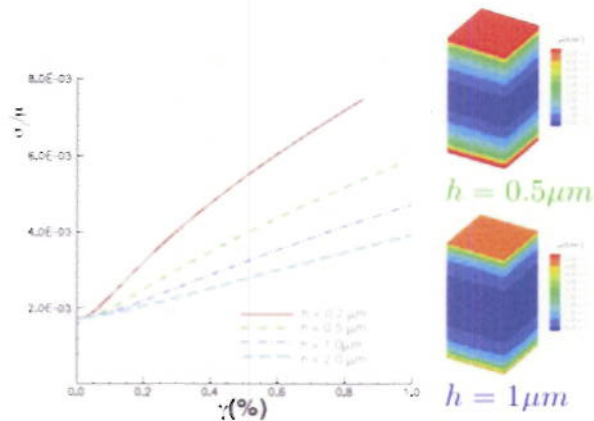


Figure 1: Simulated stress strain curve and dislocation density profiles of a Ni thin film [3].

to hardening in the mechanical response as the film thickness decreases. These findings resulted in a manuscript published in Modeling and Simulations in Materials Science and Engineering [3].

4. We have developed a new parallel C code denoted PFMM (Phase Field Micro Mechanics) to perform **large scale phase-field simulations of dislocations**. The PFMM code is able to simulate the evolution of dislocations in metallic FCC materials. The time evolution of the dislocation ensemble follows the Ginzburg-Landau equation and it is solved using an explicit time step algorithm. The non-local long-range dislocation-dislocation interactions are solved in Fourier space. In order to obtain the discrete Fourier transform of our data we use the FFTW 2.1.5¹. The FFTW 2.1.5 is a free, open source parallel C subroutine library that computes the discrete Fourier transform in one or more dimensions. We benchmarked our code for several grid sizes in several architectures using Purdue's clusters. Figure 2 shows the resulting total run time for grid sizes 64^3 to 512^3 using the different architectures. A detailed analysis of the performance of the code resulted in a manuscript accepted in Journal of High Performance Computer Applications [1].
5. We performed simulations of **polycrystals** to investigate the evolution of dislocations close to grain boundaries and the effect of grain boundaries as sources and sinks of dislocations. These findings were presented in USCCM in Columbus, Ohio in July 2009 and resulted in a manuscript currently under preparation.
6. **Grain boundary sliding** can be integrated seamlessly in the phase field approach. We have already performed simulations that account for grain boundary sliding. As dislocations are confined to the grain we obtain Hall Petch effect, see Figure 3(a). As the grains become smaller the system

¹ FFTW, <http://www.fftw.org/>

accommodates the strain by grain boundary sliding resulting in inverse Hall Petch, Figure 3(b). Figure 3(c) shows the yield stress as function of the grain size, filled circles correspond to polycrystals without grain boundary sliding and shows Hall-Petch effect. When grain boundary sliding is included in the simulations we obtain a transition to inverse Hall-Petch behavior for grains under 8nm.

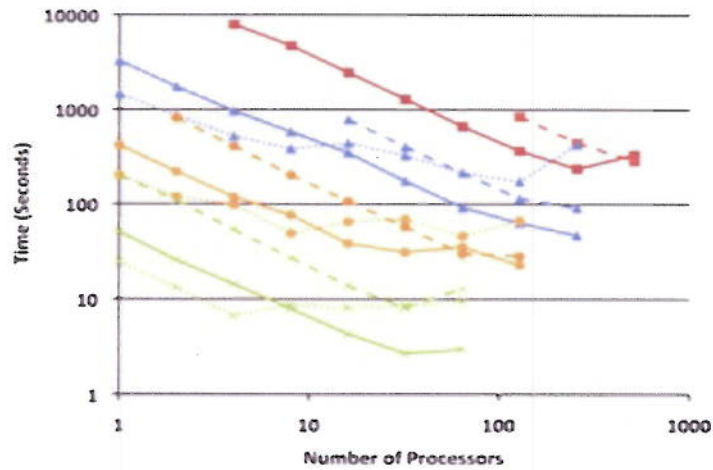


Figure 2: PFMM code performance analysis [1].

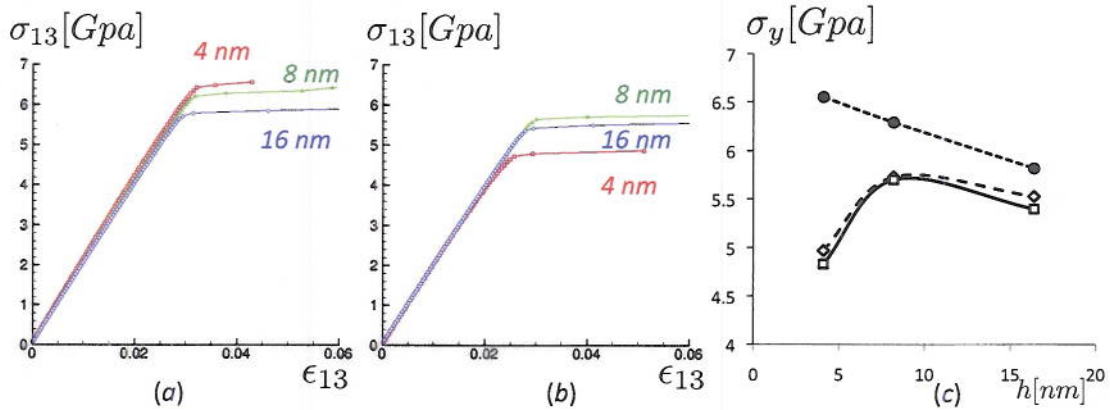


Figure 3: Simulated stress strain curves for a polycrystalline material (a) without grain boundary sliding and (b) with grain boundary sliding. (c) Yield stress as a function of the grain size, filled circles correspond to a polycrystal without grain boundary sliding and open symbols for a polycrystal with grain boundary sliding.

Future Plans

Reduction of grain size to nanometer range leads to an enhancement of several materials properties including yield and fracture strength and superior wear resistance. This reduction in grain size is responsible for new deformation mechanisms that are not present in coarse grained crystalline materials. One of these mechanisms is plastic strain recovery.

Even though, plastic deformation is not recoverable in coarse grained crystalline materials, very recent experiments in nanocrystalline aluminum, gold and nickel show plastic strain recovery after unloading. This surprising effect remains unexplained but is believed to be the result of the interaction between complex processes driven by the thermally activated motion of crystalline defects with different characteristic time and length scales, such as grain boundaries and dislocations. Numerical simulation of plastic strain recovery in nanocrystalline metals is a particularly challenging case of multiscale modeling that requires resolution of the small length scales involved while capturing the long time scales inherent to the recovery process. To address this challenge, we will develop a new approach to understand the mechanisms responsible for plastic strain recovery in nanocrystalline metals capturing both short length scales and long time scales. This new approach will incorporate thermally activated recovery mechanisms, into large-scale numerical simulations of deformation of nanocrystalline materials with a phase field theory of dislocations.

References of DOE sponsored research

[1] Abigail Hunter, Chin Le, Faisal Saied and Marisol Koslowski, *Large scale phase field dislocation dynamics simulations on high performance architectures*, Journal of High Performance Computer Applications, accepted, 2010.

[2] Marisol Koslowski, Effect of grain size distribution on plastic strain recovery, Physical Review B, accepted, 2010.

[3] Abigail Hunter, H. Kavuri and Marisol Koslowski, *A continuum plasticity model that accounts for hardening and size effects in thin films*, Modeling and Simulations in Materials Science and Engineering, **18**, 045012, 2010.

[4] A. Robison, L. Lei, S. Ramarapu and M. Koslowski, Interface effects in strained thin films. *Proceedings of the ASME 2009 International Mechanical Engineering Congress & Exposition, IMECE 2009, November 13-19, 2009, Lake Buena Vista, Florida, USA.*

[5] Abigail Hunter and Marisol Koslowski, *Direct calculation of length scales in gradient plasticity*, Journal of the Mechanics and Physics of Solids, **56** 3181-3190, 2009.

SISGR: Micro-mechanisms and Multiscale Modeling of Cyclic Plastic Deformation of Magnesium Single Crystals

Qizhen Li (PI)
Yanyao Jiang (Co-PI)
University of Nevada, Reno
1664 North Virginia Street, Mail Stop 388, Reno, NV 89557
QIZHENL@UNR.EDU

Program Scope or Definition

The primary goal of this project is to explore the fundamental deformation and failure mechanisms for the materials with a hexagonal close packed (HCP) crystal structure. Magnesium based materials (magnesium single crystal, pure polycrystalline magnesium, and some magnesium alloys) are utilized in our investigations. These materials have HCP crystal structure, excellent mechanical properties and broad structural applications in light-weight structural components. The research has three major objectives: (1) Exploration of the principal micro-mechanisms of cyclic deformation and the resulting fatigue failure, (2) Development of multiscale models for cyclic plasticity and fatigue to quantitatively describe the experimentally observed mechanical behavior of the material and predict the material properties and substructure evolution under cyclic loading and, (3) Study of the inherent and quantitative relationships among the material parameters that are used to describe the mechanical behaviors of the material at different length scales. The new knowledge resulted from the project will help understand the complex mechanical behavior of magnesium based materials under cyclic loading.

Recent Progress

We are making good progress with this project and the research is being performed as planned. For this period, there are nine publications in total as listed in the section "References of Publications", while seven of them have already been generated to date. Specifically, one journal paper is published, three journal papers are submitted and under review, three international conference abstracts are submitted and accepted, and two journal papers are under preparation. A conference symposium was proposed to TMS 2011 Annual Meeting & Exhibition, February 27 - March 3, 2011, San Diego, California. The symposium's title is "Deformation, Damage, and Fracture of Light Metals and Alloys", which is targeted to create scientific communications among researchers on deformation/failure mechanisms of magnesium, aluminum, and titanium. The symposium was accepted and received 32 abstracts. The following lists are some of the main research progress for magnesium single crystal, pure magnesium, AZ61A, and ZK60.

a. Magnesium single crystals

- The material is ordered and received. The specimen is designed and being machined for the testing under cyclic loading.
- Samples were prepared for compression tests. Static compression tests are done and dynamic compression tests under high strain rate (~1000/s) are planned to be conducted in late September or early October.

- For testing the small single crystal samples under cyclic loading, special gripping fixtures are designed and tested, and a right design of the gripping fixtures is identified.
- A vender, MTI instruments, was identified for the in-situ loading stage and its accessories in SEM. The purchasing order was processed and submitted to the vender and the parts are being manufactured. The estimated delivery time is December 2010.

b. Pure magnesium (In preparation for publishing)

- The material is obtained and prepared for different thermalmechanical processing.
- The samples are rolled under different temperatures and are prepared for microstructural observation using optical microscope. The rolled magnesium is machined into tensile testing samples. The research work allows the realization of different microstructure features, the understanding of microscopic deformation mechanisms, and the establishment of the relationship between microstructure and mechanical properties.

c. AZ61A magnesium alloy

- Microstructural analysis was performed on untested and tested AZ61A. The initial basal texture of extruded AZ61A strongly affects deformation mechanisms and microstructural features. When the strain amplitude is higher than 0.005 for a fatigue test, twinning-detwinning happens and residual twins change grain crystallographic orientations and weaken the texture. Figure 1(a), (b), and (c) show inverse pole figures for the untested and tested AZ61A samples. (More details in the Reference 4.)

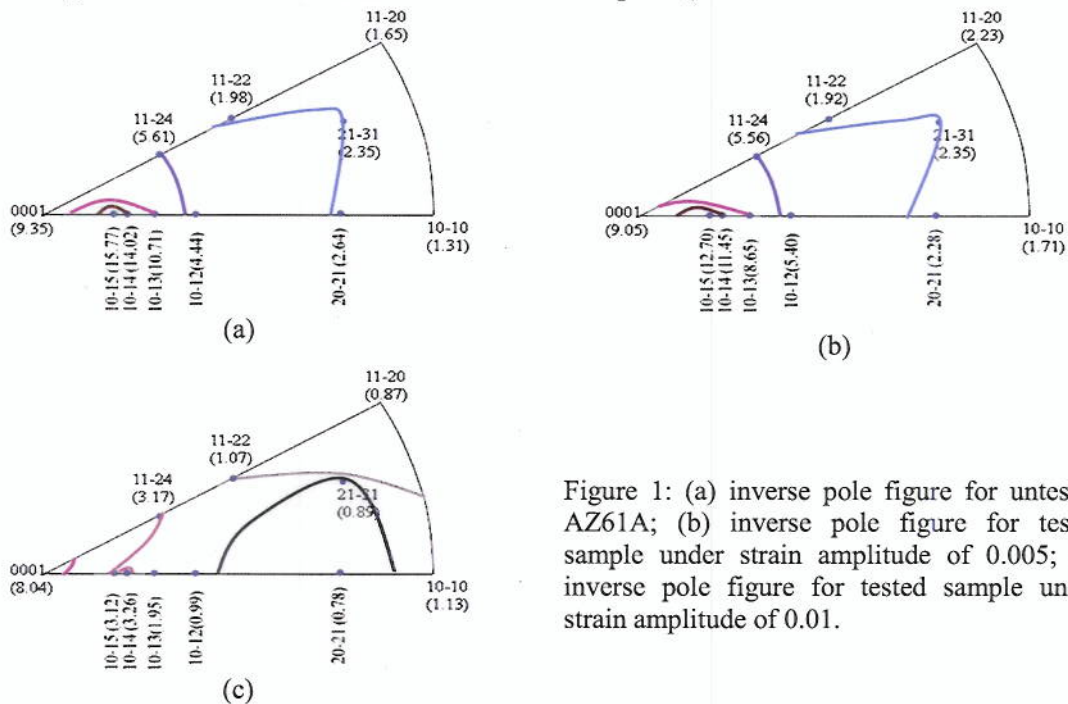


Figure 1: (a) inverse pole figure for untested AZ61A; (b) inverse pole figure for tested sample under strain amplitude of 0.005; (c) inverse pole figure for tested sample under strain amplitude of 0.01.

- Fatigue tests were conducted under the loading with static axial stress and fully reversed shear strain amplitude. A positive static axial stress reduces the fatigue life

but a negative static axial stress significantly enhances the fatigue life. Different theoretical models were utilized to interpret the testing data and a modified SWT (Smith, Watson, and Topper) criterion provides a good prediction of the fatigue life and cracking behavior for all loading paths. (More details in the Reference 3.)

- The cyclic deformation behavior was analyzed and optical microscopic observations were performed on the samples experienced different cyclic loadings to understand the deformation mechanisms and the asymmetric stress-strain hysteresis loops. (More details in the Reference 2.)
- Fatigue tests were performed on AZ61A under tension-compression cyclic loading with different strain ratios ($R_\epsilon = -\infty, -1, 0$) to explore its effect on deformation mechanisms. (In preparation for publishing, Reference 8)

d. ZK60 magnesium alloy (In preparation for publishing, Reference 9)

- Tension-compression cyclic testing was performed with strain amplitude ranging from 0.2% to 1.5%. A plateau was observed on the fatigue life versus strain amplitude curve as shown in Figure 2, indicating that deformation mechanisms change from dislocation slip to twinning-detwinning with increasing strain amplitude.

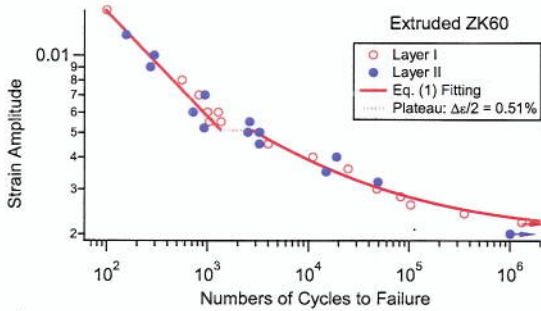


Figure 2: Strain-life curve for extruded ZK60. Equation (1) is $(\Delta\epsilon/2 - \epsilon_0)^5 N_f = C$.

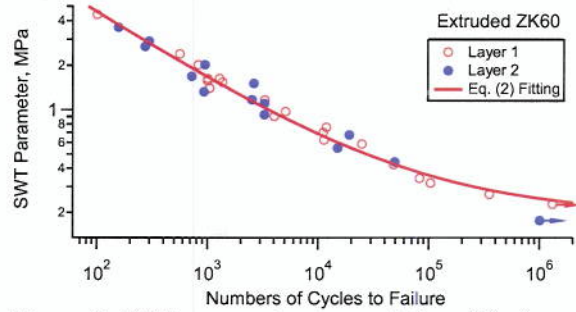


Figure 3: SWT parameter versus fatigue life for extruded ZK60.



300 μm

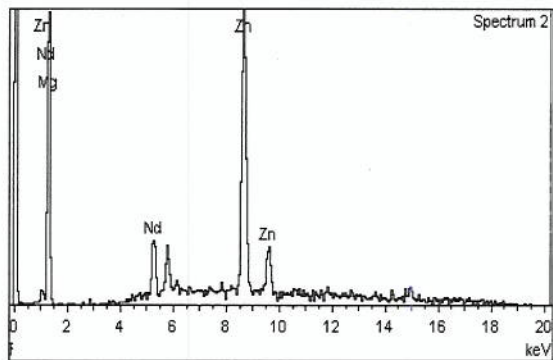


Figure 4: Fractographic observation of tested ZK60 sample and the EDS spectrum for the particle on the surface.

- SWT fatigue criterion was employed to fit the fatigue life data. The good fitting shown in Figure 3 indicates that SWT fatigue criterion based on critical plane method

relates the microstructure and deformation behavior of materials.

- Fractographic observations of tested samples were performed through scanning electron microscope. Some photos were shown in Figure 4 and there are particles on the fracture surface with Nd, which may affect the deformation mechanisms.

Future Plans

- Setting up the apparatus for performing in-situ SEM/AFM experiments under fatigue loading once the parts are received;
- Measurement of cyclic stress-strain response and fatigue for magnesium single crystals to obtain effects of crystal orientation and strain amplitude;
- Observation of fatigue crack initiation and cracking behavior;
- Microstructural and mechanical characterization of pure magnesium experienced various rolling processing and heat treatment;
- Microscopic observations of different samples using OM, SEM, TEM; Texture analysis and grain orientation characterization of different samples using XRD and EBSD;
- Development of mechanism-based constitutive model and atomic-scale model for cyclic deformation of HCP materials.

References of Publications

- [1] "Effect of Strain Amplitude on Tension-Compression Fatigue Behavior of Extruded Mg6Al1ZnA Magnesium Alloy," *Scripta Materialia*, 62, 778-781 (2010)
- [2] "An Experimental Study of Cyclic Deformation of Extruded AZ61A Magnesium Alloy," Submitted to *International Journal of Plasticity*, 2010
- [3] "Multiaxial Fatigue of Extruded AZ61A Magnesium Alloy," Submitted to *International Journal of Fatigue*, 2010
- [4] "Microstructure and Deformation Mechanism of Mg6Al1ZnA Alloy Experienced Tension-Compression Cyclic Loading," Submitted to *Scripta Materialia*, 2010
- [5] "Multiaxial Fatigue of Extruded AZ61A Magnesium Alloy", submitted to *International Conference on Fatigue Damage of Structural Materials VIII* for oral presentation, Hyannis, MA, Sept.19-24, 2010
- [6] "An Experimental Study on Cyclic Deformation and Fatigue of Extruded ZK60 Magnesium Alloy," conference abstract, Accepted to TMS 2011 annual meeting, San Diego, CA, Feb. 27-Mar. 3, 2011
- [7] "Effect of strain ratio on cyclic deformation and fatigue of extruded magnesium alloy AZ61A," conference abstract, Accepted to TMS 2011 annual meeting, San Diego, CA, Feb. 27-Mar. 3, 2011
- [8] "Effect of Strain Ratios on Deformation of Mg6Al1ZnA Magnesium Alloy under cyclic loading", a journal paper in preparation.
- [9] "Cyclic Deformation and Fatigue Behavior of ZK60 Magnesium Alloy", a journal paper in preparation.

Understanding microplasticity processes related to fatigue damage using high energy x-rays and a crystal-based modeling formulation

A New DOE BES Project

Matthew P. Miller¹, Paul R. Dawson¹ Ulrich Lienert² and James C. Williams³

¹Sibley School of Mechanical and Aerospace Engineering, Cornell University
194 Rhodes Hall, Ithaca, NY 14853
matthew.miller@cornell.edu

² Advanced Photon Source, Argonne National Laboratory

³Department of Materials Science and Engineering, The Ohio State University

Overview

The objectives of this multiyear project are:

- i the creation of a new quantitative understanding of fatigue damage accumulation and microcrack initiation processes in metallic polycrystals during cyclic plastic deformation,
- ii the creation of a new generation of cyclic deformation-based experimental capabilities at an important DOE facility, the Advanced Photon Source and
- iii the development of next generation simulation tools capable of replicating cyclic experimental loading conditions on virtual polycrystals to enable the interpretation of experimentally observed responses.

In spite of nearly a century's worth of research focus, fatigue continues to be one of the most challenging failure modes facing designers of metallic components subjected to repeated loads. While a general understanding exists of the manner in which fatigue cracks initiate from sites of concentrated damage such as persistent slip bands in ductile metals, an overarching theory - capable of predicting the nucleation of a fatigue crack has not emerged. It is qualitatively known that alloys which exhibit strain localization have lower resistance to crack initiation, but no detailed model exists that can account for this propensity in a fundamental way.

From an intellectual perspective, developing a comprehensive understanding of the microcrack initiation process associated with cyclic micro-plasticity easily ranks as one of materials engineering's "grand challenges". Attacking this problem requires the means to measure grain and subgrain loading conditions and loading-induced damage evolution as well as the modeling capability that accurately captures elastic and plastic behaviors at the grain scale. Typical cyclic plasticity and fatigue research has relied on post-mortem Transmission Electron Microscopy (TEM) studies and fractographs to hypothesize the microcrack initiation process by qualitatively connecting damage to cracking. Fatigue crack initiation is stochastic in the sense that cracks initiate at the "weakest link" in the stressed volume. TEM studies are excellent for characterizing the average damage state but cannot readily reveal the region of most severe damage (the weakest link). In this project, we will take advantage of the recent advances that have taken place in the area of synchrotron x-ray diffraction. High energy

x-rays are capable of interrogating large volumes of material *during* loading on a grain by grain basis. Since microcracks initiate on the grain scale, this creates an immediate advantage in studying fatigue.

Fatigue-life models continue to be dominated by empiricism, with very little quantitative connection to actual physical processes associated with fatigue crack initiation. Experimental methods capable of “measuring” the stress-strain response of individual crystals within a cyclically deforming polycrystal and of “observing” the microcrack initiation process have not previously been available. Detailed crystal-based simulations involving more than a handful of individual crystals or for more than a few hundred loading cycles of elastic-plastic deformation behavior have also only recently become feasible. To develop a new comprehensive understanding of microcrack initiation, we will employ some of the newest diffraction-based micromechanical characterization experiments. We also will develop capabilities that currently do not exist. In the process, we will work to lower the barriers to the use of diffraction based experiments in addressing real problems in materials science and engineering - moving the scientific discovery from the x-ray science to the improved understanding of materials. The plan for this three year project is described below. We anticipate that the findings from this project will create the opportunity for extending this research beyond three years.

Plan

The overall goal of this multi-year project is the creation of a quantitative understanding of the microcrack initiation process in ductile metallic polycrystals. The main tool we will bring to bear on this century-old nemesis is a hybrid experimental/simulation framework consisting of synchrotron x-ray *in situ* loading experiments intimately coupled with a crystal scale, finite element-based “virtual” representation of the experiment. In collaboration with the Advanced Photon Source, we will also develop a new cyclic deformation *in situ* loading capability with real time data acquisition, a sophisticated data reduction methodology and a high fidelity data archiving framework as part of the project. The specific plans and deliverables are described below. Each proposed task can be classified as either **Scientific Discovery**, **Method Development** or the creation of **High Energy Diffraction Microscopy (HEDM)** capabilities.

Scientific Discovery

These are the fundamental tasks associated with advancements in materials science and mechanics that we anticipate as part of this project.

1. We will conduct monotonic and cyclic *in situ* deformation / x-ray diffraction experiments at the Advanced Photon Source beamline 1-ID-C. We will vary the specimen control mode and investigate the effects of macroscopic stress amplitudes and average stress applied to the specimens. The diffraction experiments - collectively defined as High Energy Diffraction Microscopy (HEDM) are described in several references [1–3]. Basically, we will measure lattice strains for individual grains within a deforming aggregate using detectors placed at several distances from the sample. At approximately 1 meter from the sample when using 50 keV x-rays, we are able to measure the lattice strains within individual crystals. Based upon our previous results, we expect a significant variation of stress state at the individual crystal scale. By placing the detector farther from the sample we are able to capture high resolution diffraction patterns from each diffraction spot for a particular grain. Using these images, regions within the crystal can be imaged with high reciprocal space resolution (0.01°). Due to the variation in crystal stress state we observe throughout the aggregate, we can think of the macroscale specimen as a single crystal “test bed”. Early in its life, we will interrogate the specimen cycle by cycle - holding the load near the maximum and minimum values to conduct the diffraction experiments. During later phases in the project, we will work to develop real time data acquisition.
2. Much of our recent research employs diffraction experiments intimately coupled with a crystal scale representation of the specimen[3, 4]. Instead of following the well trodden path of motivating constitutive

models with results *thrown over the wall* from an experimental program, our approach is to create a virtual diffractometer that operates in conjunction with the physical experiment to create understanding of a material system under thermomechanical deformation. Examining a few reflections from a single crystal is a straight-forward exercise. Tracking an aggregate of crystals *during* deformation takes a sophisticated model of the experiment. We have had significant success using our finite element representation in conjunction with the experimental data in the past. In this project, we will focus on cyclic deformation and fatigue. The polycrystal simulation framework will be built in a manner to replicate various degrees of freedom of the subgrain lattice misorientation and strength distributions that develop under deformation.

3. We will conduct post-mortem TEM experiments on our samples - possibly on the exact grains that we interrogate with x-rays. These experiments are important for two reasons. First, TEM is an incredibly powerful interrogation tool. TEM micrographs coupled with HEDM data - especially the high resolution data - have the potential to yield important discoveries. Second, TEM will enable us to bridge to the enormous amount of previous research done on cyclically deformed specimens.
4. We will determine the relative importance of stress contributions from various sources (applied tractions, intragrain misorientation distributions, ...) to peak intensity distributions by conducting parametric studies of the mechanical response of virtual polycrystals subjected to macroscopically homogeneous loading states (uniaxial and biaxial tension, plane strain extension, ...).
5. Using background from dislocation mechanics together with simulations of virtual polycrystals, we will examine the role of defect induced stress fluctuations on patterns of diffraction intensity.

Method Development

We will build off our current experimental and simulation capabilities but we will need to develop new techniques and methods to meet our goals.

1. We will make several upgrades to the *in situ* loading capabilities at beamline 1-IDC. Closed loop control will be developed to accommodate strain or load control. New specimen grips and a new load train configuration will be developed to enable cyclic loading.
2. The HEDM experiment as described in [2, 3] is based on centering the grain of interest on a rotational axis. This is a laborious process for many more than a handful of grains. We have experimented with several improvements on this method, ones that will enable larger numbers of grains to be interrogated simultaneously.
3. Due to the volume of data we will acquire during cyclic loading, we will develop new data acquisition, storage and archiving capabilities early in the project.
4. We will create a methodology to instantiate virtual polycrystals with prescribed intragrain substructures (misoriented domains and slip system strength distributions).
5. We will develop a virtual diffractometer to construct diffraction intensity distribution arising from the spatial variations in stress and lattice orientations within subject grains.

HEDM Development

These are tasks that will advance the suite of experimental methods available to users at beamline 1-IDC. This is a unique time to not only understand fatigue processes at a level never before possible but to also advance the user base at APS 1-ID, an important DOE facility.

1. A general rule on the project will be that as an experiment is initially implemented, we will immediately begin to evolve it from a “one time” measurement requiring “heroic” efforts on the parts of experienced x-ray scientists into a true *capability* - an experimental setup with the associated data acquisition and reduction software capable of being performed by a non-expert. Once the cyclic individual crystal experiments are perfected - along with the requisite data reduction methodologies - spatially resolved diffraction measurements are the next “big step” for HEDM.
2. Due to the large number of cycles that will be accumulated during the experiment compared to the uniaxial tension experiments that we typically conduct, a significant increase of data throughput at beamline 1-ID-C is necessary. This cyclic project presents an ideal application for real-time data reduction. Considering the cost of maintaining a facility like APS, beamtime is easily the most costly item we will use on this project. We will be conducting entirely unique experiments within this project. Having the ability to make decisions regarding the experiments in real time would enable us to optimize the use of our beamtime.
3. The data-intense nature of both the simulations and experiment create the need for a high fidelity data archiving capability. We will design a material archiving schema for the project similar to that described in [5].

Material

Instead of focusing on the fatigue behavior of a particular alloy perhaps with a significant technical importance, in this project we seek to develop fundamental understanding of the micromechanical behavior of classes of alloys. Many of the “classic” fatigue projects tested copper as a typical wavy slip or cell forming material with alloys of copper exhibiting planar slip, such as Cu-16at.%Al, employed for contrast. In addition to the plastic deformation character, the x-ray “signature” of the material is crucial to our experiments, however, and will ultimately dictate our material choice. In particular, large lattice (elastic) strains greatly improves our lattice strain signal to noise ratio and less x-ray attenuation enables larger samples. We also seek a relatively simple material metallurgically to begin the project with. OFHC copper would be ideal - especially with its historical significance - if its strength/stiffness were greater. Nevertheless, we try high purity copper but will also explore some relatively simple copper alloys with higher strength that can be processed to produce both cell forming and planar slip behavior. Our industrial collaborator, Pratt & Whitney - Rocketdyne, will supply the copper alloys for the project. As the project proceeds, we will move towards more practical materials such as a stainless steel.

References

- [1] L. Margulies, H.F. Poulsen T. Lorentzen, and T. Leffers. Strain tensor development in a single grain in the bulk of a polycrystal under loading. *Acta Materialia*, 50(7):1771–1779, 2002.
- [2] U. Lienert, M.C. Brandes, J.V. Bernier, J. Weiss, S.D. Shastri, M.J. Mills, and M.P. Miller. In situ single-grain peak profile measurements on ti-7al during tensile deformation. *Materials Science and Engineering: A*, 524(1-2):46 – 54, 2009.
- [3] C. Efstathiou, D.E. Boyce, J.-S. Park, U. Lienert, P.R. Dawson, and M.P. Miller. A method for measuring single-crystal elastic moduli using high-energy x-ray diffraction and a crystal-based finite element model. *Acta Materialia*, 58(17):5806 – 5819, 2010.
- [4] M.P. Miller, J.-S. Park, P.R. Dawson, and T.-S. Han. Measuring and modeling distributions of stress state in deforming polycrystals. *Acta Materialia*, 56:3827–3939, 2008.
- [5] Donald E. Boyce, Paul R. Dawson, and Matthew P. Miller. The design of a software environment for organizing, sharing, and archiving materials data. *Metallurgical and Materials Transactions A*, 40(10):2301, 2009.

Mechanisms and Modeling of High Output Shape Memory Alloys

Prof. Michael J. Mills and Prof. Peter M. Anderson

Department of Materials Science and Engineering
The Ohio State University
477 Watts Hall, 2041 College Road
Columbus, OH 43220
mills.108@osu.edu and anderson.1@osu.edu

1. Program Scope

Shape memory alloys (SMAs) have remarkable properties due to a stress-induced martensitic transformation that can be reversed upon unloading (pseudoelasticity) or upon heating (1-way shape memory). This behavior is documented in a variety of alloys and it has enabled a variety of applications from valves and actuators to surgical devices. Furthermore, the crystallography of the martensitic transformation and its orientation relationship with the ordered B2 matrix have been calculated and verified in a number of cases. Nevertheless, essential aspects of shape memory and pseudoelastic behavior remain poorly understood and hinder development. Principal among these is the accommodation of the large transformation strain by the matrix. Theoretically, accommodation is achieved either by plasticity in the matrix or by inducing other transformation variants. However, there has been no verification of these mechanisms even for the most common SMA system, NiTi, and no rules have been developed to predict the nature of plasticity in the accommodation process. This fundamental issue is technologically important since the service life of components is determined by the evolution of the microstructure and defect substructure during cyclic loading or loading/heating. As a consequence, predictive, microstructure-sensitive models for static and dynamic performance are lacking. This program melds innovative mechanical testing and characterization with analytic and novel computational modeling to develop new, fundamental insight into the shape memory behavior of NiTi-based alloys, with a focus on the extremely interesting, emerging ternary and quaternary systems NiTiPt, NiTiHf and NiTiPdHf that can have much higher transformation temperatures and larger recoverable strains than the binary counterpart.

2. Recent Progress

The first year of the program has focused on three principal activities: (a) detailed microstructure characterization, (b) development of sample preparation and microcrystal testing techniques and (c) development and initial validation of a microstructure-based finite-element modeling that extends the state-of-the-art with respect to accommodation mechanisms in these alloys.

2.1 Microstructure Characterization

It is well-established in binary NiTi alloys that the precipitation of the Ni₄Ti₃ phase can strongly influence shape memory response and minimize detrimental, permanent strain. Indeed, the composition and aging of binary NiTi must be carefully controlled in order to obtain optimal performance. It is presumed that the precipitates can enhance the

transformation and/or impede matrix plasticity. In the ternary and quaternary alloys, an enormous phase space of possible compositions and thermal treatments are possible. The tremendous potential of these systems will only be fully realized with careful microstructure-property studies. Based on the ground-breaking work of Noebe and co-workers at NASA Glenn Research Center, we have focused on several of the most attractive alloy compositions in terms of their load-biased actuation response. Detailed microstructure characterization has been conducted on the following compositions:

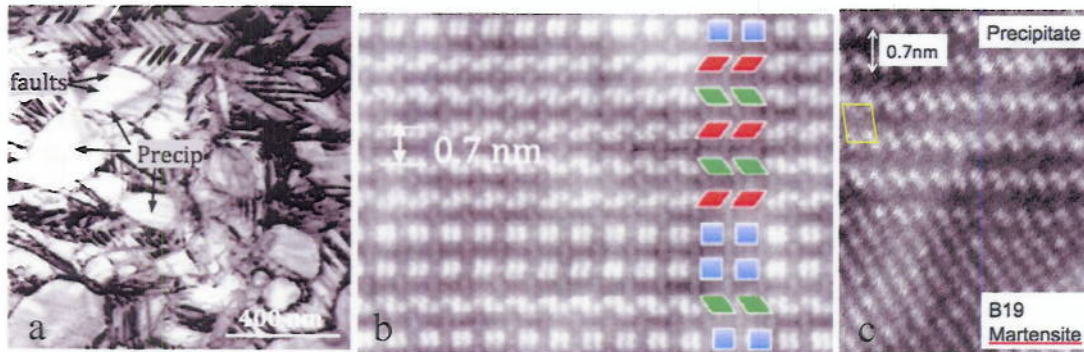


Fig. 1: (a) TEM image of microstructure of aged $\text{Ti}_{50}\text{Ni}_{30}\text{Pt}_{20}$ alloy, (b) HAADF of atomic structure of precipitate phase showing aperiodic stacking of Pt-rich layers on prior $(111)_{\text{B2}}$ planes, (Kovarik L et al., *Acta Materialia* 58 (2010), pp. 4660–4673), (c) interface region between precipitate and B19 martensite matrix.

$\text{Ti}_{50}\text{Ni}_{30}\text{Pt}_{20}$ (at.%), $\text{Ti}_{50}\text{Ni}_{30}\text{Hf}_{20}$ and $\text{Ti}_{45}\text{Ni}_{30}\text{Hf}_{20}\text{Pd}_5$. The shape memory and pseudoelastic response of these alloys are strongly affected by aging above 400°C . The austenite finish temperature for the ternary Hf alloy can approach 200°C after aging, and that for the ternary Pt alloy is nearly 300°C – both far above the near-ambient transformation temperatures in binary alloys. Aging produces a significant volume fraction of fine precipitates which are distinctly different from the conventional Ni_4Ti_3 phase. Progress on the nature of these precipitates (Fig. 1a) has only been made recently through a combination of electron diffraction, high angle annular dark field (HAADF) imaging and electronic structure calculations exploring low enthalpy structural states. In the ternary Pt alloy, the structure of the precipitates are truly remarkable (Fig. 1b). They are closely related to the high temperature cubic B2 phase, but have a unique structure due to their non-periodic character along the $[111]_{\text{B2}}$ which results from ordering of the Pt atoms combined with local relaxations. Initial investigation also indicates that this phase is present in the $\text{Ti}_{45}\text{Ni}_{30}\text{Hf}_{20}\text{Pd}_5$ alloy, as well as ternary Pd alloys. These results therefore significantly clarify the precipitation sequence in these alloys. In the next phase of microstructure work, we will be exploring the nature of the precipitate matrix interface (Fig. 1c), including assessment of coherence and possible strains associated with the interfaces.

2.2 Mechanical and Microcrystal Testing

A primary goal of the microcrystal studies is to determine the anisotropic plastic/transformation response of the alloys over a suitable range of temperature. Recent study of 5 mm pillars with $[110]$ orientation in binary NiTi have shown that the microcrystal geometry offers a unique method for studying deformation induced by isolated transformation zones. In preparation for microcrystal studies of the

pseudoelastic response of the $\text{Ti}_{45}\text{Ni}_{30}\text{Hf}_{20}\text{Pd}_5$ alloy, and shape memory response of the Pt and Hf ternary alloys, we have pursued refinement of sample preparation and testing of microcrystals of binary NiTi for several crystal orientations. Micropillar fabrication from homogeneous, polycrystalline sample has been conducted using a dual-beam focused ion beam (FIB), and improvements have been made to the script responsible for the lathing operation. Electron backscattered diffraction analysis and high-resolution SEM images have been stitched and matched to allow for the identification of useful grain orientations. Additionally, improvements have been made to the image-stitching process, which should result in better agreement between image coordinates and microscope coordinates for targeting pillar locations in the FIB. Finally, strain rate jump testing has been explored as a sensitive means to differentiate between plasticity and transformation at various stages of pseudoelastic deformation.

2.3 Microstructure-Based FEM Modeling

A central goal of the modeling activity is to successfully capture the detailed interaction between the stress or temperature-induced phase transformation and crystal-based plasticity. An important outcome from this goal will be the ability to model the thermal-mechanical response of NiTi and ternary alloys over a range of length scales and geometries, including the pillar geometries discussed in the experimental section.

The proposed approach is to pursue two levels of analysis: *martensite scale modeling* and *continuum scale modeling*. The former addresses the local interactions between discrete lattice correspondence *variants* or habit plane *plates* and the surrounding parent matrix. The scale is inherently subgranular. The latter addresses interaction between aggregates of martensite plates where the scale is larger, extending to the intergranular level. First-year activities in each of these areas is summarized:

2.3.1 Martensite scale modeling—plate formation: A cellular-automaton model has been developed in which the stress-interaction between competing plates is captured. In the current form, the model incorporates pairs of possible plates or variants in 2D or 3D. It captures the growth of plate-type morphologies in undercooled conditions, showing the extension of a primary plate along an invariant plane direction and the formation of secondary plates to relieve internal stress (Fig. 2a) or the formation of a two-variant morphology within a plate, consistent with a [110]

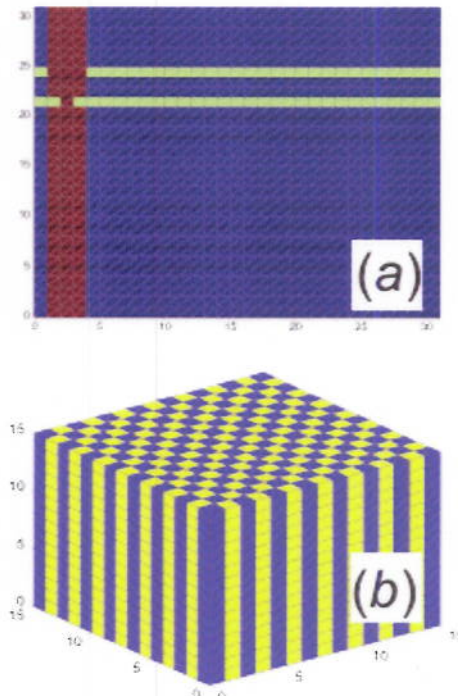


Fig. 2: Cellular automaton study of the interaction between (a) 2D martensite plates and (b) 3D martensite variants in an undercooled state.

invariant plane (Fig. 2b). This activity is viewed as an important step to inform the continuum scale modeling with a more accurate description of plate-plate and possibly plate-plasticity interaction.

2.3.2 Continuum scale modeling—NiTi experimental data: To prepare for modeling of high temperature ternary alloys, a state-of-the-art microstructural finite element model was calibrated and tested against an extensive data set for solutionized 55wt%Ni-Ti system. The calibration included incorporation of texture, DSC measurements, crystal plasticity data, a pseudoelastic response curve, and a thermal cycling response curve at small (50 MPa) bias stress. The resulting simulations capture several aspects of thermal cycling response over a range of bias stress (Fig. 3). However, the activity underscores the need for martensite scale modeling. In particular, the calibration requires modification to a phenomenological martensite plate interaction matrix frequently adopted in the literature. Further, it is difficult to quantitatively capture strain ratcheting during thermal cycling without a detailed understanding of transformation-plasticity interactions at the martensite plate scale. The outcome reinforces the need for the two-scale approach.

3. Papers

Several papers are in preparation regarding characterization, new pillar testing and modeling of in situ tension experiments.

4. Planned Activities for Next Year

The focus of the characterization work will be on confirming the nature of precipitates in the $Ti_{45}Ni_{30}Hf_{20}Pd_5$ alloy and determining those in the ternary Hf alloy as a function of aging at several temperatures (400-600°C). The significant advantage of the former system is that the matrix has a B2 crystal structure at room temperature so that the precipitate/matrix interfaces can be explored in detail at ambient conditions using HAADF. Micropillar testing will be conducted for the first time over a range of temperatures using our new variable temperature indenter system which is being purchased with supplemental DOE funding. This will enable several unique experiments, including elevated temperature pseudoelastic testing over a range of temperatures above the A_f temperature. The orientation dependence under uniaxial, load-biased conditions will also be measured for the first time. All of these experiments will be correlated with post-mortem STEM analysis of substructures developed during micropillar testing specimens will be prepared using FIB extraction of thin-foil sections. The mechanical testing and substructure analysis will be coupled with analytic and finite element simulations of the pillar response.

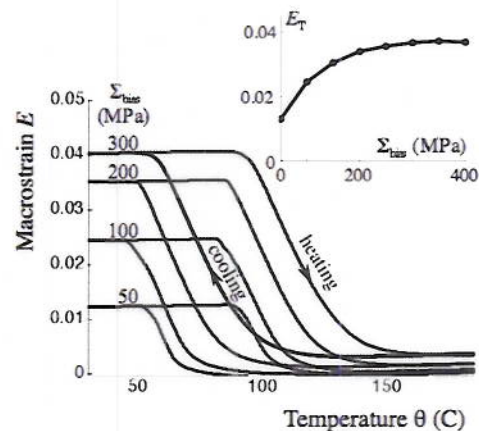


Fig. 3: Finite element simulation results for thermal cycling of solutionized 55wt%Ni-Ti at different axial bias stresses. The predicted transformation strain vs. bias stress (inset) captures the experimental trend (Manchiraju S et al., submitted to Acta Mater, Aug. 2010)

The Inverse Magnetoplastic Effect of Magnetic Shape-Memory Alloys

Peter Müllner

Department of Materials Science and Engineering, Boise State University, 1910 University Dr., Boise, ID 83725

petermullner@boisestate.edu

Program Scope

Inverse magnetoplasticity is the deformation-induced change of magnetization occurring in the martensitic phase of magnetic shape-memory alloys. Inverse magnetoplasticity is the inverse effect to magnetic-field-induced deformation (magnetoplasticity). The goal of this project is to investigate the underlying mechanisms of inverse magnetoplasticity, its potential, and limitations both, experimentally and theoretically. Project objectives cover the synthesis of high-quality single crystals, the control of twin microstructure, systematic magneto-mechanical experiments, and numerical modeling. The outcomes of this project are defect-based experimental and theoretical understanding of the micromechanisms of inverse magnetoplasticity, effects of thermo-magneto-mechanical training on twin-microstructure and magneto-mechanical properties, and knowledge about potential and limits of inverse magnetoplasticity of magnetic shape-memory alloys.

Recent Progress – Summary*

Twinning is the primary deformation mechanism in magnetic shape-memory alloys (MSMA). The effect of surface damage on the mechanical properties and twin structure of Ni-Mn-Ga single crystals was studied. Spark eroded samples were electropolished and characterized before and after each polishing treatment. Surface damage was then produced with spark erosion, ion implantation, shot blasting and abrasive wearing. Surface damage stabilizes a dense twin-microstructure and prevents twins from coarsening. The density of twins increases with increasing degree of deformation. Twinning stress and hardening rate increase with increasing surface damage and twin density.

Introduction**

The effects of composition on structure, thermal properties, and magnetic properties of Ni-Mn-Ga magnetic shape memory alloys (MSMAs) are very sensitive to subtle variations. The surface preparation procedures further impact the magneto-mechanical properties of these materials. However, data on the surface treatment and sample preparation methods is limited and of qualitative nature.

Thermo-mechanical and thermo-magnetic training increases the magnetic-field-induced strain (MFIS). Single twin domain specimen can be produced by applying simultaneously a magnetic field and a mechanical load. Variants change from a single variant state to a two variants state after thermo-mechanical training, and the variants rearrange during straining in different directions and when exposed to a rotating magnetic field. A simple two variant state can be obtained by repeated compressive deformation. This leads to a decrease of twinning stresses for a 10M martensite sample from 2.3 MPa directly after thermo-mechanical training (cooling from austenite to martensite with applied stress) to 1.1 MPa in a trained state and for a 14M martensite sample from 6.3 MPa to 2.9 MPa.

* Excerpts of two publications, Refs. [12, 14].

** References are listed in [12, 14].

The interaction of differently oriented twins leads to the formation of cracks and limits the lifetime in high-cycle dynamical actuation. While cracks nucleate very easily when twins are thick, microstructures with very thin twins are more resistant against crack nucleation. Therefore, the performance of MSMAs in dynamical loading is a compromise between large stroke and short lifetime for well trained, nearly single variant crystals, and short stroke and long lifetime for non-trained, self-accommodated crystals. Improvement of the performance may be achieved if the twin microstructure can be designed such that twins are thin but do not obstruct each other. Additionally, the twin microstructure must be stable over a large number of loading cycles.

In this work, it is shown that, polishing reduces the twinning stresses, especially in the high strain regions where the rough surface layer causes hardening. Polishing also leads to serrated flow. Surface damage caused by surface abrasion and glass ball blasting stabilizes the twin microstructure and increases the twinning stress. The larger the degree of surface damage is, the thinner the twins are. The twins are thin but extend over the entire sample and are, thus, mobile at moderate stress.

Experimental

The influence of the surface polishing treatments on twinning stress of Ni-Mn-Ga single crystals was studied on seven parallelepipeded samples, which were labeled A1 to A4 and B1 to B3, with faces parallel to $\{100\}_{\text{austenite}}$. These experiments are here referred to as test series I. The starting conditions were the freshly cut surface (spark eroded). The surface roughness and the damaged surface layer were then reduced by successive electropolishing treatments. In test series II, the starting condition was the most perfectly electropolished surface. The surface roughness and the damaged surface layer were then enhanced by exposing the samples to “successively heavier impact treatments”. Table 1 gives an overview on the surface conditions of samples A1, A3, and B2 and a reference to the figures representing results of deformation experiments, which were performed repeatedly in different directions in compression. Further details on crystal preparation, surface treatments, deformation experiments, and surface characterization are given in [12, 14].

Results

The stress-strain curves for the first deformation experiment as spark eroded and after each polishing treatment are given in Fig. 1 for test series I, for samples A3 (a) and B2 (b). For sample A3, a drastic decrease of twinning stress after the first polishing

treatment occurred. The stress-strain curves 2, 3, and 4 (treatments I2, I3, and I4, see Table 1) were very flat, and all twinning stresses were below 5 MPa. The stress-strain curve of sample B2, which was not electropolished had the same characteristics and twinning stress level as those of sample A3. The consecutive stress-strain tests of unpolished sample B2 (curves 1-4) showed a reduction of the twinning stresses from 7.4 MPa to 2.1 MPa after four stress-strain test cycles. From the second stress-strain test on, the twinning stresses decreased only slightly during the subsequent stress-strain experiment. After sample B2 was mechanically polished (treatments I5 and I6), the average twinning stress dropped further to 1.9 MPa (curves 5 and 6 in Fig. 2b). The twinning stress of B2 remained low over the entire strain range where twinning occurred. After twinning was saturated the twinning stress sharply increased. This is in contrast to the unpolished samples, for which the stress levels increased constantly with increasing strain, and transitioned slowly to the elastic region when twinning is saturated.

Samples A1 and A3 were tested again during test series II (Fig. 2) with average twinning stresses of 1.9 MPa and 3.7 MPa in the electropolished condition. After the 9 μm mechanical polish (II2), the twinning stresses increased to 3.5 MPa and 4.2 MPa.

Table 1: Summary of surface treatments for test series I and II and figures which present results.

Treatment	Details	Sample	Stress-strain results
I1	Spark eroded	A1	-
		A3	Fig. 1a, line 1
		B2	Fig. 1b, lines 1-4
I2	Electropolished once for 60 s	A1	-
		A3	Fig. 1a, line 2
I3	I2 plus second electropolish for additional 60 s	A1	-
		A3	Fig. 1a, line 3
I4	I3 plus third electropolish for additional 120 s	A1	-
		A3	Fig. 1a, line 4
I5	Mechanically polished with 9 μm and then 6 μm	B2	Fig. 1b, lines 5 & 6
II1	Electropolished for 240 s	A1	Fig. 2a, line 1
		A3	Fig. 2b, line 1
II2	Mechanically polished with 9 μm diamond particles	A1	Fig. 2a, line 2
		A3	Fig. 2b, line 2
II3	II2 plus mechanically grinded with 1200 grit SiC particles	A1	Fig. 2a, line 3
		A3	Fig. 2b, line 3
II4	II3 plus blasted with glass balls with diameters between 55 and 255 μm .	A1	Fig. 2a, line 4
		A3	Fig. 2b, line 4
II5	Chemically etched for 300 s.	A1	-
		A3	-

After grinding with 1200 grit SiC (II3), the twinning stresses increased to 4.8 MPa and 6.8 MPa with a smoothing of the stress-strain curve. Glass ball blasting (II4) increased the twinning stresses even further to 7.6 MPa and 8.4 MPa. At the same time, the twinning stress ranges increased with these surface treatments from 1.4 MPa to 7.6 MPa for sample A1 and from 4.5 MPa to 9.7 MPa for sample A3.

Fig. 3 shows micrographs taken after the stress-strain test cycles of test series II for sample A3 for the electropolished (a), mechanically polished (b), mechanically grinded (c), and glass ball blasted (d) surfaces. After each micrograph was taken, the next surface treatment was performed. While twins in the electropolished condition were rare and wide (1 mm and larger), finer twins appeared in the mechanically polished surfaces with a width of about 0.2 mm. The twins became even finer (<0.1 mm) and more homogenously distributed after glass ball blasting.

Discussion and Conclusions

Surface damage and residual stress localized in the surface layer hinder twin boundary motion. The stronger the damage in the surface layer is, the higher is the twinning stress and the larger are the slope of the stress-strain curve and, thus, the twinning stress range. In the samples with surfaces containing defects due to different surface treatments, twins are fine and the stress-strain curve is smooth due to a large number of densely dispersed pinning sites (Fig. 4a).

When the defective layer is removed, the twinning stress decreases and the twins coarsen in repeated compression experiments. Without defective surface layer, the twin boundaries are pinned mainly by the coarsely dispersed obstacles (defects) in the bulk of the sample (Fig. 4c) causing serrated flow. For an electropolished surface, the stress-strain curve is steeper and smoother due to an increased number of pinning sites (Fig. 4b). Treatments that cause surface damage prevent the coarsening of the twins.

Future Plans

The control over the twin microstructure allows studying effects of the twin thickness on inverse magnetoplasticity and on fatigue properties. We will perform deformation experiments within an orthogonal magnetic bias field. The bias field will restore the original shape upon unloading [6] allowing for repeated testing and, thus for performing a study of fatigue behavior. We have recently built an instrument with which we can carry out such experiments at a frequency of up to 500 Hz. More than 10^8 load cycles can be applied within one week. We will systematically study fatigue by varying twin thickness, displacement amplitude, and frequency. The new instrument also allows for measuring the change of the magnetization via a pick-up coil. We will systematically study inverse magnetoplasticity as a function of frequency, displacement amplitude, and twin thickness.

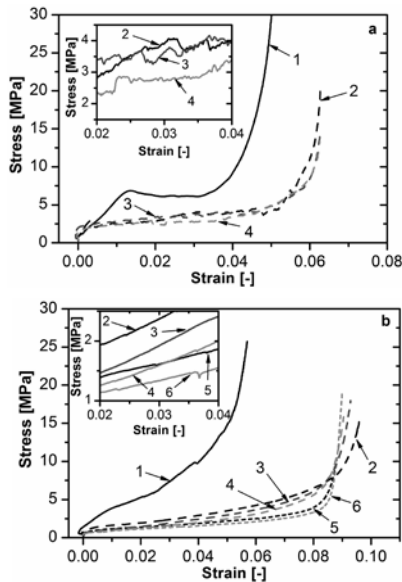


Fig. 1: Stress-strain curves of test series I for sample A3 (a) and sample B2 (b).

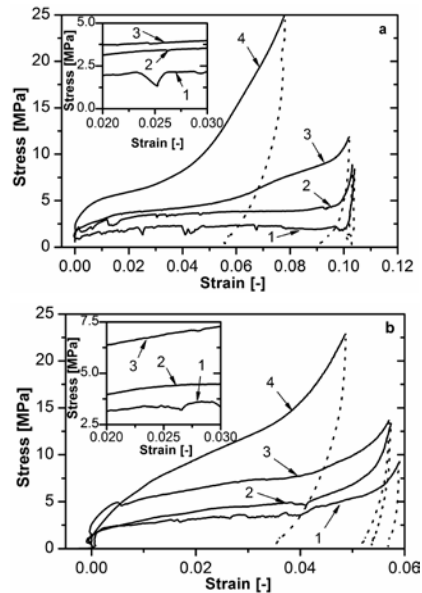


Fig. 2: Stress-strain curves of test series II for sample A1 (a) and sample B2 (b).

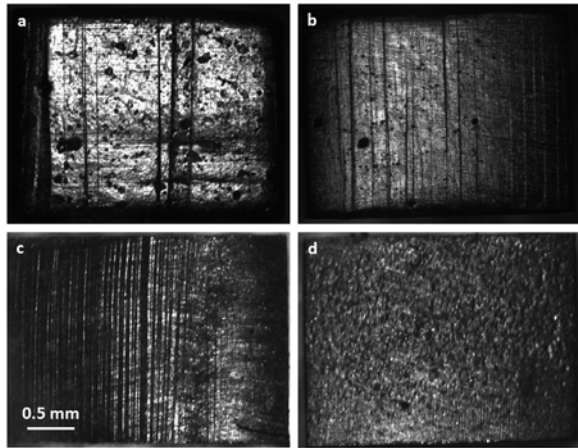


Fig. 3: Twin-micro structure after deformation following surface treatments II1 (a), II2 (b), II3 (c), and II4 (d).

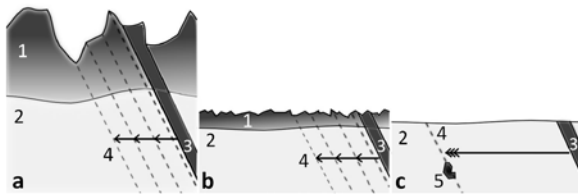


Fig. 4: Schematic of the motion of twin boundaries in samples with different surface structures.

Acknowledgments to recent progress

The PI acknowledges experimental work of M. Chmielus and C. Witherspoon at Boise State University and advice and experiments by W. Reimers, R. Schneider, C. Wimpory, and K. Rolfs at the Technical University Berlin, Germany, and at the Helmholtz Center for Materials and Energy Berlin, Germany.

Publications acknowledging support through this program in 2008-2010

- [1] P. Müllner and G. Kosterz, "Microstructure of magnetic shape-memory alloys: between magnetoelasticity and magnetoplasticity", in 'Advance Shape Memory Materials', ed. V. A. Chernenko, Mater. Sci. Forum 583 (2008) 43-65.
- [2] P. Müllner, A. S. Geleynse, D. R. Carpenter, M. S. Hagler, M. Chmielus, "Modeling magnetoplasticity and magnetoelasticity with disconnections and disclinations", MRS. Symp. Proc. 1050 (2008) 1050-BB02-01.
- [3] M. Chmielus, D. Carpenter, A. Geleynse, M. Hagler, R. Schneider, P. Müllner, "Numerical simulation of twin-twin interaction in magnetic shape-memory alloys", MRS. Symp. Proc. 1090 (2008) 1090-Z05-26.

- [4] M. Chmielus, V. A. Chernenko, W. B. Knowlton, G. Kosterz, P. Müllner, "Training, constraints, and high-cycle magneto-mechanical properties of Ni-Mn-Ga magnetic shape-memory alloys", Europ. Phys. J. S. T. 158 (2008) 79-85.
- [5] M. Chmielus, V. A. Chernenko, A. Hilger, G. Kosterz, P. Müllner, R. Schneider, "Magneto-mechanical properties and fracture of a mechanically constrained Ni-Mn-Ga single crystal after extended magnetic cycling", Proc. ICOMAT'08, Santa Fe June 30-July 4, 2008, TMS, Warrendale (2009) 683-688.
- [6] D. Carpenter, M. Chmielus, R. Schneider, P. Müllner, "Application of ferromagnetic shape memory alloys in power generation devices", ICOMAT'08, Santa Fe June 30-July 4, 2008, TMS, Warrendale (2009) 365-369.
- [7] P. Müllner, "Twin microstructure, line defects and twinning stress of magnetic shape-memory alloys", proc. ICOMAT'08, Santa Fe June 30-July 4, 2008, TMS, Warrendale (2009) 79-88.
- [8] V. A. Chernenko, K. Oikawa, M. Chmielus, S. Besseghini, E. Villa, F. Albertini, L. Righi, A. Paoluzi, P. Müllner, R. Kainuma, K. Ishida, "Properties of Co-alloyed Ni-Fe-Ga ferromagnetic shape memory alloys", J. Mater. Eng. Perf. 18, 2009, 548-553.
- [9] V. A. Chernenko, M. Chmielus, P. Müllner, "Large magnetic-field-induced strains in Ni-Mn-Ga non-modulated martensite", Appl. Phys. Lett. 95, 2009, 104103.
- [10] K. Rolfs, M. Chmielus, R. C. Wimpory, A. Mecklenburg, P. Müllner, R. Schneider, "Double twinning in Ni-Mn-Ga-Co", Acta Mater. 58 (2010) 2646-2651.
- [11] J. Guldbakke, M. Chmielus, K. Rolfs, R. Schneider, P. Müllner and A. Raatz, "Magnetic, mechanical, and fatigue properties of a $Ni_{45.4}Mn_{29.1}Ga_{21.6}Fe_{3.9}$ single crystal", Scripta Mater. 62 (2010) 875-878.
- [12] M. Chmielus, K. Rolfs, R. C. Wimpory, W. Reimers, P. Müllner, R. Schneider, "Effects of surface roughness and training on the twinning stress of Ni-Mn-Ga magnetic shape-memory alloys", Acta Mater. 10 (2010) 3952-3962.
- [13] P. Müllner and A. King, "Deformation of hierarchically twinned martensite", Acta Mater. 10 (2010) 5242-5261.
- [14] M. Chmielus, C. Witherspoon, K. Rolfs, W. Reimers, P. Müllner and R. Schneider, "Effects of surface damage on twinning stress and the stability of twin microstructures of magnetic shape-memory alloys", Acta Mater. submitted July 2010.

ABSTRACT

Program title

Roles of nanoclusters in shear banding and plastic deformation of bulk metallic glasses.

Principal Investigator

T.G. Nieh, tnieh@utk.edu, Department of Materials Science and Engineering, University of Tennessee, Knoxville, TN 37922

Program scope

The objective of this research is to establish a basic understanding of plastic deformation in metallic glasses at an atomistic scale, especially the role of nanocluster in shear band nucleation and propagation.

Recent progress

Localized shear is the dominant deformation mechanism at room temperature in metallic glasses, thereby we continue our focus on the shear band formation.

► Capture shear band propagation

With the help of a high-speed camera, rapid shear band propagation in a Zr-based metallic glass during compression was captured and images were analyzed using a digital image correlation (DIC) method. As shown in the figure below, the images indicate that localized shear occurs in a simultaneous fashion, i.e. shear band operates simultaneously across the entire shear plane, rather than in a progressive manner. This study settles the long-time debate as to whether the shear is simultaneous or progressive.

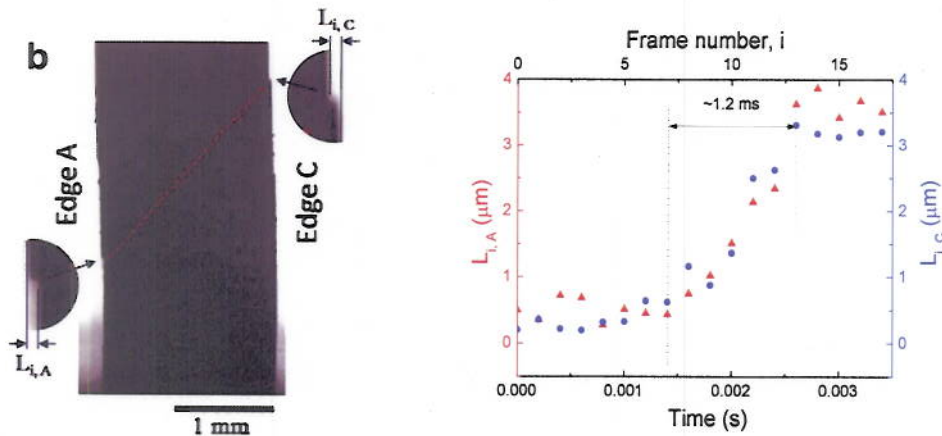
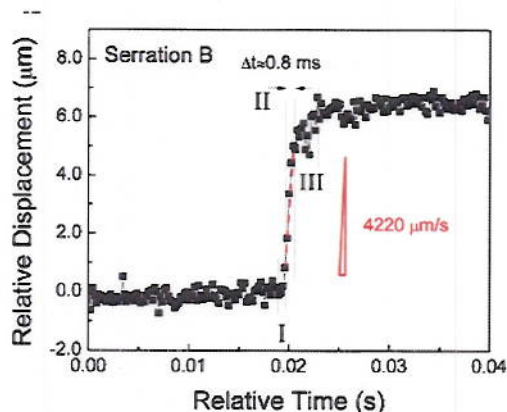


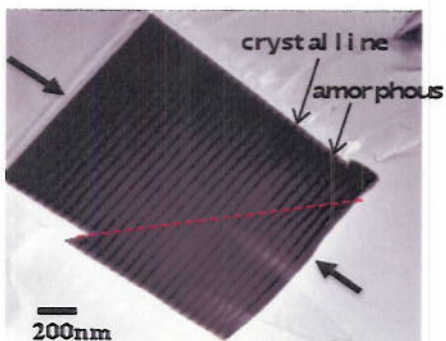
Figure: (left) Zr-BMG in-situ compression using a high-speed camera at 5000 fps. (right) Horizontal displacement at shear steps plotted as a function of time or frame number.

In using high-speed camera, shear band propagation was timely captured and measured to be about 4 mm/s, which corresponds to a high strain rate of about 10^5 s^{-1} , as shown in the following figure. In addition, the curve in the figure indicates that shear band propagation consists of three steps: acceleration, steady state, and deceleration.



► Shear-band nucleation

Kinetically, shear band formation consists of shear band nucleation and propagation. In view of the fact that a shear band can propagate at such a high rate (above), the rate controlling process for shear banding is most probably the nucleation, not propagation. We previously developed a mechanistic model for shear band formation. From the model, the size of a shear-band nucleus in metallic glasses is calculated to be 10^6 atoms, or a sphere of ~ 20 nm in diameter. This size is, in fact, consistent with the dimension of shear bands often observed under TEM, which is about 10-20 nm thick. Based upon these results, we predict that when the characteristic length scale of an amorphous phase is less than 10-20 nm, it would be impossible to initiate shear bands. Several recent experiments on nanolayers provided convincing supports of the prediction. For example, large tensile ductility (~ 5 -15%) was observed in a crystalline-amorphous nanolayer (35 nm Cu + 5.7nm amorphous Cu-Zr) by our group and Wang et al in LLNL. Additional evidence of shear-band nucleation suppression to achieve high plasticity was given by Donohue *et al* in Harvard, who studied the cold rolling of a 10/90 nm PdSi/Cu multilayer. To demonstrate the opposite end of the nucleation effect, we recently synthesized thin crystalline-thick amorphous nanolayer (5 nm Zr + 50nm amorphous Cu-Zr) and subsequently tested it. As expected, in this case, localized shear band formation dominates the deformation mode.



Future plane

The program was scheduled to end on August 14, 2010. It is now extended to August 14, 2011, without additional cost. In the original proposal, we proposed to conduct *in situ* straining experiments under neutron diffraction to explore the possibility to identify the

diffraction signature of shear transformation zone (STZ, the basic unit for plastic flow). However, due to facility malfunction it is now rescheduled to the end of this year. This effort will be collaborated with Dr. Xunli Wang in ORNL.

A list of publications of DOE sponsored research that have appeared in 2008-2010

1. C.L. Wang, M. Zhang, J.P. Chu, and T.G. Nieh, 'Structures and nanoindentation properties of nanocrystalline and amorphous Ta-W thin films,' *Scripta Mater.* 58(3) 95-198 (2008).
2. Y.C. Chang, J.C. Huang, Y.T. Cheng and C.J. Lee, X.H. Du, and T.G. Nieh, 'On the fragility and thermomechanical properties of Mg-Cu-Gd-(B) bulk metallic glasses,' *J. Appl. Phys.* 103, 103521, 2008.
3. Y.H. Lai, C.J. Lee, Y.T. Cheng, H.S. Chou, H.M. Chen, X.H. Du, C.I. Chang, J.C. Huang, J.S.C. Jang, S.R. Jian, and T.G. Nieh, 'Bulk and microscale compressive behavior of a Zr-based metallic glass,' *Scripta Mater.* 58, 890-893 (2008)
4. S.X. Song, J.S.C. Jang, and T.G. Nieh, 'Analyses of shear band emission in a Mg-based bulk metallic glass deformed at different nanoindentation rates,' *Intermetallics*, 16(5), 676-681 (2008).
5. L. Wang, S.X. Song, and T.G. Nieh, 'Assessing plastic shear resistance of bulk metallic glasses under nanoindentation', *Appl. Phys. Lett.* 92, 101925, 2008.
6. S.X. Song, H. Bei, J. Wadsworth, and T.G. Nieh, 'Flow serration in a Zr-based bulk metallic glass in compression at low strain rates,' *Intermetallics*. 16, 813-818, 2008.
7. K. Wang, T. Fujita, D. Pan, T.G. Nieh, A. Inoue, D.H. Kim, and M.W. Chen, 'Interface structure and properties of a brass-reinforced Ni₅₉Zr₂₀Ti₁₆Si₂Sn₃ bulk metallic glass composite', *Acta Mater.* 56(13), 3077-3087, 2008.
8. J. Wadsworth and T.G. Nieh, 'Bypassing shear band nucleation and ductilization of amorphous-crystalline nanolaminate in tension,' *Intermetallics* 16, 1156-1159, 2008.
9. H.S. Chou, J.C. Huang, L.W. Chang, and T.G. Nieh, 'Structural relaxation and nano-indentation response in Zr-Cu-Ti amorphous thin films,' *Appl. Phys. Lett.* 93, 191901 (2008).
10. S.X. Song, Y.H. Lai, J.C. Huang, and T.G. Nieh, 'Homogeneous deformation of Au-based metallic glass micro-pillars in compression at elevated temperatures,' *Appl. Phys Lett.* 94, 061911 (2009).
11. H.M. Chen, X.H. Du, J.C. Huang, J.S.C. Jang, and T.G. Nieh, 'Analysis of plastic strain and deformation mode of a Zr-based two-phase bulk metallic glass in compression,' *Intermetallics* 17, 330-335 (2009).
12. C.L. Wang, T. Mukai, and T.G. Nieh, 'Nanoindentation creep of fine-grained pure magnesium,' *J. Mater Res.* 24(5), 1615-1618 (2009).
13. H.M. Chen, S.X. Song, J.C. Huang, H.S. Chou, J.S.C. Jang, and T.G. Nieh, 'Flow serration and shear band propagation in bulk metallic glasses,' *Appl. Phys Lett.* 94, 141914 (2009)
14. S.X. Song and T.G. Nieh, 'Flow serration and shear-band viscosity during inhomogeneous deformation of a Zr-based bulk metallic glass,' *Intermetallics* 17, 762-767 (2009)
15. M.C. Liu, J.C. Huang, H.S. Chou, Y.H. Lai, C.J. Lee, and T.G. Nieh, 'A nano-scaled underlayer confinement approach in achieving extraordinarily plastic amorphous thin film,' *Scripta Mater.* 61, 840-843(2009)
16. C.J. Chen, J.C. Huang, Y.H. Lai, H.S. Chou, L.W. Chang, X.H. Du, J.P. Chu, and T.G. Nieh, 'On the amorphous and nanocrystalline Zr-Cu and Zr-Ti Co-sputtered thin films,' *J. Alloys Compounds*, 483, 337-340 (2009).
17. H.S. Chou, J.C. Huang, Y.H. Lai, L.W. Chang, X.H. Du, J.P. Chu, and T.G. Nieh, 'Amorphous and nanocrystalline sputtered Mg-Cu thin films,' *J. Alloys Compounds*, 483, 341-345 (2009).

18. Hirata, Y. Hirotsu, S. Kuboya, and T.G. Nieh, 'Local structural fluctuation in Pd-Ni-P bulk metallic glasses examined using nanobeam electron diffraction,' *J. Alloys Compounds*, 483, 64-69 (2009).
19. J.G. Wang, D.Q. Zhao, M.X. Pan, W.H. Wang, S.X. Song, and T.G. Nieh, 'Yielding and free volume of metallic glasses' *Scripta Mater* 62, 477-480, 2010.
20. Jason S.C. Jang, J.Y. Ciou, T.H. Li, J.C. Huang, and T.G. Nieh, 'Dispersion toughening of a Mg-based bulk metallic glass reinforced with porous Mo particles,' *Intermetallics* 18, 451-458, 2010.
21. J.S.C. Jang, S.R. Jian, D.J. Pan, Y.H. Wu, J.C. Huang, and T.G. Nieh, 'Thermal and mechanical characterizations of a Zr-based bulk metallic glass composite toughened by in-situ precipitated Ta-rich particles' *Intermetallics* 18, 560-564, 2010.
22. S.X. Song, J.S.C. Jang, J.C. Huang, and T.G. Nieh, 'Inhomogeneous to homogeneous transition in an Au-based metallic glass and its deformation maps,' *Intermetallics* 18, 702-709, 2010.
23. S.X. Song, X.-L. Wang, and T.G. Nieh, 'Capturing shear band propagation in a Zr-based metallic glass using a high speed camera' *Scripta Mater* 62(11) 847-850, 2010.
24. C. J. Lee, Y. H. Lai, J. C. Huang, X. H. Du, L. Wang, and T.G. Nieh, 'Strength variation and cast defect distribution in metallic glasses,' *Scripta Mater* 63, 105-108, 2010.
25. Ying Liu, Binghong Li, Jun Li, Lin He, Shengji Gao, and T.G. Nieh, 'Effect of titanium on the ductilization of Fe-B alloys with high boron content,' *Materials Letters* 64(11) 1299-1301, 2010.
26. J.S.C. Jang, W.J. Li, T.H. Li, S.R. Jian, Y.H. Wu, J.C. Huang, and T.G. Nieh, 'Thermoplastic forming ability of a Mg-base bulk metallic glass composites reinforced with porous Mo particles' *Intermetallics*. 18, 1964-1968, 2010.

Mechanical Properties of Materials with Nanometer Scale Microstructures

William D. Nix

nix@stanford.edu

Department of Materials Science and Engineering

Stanford University, Stanford CA 94305-4034

Program Scope

The rapid development of functional materials and devices with nanoscale and microscale features has brought about the need to understand and control the mechanical properties of materials at small length scales. Such important mechanical properties as the yield and fracture strength are strongly dependent on microstructure and are very different for materials in small dimensions compared to their bulk counterparts. The objective of this work is to devise techniques for studying the mechanical properties of materials at the nanoscale and to understand the fundamental defect processes that cause mechanical properties to be length-scale dependent. Such understanding and such small-scale testing techniques might be useful in characterizing the effects of radiation on structural materials, where small irradiated specimens are typically required.

Recent Progress

Much of our recent work has focused on determining the role of dislocation content (density) on the strength and plasticity of metals at the sub-micrometer scale. For this purpose we have been studying the compression deformation properties of sub-micron sized pillars of gold, grown epitaxially onto MgO substrates by sputter deposition. By growing gold films epitaxially onto (001) MgO substrates and making micropillars using focused ion beam milling, we are able to control the length of the gold micropillars precisely and also have a rigid support for the compression deformation experiment [1]. Figure 1 shows such a nanopillar ready for testing. The compression deformation experiments show that the pillars of this dimension are more than an order of magnitude stronger than bulk gold, an effect that is in keeping with other experiments on micro- and nanopillars. In our recent experiments we have developed a technique for studying the effects of pre-straining and annealing on the strength properties of these Au pillars and found that these effects are opposite to those found for bulk samples. Surprisingly, pre-straining leads to softening, not hardening as in the case of bulk metals, and annealing leads to hardening, not softening as in bulk metals. We have argued that these effects can be understood by considering the role of dislocations as carriers of plasticity as opposed to their role as obstacles for dislocation motion, as in the case of bulk metals.

In related work we are also studying the deformation properties of epitaxial gold microcrystals formed on sapphire substrates. These crystals are made by de-wetting a continuous film of gold by annealing at a very high temperature [2]. The sub-micrometer sized microcrystals are nearly dislocation free and have ideal strengths, much like the whiskers of Brenner in the 1950's. Subjecting these pristine microcrystals to very slight exposure to a focused ion beam of Ga ions causes a severe reduction in strength. Also, prestraining these microcrystals leads to a weakening effect, much like the work of Bei et al. [3]. These

experiments underscore the conclusion that at this dimensional scale plasticity is dislocation source-controlled and that FIB processing reduces the strength instead of causing strengthening, as some have assumed.

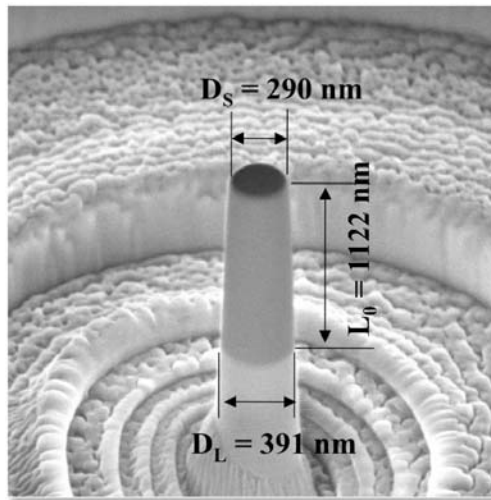


Figure 1. Nanopillar of [001] Au grown epitaxially onto a [001] MgO substrate.

Recent work has shown that plasticity in BCC micropillars might be quite different from that in FCC micropillars. Theoretical work has indicated that the ease with which screw dislocations cross-slip (and multiply) in BCC metals compared to FCC metals may be responsible for these differences [4]. In an effort to shed new light on this we have grown epitaxial films of BCC vanadium onto MgO substrates by vapor deposition and are making and testing micropillars using these films [5]. Vanadium has been chosen for this work because it has a sufficiently low atomic number to allow in situ TEM studies of pillar compression. We are planning to conduct in situ TEM studies on these vanadium pillars by making use of the Pico-Indenter in our lab.

Through our collaborations with Prof. Wei Cai at Stanford we are also conducting modeling studies of the behavior of dislocations in small crystal volumes. In recent work we have studied the stability of dislocation junctions and jogs in a free standing FCC thin film using 3-dimensional discrete dislocation dynamics simulations. We are making use of our recently developed technique for removing the singularities associated with the termination of dislocations at free surfaces in this work [6]. Due to the unconstrained motion of surface nodes and dislocation annihilation at the free surfaces, junctions and jogs in thin slabs are unstable except for some special (uncommon) conditions. If the film thickness is comparable to the mean spacing between dislocations, a significant portion of the dislocation network is terminated at the free surfaces, so that junctions and jogs can exist for only a finite time during deformation. Junction and jog-related dislocation sources are thus more limited as the film thickness decreases, with the consequence that there might be insufficient dislocation multiplication to balance dislocation annihilation at the free surfaces.

Future Plans

Our experiments on the nearly ideal strengths of gold microcrystals show a surprisingly strong size dependence, which we are trying to understand. Future efforts will be aimed at

determining whether shape defects grown into the microcrystals might be responsible for this dependence. We have also recently become aware of a delicate technique for removing the FIB damage and the implanted Ga ions in FIB processed metallic nanopillars. We plan to use this technique to alter the properties of FIB machined gold nanopillars in an effort to better understand the role of free surfaces in controlling strength and plasticity at this scale. We are also pursuing a new technique for mechanical testing of metallic nanowires, wherein a pedestal is first made on a substrate using focused ion beam machining and then a nanowire is placed on top of the pedestal and tested using the nanoindenter fitted with a flat ended diamond punch. The aim of this method is to be able to test chemically synthesized nanowires without the complications of gripping the ends of the nanowire. We are also extending previous work at Stanford on DD modeling of dislocations in cylinders in an effort to study both axial (without strain gradients) and torsional (with strain gradients) deformation at a small scale.

References

1. Seok-Woo Lee, Seung Min Han and William D. Nix, "Uniaxial compression of fcc Au nanopillars on an MgO substrate: The effects of prestraining and annealing," *Acta Materialia*, **57**, 4404–4415 (2009).
2. H. Sadan and W. D. Kaplan, *J Mater Sci*, **41**, 5099-5107 (2006).
3. H. Bei, S. Shim, G.M. Pharr and E.P. George, "Effects of pre-strain on the compressive stress-strain response of Mo-alloy single-crystal micropillars," *Acta Mat.*, **56**, 4762-4770 (2008).
4. C.R. Weinberger and W. Cai, "Surface-controlled dislocation multiplication in metal micropillars," *PNAS*, **105**, 14304-14307 (2008).
5. Seung Min Han, Tara Bozorg-Grayeli, James Groves and William D. Nix, "Size effects on strength and ductility of vanadium nanopillars," (accepted in *Scripta Materialia*)
6. C.R. Weinberger, S. Aubry, S-W Lee, W.D. Nix and W. Cai, "Modeling dislocations in a free standing thin film," *Modeling and Simulation in Materials Science and Engineering*, **17**, No.7, 075007 (2009).

Other DOE Sponsored Publications in 2008-2010

1. A.S. Budiman, S.M. Han, J.R. Greer, N. Tamura, J.R. Patel and W.D. Nix, "A search for evidence of strain gradient hardening in Au submicron pillars under uniaxial compression using synchrotron X-ray microdiffraction," *Acta Materialia*, **56**, 602–608 (2008).
2. Lucas A. Berla, Young-Chang Joo and William D. Nix, "A model for power law creep controlled hillock growth," *Materials Science and Engineering A.*, **488**, 594–600 (2008).
3. Jia Zhu, Hailin Peng, A.F. Marshall, D.M. Barnett, W.D. Nix and Yi Cui, "Formation of chiral branched nanowires by the Eshelby Twist," *Nature Nanotechnology*, **3**, No. 8, 477-481 (2008).
4. Kevin J. Hemker and William D. Nix, "Nanoscale deformation - Seeing is believing,"

- Nature Materials, **7**, 97-98 (2008).
5. G. Feng, A.S. Budiman, W.D. Nix, N. Tamura and J.R. Patel, "Indentation size effects in single crystal copper as revealed by synchrotron x-ray microdiffraction," *J. Applied Physics*, **104**, 043501 (2008).
 6. W.D. Nix, "Yielding and Strain Hardening in Metallic Thin Films on Substrates: an Edge Dislocation Climb Model," *Mathematics and Mechanics of Solids*, **14**, 207 (2009).
 7. A.S. Budiman, P.R. Besser, C.S. Hau-Riege, A. Marathe, Y.-C. Joo, N. Tamura, J.R. Patel and W.D. Nix, "Electromigration-Induced Plasticity: Texture Correlation and Implications for Reliability Assessment," *Journal of Electronic Materials*, **38**, No. 3, 379-391 (2009).
 8. William D. Nix, "Exploiting new opportunities in materials research by remembering and applying old lessons," *MRS Bulletin*, **34**, 82-91 (2009).
 9. Valeriy Sukharev, Armen Kteyan, Ehrenfried Zschech, and William D. Nix, "Microstructure Effect on EM-Induced Degradations in Dual Inlaid Copper Interconnects," *IEEE Transactions on Device and Materials Reliability*, **9**, No.1, 87-97 (2009).
 10. Wendelin J. Wright and W.D. Nix, "Storage and loss stiffnesses and moduli determined by dynamic nanoindentation," *Journal of Materials Research*, **24**, No.3, 863-871 (2009).
 11. Gang Feng, Shaoxing Qu, Yonggang Huang and William D. Nix, "A quantitative analysis for the stress field around an elastoplastic indentation/contact," *Journal of Materials Research*, **24**, No.3, 704-718 (2009).
 12. Seung Min Han, Mark A. Phillips and William D. Nix, "Study of strain softening behavior of Al–Al₃Sc multilayers using microcompression testing," *Acta Materialia*, **57**, 4473–4490 (2009).
 13. Seok-Woo Lee and William D. Nix, "Geometrical analysis of 3D dislocation dynamics simulations of FCC micro-pillar plasticity," *Materials Science and Engineering A*, **527**, 1903-1910 (2010).
 14. Lucas Berla, Aileen Allen, Seung Min Han and William Nix, "A Physically Based Model for Indenter Tip Shape Calibration for Nanoindentation," *Journal of Materials Research*, **24**, 735-745 (2010).
 15. William D. Nix and Seok-Woo Lee, "Micro-pillar plasticity controlled by dislocation nucleation at surfaces," (accepted in *Phil. Mag.* (2010)).

Understanding the Role of High-Angle Grain Boundaries in Failure of Thin Film Materials

(Grant No.: DE-FG02-07ER46355)

Principle Investigator: Dr. Yu Qiao

*Program of Materials Science and Engineering
Department of Structural Engineering
University of California, San Diego
9500 Gilman Dr. MC 0085
La Jolla, CA 92093-0085
Phone: 858-534-3388 · Email: yqiao@ucsd.edu*

1. Scope and Definition

In polycrystalline materials, grain boundary is an important obstacle to cleavage crack propagation. The important role of grain-sized cracks was reported frequently. In the classic linear elastic fracture mechanics (LEFM), the onset of catastrophic cleavage failure is associated with the break-through of pre-cracks across grain boundaries. That is, the effective fracture toughness of a brittle material is not directly determined by the fracture resistance of crystallographic planes (e.g. the surface free energy). Rather, the grain boundary toughness is the dominant factor.

Our previous study indicates that the fracture resistance offered by a high angle grain boundary to cleavage cracking is related to the penetration of crack front across the grain boundary, the crack trapping and pinning effects of persistence grain boundary islands (PGBI), the shearing and shear fracture of PGBI, the plastic bending and shearing of parallel ligaments, as well as crystallographic orientation. The average distance between adjacent break-through points, w , is the key parameter.

Compared with bulk materials, cleavage cracking in thin solid films of through-thickness grain structures is of difference characteristics, especially when the film thickness (t) is comparable with or smaller than the characteristic length scale of crack front transmission, w . Understanding their behaviors is of important relevance to MEMS/chips design, e.g. for the development of “unbreakable” electronics. The current project is focused on the crack-boundary interaction in free-standing bicrystal and polycrystalline silicon thin films.

2. Major Achievements

Through our experimental study, a new size effect was discovered: when the film thickness, t , is below 10 μm , as t decreases the grain boundary toughness is no longer a material constant. Rather, it would decrease rapidly with t , as shown in Fig.1.

The experiments were performed on specially designed silicon bicrystal thin films, with the film thickness ranging from 1 to 100 μm . Altogether four groups of bicrystal samples were tested. In each group, all the samples were harvested from the same bicrystal piece and, thus, had the same crystallographic orientation. The only difference among them was the film thickness. Samples in different groups had different crystallographic orientations.

In each sample, a precrack was produced normal to the grain boundary, with the crack tip arrested at the boundary. As a tensile load was applied, the crack would eventually overcome the boundary and the fracture resistance offered by the grain boundary was directly measured.

A detailed fractography analysis revealed that the size effect could be attributed to the non-scalable grain boundary behaviors at the microscopic length scale. As shown in Fig.2, in a thick film, as a cleavage crack propagates across a high-angle grain boundary, due to the twist misorientation of the cleavage planes across the boundary, the crack front must be geometrically necessarily broken down into a number of parallel terrains. The width of the terrains, w , is dominated by the competition between the grain boundary separation and the crack trapping/pining effect of PGBI. As a result, the overall fracture toughness is a material constant, governed by the averaged contributions of all break-through points.

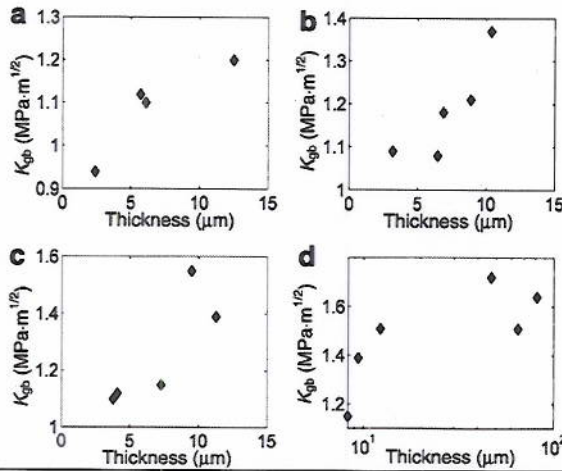


Fig.1 The measured grain boundary toughness, K_{gb} , as a function of the film thickness, t , of four groups of bicrystal samples. The samples in the same group have identical crystallographic orientation; the only difference among them is the film thickness. The crystallographic orientations of different groups are considerably different.

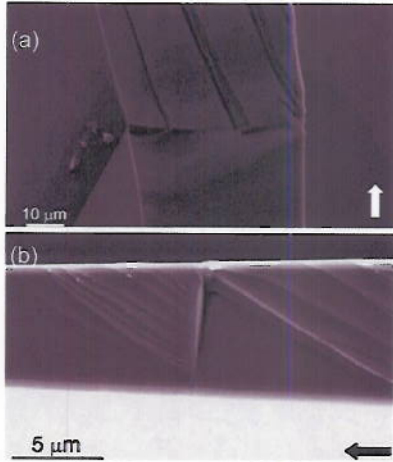


Fig.2 Cleavage cracking modes across high angle grain boundaries in (a) a thick film and (b) a thin film. The arrows indicate the crack propagation directions. In the thin film sample, there is only one break-through point along the grain boundary.

In a thin film, because of the constraints of the lateral surfaces, there would be only one break-through point along the crack front, and, thus, as t is reduced, the separated grain boundary area decreases, causing the observed size effect. Under this condition, conventional fracture theory would significantly over-predict the effective material toughness, which must be taken into consideration for materials selection and microstructural design.

Based on this understanding, we proposed a unique concept to toughen thin film structures by creating multiple grain layers. As shown in Fig.3, when a crack front encounters an array of grain boundaries, e.g. in a thin film containing a few grain layers, the cracking paths may be parallel in the grains, quite similar with what would happen at a wide grain boundary. Particularly, a number of break-through points would be formed (one in each

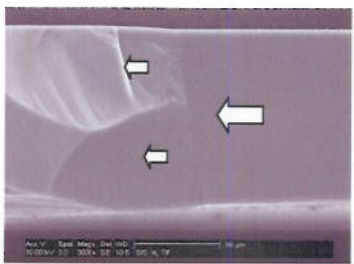


Fig.3 Parallel crack advance in a double grain layer.

individual grain). On the one hand, each break-through point would offer additional fracture resistance due to the crack trapping effect and the fracture work associated with the ligaments between parallel cleavage terrains. On the other hand, with a constant film thickness, if the number of break-through points is too large, the involved grain boundary area would be small, which tends to lower the overall resistance. Our preliminary analysis indicates that the optimum number of grain layers that results in the maximum fracture resistance is 3-4 for a variety of conditions. We are conducting a series of experiment to validate this concept.

It was also noticed that twin boundaries could offer important resistance to cleavage crack propagation. There are three possible crack transmission modes across a twin: smooth transmission, planar transmission (Fig.4), and sectioned transmission. The crystallographic misorientation across the first twin-matrix boundary is the key factor, the increasing of which causes more jerky crack front behaviors and a much higher effective fracture toughness. Another important factor is the film thickness. In a thinner film, the nonsingular components of crack-tip stress field are significant and the free surface effect is more pronounced. Thus, the crack-twin interaction tends to be smooth. As the film becomes thicker, the crack front would break through the twin boundary at multiple sites, resulting in the sectioned transmission mode.

With a certain orientations, as shown in Fig.5, secondary cracking can take place in the near-boundary zone, so that the crack front effectively “tunnels” through the grain boundary and the boundary toughness would be reduced to the lowest possible level. These special grain orientation patterns can be quite dangerous and must be avoided in thin film and microstructural design.

Our experimental observation shows that, as depicted in Fig.6(a). If the projected twist angle between two cleavage planes on the grain boundary plane is relatively small, and the tilt angle of the outbound plane is energetically favorable, as the inbound crack surface extends across the boundary into the adjacent grain, it may also bifurcates. The secondary cracking can either increase or decrease the overall grain boundary fracture resistance, associated with the shielding and weakening effects, respectively.

Figure 6(b) shows that, if the crack front penetration across the grain boundary is relatively difficult, the crack may only propagate along

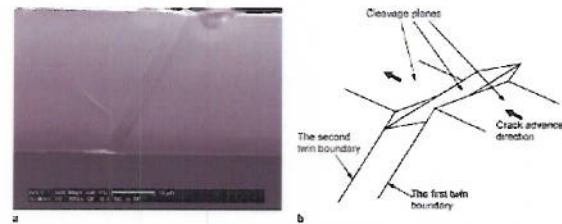


Fig.4 (a) A SEM image and (b) a schematic of cleavage cracking across a twin.

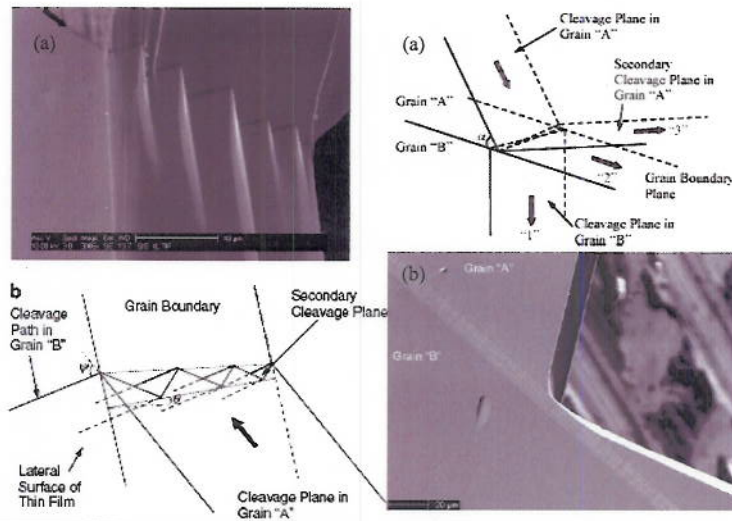


Fig.5 (a) A SEM image and (b) schematic of secondary cracking.

Fig.6 (a) Schematic of crack bifurcation. (b) crack reflection at grain boundary.

the outbound plane in the same grain, causing the abrupt change in crack propagation direction, as if the crack were “reflected” by the grain boundary.

3. Future Research Plan

Through the aforementioned investigation on bicrystal thin films and the previous study on large bicrystals, the fracture resistance of high-angle grain boundaries in brittle materials is now relatively adequately understood. We plan to extend our study to high-angle grain boundary behaviors under fatigue loadings in ductile materials, where dislocation activities are critical.

Note that, in ductile fracture the grain boundary behaviors are more dependent on plastic shearing and microvoiding, and the crystallographic characteristics are less important, similar to the role of grain boundaries in long fatigue crack growth, where the contribution of grain boundaries in crack-tip zone may be homogenized.

For the crystallographic growth of a short fatigue crack (SFC), however, the behavior of individual grain boundary must be taken into consideration. The boundary-SFC interaction involves the primary persistent slip band (PSB), the secondary PSB, the PSB across boundary, the dislocation reactions at grain boundary, and the microscopic crack front transmission mode.

The key questions to be answered include: (1) What are the fundamental mechanisms and processes associated with the primary and secondary PSB in SFC growth in grain boundary affected zone (GBAZ)? (2) What is the role of dislocation reactions at grain boundary in the crack front transmission process, and what is the role of the PSB ahead of the boundary? (3) Whether and how the SFC transmission is dominated by the crack front “branching,” and how does this affect the dislocation behaviors in the angular sectors at crack tip? (4) Is there any size effect at the microscopic level?

4. List of Publications in 2008-2010 Supported by the Project

1. Lu W, Chen J, Chakravarthula SS, Qiao Y. Resistance to cleavage cracking and subsequent shearing of high angle grain boundary. *Eng. Fract. Mech.* **77**, 768-775 (2010).
2. Chen J, Lu W, Qiao Y. Resistance of grain boundary array to cleavage cracking in free-standing thin film. *Mech. Mater.* **41**, 131-138 (2009)
3. Chen J, Qiao Y. Cleavage cracking across triple grain boundary junctions in free-standing silicon thin films. *J. Mater. Res.* **23**, 1647-1651 (2008).
4. Qiao Y, Chen J. Resistance of through-thickness grain boundaries to cleavage cracking in silicon thin films. *Scripta Mater.* **59**, 251-254 (2008).
5. Chen J, Qiao Y. Bifurcation and deviation of cleavage paths at through-thickness grain boundaries. *Metal. Mater. Trans. A* **39A**, 2040-2044 (2008).
6. Chen J, Qiao Y. Interaction of cleavage ridges with grain boundaries in polysilicon films. *Appl. Phys. A* **91**, 127-130 (2008).
7. Chen J, Lu W, Qiao Y. Cleavage cracking across twin boundaries in free-standing silicon thin films. *Appl. Phys. A* **91**, 663-666 (2008).
8. Qiao Y, Chen J, Kong X, Chakravarthula SS. Energy equilibrium of cleavage front transmission across a high-angle grain boundary in a free-standing silicon thin film. *Eng. Fract. Mech.* **75**, 2444-2452 (2008)
9. Chen J, Qiao Y. Characteristic length scale in cleavage cracking across high-angle grain boundary. *Comput. Mater. Sci.* **42**, 664-669 (2008).

DOE-BES
2010 Mechanical Behavior and Radiation Effects Contractors Meeting
September 28–October 01, 2010, Washington DC

Program Title:
**The Coupling Between Interfacial Charge and Mechanical Deformation at High
Temperatures in Ceramics**

PI:
Rishi Raj
Department of Mechanical Engineering
University of Colorado at Boulder
Boulder, CO 80309-0427
rishi.raj@colorado.edu

PROGRAM SCOPE

The overall scope of this research effort is to develop a scientific foundation for phenomena where externally applied electrical fields interact with stress-induced interfacial phenomena in ceramics at high temperature. The work adds a new dimension to topics of general interest to the ceramics community: creep, superplasticity, and sintering. Traditionally, the thermodynamic forces for these phenomena have been described by the stress-dependent chemical potential of the species at the grain boundaries. The new dimension is to include the effect of electrical fields by defining and exploring the electro-chemico-mechanical potential as the driving force. The kinetics of these processes is also likely to be influenced by electrical fields. Intrinsic fields within space charge layers adjacent to the grain boundaries can affect defect concentrations, and thereby the rate of mass transport. Applied fields and currents can produce Joule heating, especially at grain boundaries if they have a high electrical resistance. The higher local temperature can have a remarkable effect on grain boundary kinetics.

The objective of this BES program is to discover new phenomena related to the coupling between electrical fields and high temperature mechanical behavior and sintering, and then to develop fundamental, mechanistic understanding of these phenomena through modeling and further experiments that are targeted to test the predictions from fundamental concepts and models.

RECENT PROGRESS

Brief Background: The earliest work on the influence of electrical fields on mechanical behavior was carried out on NaCl crystals where it was shown that fields (several kVcm^{-1}) could move dislocations. The next phase, over the last ten years, was to show that electrical fields could produce a significant reduction in the flow stress of ceramics in superplastic deformation. Other developments, work published under this PI, include the theory and then, the measurement of interfacial electro-chemico-mechanical potential in zirconia, and a model for the influence of interfacial space charge on diffusion kinetics as related to diffusional creep.

Narrowing the Scope of this BES Program: The results summarized above, as well as the application oriented experiments, as in microwave sintering and spark-plasma-sintering, present a wide landscape of phenomena encompassing the interaction between electrical fields and high temperature properties and processing of ceramics. For the present, we have sought to focus our research on two basic issues: (a) is it possible that electrical fields can influence grain growth kinetics in ceramics, and (b) how may electrical fields influence the sintering process. The arguments for choosing these topics are (i) that grain growth is implicit in diffusional creep (and sintering) of polycrystalline ceramics, and (ii) that since sintering and superplastic deformation have the same mechanistic basis, the study of sintering would provide not only a basic understanding of superplasticity but could also elucidate the science underlying microwave and spark-plasma sintering behavior.

New Results:

We have recently obtained two new results: the first is related to grain growth, and the second to sintering. Both experiments were carried out on yttria stabilized zirconia (3YSZ).

Grain Growth Experiments: The flow stress in superplastic deformation depends on diffusion kinetics, and inversely on the third power of the grain size. In order to differentiate between these two aspects, experiments were carried out to measure grain growth under an electrical field under static conditions. Remarkably, the results described in Fig. 1, show that grain growth is retarded under an applied field. The field was applied by two wire electrodes placed on opposite sides of the specimen as shown in cross section in this figure. This geometry creates a spectrum of electrical fields, which can be

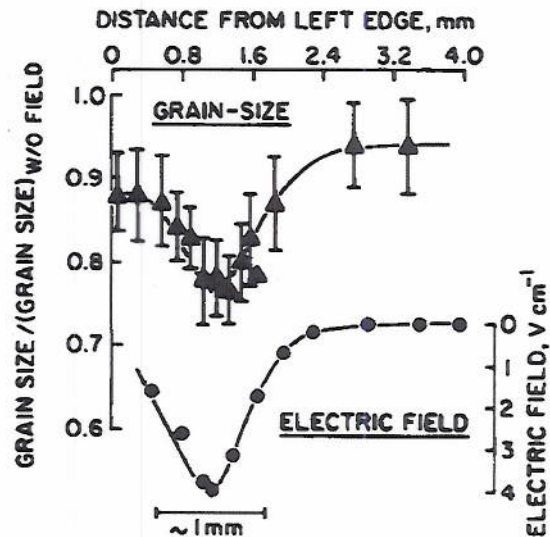
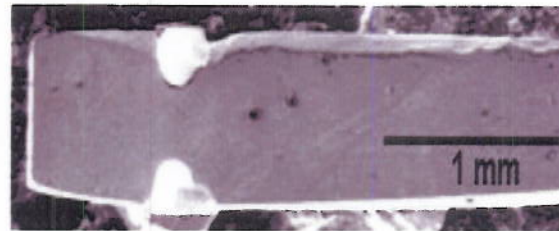


Figure 1: Rather weak DC fields have the effect of retarding the rate of grain growth in 3YSZ, as seen above where the field varies spatially along the x-axis.

calculated, and then correlated to the grain size within the specimen. This correlation is shown clearly in the lower half of the figure, where it is seen that the grain size is smaller when the field is higher.

The results presented in Fig. 1 help to differentiate between the kinetics and thermodynamic aspects of the effect of electrical fields on superplastic deformation. A lower grain size implies a reduction in the thermodynamic force for grain growth (it is not intuitively obvious how electrical fields can reduce grain boundary diffusion kinetics, though this idea should not be ruled out). This finding has been explained by postulating that the higher electrical resistance of the boundary raises the local temperature, and therefore produces an energy "well" which pins the boundaries (the free energy of the boundary decreases with temperature because boundaries have a significant entropy).

Flash-Sintering:

We are conducting experiments where traditional sintering experiments are combined with externally applied electrical fields. Samples are prepared in the shape of dog-bones, and the field is applied via platinum electrodes attached to the handles of the specimen, and the shrinkage rate is measured. In this way, the influence of fields on sintering can be studied explicitly, avoiding the complexities inherent in microwave and spark-plasma sintering processes.

The results for 3YSZ show the densification strain as a function of temperature in constant heating rate experiments, at applied fields varying from 0 Vcm⁻¹ to 120 Vcm⁻¹. The effect is clearly distinguished into two regimes. At lower fields, the sintering rate is gradually enhanced, as seen the movement of the sintering curves to a lower temperature. But at fields ≥60 Vcm⁻¹, sintering is accomplished in just a few seconds at temperatures well below 1000°C (the conventional sintering of zirconia requires several hours at 1400°C). This new phenomenon is being called "flash sintering". On going experiments with other ceramics, are showing that flash sintering prevails in all instances.

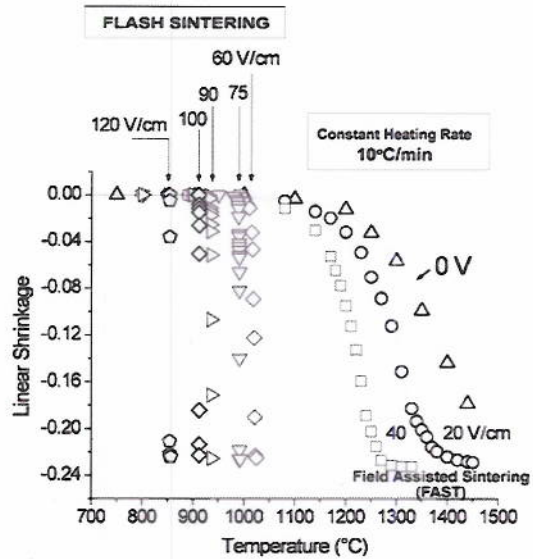


Figure 2: Influence of electrical fields on sintering behavior of 3YSZ in constant heating rate experiments.

FUTURE PLANS

Future plans are focused on understanding the fundamental mechanisms for the grain growth and flash sintering phenomena summarized above. The following hypotheses are being pursued:

- (a) Grain boundaries could have a higher electrical resistance than the crystal, which can cause a local rise in temperature from Joule heating, relative to the adjacent matrix. The higher temperature can produce a spatial minimum in grain boundary energy, thereby having a pinning effect which could then explain the slower rate of grain growth.
- (b) As seen in Fig. 2, field enhanced sintering of ceramics has two different characters, at low fields the sintering rate increases gradually with applied field, but in the high field regime sintering occurs nearly instantaneously, as in flash-sintering. These effects may be explained, partly, by the slower rate of grain growth under applied fields, and partly by enhanced kinetics, presumably due to Joule heating. The separation of these two effects is an explicit goal of future plans.
- (c) The onset of flash sintering is accompanied by a sharp increase in power dissipation in the specimen. We are exploring two possible ways to explain this finding:
 - (i) First, that runaway heating at grain boundaries produces the instability: local rise in temperature lowers the resistance which increases the power dissipation, thereby precipitating an instability.
 - (ii) A second possibility is that the applied field nucleates vacancy-interstitial pairs which greatly enhances mass transport kinetics. This mechanism can also lower electrical resistivity, and produce the "flash" effect. The argument for the nucleation of Frenkel pairs is that the applied fields helps to overcome the electrostatic binding force between the vacancy-interstitial pairs.

Experiments and models in future plans include modeling the nucleation of Frenkel pairs under an applied electrical field (in a possible collaboration at LANL), measuring the change in conductivity as a function of the applied field using non-contact electrodes, measuring the temperature profile with infrared microscopy (in collaboration with Dr. Dinwiddie at ORNL), and conducting experiments with different material systems to test the generality of the concepts and models.

Publications (2008-2010)

1. S. Ghosh, A. H. Chokshi, P. Lee and R. Raj, "A Huge Effect of Weak dc Electrical Fields on Grain Growth in Zirconia," *J. Am. Ceram. Soc.*, 92[8], 1856-1859 (2009).
2. D. Yang, R. Raj and H. Conrad, "Enhanced Sintering Rate of Zirconia (3Y-TZP) Through the Effect of a Weak dc Electric Field on Grain Growth," *J. Am. Ceram. Soc.*, in press (2010).
3. M. Cologna and R. Raj, "Surface Diffusion Controlled Neck Growth Kinetics in Early Stage Sintering of Zirconia, with and without DC Electrical Field," *J. Am. Ceram. Soc.*, in press (2010).
4. M. Cologna, B. Rashkova and R. Raj, "Flash Sintering of Nanograin Zirconia in < 5s at 850°C," *J. Am. Ceram. Soc.*, in press (2010).

Controlling Transformations for Desirable Mechanical Response

PIs: Ivar Reimanis* and Cristian Ciobanu**

*Metallurgical and Materials Engineering Department

**Engineering Division

Colorado School of Mines

Golden, CO 80401 USA

Email: reimanis@mines.edu

Program Scope

The study of materials with unusual properties offers new insight into structure-property relations as well as promise for the design of novel composites. In this spirit, the PIs seek to (1) understand fundamental mechanical phenomena in ceramics that exhibit pressure-induced phase transitions, negative coefficient of thermal expansion (CTE), and negative compressibility, and (2) explore the effect of these phenomena on the mechanical behavior of composites designed with such ceramics. The broad and long-term goal is to learn how to utilize these unusual behaviors to obtain desired mechanical responses.

Eucryptite, a lithium aluminum silicate (LiAlSiO_4), has been targeted because it exhibits a pressure-induced phase transition at a sufficiently low pressure to be accessible during conventional materials processing [1]. Specifically, the hexagonal polytype β -eucryptite transforms to ε -eucryptite under about 0.8 GPa hydrostatic pressure. Thus, it is theoretically possible to design eucryptite-containing composites that exhibit a novel type of transformation toughening involving the reverse phase transformation ε -to- β eucryptite. This rests on the premise of being able to fabricate composites in which the high pressure phase ε -eucryptite is stabilized. The functionality of this type of transformation toughening depends on the difference between the pressure to form ε -eucryptite and that for the reverse transformation back to β -eucryptite; this hysteresis in loading vs. displacement should correlate with the amount of toughening. We perform a combination of activities, including synthesis and processing to control structures, atomistic modeling, and mechanical characterization. Synthesis studies are focused to understand how particular structures are formed and how to utilize this understanding to control modify the critical pressure at which the phase transformation occurs. In particular, the additions of dopants such as Mg^{2+} and Zn^{2+} to the structure are expected to modify the transformation pressures. The atomistic modeling allows fundamental insight into the stability of different structures of eucryptite under different thermodynamic conditions. Mechanical characterization brings together micromechanical modeling to describe this unique toughening mechanism and experiments that measure crack growth in eucryptite-containing composites.

Recent Progress

The sequence of chemical reactions when β -eucryptite is formed from raw constituents SiO_2 , Al_2O_3 and Li_2CO_3 has been successfully identified with thermal analysis techniques [2]. Understanding this synthesis reaction path is the first step to alloying β -eucryptite with a dopant in order to alter its thermomechanical properties (specifically, the critical pressure at which the

pressure-induced phase transformation occurs). A model of the β -eucryptite structure is shown in Figure 1. The Li ions are believed to ‘prop’ open the relatively open β -quartz structure of β -eucryptite, and thus, it would be expected that any strategy to alter the phase transformation characteristics (e.g., critical pressure for the transformation) would involve Li ions. Dopants such as Zn^{2+} and Mg^{2+} have been shown to substitute for Li^+ in the structure; the ionic charge differences may lead to structural defects. Formulations in which some of the Li_2CO_3 is replaced with either ZnCO_3 or MgCO_3 are being prepared.

A relatively new atomistic modeling approach developed by van Duin, et al. [3], termed ReaxFF, has been successfully extended for the four-component (Li-Al-Si-O) system examined in our work [4,5]. Van Duin, et al. have developed a new generation of force field to describe the bonding between atoms that eliminates certain problems with conventional empirical force field methods. Our work has involved significant benchmarking with well-established density function theory (DFT) and experimental results for numerous known compounds comprising combinations of the elements Li, Al, Si, and O. An example result comparing the relative stability of the three major polytypes of eucryptite in which both DFT and ReaxFF were used independently is shown in Figure 2. We have successfully developed atomistic bonding descriptions for Li, Al, Si and O.

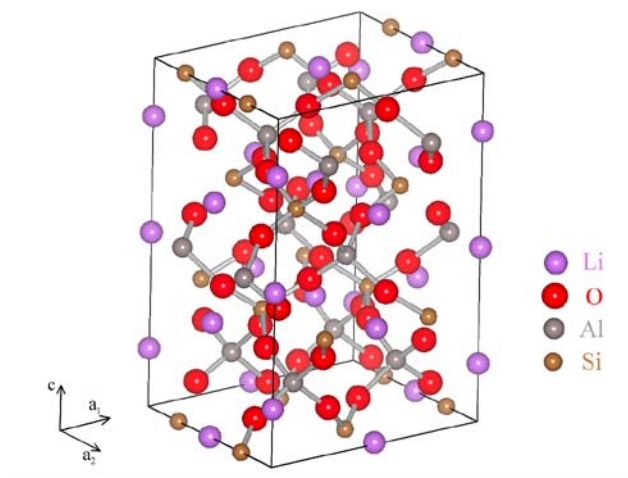


Figure 1. Depiction of the atomic structure of β -eucryptite. The structure is β -quartz, a relatively open structure in which Li ions prevent it from collapse to α -quartz. The structure of ϵ -eucryptite is not known.

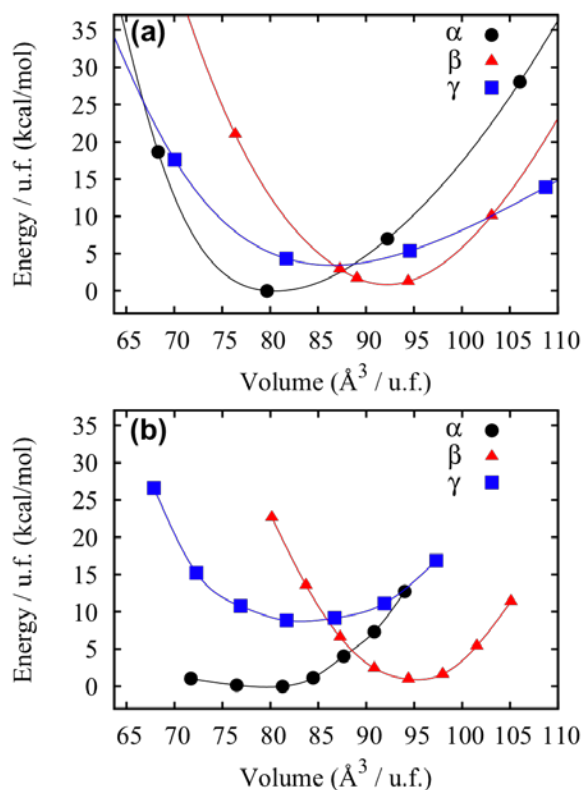


Figure 2. Equations of state of various phases of eucryptite calculated using (a) DFT and (b) ReaxFF. Both techniques predict an identical order of stability of the three polymorphs with α being the most stable phase in each case.

Micromechanical modeling work has been performed to predict the level of toughening expected from this class of composites. It is noted that the difference in coefficient of thermal expansion between a matrix (e.g., ZrO_2 or Al_2O_3) and the particle (β -eucryptite) leads to the compressive stress required to transform β -eucryptite to ϵ -eucryptite. The corresponding tensile stress in the matrix is expected to lower the toughness, countering the raise in toughness expected from the reverse ϵ -to- β transformation. The micromechanical model combines a classical transformation toughening prediction of toughness with a model developed by Taya, et al. based on thermal residual stresses. The result shows that a net toughening of up to about 100 percent is possible. If there is hysteresis (i.e., a difference in the pressure for the forward transformation of β -to- ϵ eucryptite and that for the reverse of ϵ -to- β), it is expected that the amount of toughening would increase.

To verify the proposed toughening mechanism, composites comprising varying volume fractions (from 0.5 to 0.2) of β -eucryptite particles in a matrix of ZrO_2 have been fabricated with varying β -eucryptite particle sizes. ZrO_2 was chosen because it has a sufficiently high coefficient of thermal expansion compared with β -eucryptite that cooling from a processing temperature leads to a hydrostatic stress in the β -eucryptite particles in excess of that required for β -eucryptite to transform to ϵ -eucryptite. The particle size of eucryptite was varied by milling for different times. It is expected that the transformation characteristics would depend on particle size; also, the tensile residual stress distribution in the matrix depends on particle size. A significant challenge has been to prevent cracking due to the large tensile thermal residual stresses that develop during fabrication. Figure 3 shows fracture surfaces from YSZ and two composites. A reasonably good dispersion of β -eucryptite has been achieved. The toughness has not yet been measured.

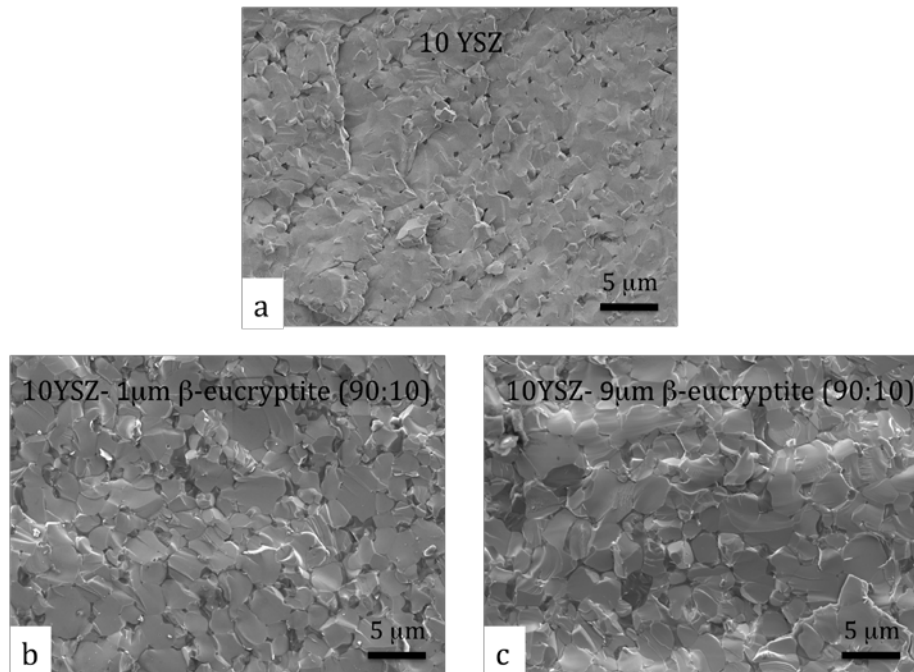


Figure 3. Scanning electron micrographs showing the microstructure of (a) YSZ, and YSZ with 10 percent by volume β -eucryptite particles with average particle sizes (b) 1 μm and (c) 9 μm . The dark phase in (b) and (c) is β -eucryptite.

Future Plans

We plan to perform in-situ Raman spectroscopy experiments in which β -eucryptite (doped and un-doped) is exposed to pressures and temperatures to map out the thermodynamic stability of the phase transformation; it may be possible to study the phase transformation kinetics as well. A limited number of single crystals is available for this as well.

Atomistic modeling will focus on utilizing the newly developed descriptions for interactions between Li, Al, Si and O to (1) describe the pressure-induced phase transformation, (2) describe the crystal structure of the newly discovered ε -eucryptite phase, (3) predict the Raman spectroscopy response of ε -eucryptite to compare with the experimental measurements, and (4) develop a method by which to examine the role of dopants (Mg^{2+} and Zn^{2+}) on phase stability.

Composites are being fabricated for fracture toughness measurements. Subcritical crack growth will be evaluated using a dynamic indentation method recently developed by our group [6]. Microcracking is still prominent in most of the eucryptite- ZrO_2 composites, and a strategy must be developed to prevent this; particle dispersion probably plays a key role. A micromechanical model is being developed to examine the role of hysteresis in governing toughening.

References (* indicates references published with DOE funding)

1. *T. Jochum, I. E. Reimanis, M. Lance and E. R. Fuller, "In-Situ Raman Indentation of Eucryptite: Characterization of the Pressure-Induced Phase Transformation", *Journal of the American Ceramic Society* [92]4 857-863, (2009).
2. *T. Jochum and I. E. Reimanis, "Reactions in Eucryptite-Based Lithium Aluminum Silicates", *Journal of the American Ceramic Society*, 93[6] 1591-1596, (2009).
3. A. C. T. van Duin, A. Strachan, S. Stewman, Q. Zhang, X. Xu, and W. A. Goddard, "ReaxFF_{SiO} Reactive Force Field for silicon and silicon oxide systems", *J. Phys. Chem. A*, **107**, p 3803 (2003).
4. *B. Narayanan, I. E. Reimanis, E. R. Fuller and C. Ciobanu, "Elastic constants of β -eucryptite studied by density functional theory", *Phys. Rev. B* 81, 104106 (2010). DOI: 10.1103/PhysRevB.81.104106.
5. B. Narayanan, A. C. T. van Duin, B. B. Kappes, I. E. Reimanis and C. V. Ciobanu, "Parametrization of a reactive force field for lithium aluminum silicates with application to elastic properties of eucryptite phases", manuscript ready for submission to *Phys. Rev. B* (2010).
6. *S. Ramalingam, I. E. Reimanis, E. R. Fuller, Jr., and J. Haftel, "Slow Crack Growth Behavior of Zirconia Toughened Alumina (ZTA) and Alumina using the Dynamic Fatigue Indentation Technique", in press in *Journal of the American Ceramic Society* (2010).

Elisa Riedo

Georgia Institute of Technology

Address: School of Physics, 837 State St, Atlanta GA 30332-0430

Phone number: 404-694-6580

Email: elisa.riedo@physics.gatech.edu

DOE Division of Materials Sciences and Engineering, Office of Basic Energy Sciences

NanoMechanics: Elasticity and Friction in Nano-Objects

Nanotubes, nanowires, nanosheets, and nanobelts hold the potential to become building blocks in integrated nano-electronic and photonic circuits, nano-sensors, batteries electrodes, energy harvesting nano-systems, and nano-electro-mechanical systems (NEMS). While several experiments and theoretical calculations have revealed a plethora of novel phenomena in these nanostructures, many fundamental and technological questions remain open. For example, it is still unclear how the structural defects contribute to the mechanical properties of nanotubes and nanowires, what are the scaling effects on the mechanical, electro-mechanical and opto-mechanical properties of different nano-objects (N-O). Another crucial issue in nanotechnology is related to the ability to assemble nano-objects on a substrate. This issue is intimately connected with the problematic of controlling friction and adhesion. Friction is one of the oldest problems in Physics and yet, one of the least understood. The study of friction and adhesion in nano-objects offers the opportunity to either understand at a fundamental level the energy dissipation mechanisms in friction, or learn about the interaction forces acting between N-O/N-O and N-O/substrate so that they can be assembled on a surface and/or used in NEMS. The long term goal is to understand, predict and manipulate the interactions between atoms, molecules, and small particles, for producing nano-objects with tailored optimum mechanical, electro-mechanical and opto-mechanical properties.

Here, we propose a research program to study, simultaneously with the morphological, structural and chemical properties, the frictional and elastic properties of individual carbon nanotubes, nanowires, 2D nanosheets, and piezoelectric and photostrictive nanostructures. The research activity is focused on three Topics:

1. Friction and frictional anisotropy in carbon nanotubes
2. Elastic properties of nanowires, and nanosheets as a function of their size, structure, defects and temperature.
3. Piezoelectricity, photostiction, and pseudoelasticity in piezoelectric nanostructures produced by a method, thermochemical nanolithography, recently developed by the PI. The focus will be on the role of size, geometry, and defects.

Related to Topic 1, in our past work we have performed a joint experimental and theoretical investigation of the frictional forces encountered by a nano-size tip sliding on top of a supported multiwall CNT along a direction parallel or transverse to its axis, as a function of normal load, sliding velocity, and tube radius. Experimentally, the longitudinal shear stress is found to remain almost constant with varying CNT radius, whereas the transverse shear stress decreases with increasing radius, reaching the value of the longitudinal shear stress for radii larger than 10 nm. Experiments and theory find that for a fixed total normal force, i.e., applied normal load plus adhesion force, the friction force, F_F , in the transverse direction is higher than in the longitudinal direction. This

result appears clear in the AFM data reported in Figure 1, where it is shown a typical plot of F_F acquired on top of a CNT as a function of the normal load, F_N , for transverse and longitudinal sliding. In each graph we also add the results for the silicon substrate, which is the reference surface. The slope of the F_F vs. F_N curve for the transverse CNT is similar to the slope measured on Si, and it is about three times the slope measured on the longitudinal CNT. On the other hand, the adhesion force remains almost the same for the two sliding. No substantial differences have been detected in the F_F vs. F_N curves acquired on the same CNT and for the same sliding direction but for different sliding velocities, in the range $v = 0.8 - 4 \mu\text{m/s}$. This unanticipated behavior was explained with the help of the theoretical simulations. We found that transverse sliding probes not only the elastic deformations of the stiff carbon-carbon bonds of the graphitic basal planes, common to the longitudinal sliding, but also a much softer overall swaying motion of the tube, akin to a "hindered rolling". This added softness is the source of the additional transverse tip dissipation and increased friction in the transverse direction. This friction anisotropy should be observable in very different geometries/situations, e.g., when a CNT slides on a substrate parallel or perpendicularly to its axis. Our findings could thus help in developing better strategies for large scale self-assembling of surface deposited nanotubes [59], design of CNT adhesives and nanotube/polymer composite materials. These results have been published in Nature Materials in 2009 [1].

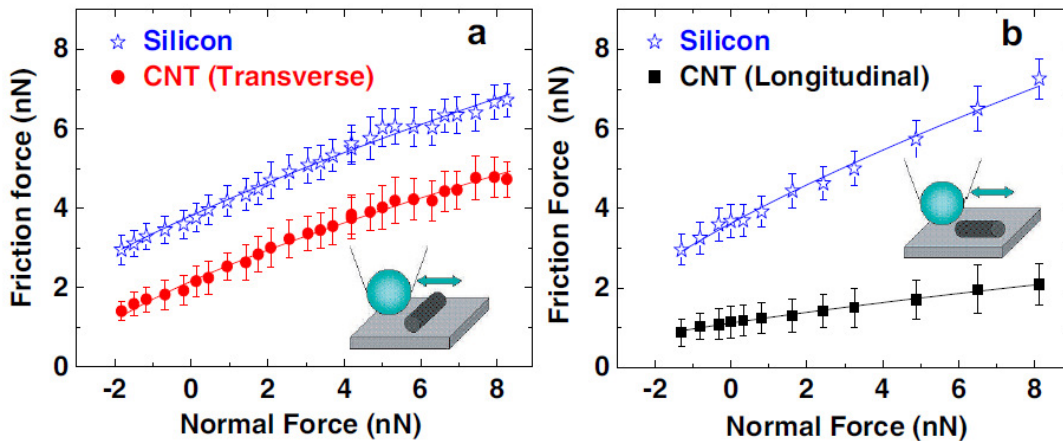


Figure 1: Frictional force as a function of the normal load for silicon (blue stars) and for transverse (a) and longitudinal (b) sliding on top of a CNT.

Related to Topic 2, in our past work, the elastic properties of ZnO nanobelts have been investigated with an AFM by means of the modulated nanoindentation technique [2, 3]. Their Young's modulus is found to decrease significantly from about 100 GPa to 10 GPa, as the width-to-thickness ratio increases from 1.2 to 10.3. In order to understand the origin of the low elastic modulus of nanobelts with high w/t, surface effects and the possibility of a structural phase transition were investigated. However, the surface to volume ratio reported in our study is more than one order of magnitude smaller than the value required for noticeable surface effects in previous investigations. Also, no hysteresis or sudden force variations have been observed in our experiments when the tip

is approaching or retracting during the indentation process. Since no surface effects or structural phase transitions can be invoked to explain the observed w/t dependence, it was necessary to understand if this dependence was related to any structural property/defects of the nanobelts. We have thus developed a system to investigate in-situ the structure, meaning growth direction and presence of defects, and the mechanical properties of an individual nano-object. This system combines an AFM with a Raman microscope through an inverted optical microscope, see Fig. 2. The morphology and the mechanical properties of individual ZnO nanobelts were then determined by AFM, while polarized Raman (PR) spectroscopy was used to characterize in-situ and non-destructively the growth direction and randomly distributed defects in the same individual nanobelts. Indeed, this investigation shed light on the origin of the observed elastic behavior of ZnO nanobelts. We found that the presence of point defects decreased the elastic modulus of the nanobelts by almost one order of magnitude. Furthermore, PR-AFM data revealed two growth modes during the synthesis of ZnO nanobelts by physical vapor deposition. In the thermodynamics-controlled growth mode, nanobelts grow along a direction close to $[0001]$, however the growth-direction is increasingly moving far away from the c -direction as the w/t ratio increases from 1 to 2, and they exhibit no point defects. In the kinetics-controlled growth mode, nanobelts grow along directions almost perpendicular to $[0001]$, they exhibit point defects, and they can have $w/t > 2$. The origin of a larger Young's modulus for nanobelts with $w/t = 1$ as compared with nanobelts with $w/t = 2$ is still unclear. However, we remark that the majority of the nanobelts presenting the highest modulus values were identified as nanowires with an hexagonal cross section from AFM topography measurements. The symmetry of the structure seems thus to play a role. These results have been published in the References [2, 3].

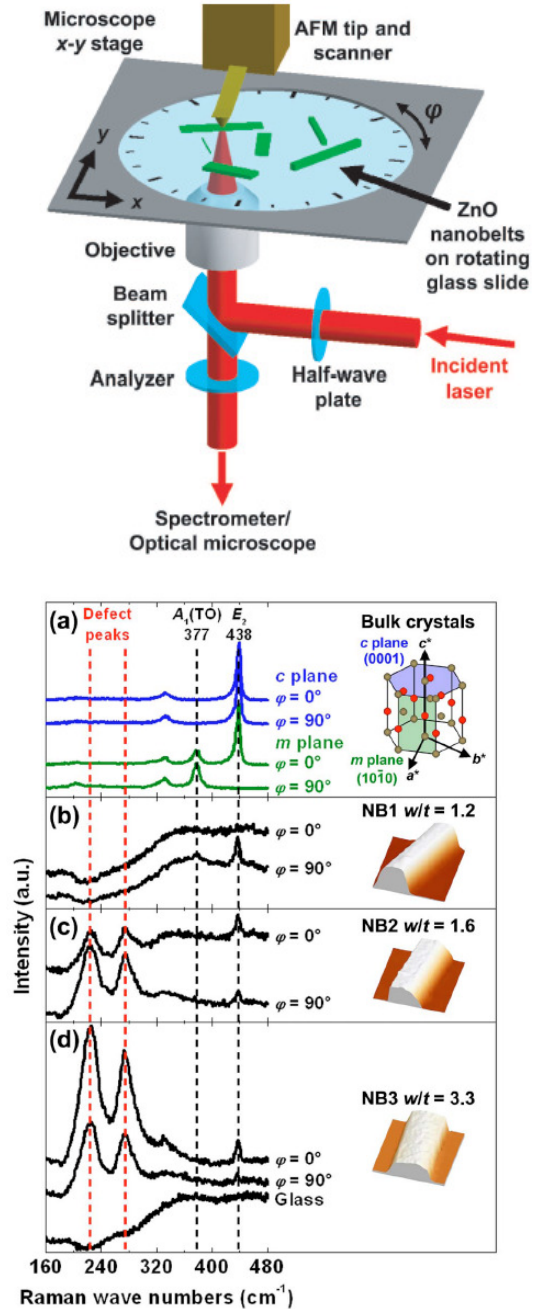


FIG. 2. (Color online) (a) PR spectra from the c and m planes of a ZnO crystal, shown in blue and green, respectively. The wurtzite structure (Zn atoms are brown, O atoms red) is also shown, where a^* , b^* , and c^* are the reciprocal lattice vectors. [(b)–(d)] AFM images ($3 \times 3 \mu\text{m}$) of three NBs labeled NB1, NB2, and NB3 and corresponding PR spectra. In (d) a PR spectrum of the glass substrate is shown at the bottom. All the PR spectra in (a)–(d) are collected in the copolarized configuration for $\varphi = 0^\circ$ and 90° . The spectra are offset vertically for clarity.

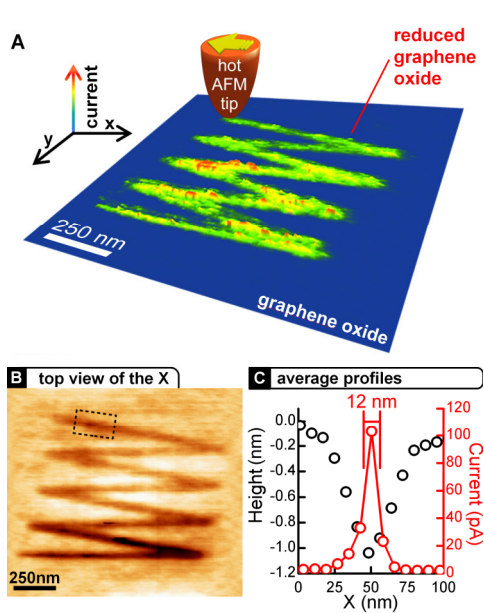


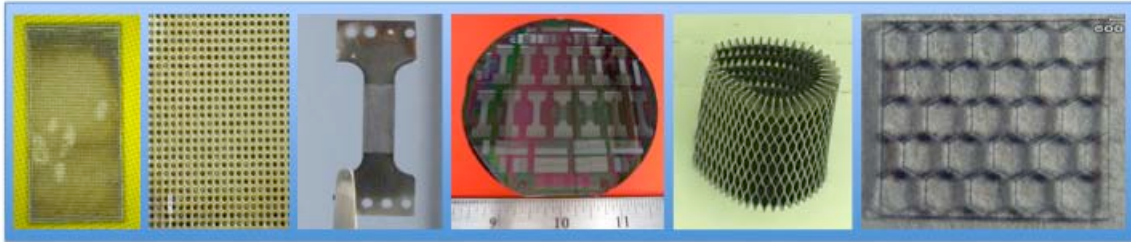
FIG 3. Local thermal reduction of a GO_{epi} film: current and topographical images. (A) Room temperature AFM current image of a zigzag shaped graphene-like nanoribbon fabricated by TCNL on GO_{epi} . (B) Corresponding topography image taken simultaneously with (A). (C) Averaged profiles of current and height.

Nanofabrication and in-situ mechanical and electrical characterization of nanostructures is considered the ultimate goal in nano-electrical mechanical systems. Related to Topic 3, recently, by using a resistively-heated atomic force microscopy tip, the PI in collaboration with a team of people from GeorgiaTech and the University of Illinois has demonstrated the ability to thermally activate a chemical reaction at the nm scale at the surface of a material. Local chemical and topographical changes with feature sizes down to 12 nm at scan speeds up to 1 mm/s have been obtained with this new technique, ThermoChemical NanoLithography (TCNL). Thus far, the material used in our TCNL experiments consisted of copolymers containing thermally labile groups, precursors/conjugated polymers, and epitaxial graphite oxide/graphene (see Fig. 3). The process is quite versatile, can produce simultaneous partially independent chemical and topographical changes, and can be extended to a wide range of thermally activated chemical transformations.

In the future we plan to use this technique to produce ferroelectric and piezoelectric nanostructures with controlled size and geometry. The results related to the TCNL project are published in the References [7-11].

Publications (2008-2010) from Current DoE-BES Funding

1. Marcel Lucas, Xiaohua Zhang, Ismael Palaci, Christian Klinke, Erio Tosatti, and Elisa Riedo, Hindered rolling and friction anisotropy in supported carbon nanotubes, *Nature Materials* 8, 876 (2009). Featured in News&Views of Nature Materials.
2. M. Lucas, Z.L. Wang, and E. Riedo, Growth direction and morphology of ZnO nanobelts revealed by combining in situ atomic force microscopy and polarized Raman spectroscopy, *Phys. Rev. B* (2010), in press.
3. M. Lucas, Z.L. Wang, and E. Riedo, Combined polarized Raman and atomic force microscopy: In situ study of point defects and mechanical properties in individual ZnO nanobelts, *Appl. Phys. Lett.* 95, 051904 (2009).
4. M. Lucas, K. Gall, and E. Riedo, Tip size effects on AFM nanoindentation of a gold single crystal, *J. Appl. Phys.* 104, 113515 (2008).
5. M. Lucas, A. M. Leach, M. T. McDowell, S. E. Hunyadi, K. Gall, C. J. Murphy, and E. Riedo, Plastic deformation of pentagonal silver nanowires: Comparison between AFM nanoindentation and atomistic simulations, *Phys. Rev. B* 77, 245420 (2008).
6. M. Lucas, T.-D. Li, E. Riedo, "Nanomechanics: Fundamentals and NEMS," book chapter in *Nanoelectronics and Photonics, From Atoms to Materials, Devices, and Architectures, Nanostructure Science and Technology* (Springer, 2008).
7. Z. Wei, D. Wang, S. Kim, S. Y. Kim, Y. Hu, M.K. Yakes, A.R. Laracuente, Z. Dai, S. R. Marder, C. Berger, W. P. King, W. A. de Heer, P. E. Sheehan, E. Riedo, "Nanoscale Tunable Reduction of Graphene Oxide for Graphene Electronics" *Science* (2010).
8. W. P. King S. Marder E. Gnecco, E. Riedo and R. Szoszkiewicz, Linear ripples and traveling circular ripples produced on polymers by thermal AFM probes, *Phys. Rev. B* 79, 235421 (2009).
9. D. Wang, Kod ali V.K., Underwood W.D., Jarvholm J.E., Okada T., Jones S.C., Rumi M., Dai Z.T., King W.P., Marder S.R., Curtis J.E., and Riedo E., Thermochemical Nanolithography of Multifunctional Nanotemplates for Assembling Nano-objects, *Adv. Funct. Mat* 19, 3696 (2009), cover Article.
10. Wang D.B., Kim S., Underwood W.D., Giordano A.J., Henderson C.L., Dai Z.T., King W.P., Marder S.R., and Riedo E., Direct writing and characterization of poly(p-phenylene vinylene) nanostructures, *Appl. Phys. Lett.* 95, 233108 (2009).
11. D. Wang, R. Szoszkiewicz, J. Curtis, E. Riedo "ThermoChemical Nanolithography (TCNL)" book chapter in *Applied Scanning Probe Methods, NanoScience and Technology* (Springer, 2010).
12. T.-D. Li and E. Riedo, Nonlinear viscoelastic dynamics of nanoconfined wetting liquids, *Phys. Rev. Lett.* 100, (2008).



USING ARTIFICIAL MICROSTRUCTURES TO UNDERSTAND MICROSTRUCTURE PROPERTY RELATIONSHIP IN METALLIC GLASSES

Jan Schroers, Yale University, Mechanical Engineering and Materials Science

Materials science seeks to correlate microstructure with (mechanical) properties. Various approaches have been employed to understand this correlation including conventional direct approaches where the microstructure is varied through processing parameters and composition and the effects on the mechanical properties determined. “Virtual experiments” through molecular dynamics simulations have been widely used to investigate structure-property relationships but are limited by today’s available computing power, which limits the system size and simulation time. Alternatively, model systems such as colloidal systems have also been employed which exhibit limitations in terms of the limited number of properties that can be varied. Technologically relevant materials have reached a level of complexity that conventional metallurgical strategies as well as above mentioned model and simulation strategies are at their limit.

Therefore, we propose a novel approach to study microstructure-property relationship; artificial microstructures, which allow us to individually and independently vary parameters and thereby determine their individual effects on mechanical properties. The artificial microstructure is fabricated using our recently developed miniature fabrication method, which allows us to manipulate the material on a length scale ranging from 10 nm to millimeters. Examples where this novel approach can be applied include toughening mechanism in metallic glasses, size effects, and the transition from plastic deformation to elastic buckling in metallic glass heterostructures.

Deformed materials: Towards a theory of materials morphology dynamics

James P. Sethna, sethna@lassp.cornell.edu, (607) 255-5132, <http://www.lassp.cornell.edu/sethna>
Clark Hall, Cornell University, Ithaca, NY 14853-2501

1 Program Scope

The mechanical properties of structural materials (strength, toughness, and transport) are sensitively dependent on its mesoscale morphology (dislocation structures, grain boundaries, composite and multiphase structure, microcracks...). These morphologies are in turn sensitively dependent on how it is annealed and deformed during manufacturing. Even now, with our microscopic probes into the relevant mechanisms of ductility and failure and our vast computational resources for simulating materials evolution and properties, our fundamental understanding even of basic features in the evolution of single crystals of pure materials remains limited. Dislocation structures, and the dislocation avalanches that mediate their response to strain, are the motivation and focus of our research. Our objectives are

(1) To study the formation and evolution of emergent dislocation structures – grain boundaries and grain growth at high temperatures, cellular dislocation structures and refinement at low temperature, and the joint effects of temperature and strain variation. We build on our continuum theory of dislocation dynamics [3, 4] which (despite enormous simplifications of the microscopic dynamics) provides realistic formation of grain boundaries and cell structures (Section 2), providing an unusual opportunity to develop the analytical and computational machinery to systematically explore and characterize the materials evolution in a model materials system.

(2) To study avalanches in materials plasticity – the emergent collective dynamics of dislocations. We propose new, simple models to understand experimental data, and also propose to incorporate disorder into our existing model to generate metastability and avalanches. In studying avalanches, we build on universal scaling properties that allow quantitative under-

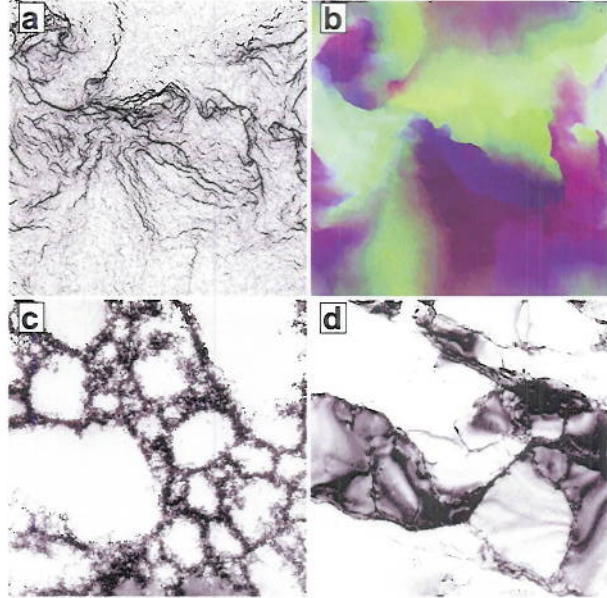


Figure 1: **Simulated grain boundaries and cell structures.** *Our model, initialized with a Gaussian random plastic distortion field, develops fractal cell wall patterns when only glide is allowed [(a) Dislocation density; (b) Orientation map, converted to RGB.] These simulations reproduce realistic dislocation cell wall patterns found experimentally. [(c) from Hughes et al. [1], analyzed in terms of scaling distributions with a single characteristic scale. (d) from Hähner et al. [2], shown to be fractal without a characteristic scale.*

standing of the emergent properties. We go beyond universality, introducing corrections to scaling and studies of crossover effects, both to expand the ranges of validity of the theory and to connect to microscopic materials properties.

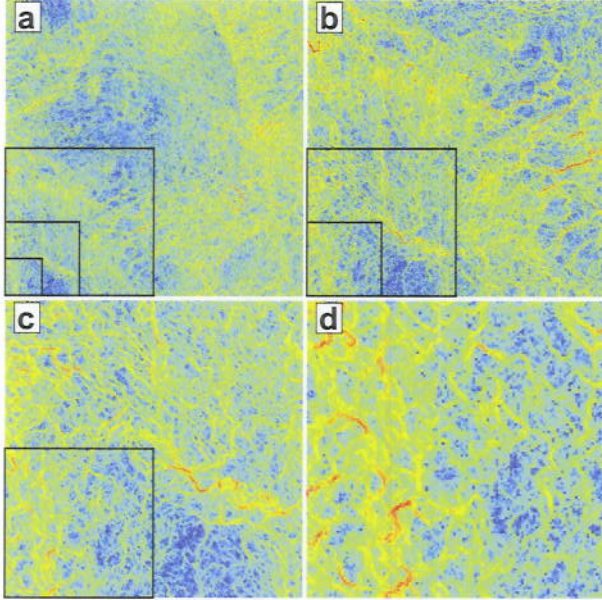


Figure 2: **Self-similar cell walls: real-space renormalization group.** Each frame is the lower left-hand quarter of the previous frame, rescaled in amplitude by the appropriate factor.

tions. At low temperatures, where vacancies and interstitials are immobile and climb is forbidden, our dislocations form fuzzier boundaries (Fig. 1 a,b), with strikingly similar morphologies to the dislocation cell structures [6, 7], seen experimentally in stage II and III hardening (Fig. 1 c,d). This work has recently been published in *Phys. Rev. Lett.* [4].

There is a longstanding controversy in the plasticity community about whether the experimental cell-wall structures have a fractal structure [2, 9–11] or whether they are characterized by a single length scale [12–14]. Our model generates self-similar dislocation structures – invariant under a rescaling of length and dislocation density (Fig. 2) with power-law decays of the relevant order

We view our studies as the first steps in a systematic analysis of the history dependence of materials morphology and properties: how do materials evolve under heating and beating?

2 Plasticity and fractals

Crystals, when deformed by the creation and movement of dislocation lines, relax to low-energy structures formed to screen the long-range strain fields of these topological defects. Our continuum theory [3–5] reproduces this behavior, despite leaving out many important features of real material dislocations (glide planes and slip systems, entanglement and pinning, geometrically unnecessary dislocations, ...). At high temperatures, where our dislocations can climb, they form into sharp grain boundaries separating nearly undeformed crystals with different crystalline orienta-

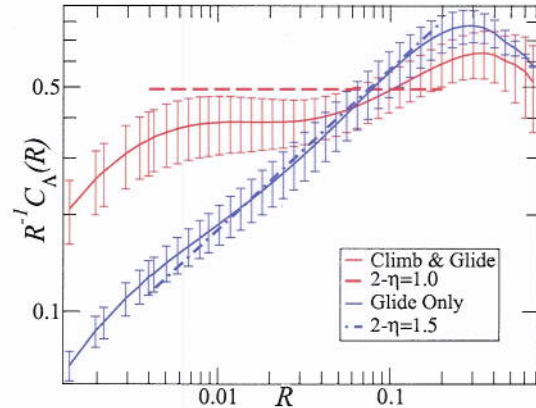


Figure 3: **Orientation correlations decay as a power law.** The orientations allowing climb have $C_{\Lambda} \sim R$ as expected for non-fractal sharp grain boundaries, while the glide-only simulations show $C_{\Lambda} \sim R^{\eta}$ with $\eta \approx 1.5$, indicating a fractal, fuzzy cell wall structure.

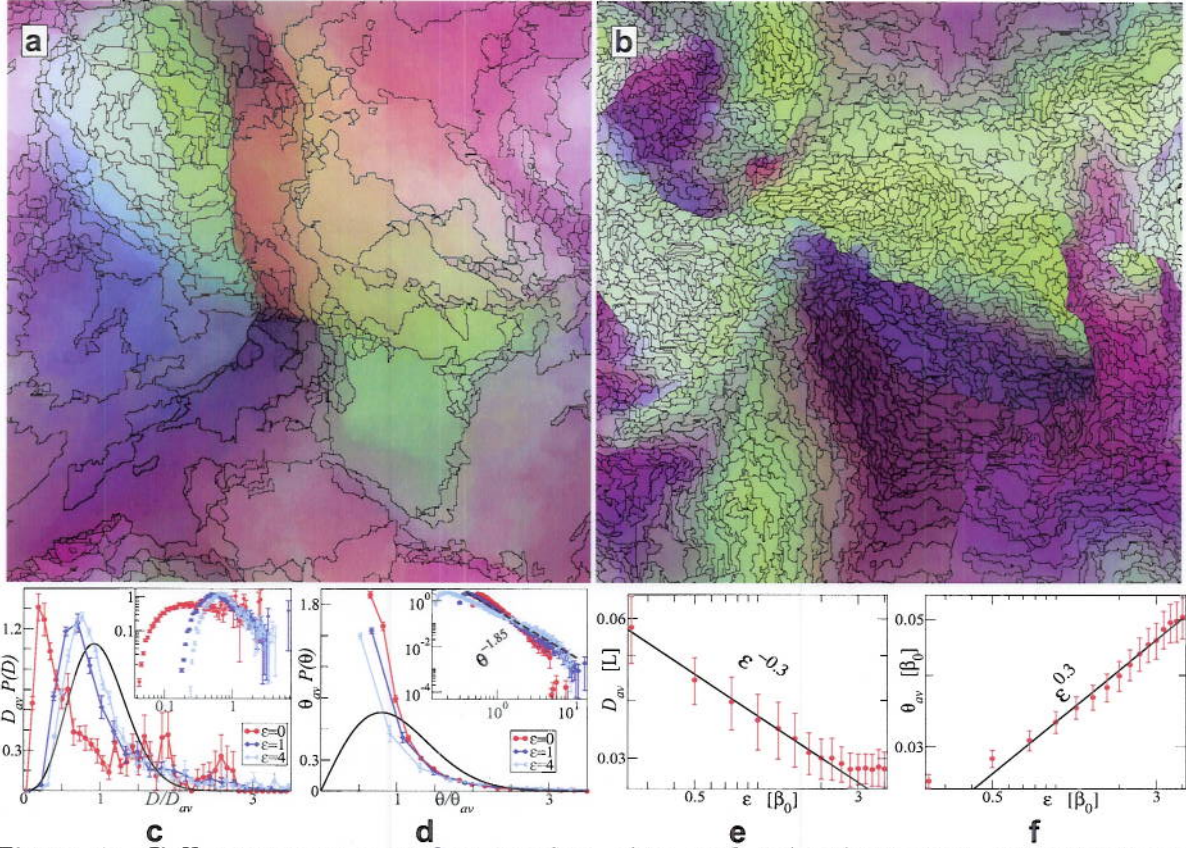


Figure 4: **Cell structures under strain: size and misorientation distributions.** (a) The relaxed state of Fig. 1(b), decomposed into cells. (b) The final state after a strain of $\epsilon_{zz} = 3\beta_0$ is applied; notice the cells refine to shorter length scales. (c,d). The cell size and misorientation angle distributions, scaled by their means, at various external strains. Both distributions are closer to power laws (insets) than are the experimental distributions [1, 8] (solid curves). (e,f) Mean cell size D_{av} and misorientation angle θ_{av} as functions of external strain. Notice that the product $D_{av}\theta_{av}$ is approximately constant, as observed experimentally [8]. The power law dependence $\epsilon^{0.3}$ is weaker than the powers $\epsilon^{1/2}$ and $\epsilon^{2/3}$ observed experimentally for incidental dislocation boundaries and geometrically necessary boundaries.

parameters (Fig. 3). Using a boundary-pruning algorithm to identify cell walls (Fig. 4a), we have estimated the fractal dimension to be about 1.5 over a range of about a decade, somewhat less than the experimental values of 1.64 – 1.79 [2]. We thus have provided a concrete evolution law that generates fractal cell walls. It is interesting to note that previous theoretical approaches explaining the appearance of fractals [2, 15] involve random noise in the evolution laws; our model generates fractal structures without any stochasticity.

Our model does not, however, generate a simple “black-and-white” fractal: it is self-similar when both length *and* amplitude are rescaled. Thus smaller cells are generally associated with lower misorientation angles. We can use our decomposition into cells to directly compare our model to the experiments of Hughes and collaborators [12–14], who find a scaling form emerges for the cell size and misorientation distribution functions as the system is

strained, with cell sizes shrinking with strain (refinement) and misorientations growing. Our model also exhibits refinement (Fig. 4b) under external strain. We observe a similar scaling collapse with external strain (Fig. 4c,d), but with scaling functions that are much closer to power laws. (The experimental paucity of small cells and small misorientation angles may be due to the human tendency to merge tiny cells with neighboring large ones; most of our small cells are near large-angle boundaries.) Figures 4e&f show that we can duplicate (with large error bars) the experimentally observed inverse relation between the average cell size $D_{av}(\epsilon)$ and misorientation angle $\theta_{av}(\epsilon)$, and replicate the observed power-law scaling, but the power law for our 2D model material is smaller than that observed experimentally.

References

- [1] D. A. Hughes, D. C. Chrzan, Q. Liu, and N. Hansen. Scaling of misorientation angle distributions. *Phys. Rev. Lett.*, 81:4664–4667, 1998.
- [2] Peter Hähner, Karlheinz Bay, and Michael Zaiser. Fractal dislocation patterning during plastic deformation. *Phys. Rev. Lett.*, 81(12):2470–2473, Sep 1998.
- [3] S. Limkumnerd and J. P. Sethna. Mesoscale theory of grains and cells: Crystal plasticity and coarsening. *Physical Review Letters*, 96:095503, 2006.
- [4] Yong S. Chen, Woosong Choi, Stefanos Papanikolaou, and James P. Sethna. Bending crystals: the evolution of grain boundaries and fractal dislocation structures. *Phys. Rev. Lett.*, 105:105501, 2010.
- [5] Anish Roy and Amit Acharya. Finite element approximation of field dislocation mechanics. *Journal of the Mechanics and Physics of Solids*, 53:143–170, 2005.
- [6] D. Kuhlmann-Wilsdorf. *Mater. Sci. Eng.*, A113:1, 1989.
- [7] A. S. Argon. Mechanical properties of single-phase crystalline media: Deformation at low temperatures. In R. W. Cahn and P. Haasen, editors, *Physical Metallurgy*, pages 1877–1955. North Holland, Amsterdam, 1996.
- [8] D. A. Hughes and N. Hansen. Graded nanostructures produced by sliding and exhibiting universal behavior. *Phys. Rev. Lett.*, 87:135503, 2001.
- [9] H Mughrabi, T Ungar, W Kienle, and M Wilkens. Long-range internal-stresses and asymmetric x-ray line-broadening in tensile-deformed [001]-orientated copper single-crystals. *Philos. Mag. A*, 53(6):793, JUN 1986.
- [10] C Schwink. Flow-stress dependence on cell geometry in single-crystals. *Scr. Metall.*, 27(8):963, OCT 1992.
- [11] Y Kawasaki and T Takeuchi. Cell structures in copper single-crystals deformed in the [001] and [111] axes. *Scr. Metall.*, 14(2):183, 1980.
- [12] D A Hughes, Q Liu, D C Chrzan, and N Hansen. Scaling of microstructural parameters: misorientations of deformation induced boundaries. *Acta Mater.*, 45(1):105–112, 1997.
- [13] D A Hughes, D C Chrzan, Q Liu, and N Hansen. Scaling of misorientation angle distributions. *Phys. Rev. Lett.*, 81(21):4664, Nov 1998.
- [14] D A Hughes and N Hansen. Graded nanostructures produced by sliding and exhibiting universal behavior. *Phys. Rev. Lett.*, 87(13):135503, Sep 2001.
- [15] I Groma and B Bakó. Dislocation patterning: From micro- to mesoscale description. *Phys. Rev. Lett.*, 84(7):1487, Feb 2000.

Understanding and Controlling Toughening Mechanisms in Nanotube Reinforced Ceramic Coatings

Brian W. Sheldon and William A. Curtin
School of Engineering, Brown University, Providence, RI 02912

This project consists of integrated experimental, theoretical, and computational efforts that are designed to understand the basic mechanisms that can toughen nanotube and nanofiber reinforced ceramics. These nanocomposites have the potential to provide substantial toughening at the length scales where damage and failure initiation typically occur in coating systems. Our work in this area demonstrates that there are significant differences between behavior at the nanoscale and conventional micron-scale fiber-reinforced ceramics. In particular, reducing the reinforcement dimensions by roughly two orders of magnitude leads to important new questions. In nanomaterials, the scale over which fracture and decohesion occur are comparable to the fiber dimensions (e.g., nanotube diameter). The intrinsic lengths and nanotube lengths are thus intertwined, and a key feature of our work is to examine how crack deflection, nanoscale interface deformation and fracture occur. In these materials the distinction between the fiber, the matrix, and the interface must be considered in light of the fact that the entire reinforcement is within a few atomic spacings of the matrix. Exploring the ways in which these inherently smaller size scales will impact toughening mechanisms is the central idea that motivates our work. The current experiments are focused on coatings that consist of multiwalled carbon nanotubes in a silicon nitride matrix produced by chemical vapor infiltration, where we have demonstrated that multiwalled carbon nanotubes can provide substantial mechanical properties improvements. The fabrication methods employed make it possible to systematically vary the structure of these materials in a variety of ways, including the internal carbon structure (primarily graphene ordering); nanotube dimensions (diameter and wall thickness); the nanotube-matrix interface (roughness and bonding); and residual stresses.

DOE award number: DE-FG02-07ER46399

Institution: Purdue University

Project title: Shape memory in nanoscale metallic alloys

PI: Alejandro Strachan

School of Materials Engineering and Birck Nanotechnology Center

1205 W State Street, West Lafayette, IN 47907-2057

Email: strachan@purdue.edu

1. Program scope and Definition

The objectives of this project are to i) use electronic structure calculations and large-scale molecular dynamics (MD) to characterize the size and dimensionality dependence of the martensitic nanostructure of nanoscale NiTi alloys and the resulting thermo-mechanical response including shape memory and superelasticity, and ii) computationally explore avenues to optimize the performance of nanoscale SMA samples for applications that require active components.

The following three sections describe our accomplishments in three areas: i) size effects in martensitic nanostructure of Zr wires; ii) First principles calculations of the crystal structures involved in the thermo-mechanical response of NiTi, the shape memory alloy of choice for this project; and iii) large-scale MD simulations.

2. Recent Progress

The work during the first funding period of this project can be divided in two main categories: i) *ab initio* calculations of NiTi alloys using density functional theory (DFT), and ii) MD calculations to predict size effects on the martensitic nanostructure of nanoscale samples. In the following paragraphs I summarize the key results.

2.1 Ab initio calculations of NiTi crystal structures and phase transformations

We used DFT within the generalized gradient approximation (GGA) to characterize the various crystalline structures that govern NiTi alloys: i) high-temperature austenite phase B2; ii) orthorhombic B19; iii) the monoclinic martensite phase B19'; and iv) a body-centered orthorhombic phase (BCO). Our calculations confirm, as theoretically observed earlier, that BCO is the ground state structure of NiTi. We also investigated possible transition pathways between the various phases and the energetics involved, see Figure 1. We found B19 to be metastable with a 1 meV energy barrier separating it from B19'. Interestingly, we predicted a new phase of NiTi, denoted B19'', that is involved in the transition between B19' and BCO. B19'' is monoclinic and, unlike BCO, it can exhibit shape memory, see bottom panel of Figure 2.5. We find that the presence of this intermediate phase reduces the internal stress required to stabilize the experimentally observed B19' structure, and, consequently, it plays a key role in NiTi's properties. This work was published in Acta Materialia, see Section 4.

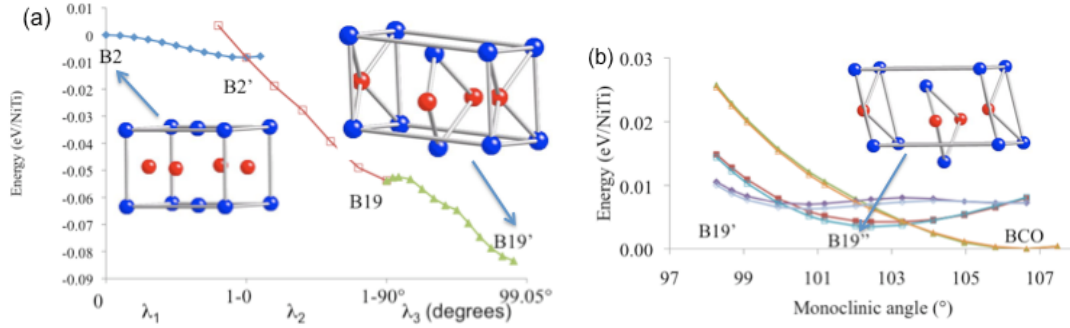


Figure 1. Energetics of phase transitions between NiTi phases.

2.2 Ab initio predictions of surface energies and size effects in NiTi

Surface energy differences between crystalline phases can play an important role in solid-solid phase transformation of nanoscale materials. Thus, we used DFT-GGA to characterize the surface energies of the various crystal structures of NiTi. We focused on low energy (110) surfaces of which there are two kinds (see Fig. 2): i) surfaces with in-plane atomic displacements and ii) ones with out-of-plane atomic displacements. Our results show that the B2' phase (the high temperature austenite phase) exhibits the lowest free surface energy, followed by B19, B19' (martensite) and BCO, see right panel of Fig. 2, although the energy difference is smaller for out-of-plane surfaces.

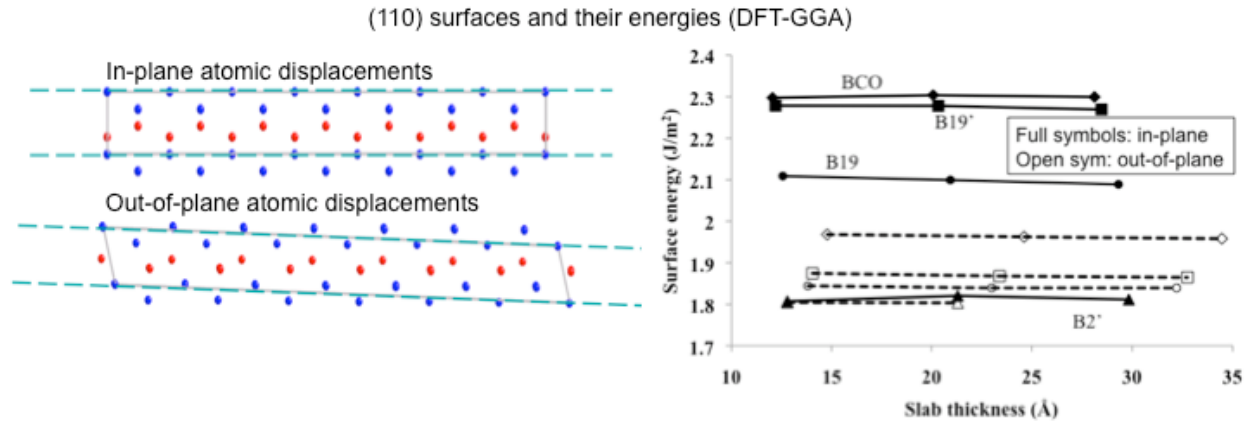


Figure 2. Atomic snapshots of (110) NiTi surfaces with in-plane and out-of-plane atomic displacements (left) and their corresponding formation energies computed from slabs of various lengths.

The total energy difference of slabs of the various phases with thickness N (number of unit cells) can then be determined from the relative energy of the bulk (E^{bulk}) and their surface energies (γ) and cross-sectional areas (A) in the following way:

$$E_{\alpha}^{\text{slab}}(N) - E_{\beta}^{\text{slab}}(N) = N(E_{\alpha}^{\text{bulk}} - E_{\beta}^{\text{bulk}}) + 2(A_{\alpha}\gamma_{\alpha} - A_{\beta}\gamma_{\beta}),$$

where the subscripts indicate the phase. The difference in surface energies between the various phases cause the relative energy of slabs of different crystal phases to become size dependent; consequently the martensite transition temperature will also be expected to be size dependent. Figure 3 shows the predicted relative energy between B2' and the martensite (B19') and ground state (BCO) slabs as a function of their thickness. Our DFT-GGA calculations predict different

trends: i) for out-of-plane slabs where B19' and BCO phases become more stable as thickness is reduces (thus increasing the transition temperature for nanoscale samples); ii) for in-plane slabs the B2' phase increases its stability with respect to B19' and BCO with decreasing slab thickness leading to a decrease of transition temperature. In summary our results show that reducing the size of NiTi samples affects the relative stability of the martensite and austenite phases and consequently the transition temperature. For slabs with in-plane displacements we predict a critical thickness below which the martensite transition would not occur.

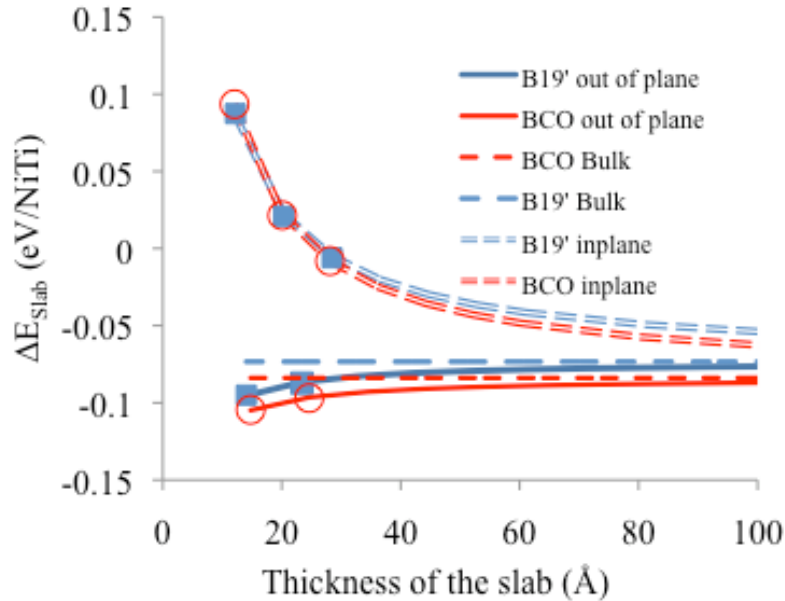


Figure 3. Energy of B2' slabs and B19' (martensite) and BCO as a function of thickness.

3. Future plans

During the next stage of this project we will perform large-scale MD simulations to characterize hetero-epitaxial or lattice coherent integration of shape memory alloys. Coherent integration of dissimilar materials at the nanoscale is a powerful technique to tune materials response and achieve properties not possible with bulk materials. This approach is widely used in microelectronics to engineer the band structure of semiconductors and in metamaterials for optical and energy conversion applications. Strain engineering via hetero-epitaxial integration has the potential to revolutionize the field of shape memory alloys (SMAs) since changes in lattice parameter can be used to control martensitic phase transformations which are responsible for the unique properties of these materials: their ability to remember shape and superelasticity. Experimental efforts in hetero-epitaxial SMAs are at a nascent stage and progress is hindered by a poor understanding of coherent (defect free) integration of these materials and the properties of the resulting nanostructures. **Our efforts will focus on large-scale MD simulations to characterize the thermo-mechanical response of epitaxial shape memory heterostructures consisting of NiAl alloys** designed to achieve properties not possible with bulk samples. We will focus on two classes of nanostructures:

- *Hetero-epitaxial nanolaminates* consisting of two NiAl alloys with different composition and, consequently, different lattice parameter and thermo-mechanical properties. We will focus on alloy combinations designed to result in heterostructures with martensitic

transformation temperature and mechanical damping fully tunable not only by composition but also by the characteristic sizes of the nanostructure.

- *Axial and core-shell hetero-epitaxial nanopillars*. Surface relaxation in 1-D nanomaterials enables the epitaxial integration of materials with very different lattice parameters (over 10% in some cases) beyond what is possible in planar geometries. We propose to use this additional flexibility in material selection and partial strain relaxation to achieve properties beyond those in planar configurations.

Our goal is to provide a quantitative assessment of the potential and limitations of hetero-epitaxial integration as an avenue to develop shape memory materials with tailored properties. This may address some of the limitations that currently restrict the use of SMAs as active materials. From the point of view of basic science our effort will shed light into the fundamental phenomena that govern and limit the fabrication and performance of hetero-epitaxial SMAs nanostructures: i) coherency limits in terms of materials and size, and ii) the role of strain, interfaces, and free surfaces in their martensitic transformation and thermo-mechanical response. Shape memory materials have an enormous potential for a wide range of applications from nanoscale switches for communications and low power electronics to microfluidics and this project will contribute to the knowledge base necessary for the development of next-generation materials nanoengineered to achieve specific functionalities.

4. References of DOE sponsored work

Publications entirely supported by this effort

“*Size effects on martensitic microstructure in Zr nanowires via molecular dynamics*”, A. Thompson and A. Strachan, *Physical Review B*, **81** 085429 (2010).

“*Phase stability and transformations in NiTi from density functional theory calculations*”, K. Guda Vishnu and A. Strachan, *Acta Materialia* **58** 745–752 (2010).

Publications closely related to this project

“*Nanoscale metal-metal contact physics from molecular dynamics: the strongest contact size*”, H. Kim and A. Strachan, *Physical Review Letters* **104**, 215504 (2010).

“*Strain relaxation in Si/Ge/Si nanoscale bars from molecular dynamics simulations*”, Y Park, M. Aktuga, A. Grama and A. Strachan, *Journal of Applied Physics*, **106**, 034304-1-6 (2009).

RADIATION EFFECTS IN NANOCRYSTALLINE SILICON CARBIDE

PROGRAM TITLE:

Radiation effects in nanocrystalline ceramics: Multi-scale model and experiment

LEAD PRINCIPAL INVESTIGATOR: Izabela Szlufarska, Associate Professor (Department of Materials Science & Engineering, Department of Engineering Physics, University of Wisconsin - Madison)

Address: 242 MSE, 1509 University Ave., Madison, WI, Ph: 608-265-5878. E-mail: izabela@engr.wisc.edu.

CO-PIs: Prof. Dane Morgan and Prof. Todd Allen (Department of Materials Science & Engineering, Department of Engineering Physics, University of Wisconsin – Madison)

SCIENTIFIC STAFF: Dr. Narasimhan Swaminathan, Dr. Peng Xu, Laura Jamison

PROGRAM SCOPE: The scope of this program is to determine relationships between the structure and radiation response of nanocrystalline (nc) silicon carbide (SiC) and to determine under what conditions refining the grain size leads to improved radiation resistance. The efforts involve both computational modeling and experiments. On the computational side, we are developing a continuum model of irradiation-induced defect evolution and overall radiation response, which model is based on input from molecular dynamics (MD) simulations and *ab initio* calculations. Experiments are being carried out to validate predictions of our models and to compare radiation resistance of nc and polycrystalline samples.

PROJECT PROGRESS

Abstract

We hypothesized that two mechanisms can lead to differences in radiation responses of nc and coarse-grained materials. Firstly, the large GB fractions in nc materials may alter the defect production rates and secondly, increased GB fraction can also lead to more efficient annihilation of the irradiation defects. To understand the former phenomenon, we performed MD simulations of radiation cascades in nc SiC with varying grain sizes. We found that grain size does not have a significant effect on the initial (a few picoseconds after cascade initiation) defect production rates. This result suggests that size effects on radiation damage may be due to long-term evolution of the point defects, as they interact with each other and with GBs. To investigate this long-term behavior of defects we extended a rate theory model to binary alloys and we used this model to predict size effects on radiation-induced amorphization. Defect production rates are derived from MD simulations while the kinetic parameters for diffusion and defect reaction rates are taken from *ab initio* calculations. Our model reveals a complex dependence of dose to amorphization on grain size and temperature. Results show that grain size can both enhance and reduce the dose to amorphize SiC depending on the temperature regime.

In the experimental part of the project we spent a significant amount of time synthesizing nc SiC samples. We have succeeded on preparing CVD grown nc SiC and we are now investigating its response to radiation. In the meantime we irradiated nc SiC powders to

determine the dependence of a critical temperature to amorphization on the grain size. The preliminary results are in a qualitative agreement with predictions of our models.

Results and key findings: A brief description of the methods and key findings are summarized in the following sections.

MD simulations: MD simulations of displacement cascades were conducted on single crystal (sc) and nc SiC with grain sizes (5,7,10 and 12 nm) with 4KeV and 10KeV Si atom as the PKA (Primary Knock on Atom). The primary motivation was to discover whether the increased GB fraction in the nc material actually affected defect production. The simulations used the Tersoff [1] force field for long range interactions and the ZBL force field [2] to capture the short range interactions occurring during collisions. The defect production (p) is defined as:

$$p = \frac{D_{IG}^{nc} - D_{IG}^{sc}}{D_{IG}^{sc}}$$

where D_{IG}^{nc} is the total number of defects inside the grains of the nc and D_{IG}^{sc} is the total number of defects in an equivalent volume of the sc. The equivalent volume in the sc was determined using a new mapping method the details of which can be found in Ref. [3]. The parameter p (for 4KeV simulations) is plotted in Fig. 1 and we found that the increased GB fractions for the grain sizes we considered did not affect the initial defect production. The 10KeV simulations showed the same qualitative trends.

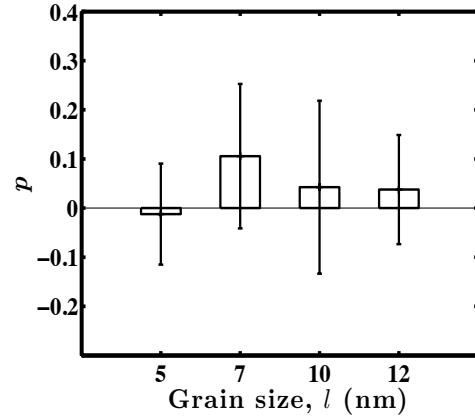


Figure 1: Defect production p showing that GBs do not alter defect production in the primary cascade regime

Continuum Modeling: Although the effect of GBs on primary defect production in nc SiC is insignificant, the GB can act as sinks for defects and therefore affect a long-term damage evolution. Processes like radiation-induced amorphization typically take place on time scales from a few seconds to several years. To determine whether the presence of GBs affected the amorphization response of nc SiC, we developed a continuum model by extending the rate-theory framework to include multiple sub-lattices. Relative concentration of defects of a given type was estimated based on our MD simulations of radiation cascades, while the migration, formation [4, 5] and recombination [6] energies needed for the diffusion and recombination reactions were taken from published *ab initio* data. In Fig. 2 we plot the dose to amorphize SiC of various grain sizes at different temperatures. We show that the resistance to amorphization displays a cross over in its behavior at 448K. Below this critical temperature of 448K, there is an optimum grain size for which the resistance is maximum. For temperatures larger than 448K, larger grain sizes seem to have a higher resistance to amorphization than smaller ones, which means that at these temperatures refining the grain size is not a promising path to increasing radiation resistance. It is therefore very important to consider operating temperatures of nc materials. As shown in Fig. 3 we also found that the critical temperature for amorphization was higher for finer grains than for coarser ones. For example, at 10nm the critical temperature is about 1280K and for 5 μ m it is about 600K.

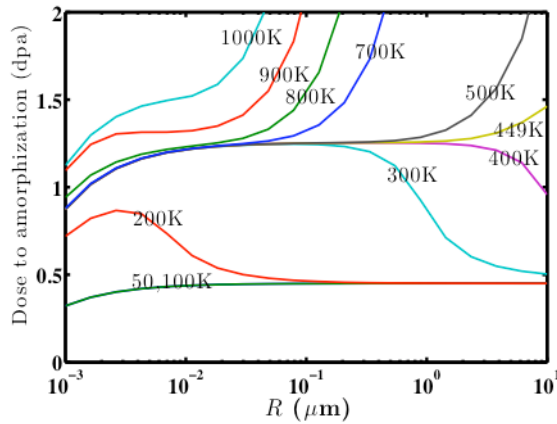


Figure 2: Dose to amorphization vs. grain sizes for various temperatures

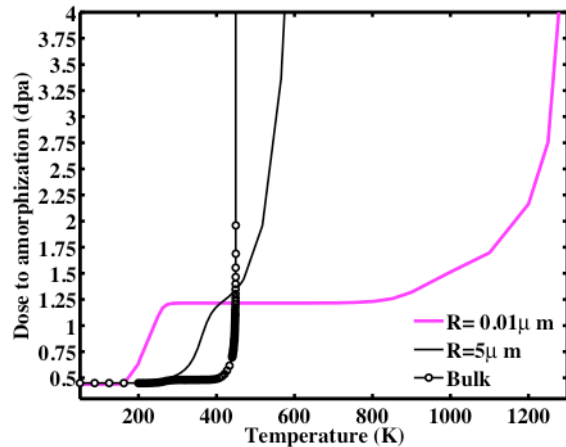


Figure 3: Dose to amorphization vs. Temperature curves for bulk, and grain sizes of 5μm and 10nm

Experiments: Irradiation experiments were conducted on 10nm and 45-55nm SiC powders

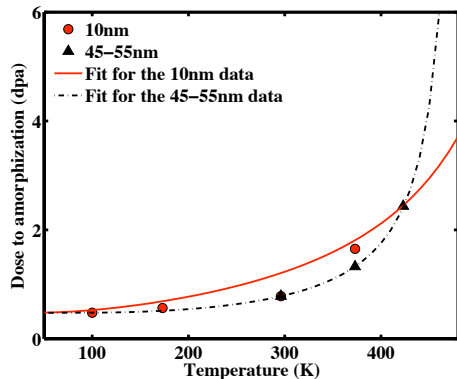


Figure 4: Dose to amorphization vs Temperature experimental data and fit for 10nm and 45-55nm SiC samples

using Kr^{2+} . The main motivation was to determine the critical dose to amorphization. Figure 4 shows the dose to amorphization for several temperatures for both the 10nm, and the 45-55nm samples. Also shown are curve fits of the data to the equation $\ln(1-D_0/D)=C-(E/kT)$ [7], where D_0 is the extrapolated dose to amorphization at 0K and D is the dose to amorphization at a particular temperature (T). From this fit, the critical temperature for 10nm grain size was determined to be 625K, and for 45-55nm grain size 410K. While this data is still preliminary, from the fit it appears that the critical temperature for amorphization is higher for smaller sized grains (10nm) than for coarser ones (45-55nm). This result is qualitatively agrees with the modeling results discussed in the previous sections (see Fig. 3).

Summary and key findings: In conclusion we have shown that the initial defect production remains unaffected by the GBs in SiC. Over longer time scales, the interaction between temperature, GB and the various point defects is quite complex. Whether the smaller grain sizes will enhance resistance to amorphization or not actually depends on the temperature regime. At smaller temperatures and small grain sizes the diffusion of interstitials and their annihilation at GB enhance the resistance to amorphization ($T < 448\text{K}$). At higher temperatures ($T > 448\text{K}$) however, excessive annihilation of the interstitials at GBs leave behind vacancies, which actually decrease the resistance to amorphization. The experiments also show that smaller sized grains

might have a higher critical temperature for amorphization than coarser grains. This conclusion is in qualitative agreement with the physics explained by the theoretical modeling using rate theory methods as described above.

References

1. Tersoff, J., *Chemical order in amorphous silicon carbide*. Physical Review B, 1994. **49**(23): p. 16349-16352.
2. Ziegler, J.F., J.P. Biersack, and U. Littmark, *The stopping and range of ions in solids*. Vol. 1. 1985: Pergamon, Oxford.
3. Swaminathan, N., Kamenski, P.J., Morgan, D., Szlufarska, I., *Effects of grain size and grain boundaries on defect production in nanocrystalline 3C-SiC*. Journal of Nuclear Materials, 2010. **58**(8).
4. Bockstedte, M., A. Mattausch, and O. Pankratov, *Ab initio study of the migration of intrinsic defects in 3C-SiC*. Physical Review B, 2003. **68**(20).
5. Schrader, D., Khalil, S., Heim, A., Gerczak, T., Allen, T., Szlufarska, I., Morgan, D., *Ag Diffusion in cubic silicon carbide*. Journal of Nuclear Materials, 2010. Submitted.
6. Roma, G. and J.P. Crocombette, *Evidence for a kinetic bias towards antisite formation in SiC nano-decomposition*. Journal of Nuclear Materials, 2010. **403**(1-3): p. 41.
7. Weber, W.J., *Models and mechanisms of irradiation-induced amorphization in ceramics*. Nuclear Instruments and Methods in Physics Research B, 2000. **166-167**: p. 98-106.

Electrical, mechanical and thermal properties of single molecules

Nongjian (NJ) Tao

Arizona State University, Tempe, AZ 85287-3503, email: njtao@asu.edu

Program Scope

Building a device using a single or a few molecules is one of the ultimate goals in technology. Owing to many unique electronic properties of molecules, electronic applications have been a focus of molecular devices. In addition to wonderful electronic properties, many molecules have attractive electromechanical, thermal electrical and molecular recognition properties that are fundamentally different from conventional bulk materials, which may lead to new devices. In this project we:

- Determine the lifetime and stability of a single molecule bound to two electrodes;
- Study local heating and cooling in single molecule junctions due to electron-phonon and electron-electron interactions;
- Measure electron-phonon interactions in single molecule wires;
- Explore piezoelectric properties of single molecules.

The project has led to new insights into some of the most fundamental properties of single molecule junctions, and provided us with basic knowledge and skills required for reaching the ultimate goal of building functional devices based on single molecules.

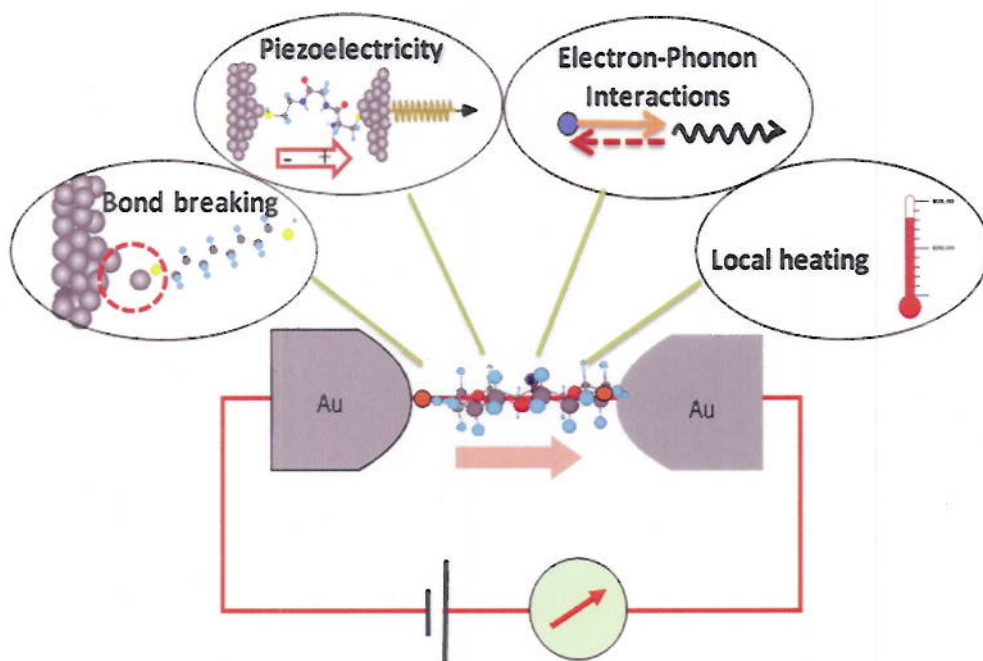


Fig. 1 A molecule electrically “wired” to two electrodes serves a model system for studying charge transport in single molecules and basic building block for developing device applications. This project focuses on the electrical, thermal and mechanical properties of single molecules, in order to achieve a better understanding of charge transport and to explore new functions of single molecules.

Progress Report

To date we have completed most of the proposed tasks and expect to complete the rest by the end of the project. We summarized here some of the findings.

Current-induced local heating and cooling in single molecule junctions

Current-induced local heating of molecules is a critical issue both for understanding energy dissipation mechanisms in molecules, and for developing device applications with molecules. We have carried out a systematic study of local heating in single molecules (*n*-alkanedithiol, *n*=6, 8 and 10, or C6, C8 and C10) covalently attached to two gold electrodes as a function of molecular length and applied bias. In order to determine the effective temperature, we studied the breakdown of thousands of molecular junctions and measured the average distance *L* over which the molecular junctions can be stretched before breakdown. Since the breakdown process is thermally activated, *L* is directly related to the effective local temperature of the molecule–electrode contacts. We find that at fixed bias the

effective temperature of a molecular junction decreases with the molecular length. More interestingly, the effective temperature first increases with applied bias, and then decreases after reaching a maximum, indicating an effective cooling in single molecules at large biases (Fig. 2). Current-induced cooling is less intuitive than current-induced heating but may be understood based on the following considerations. When electrons traverse the molecule from one electrode to the other, a portion of their energy is transferred to the ionic degrees of freedom via electron-phonon interactions and another portion to the electronic degrees of freedom via electron-electron interactions, i.e., the underlying Fermi gas heats up. With increasing bias, the current-carrying electrons transfer an ever-increasing portion of energy to the other electrons, which leaves a decreasing available energy to heat the ions. Since the heated electrons carry energy away from the molecular junction and eventually dissipate it to the bulk of the electrodes, the electron heating effect lowers the effective temperature of the ionic degrees of freedom in the molecular junction.

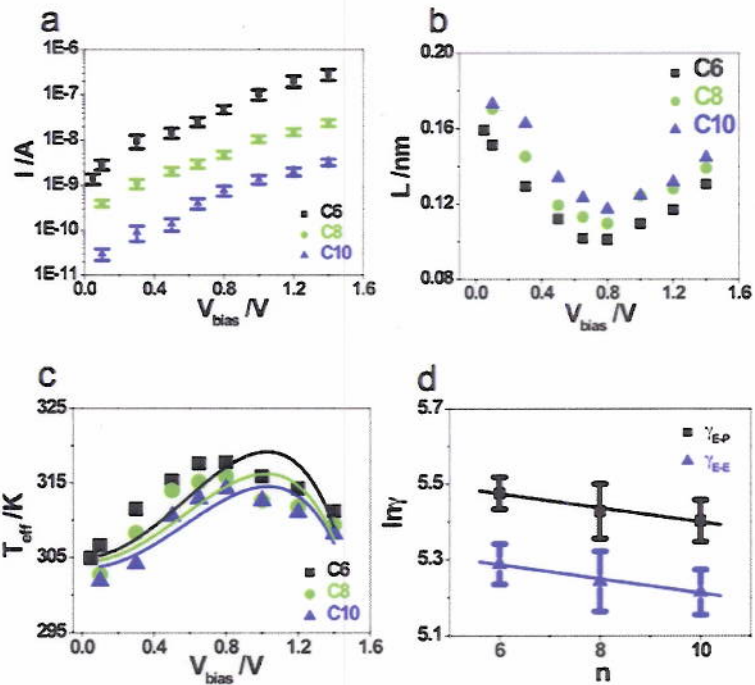


Fig.2. (a) Current through single molecule junctions vs. applied bias (V_{bias}). (b) Average stretching distance (L) vs. bias voltage. (c) Effective temperature (T_{eff}) vs. bias and the black (C6), green (C8) and blue (C10) curves are the fits with Equation 1. (d) The semi-logarithmic plots of γ_{e-p} (black squares) and γ_{e-e} (blue triangle) vs. molecular length. All the measurements are carried out at room temperature with stretching rate fixed at 20nm/s.

Rectification and asymmetric current-induced instability

One of the most exciting device functions is the diode or rectification behavior, which was first envisioned by Aviram and Ratner. The Aviram-Ratner molecular diode consists of a donor (D) and an acceptor (A) separated with a σ -bridge in which the forward current is from A to D. To date most experimental studies of molecular diodes have been carried out using Langmuir-Blodgett films and self-assembled monolayers, which involve many molecules. The diode behavior in single molecules is much less studied. To achieve single molecule rectification effect, one must 1) provide a reliable and symmetric contact between an asymmetric molecule and two electrodes, and 2) be able to determine and control the orientation of the molecule relative to the polarity of the applied bias voltage. Reliable and symmetric contacts can be achieved via covalent binding between two terminal groups of the molecule and two metal electrodes, allowing for statistical analysis of electron transport of thousands of repeated formed metal-molecule-metal junctions using STM break junction techniques. However, the orientation of the molecule with respect to the polarity of the bias is difficult to control and determine using these methods. We have combined an AC-modulation STM-break junction method with selective deprotection of terminal groups of molecules to measure unambiguously the I-V characteristics of single molecules and to control their orientation.

Using this approach, we have measured the conductance of two structurally similar molecules, one symmetric and one asymmetric. The asymmetric molecule shows a pronounced rectification in the I-V curves (Fig. 3a), which is interpreted in terms of asymmetric localization of the hole ground state wave function of the molecule in the applied electric field. The work demonstrates that symmetry breakdown in a molecule introduced by chemical substitution gives rise to a dramatic change in the

electron transport and leads to significant rectification. Moreover, proper engineering of the protection groups of the molecule allows control of the molecular orientation. In addition to rectification, we have also studied the stability of the molecule diode (Fig. 3b). The current increases rapidly in the forward direction when the bias reaches ~ 1.8 V. At large currents (few μA), the Au-molecule-Au junction becomes unstable. However, instead of breakdown of the molecular junction, the instability leads to the formation of Au point contacts between the two electrodes (Fig. 3a). The absence of the instability under a reverse bias rules out electric field as the direct cause of the instability. We believe current induced local heating is at least partially responsible for the observed instability.

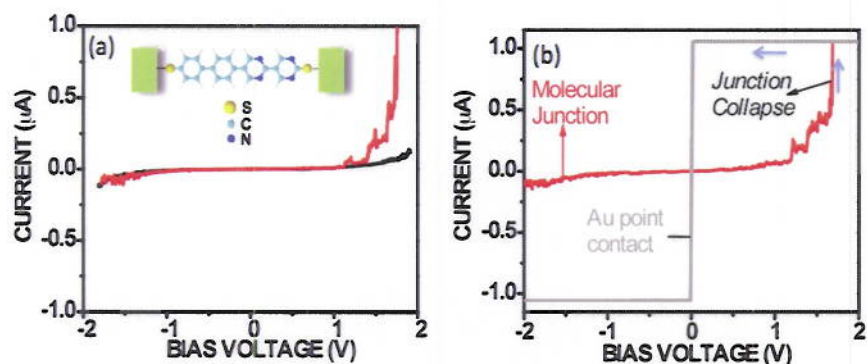


Fig. 3.(a) **Rectification:** I-V curve the asymmetric dipyrindinyl-diphenyl showing rectification (red line). (b) **Current-induced instability:** When the forward current reaches $\sim 1 \mu\text{A}$, the molecular junction becomes unstable, and a point contact forms between the two electrodes.

Electron-phonon interactions and energy dissipation

We have studied electron-phonon interactions in many individual junctions to determine the variability of the phonon modes between junctions, and the dependence of the phonon modes on atomic scale details of the molecule-electrode contact geometry (Fig. 4). Furthermore, by studying a single molecule that is covalently bound to two electrodes, the conductance changes due to individual phonon modes in the molecular junction were precisely measured, making it possible to estimate the phonon damping rates from the conductance changes. We also explored certain cases where decreases in the conductance were observed in single molecule junctions. These observations demonstrate that electron-phonon coupling can contribute significantly to the total conductance of a molecular junction, and that the specific configuration of the molecular junction can affect how a phonon mode changes the conductance.

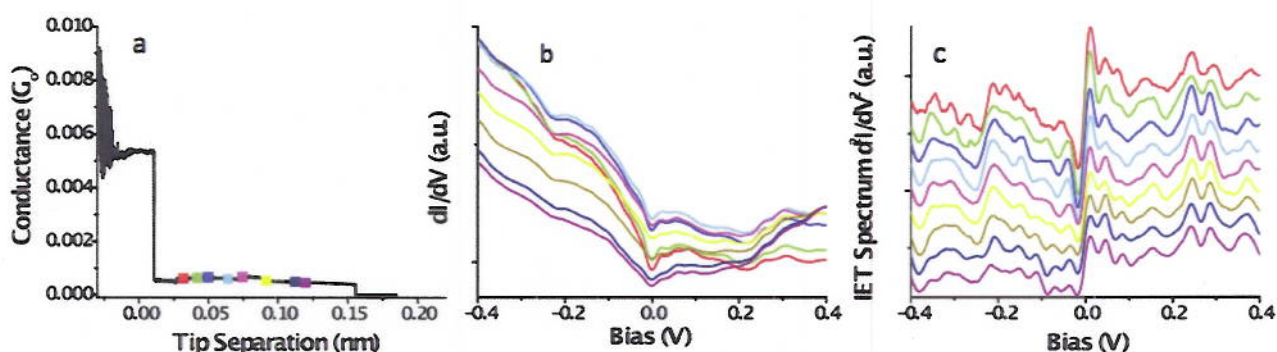


Fig. 4. a) Conductance of a single molecule junction vs. stretching distance. The colored squares mark the positions where IET spectrum was measured. b) First derivatives of I-V curves. c) Second derivatives of I-V curves.

Energy dependent conductance switching

We have developed a low temperature setup to create highly stable molecular scale junctions, which leads to an opportunity to explore unexpected behavior in molecular junctions. One phenomenon that we have observed in many different molecular junctions is voltage dependent conductance switching in molecular junctions. Several junctions have clearly demonstrated conductance switching with an onset that is energy dependent. As is shown in Fig. 5, a clear change in the conductance of the

molecular junction occurs at ~ 200 mV bias for this junction. Between ± 200 mV the conductance is relatively constant, but at higher absolute energies the conductance becomes unstable and switching occurs in the junction. It is currently unclear whether this switching is due to contact changes, where the charge carriers are losing energy in the leads and causing changes in the contact geometry. What is apparent is that the switching is symmetric about zero bias, and it occurs at different biases in different junctions. Continued work during the rest of the current funding period may reveal important information about the inherent stability of molecular-scale devices.

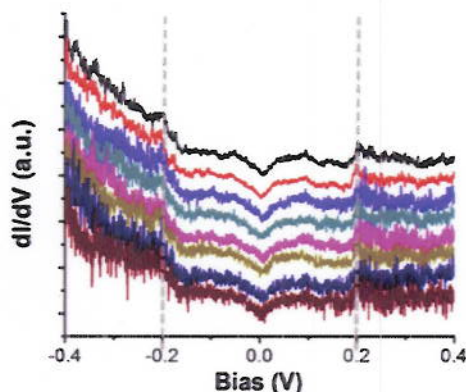


Fig. 5. Energy dependent conductance switching in single molecule junctions. The data shows that the conductance of a molecular junction begins switching at well-defined applied biases (marked by two vertical dashed lines).

Publications

1. Joshua Hihath, Christopher Bruot, and N.J. Tao, "Electron-Phonon Interactions in Single Octanedithiol Molecular Junctions", *ACS Nano*, 2010, in press.
2. Ismael Díez-Pérez, Joshua Hihath, Youngu Lee, Luping Yu, Lyudmyla Adamska, Mortko A. Kozhushner, Ivan I. Oleynik and N.J. Tao, "Gate-controlled electron transport in coronenes as a bottom-up approach towards graphene transistors", *Nature Communication*, 2010, in press.
3. Ismael Díez-Pérez, Joshua Hihath, Youngu Lee, Luping Yu, Lyudmyla Adamska, Mortko A. Kozhushner, Ivan I. Oleynik and N.J. Tao, "Rectification and Stability of a Single Molecular Diode with Controlled Orientation", *Nature Chemistry*, 1, 635-641(2009).
4. N.J. Tao, "Push the right button", *Nature Chemistry*, 1, 108(2009).
5. J.L. Xia, F. Chen, J.H. Li and N.J. Tao, "Measurement of Quantum Capacitance of Graphene", *Nature Nanotechnology*, 4, 505-509(2009).
6. F. Chen, J.L. Xia, D.K. Ferry and N.J. Tao, "Dielectric screening enhanced performance in graphene FET", *NanoLetters*, 6, 2571-2574(2009).
7. F. Chen, J.L. Xia and N.J. Tao, "Ionic Screening of Charged-Impurity Scattering in Graphene", *NanoLetters*, 9, 1621-1625(2009).
8. F. Chen, Q. Qing, J.L. Xia, J.H. Li and N.J. Tao, "Electrochemical gate-controlled charge transport in graphene in ionic liquid and aqueous solution", *J. Am. Soc.*, 131, 9908-9909(2009).
9. F. Chen and N.J. Tao, "Electron transport in single molecules: from benzene to graphene", *Acc. Chem. Res.*, 42, 429-438(2009).
10. J. Hihath and N.J. Tao, "Rapid measurement of single-molecule conductance", *Nanotechnology* (2008), 19(26), 265204/1-265204/7.
11. J.L. Xia, I. Diez-Perez, N.J. Tao, "Electron Transport in Single Molecules Measured by a Distance-Modulation Assisted Break Junction Method." *Nano Letters* (2008), 8(7), 1960-1964.
12. J. Hihath, C.R. Arroyo, G. Rubio-Bollinger, N.J. Tao and N. Agrait. "Study of electron-phonon interactions in a single molecule covalently connected to two electrodes", *Nano Letters* (2008), 8(6), 1673-1678.
13. Z.F. Huang, F. Chen, R. D'Agosta, P. A. Bennett, M. Di Ventra and N.J. Tao. "Local-Heating in Single Molecule Junctions: Evidence of Electron-Phonon and Electron-Electron Interactions", *Nature Nanotechnology*, 2, 698-703(2007).
14. Fang Chen, Zhifeng Huang, N.J. Tao, "Forming single molecular junctions between ITO electrodes", *Appl. Phys. Lett.*, 91, 162106(2007).
15. Xiulan Li, Joshua Hihath, Fang Chen, Takuya Masuda, Ling Zang and N.J. Tao, "Thermally Activated Electron Transport in Single Redox molecules", *J. Am. Chem. Soc.*, 129, 11535-11542(2007).
16. Zhifeng Huang, Feng Chen, Peter A. Bennett and Nongjian Tao "Single Molecule Junctions Formed via Au-Thiol Contact: Stability and Breakdown Mechanism", *J. Am. Chem. Soc.*, 129, 13225-13231(2007).
17. J. Hihath, F. Chen, P.M. Zhang and N.J. Tao, "Thermal and Electrochemical Gate Effects on DNA Conductance", *J. Phys.*, 19, 215202-215221(2007).
18. F. Chen, J. Hihath, Z.F. Huang, X.L. Li and N.J. Tao, "Measurement of single molecule conductance", review, *Annual Review of Physical Chemistry*, 58, 535-564(2007).

Chemomechanics of Far-From-Equilibrium Interfaces (COFFEI)

Principle Investigators: Harry L. Tuller (Rm.13-3126; tuller@mit.edu), Craig Carter (13-5018; ccarter@MIT.EDU), Yet Ming Chiang (13-4086; ychiang@MIT.EDU), Yang Shao-Horn (3-342A, shaohorn@mit.edu) Krystyn Van Vliet (8-237; krystyn@mit.edu), Bilge Yildiz (24-210; byildiz@mit.edu), Sidney Yip (24-208; syip@MIT.EDU). 77 Massachusetts Ave. Cambridge, MA 02139

COFFEI Thrust I (PIs: Carter, Chiang and Van Vliet; Students/postdocs: Woodford, Qu):

Scope: Develop continuum models linking electrochemical cycling conditions to fracture mechanics failure criteria for lithium intercalation compounds. Study how electrochemical duty cycles and electrode microstructures influence mechanical damage accumulation in lithium-ion battery active materials. This requires a novel synthesis of electrochemistry, battery engineering, and solid mechanics. To the best of our knowledge, this work represents the first synthesis of electrochemical kinetics and fracture mechanics as applied to battery materials.

Recent progress: We have derived a fracture mechanics failure criterion for individual electrode particles subjected to constant current electrochemical cycling [1]. To demonstrate the utility of our method, we use galvanostatic charging of $\text{Li}_x\text{Mn}_2\text{O}_4$ as a model system. Our fracture mechanics analysis predicts a critical C-rate above which active particles fracture; this critical C-rate decreases with increasing particle size. We produce an electrochemical shock map, shown in Figure 1(a), a graphical tool that shows regimes of failure depending on C-rate, particle size, and the material's inherent fracture toughness K_{Ic} . The different curves on the map indicate different possible values of fracture toughness, which is presently unknown for most lithium-ion battery materials. We are measuring fracture toughness for LiCoO_2 and LiFePO_4 , two commercially important positive electrode materials. Preliminary results showed that both the fracture toughness (K_{Ic}) and elastic modulus (E) varied significantly between grains. From our analysis, we find that the fracture dynamics are sensitive to the gradient of diffusion-induced stresses at the crack tip; as a consequence, small initial flaws grow unstably and are therefore potentially more damaging than larger initial flaws, which grow stably. This can be seen from the changing slope of the stress intensity factor – flaw size relationship shown in Figure 1(b).

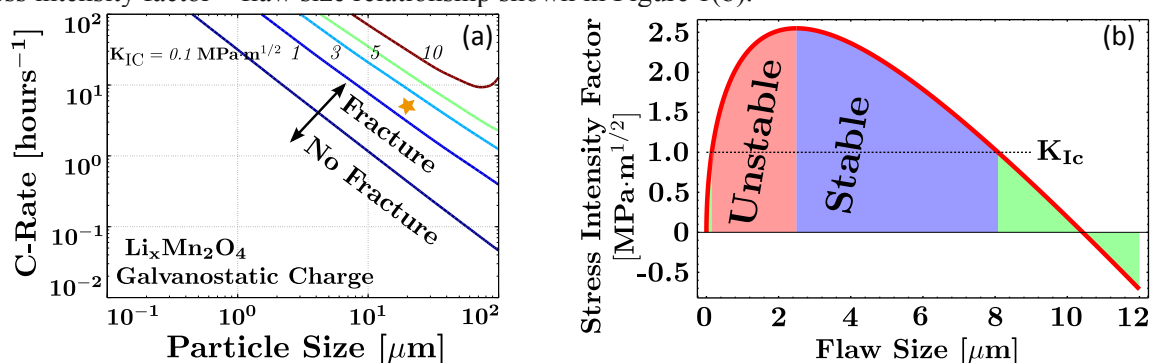


Figure 1: (a) Electrochemical Shock Map for LiMn_2O_4 showing critical combinations of particle size and charging rate for fracture of individual particles; (b) Calculated stress intensity factor - flaw size relationship for one particular set of conditions.

Future Plans:

1. Experimental validation of the electrochemical shock model using in situ optical imaging of single particle electrodes and/or acoustic emission measurements of composite electrodes during electrochemical cycling.
2. Embedding the electrochemical shock model [1] in existing mean-field models for composite battery electrodes. This will allow us to model cyclic fatigue of these electrode particles during different “real-world” duty cycles.

3. Finite element modeling of compatibility stresses due to anisotropic phase transformation strains in polycrystalline particles using LiCoO_2 as a model system.
4. Determination of distribution of E and fracture toughness within and among grains. Here, we aim to determine whether correlations exist between grain orientation and fracture toughness.
5. Establish the elastic properties and fracture toughness of LiCoO_2 grains and bulk compacts, possibly extending to elevated temperature and pre-/post-cycling.
6. Measurement of fracture toughness for an additional oxide of interest, LiFePO_4 .

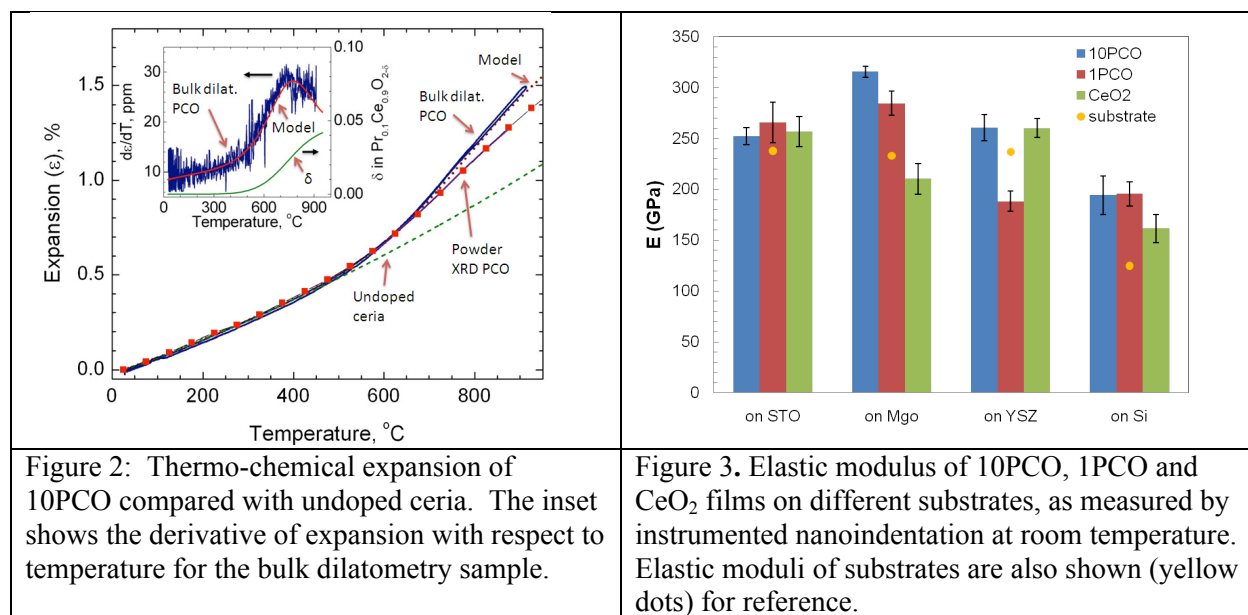
Publications:

[1] W.H. Woodford, Y.-M. Chiang, and W.C. Carter, “‘Electrochemical Shock’ of Intercalation Electrodes: A Fracture Mechanics Analysis,” *J. Electrochem. Soc.*, 157 [10] A1052-A1059 (2010).

COFFEI Thrust II (PIs: Tuller, Van Vliet & Yip; students/posdocs: Bishop, Jung, Kuru & Qu):

Program Scope: Investigate interplay between chemical and mechanical behavior of solid oxide fuel cell materials and related thin films. Nonstoichiometry and high point-defect densities lead to oxygen “breathing modes” i.e. dilation connected with formation of oxygen vacancies. Resulting *chemical strain* effects induce mechanical stresses leading to membrane fracture; routes for reducing chemical expansion are therefore important for stabilizing such structures. Objectives include quantification of elastic and plastic properties at elevated temperature (up to 800°C) and oxygen rich environments using nano-mechanical and other tools and to investigate role of strain in influencing defect formation and transport. Two metal oxide systems were chosen as model systems: $\text{SrTi}_{1-x}\text{Fe}_x\text{O}_{3-\delta}$ (STF) and $\text{Pr}_{1-x}\text{Ce}_x\text{O}_{2-\delta}$ (PCO).

Recent Progress: Study of thermo-chemical expansion and defect equilibria in bulk $\text{Pr}_{0.1}\text{Ce}_{0.9}\text{O}_{2-\delta}$ was initiated. We also report on nano-indentation measurements of thin films of $\text{Pr}_{0.1}\text{Ce}_{0.9}\text{O}_{2-\delta}$. $\text{Pr}_{1-x}\text{Ce}_x\text{O}_{2-\delta}$ (PCO) is a particularly interesting material given that it releases significant oxygen with decreasing oxygen partial pressure ($p\text{O}_2$) and/or heating. Figure 2 shows our measurements for expansion as a function of temperature in 10PCO ($\text{Pr}_{1-x}\text{Ce}_x\text{O}_{2-\delta}$ $x=0.1$). The sample initially undergoes thermal expansion followed by a significant positive deviation from “linear” thermal expansion above $\sim 500^\circ\text{C}$ where non-stoichiometry (δ) begins to increase. This *chemical expansion* can increase the measured coefficient of thermal expansion from ~ 10 to ~ 28 $\text{ppm}^\circ\text{C}^{-1}$ as shown in the inset of figure 1. Using this data and a defect equilibria model that we have developed, we extract a chemical expansion coefficient (α_c), analogous to the thermal expansion coefficient, $\epsilon_c = \alpha_c \Delta\delta$ where $\Delta\delta$ is the change in stoichiometry. We find $\alpha_c = 0.086$ per δ for 10PCO, similar to literature values for the reduction of undoped and acceptor doped ceria. The elastic modulus may also vary with these chemical and strain changes. One way to induce strain is to deposit PCO on substrates with different lattice parameters. We have initiated instrumented nanoindentation experiments in air at room temperature on $\text{Pr}_{0.01}\text{Ce}_{0.99}\text{O}_{2-\delta}$ (01PCO films), $\text{Pr}_{0.1}\text{Ce}_{0.9}\text{O}_{2-\delta}$ (10PCO) and CeO_2 films on four different substrates: STO, MgO, YSZ and Si. Thin films with thickness $\sim 500 - 700$ nm were produced using pulsed laser deposition. Indentation results are shown in Fig. 3. To the best of our knowledge, these data represent the first measurements of elastic modulus on PCO films. We found that although the elastic moduli of 10PCO, 1PCO and CeO_2 on STO are the same within measurement error, the elastic properties showed significant differences among samples when deposited on MgO substrates: $E_{10\text{PCO}} > E_{1\text{PCO}} > E_{\text{CeO}_2}$. On YSZ, $E_{10\text{PCO}}$ is about 23% higher than $E_{1\text{PCO}}$, while $E_{10\text{PCO}}$ is comparable to E_{CeO_2} . On Si, films of both 10PCO and 1PCO exhibited a higher E than films of CeO_2 . These films are residually strained by the deposition process, due to both peening effects and thermal mismatch between films and substrates. Thus, we find that the elastic properties and fracture toughness of films on different substrates can be tuned by changing the deposition parameters and substrate materials. AFM images were also acquired on these films to quantify the surface roughness and film morphology as a function of film composition and substrate.



Future Plans:

1. Correlation of film elastic modulus to film texture.
2. Receipt and installation of new instrumentation that will enable nanoindentation experiments at elevated temperature and controlled partial pressure of oxygen.
3. Measurement of $E(T)$ and $E(P_{O_2})$ for 10PCO, 1PCO and CeO₂ films up to 800°C.
4. Measurement of the chemical and thermal expansion of films at high temperature, via expansion-induced displacement of the nanoindenter probe during expansion.
5. Measurement of the chemical and thermal expansion of films at high temperature and controlled p_{O_2} using XRD

List of Papers:

[2] *Tailoring Material Properties Through Defect Engineering*, H. L. Tuller and S.R. Bishop, *Chemistry Letters*, (invited review; in print)

COFFEEI Thrust III (PIs: Tuller, Yildiz & Shao-Horn; students/posdocs: Jung, Kushima, Han, Chen, Cai, Crumlin, Mutoro):

Program Scope: For enabling durable and economic solid oxide fuel cells (SOFCs) at intermediate temperatures, highly active cathode surface chemistries are needed for oxygen reduction. For this purpose, the equilibrium surface structure, chemistry and electronic and catalytic properties of *thin film cathodes* are being investigated at SOFC working conditions of temperature, pressure. In addition, our goal is to assess the mechanistic role of “lattice strain” as a thermodynamic and kinetic driver of the oxygen reactions and transport in SOFC materials. We have taken a multidisciplinary approach integrating new surface sensitive measurements (High resolution Scanning Tunneling Microscopy and Spectroscopy (STM, STS), X-ray Photoelectron Spectroscopy (XPS)), Electrochemical Impedance Spectroscopy (EIS), together with first principles-based modeling and simulations to improve our understanding of the interactions between energy band and defect structures, surface chemistry, strain and electrochemical performance.

Recent Progress: Two related perovskite oxide systems are under investigation. The first, Sr(Ti_{1-x}Fe_x)O₃ (STF), in the form of dense thin films, exhibits superior mixed-conductivity with capability of controlling properties through Fe substitution renders STF an attractive model cathode material. The surface exchange kinetics of STF were examined over a wide range of x and were found to be charge transfer limited at high p_{O_2} and oxygen adsorption limited at low p_{O_2} . The charge transfer limitation was directly tied to the energy band structure of STF that could be varied systematically by control of the Fe/Ti ratio on the B-site. The surface of highly textured PLD prepared Sr(Ti_{0.65}Fe_{0.35})O₃ films exhibited clear Sr

enrichment with the A to B site ratio of 2.1 compared to the bulk nominal value of 1. STS (first-of-a-kind designed to operate at temperatures to 700°C and gas pressures to 1 mbar – 1 bar range) showed the electronic structure to transition from an insulator to the metallic state from room temperature to 400°C, as opposed to the bulk semiconducting characteristics. The oxygen exchange kinetics were found to slow with increasing Sr segregation. Our early observations show that the surface electronic state, topography and chemistry are sensitive to temperature and partial pressure of oxygen, and that they respond in a way different from the bulk studies of this material.

The second system examined is the perovskite $\text{La}_{1-x}\text{Sr}_x\text{CoO}_{3-\delta}$ (LSC), Fig. 4, which exhibits very good cathode behavior at intermediate temperatures. To understand how strain could be playing a role in Oxygen Reduction Reaction (ORR) kinetics, it is important to establish what the strain state is at high temperatures comparable to SOFC operating conditions. A Panalytical four-circle diffractometer with gas chamber and in-situ heating stage was used to obtain XRD spectra of ~100 nm thick epitaxial LSC(80:20) and LSC(60:40) films in air from RT to 550 °C. Table 1 provides in-plane, normal, and relaxed lattice parameters thermal expansion coefficients for LSC(80:20) and LSC(60:40) thin-films. While both epitaxial LSC(80:20) and LSC(60:40) thin-films relaxed thermal expansion coefficients are ~20% larger than reported bulk values, the in-plane and normal coefficients were significantly different (60% and -50%) relative to bulk values. EIS measurements at elevated temperatures are therefore performed on films are under tensile strains normal to the film and compressive strain in-plane. These show distinctively different performance than *bulk* electrodes.

In related work, we apply density functional theory (DFT) formalism with Hubbard-U correction for strongly correlated electronic systems, to determine the dominant strain-driven mechanisms governing both the thermodynamics and kinetics of unit processes that influence the oxygen reduction kinetics; namely the oxygen vacancy formation energy in the bulk, and oxygen molecular adsorption and vacancy formation energies on the surface, and the energy barriers of dissociation, adsorbed oxygen transport, and vacancy transport on the surface of LaCoO_3 . We show that elasto-plastic effects cause a transition in the adsorption mechanism from chemisorption to physisorption. An implication of this work is the prospect of controlling the oxide reactivity through strain to develop highly active ionic nano-structures in, for example, solid oxide fuel cells, sensors, and batteries.

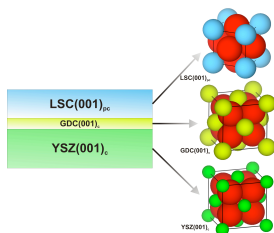


Figure 4: (a) schematic of LSC/GDC/YSZ(001) thin-film with oriented unit cell representations for each material and their relative alignment with respect to each other.

Table 1: LSC(80:20) and (60:40) normal, in-plane, and relaxed average thermal expansion coefficient.

	Average Thermal Expansion Coefficient $10^{-6}/\text{C}^\circ$ (stdev)		
	normal (<i>c</i>)	in-plane (<i>a</i>)	relaxed (\hat{a})
LSC(80:20)	27.22 (1.50)	8.54 (0.92)	19.84 (1.11)
LSC(60:40)	27.19 (4.08)	8.08 (2.46)	19.53 (1.28)

List of Papers:

- [3] Akihiro Kushima, Sidney Yip, and Bilge Yildiz, Competing Strain Effects in Reactivity of LaCoO_3 with Oxygen, *Physical Review B*, in print,
 [4] *Catalytic Activity Enhancement for Oxygen Reduction on Epitaxial Perovskite Thin Films for Solid Oxide Fuel Cells*, Gerardo Jose la O', Sung-Jin Ahn, Ethan Crumlin, Yuki Oriksa, Michael D. Beigalski, Hans M. Christen and Yang Shao-Horn, *Angew. Chem. Int. Ed.*, accepted, 2010.

COMBINED ATOMISTIC AND MESOSCOPIC STUDY OF DEFORMATION OF BODY-CENTERED-CUBIC TRANSITION METALS: EFFECTS OF ALLOYING AND MAGNETISM

V. Vitek

Department of Materials Science and Engineering, University of Pennsylvania,
Philadelphia, PA 19104
e-mail: vitek@seas.upenn.edu

Grant No. DE FG02-98ER45702

Body-centered-cubic (BCC) transition metals from groups 5B and 6B, α -iron, as well as their alloys, are the most important materials employed in technologies of energy production and conversion. Understanding of microscopic phenomena that govern processes of their fabrication as well as failures, acquired in materials science, physics and chemistry, increased tremendously the efficiency of the development of new materials needed for ever progressing technologies. The goal of this research is to advance our fundamental understanding of the deformation behavior that is, together with the fracture processes, the major failure mechanism encountered in service. The aim is to start from the electronic structure and proceed via atomistic modeling and mesoscopic models with atomistic input to constitutive relations usable at levels where atomistic approach is neither feasible nor needed. This is shown schematically in Fig. 1.

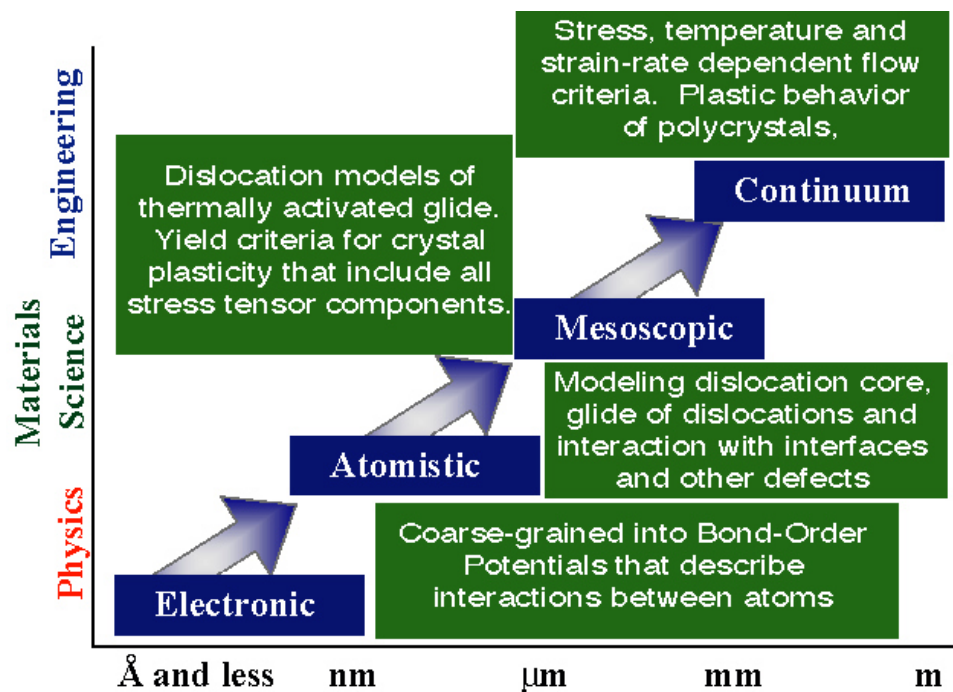


Fig. 1. Scheme of the studies proceeding from electronic structure up to continuum plasticity.

Using this approach we studied the glide of the $1/2[111]$ screw dislocation in Mo and W under the effect of shear, tensile and compressive stresses and combination of shears parallel and perpendicular to the Burgers vector. The most important finding is that the critical resolved shear stress (CRSS) in the maximum resolved shear stress plane (MRSSP) at which the dislocation moves depends not only on the orientation of the MRSSP but also on the shear stress perpendicular to the Burgers vector. Based on this finding we constructed the Peierls barrier that reflects these fundamental features and used earlier dislocation models of the mechanism of formation of kink pairs that controls the glide of screw dislocations at finite temperatures and strain rates. Using these results we then formulated flow criteria for deformation of Mo and W and, as an example, a comparison between calculated and experimentally measured flow stress of W is shown in Fig. 2

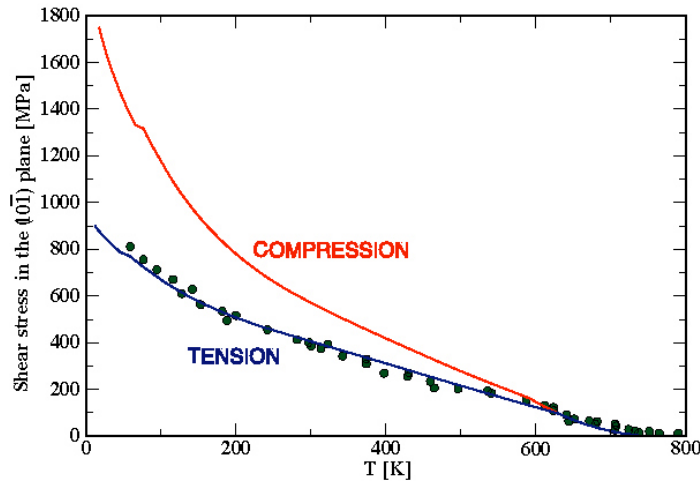


Fig. 2. The temperature dependence of the flow stress in W. Curves are calculated using the present research that demonstrate strong difference between tension and compression arising due to the effect of shear stresses perpendicular to the Burgers vector. Points are measured values but no measurements for compression are available.

Further results of this research encompass explanation of the choice of slip systems in B2 compounds that was achieved by combining investigation of possible APB type faults on $\{101\}$ planes using a density-functional theory (DFT) based method combined with elastic analysis of possible dislocation splittings. The most important finding is that these faults vary from material to material and are not the usually assumed $1/2[111]$ APBs. Similarly, the dislocation splittings were studied in MoSi₂ with the C11_b structure and a possible non-planar dissociation of the $1/2\langle 331 \rangle$ screw dislocations that explains the very low ductility for compression along the $[001]$ direction was identified.

The present studies follow the scheme outlined in Fig. 1. We again employ the bond-order-potentials (BOPs) to describe atomic interactions. While the DFT is at present the state of the art when including fully the electronic structure, the size of the atomic blocks that can be studied and periodic boundary conditions are severe limitation when treating extended crystal defects. Hence, coarse-graining the problem such that the electronic degrees of freedom are removed and the atoms are considered to interact with each other via potentials, is an essential step forward. Earlier we constructed BOPs for several non-magnetic transition metals and the development of the BOP for iron, in which magnetism stabilizes its BCC structure, is now complete. Two new developments proposed are constructions of BOPs for Fe-Cr, which is the primary structural material in advanced nuclear reactors, and for B2 intermetallic compounds based on transition metals, which are all important high-temperature materials. A very important recent

development is advancement of analytical BOPs which will be introduced to our studies in collaboration with the group at University of Bochum.

Similarly as in non-magnetic transition metals, we will investigate the dislocation glide at finite temperatures and strain rates assuming that screw dislocations move via thermally activated formation of kink pairs. This mechanism will be treated in the framework of dislocation models developed earlier but with the stress-dependent Peierls barrier determined so as to reproduce atomistic calculations of the Peierls stress. Here the crucial step is establishment of the Peierls barrier that cannot be done uniquely just from knowledge of the Peierls stress. Hence, we will employ the nudged elastic band model to evaluate the Peierls barrier within the atomistic model which will self-consistently enhance the approach utilizing the Peierls stress the calculation of which is much less time consuming.

An important reserach proposed is study of the possible observation of screw dislocations in BCC metals. Although it is generally assumed that $1/2\langle 111 \rangle$ screw dislocations with non-planar cores control the plastic behavior of BCC metals, the cores of such screw dislocations have never been observed. Hence, we will be modeling a realistic thin foil (Mo and Nb) employed in the high-resolution electron microscopy with the screw dislocation running through the foil. The results will then be used in contrast calculations and provide basis for interpretation of experimental observation.

Summarizing the main thrust of this research, we first develop potentials in order to enable atomistic studies of dislocations and their glide in all non-magnetic transition metals, ferromagnetic iron, Fe-Cr and a number of B2 intermetallic compounds. We then proceed to advance mesoscopic models of dislocation glide at finite temperatures and strain rates using the results of atomistic studies as input for construction of the stress-dependent Peierls barrier that enters these models and develop corresponding yield and flow criteria for crystal plasticity.

Publications from 2008-2010

1. V. Vitek and V. Paidar: Non-planar dislocation cores: A ubiquitous phenomenon affecting mechanical properties of crystalline materials, *Dislocations in Solids*, edited by J. P. Hirth, Elsevier: Oxford, Vol. 14, p. 441, 2008.
2. R. Gröger, A.G. Bailey and V. Vitek: Multiscale modeling of plastic deformation of molybdenum and tungsten: I. Atomistic studies of the core structure and glide of $1/2\langle 111 \rangle$ screw dislocations at 0K, *Acta Materialia* **56**, 5401, 2008.
3. R. Gröger, V. Racherla, J. L. Bassani and V. Vitek: Multiscale modeling of plastic deformation of molybdenum and tungsten: II. Yield criterion for single crystals based on atomistic studies of glide of $1/2\langle 111 \rangle$ screw dislocations, *Acta Materialia* **56**, 5412, 2008.
4. R. Gröger and V. Vitek: Multiscale modeling of plastic deformation of molybdenum and tungsten: III. Effects of temperature and plastic strain rate, *Acta Materialia* **56**, 5426, 2008.
5. R. Gröger and V. Vitek: Temperature and strain rate dependent flow criterion for bcc transition metals based on atomistic analysis of dislocation glide, *Int. J. Materials (Zeit. Metallkunde)* **100**, 315, 2009.
6. M. Cak, M. Sob, V. Paidar and V. Vitek: Stacking Faults and Dislocation Dissociation in MoSi_2 , in *Advanced Intermetallic-Based Alloys for Extreme Environment and Energy Applications*, edited by M. Palm, B.P. Bewlay, M. Takeyama, J.M.K. Wiezorek, Y-H. He, MRS Symposium Proceedings, Vol. 1128, U7-10, 2009.

7. Yi-Shen Lin: Relation between electronic structure and deformation properties of B2 compounds, *MSc Thesis, University of Pennsylvania*, 2009.
8. R. Gröger and V. Vitek: Directional versus central-force bonding in studies of the structure and glide of $1/2\langle 111 \rangle$ screw dislocations in BCC transition metals, *Philos. Mag*, **89**, 3169, 2009.
9. V. Paidar, M. Cak, M. Sob and V. Vitek: Theoretical analysis of dislocation splitting in MoSi_2 , *J. Phys: Conference Series* **240**, 012007, 2010.
10. V. Paidar, Yi-Shen Lin, M. Cak, and V. Vitek: Why is the slip direction in CuZn and FeAl different than in CoTi, *Intermetallics*, **18**, 1285, 2010.

NANOSTRUCTURE PATTERNING UNDER ENERGETIC PARTICLE BEAM IRRADIATION

(Supported by DOE BES under Grant # DF-FG02-02ER46005)

Lumin Wang^{1,2} (Principal Investigator)

Wei Lu³ (Co- Principal Investigator)

¹Department of Nuclear Engineering and Radiological Sciences

²Department of Materials Science and Engineering

³Department of Mechanical Engineering

University of Michigan, Ann Arbor, MI 48109-2104

lmwang@umich.edu

Program Scope

Energetic particle beam irradiation provides a highly controlled means of manipulating material microstructures at the nanoscale, representing an effective way to modify physical properties of materials. This research program explores the unique one step process for creating various forms of patterned nanostructures by using energetic particle beam irradiation. During the previous years, we have demonstrated particle beam induced formation of 1-D periodic surface arrays of nanodots and ripples, 2-D ordered nanodroplets or nanoholes, as well as 3-D networks of nanofibers and void/bubble superlattices that extended underneath the irradiated surface of various materials. The amazing common feature in those nanopatterns is the uniformity of the size of nanoelements (nanoripples, nanodots, nanovoids or nanofibers) and the distance or wavelength separating those features. Our research focuses on understanding of the possible link between those nanoscale patterning of different dimensions and the fundamental scientific basis for nanoscale self-organization processes under irradiation. Defect production and migration, sputtering, redeposition, viscous flow, diffusion and anisotropic movement of species, all of which contribute to the formation of nanopatterns, have been investigated through a combination of *in situ* and *ex situ* microscopic observations and computer modeling.

Recent Progress

Through a systematic study of ion and electron beam irradiation study, we have explored nanostructure patterning on the surface of various material substrates as well as imbedded nanostructures with higher energy irradiation. The roles of material property, initial surface morphology and irradiation parameter control (temperature, incident beam angle, beam energy and flux) have all been explored. The following are some example findings:

The quality of focused ion beam (FIB) induced 1-D nanoripple structures on material surface was found to be greatly dependant on the prior surface treatment (e.g. carbon coating) that changes the initial surface roughness that in turn greatly affects the dynamic competition between the roughening and smoothing processes on the irradiated surface as the irradiation parameter and material properties (G. Ran, et al, APL 2009; Q. Wei et al, PRB 2009).

Ostwald ripening or coalescence that often leads to non-uniform particle sizes during particle growth on material surfaces thus preventing 2-D ordering of particles can be hindered under low energy ion bombardment, and highly ordered and uniform hexagonal patterns of

nanoparticles can be induced at an optimal irradiation condition (Q. Wei, et al, PRL 2009).

Interplay among ion sputtering, redeposition, viscous flow, and surface diffusion is responsible for the 2-D ordered nanohole pattern formation on ion bombarded germanium surface. Simulation of surface morphology evolution based on a damped Kuramoto-Sivashinsky (DKS) growth model has been performed to facilitate the interpretation of the experimental findings (Q. Wei, et al, Adv. Mater. 2009. Fig. 1).

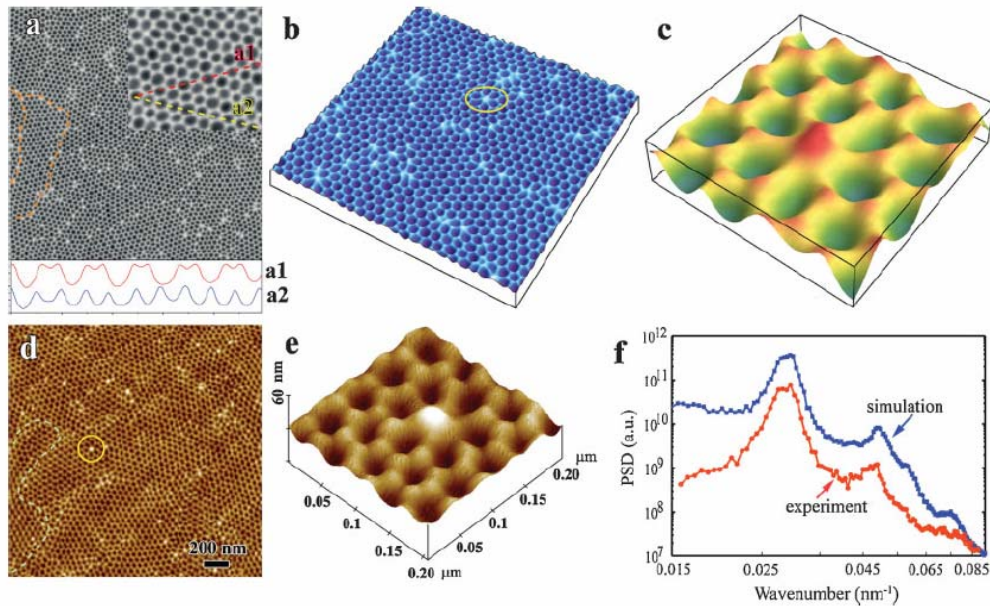


Fig. 1. Comparison of surface morphology calculated by DKS equation with experimental observations of ordered nanoholes on 5 kV Ga ion irradiated Ge surface. a) 2-D result of simulation, b) 3-D result of simulation, c) an enlarged segment of b), d) AFM image of the irradiated surface, e) an enlarged segment of d), f) Log-log plot of the PSD curves obtained from a) and d). (Q. Wei et al, Adv. Mater. 2009)

Four main formation mechanisms have been considered: sputtering, surface diffusion, redeposition, and viscous flow. It was found that the DKS growth model can describe these four mechanisms well for the long-time limit. Visible light emission or absorption from the ordered semiconductor nanostructure patterns has been observed (Q. Wei, et al, Adv. Mater. 2009; X. Zhou, et al, J. Appl. Phys: A 2009; X. Zhou, et al, APL 2009).

The formation process of 3-D nanoscale void superlattice in electron beam irradiated CaF_2 has been observed by in situ TEM, but the formation of such a structure in different materials requires very precise irradiation conditions that have not been predicted by the current models. The exact controlling mechanisms are still unclear. Through collaboration with V.N. Kuzovkov, E.A. Kotomin at the University of Latvia, we have been making progress in understanding the mechanism for the 3-D superlattice formation by a kinetic Monte Carlo simulation (V.N. Kuzovkov et al, NIMB 2010, in press).

Although another type of ion beam induced nanoscale patterns we have studied does not seem to have a periodic stacking of nanoelement, but it contains 3-D nanoscale features (e.g., nanofibers and nanoholes) of uniform dimensions. We have observed these nanostructures in the

surface region of several semiconductors. Once formed, the nanoscale dimension of the fibers is quite stable upon further irradiation. After annealing, the crystalline nanofibers may demonstrate unique photoluminescent properties. Under high energy ion irradiation, the structure can form underneath an intact surface indicating the process is not sputtering controlled but rather a void formation induced phenomenon (A. Perez-Bergquist et al, *Small* 2008, *JMR* 2009, *Nanotechnology* 2010). A phase field model has been developed to successfully simulate the formation process and the irradiation parameter control of such nanostructure patterns (K.D. Li et al, *NIMB* 2009, *JCTN* 2010, *IJMCE* 2010).

Future Plans

We will incorporate the results of previous research to improve the scientific understanding of the common self-organization mechanism responsible for the formation of the very different but apparently related nanopatterns under irradiation as demonstrated in the previous section. We will also explore the potential for technological utilizations of the self-organization process by establishing relationships between the morphology of the nanopatterns and their mechanical, optical, and electronic properties. We will focus on the dimension and wavelength control nanopatterns by conducting both high energy electron and ion beam bombardment as well as continued theoretical modeling and computer simulation. For modeling and simulation, we will expand our effort from the phase-field modeling to multiscale modeling by incorporating first principal, molecular dynamic and Dynamic Monte Carlo simulations. Through renewed effort, we seek for improved understanding on the roles of experimental parameters (particle mass, energy, dose rate, irradiation temperature) and intrinsic material parameters on pattern formation. Based on the improved understanding of mechanisms, it is expected that the morphology, size, shape, density, and distribution of particle beam induced nanostructures shall be precisely controlled. The research shall have a great impact on the future development of innovative irradiation-based nanoscale material processing techniques and technological applications of the processed nanostructures.

References (journal publications generated during 2008-2010 under this DOE BES grant)

1. Qiangmin Wei, Jie Lian, Sha Zhu, Weixing Li, Kai Sun and Lumin Wang, Ordered nanocrystals on argon ion sputtered polymer film, **Chemical Physics Letters** 452 (2008) 124-128.
2. Qiangmin Wei, Kie Lian, Wei Lu and Lumin Wang, Highly ordered Ga nanodroplets on a GaAs surface formed by a focused ion beam, **Physical Review Letters** 100 (2008) 076103.
3. Qiangmin Wei, Weixing Li, Kai Sun and Lumin Wang, Morphological instability of Cu nanolines induced by Ga⁺-ion bombardment: *In situ* scanning electron microscopy and theoretical model, **Journal of Applied Physics** 103 (2008) 074306.
4. K.-D. Li, H.Y. Xiao and L.M. Wang, Computer simulation study of defect formation and migration energy in calcium fluoride, **Nuclear Instruments & Methods in Physics Research B** 266 (2008) 2698-2701.
5. K. Sun, L.M. Wang and R.C. Ewing, Fabrication of nano-/micro-patterns on iron phosphate glass surfaces by focused energetic beams, **Nuclear Instruments & Methods in Physics Research B** 266 (2008) 3133-3137.
6. Qiangmin Wei, Kun-Dar Li, Jie Lian and Lumin Wang, Angular dependence of sputtering yield of amorphous and polycrystalline materials, **Journal of Physics D: Applied Physics** 41 (2008) 172002.

7. Alejandro Perez-Bergquist, Sha Zhu, Kai Sun, Xia Xiang, Yanwen Zhang, and Lumin Wang, Embedded nanofibers induced by high-energy ion irradiation of bulk GaSb, **Small** 4(8) (2008) 1119-1124.
8. X. Xiang, X.T. Zu, S. Zhu, L.M. Wang, V. Shtthanandan, P. Nachimuthu and Y. Zhang, Photoluminescence of SnO₂ nanoparticles embedded in Al₂O₃, **Journal of Physics D: Applied Physics** 41 (2008) 225102.
9. X.L. Zhou, Q.M. Wei, L.M. Wang, K. Sun, Optical characteristics of highly ordered gallium oxide nano-islands on GaAs, **Applied Physics B: Lasers and Optics** 94 (2009) 3360.
10. G. Ran, J.M. Zhang, Q.M. Wei, S.Q. Xi, X.T. Zu and L.M. Wang, The effects of carbon coating on nanoripples induced by focused ion beam, **Applied Physics Letters** 94 (2009) 073103.
11. Qiangmin Wei, Xiuli Zhou, Bhuwan Joshi, Yanbin Chen, Kundar-Li, Qihuo Wei, Kai Sun and Lumin Wang, Self-assembly of ordered semiconductor nanoholes by ion beam sputtering, **Advanced Materials** 21 (2009) 2865-2869.
12. Xiuli Zhou, Qiangmin Wei, Kai Sun and Lumin Wang, Formation of ultrafine uniform gold nanoparticles by sputtering and redeposition, **Applied Physics Letters** 94 (2009) 133107.
13. Q.M. Wei, M. Eddy, K.D. Li and L.M. Wang, Influence of surface morphology on sputtering yields, **Journal of Physics D** 42 (2009) 165304.
14. X.L. Zhou, Q.M. Wei, L.M. Wang, B.W. Joshi, Q.H. Wei and K. Sun, Enhanced photoluminescence from gallium arsenide semiconductor coated with Au nanoparticles, **Applied Physics A: Materials Science & Processing** 96 (2009) 637-641.
15. A.G. Perez-Bergquist, K. Sun, L.M. Wang, Y.W. Zhang, Formation of GaSb core-shell nanofibers by a thermally induced phase decomposition process, **Journal of Materials Research** 24 (2009) 2286-2292.
16. Qiangmin Wei, Jie Lian, L.A. Boatner, L.M. Wang, and R.C. Ewing, Propagation of ripples on pyrochlore induced by ion beam bombardment, **Physical Review B** 80 (2009) 085413.
17. K.D. Li, A. Perez-Bergquist and L.M. Wang, Computer simulation of radiation-induced nanostructure formation in amorphous materials, **Nuclear Instruments & Methods in Physics Research B** 267 (2009) 3063-3066.
18. Q.M. Wei, N. Li, K. Sun and L.M. Wang, The shape of bubbles in He-implanted Cu and Au, **Scripta Materialia** 63 (2010) 430-433.
19. K.D. Li, A. Perez-Bergquist, Q.M. Wei, L.M. Wang and W. Lu, Energy-dependant irradiation-induced nanostructure formation in amorphous germanium, **Journal of Computational and Theoretical Nanoscience** 7 (2010) 522-527.
20. A.G. Perez-Bergquist, K. Li, Y.W. Zhang and L.M. Wang, Ion irradiation-induced bimodal surface morphology changes in InSb, **Nanotechnology** 21 (2010) 325602.
21. V.N. Kuzovkov, E.A. Kotomin, P. Merzlyakov, G. Zvejnieks, K.D. Li, T.H. Ding, L.M. Wang, Void superlattice formation in electron irradiated CaF₂: Theoretical analysis, **Nuclear Instruments & Methods in Physics Research B** 267 (2010) 3055-3058.
22. Kun-Dar Li, Qiangmin Wei, Lumin Wang and Wei Lu, Dynamics of nanoscale void/fiber assembly formation in irradiated amorphous materials, **International Journal for Multiscale Computational Engineering** (2010) in press.

Localized Deformation and Intergranular Fracture of Irradiated Alloys under Extreme Environmental Conditions

Gary S. Was, University of Michigan
Ian M. Robertson, University of Illinois
Diana Farkas, Virginia Tech

Program Scope and Approach

While it is well known that irradiation accelerates intergranular stress corrosion cracking (IGSCC) in high temperature water, the mechanism remains unknown. The dramatic change in the nature of plastic deformation due to irradiation results in large amounts of slip, in the form of dislocation channels, impinging on grain boundaries in very local regions. Understanding the nature of the interaction of these channels with the grain boundaries is the primary objective of the project. A discovery-based approach is being pursued to determine the processes by which localized deformation in irradiated materials leads to intergranular cracking in alloys in aggressive environments at high temperature. To reach our objective, we are focusing on four controlled purity alloys and one commercial purity alloy. These are: commercial purity 304 SS (18Cr-8Ni), and controlled-purity alloys 18Cr-10Ni, 13Cr-15Ni, 21Cr-32Ni and 18Cr-12Ni-1Si. These alloys span a range of stacking fault energy ($15 - 61 \text{ mJ/m}^2$) and a wide range of known cracking susceptibilities; 18Cr-8Ni and 18Cr-12Ni-1Si are very susceptible to cracking, 13Cr-15Ni is moderately susceptible and 21Cr-32Ni is very resistant. We will evaluate the nature of deformation and cracking by conducting stress corrosion cracking experiments in high temperature water at low values of plastic strains. The nature of cracking, the localized deformation structure and their interaction will be evaluated to understand how they work together to induce cracking. A simulation effort is being conducted on digital samples generated using Voronoi constructions in which the orientation of each grain is taken from the characterization of the alloys. The simulations seek to understand unit processes such as dislocation generation, emission and absorption and the role of the grain boundary structure in these processes. The in-situ microscopy will tie the macroscopic SCC and deformation behavior with the modeling results by probing the nature of dislocation channel-grain boundary interaction, which is believed to be at the root of the IASCC initiation process.

Recent Progress

Stress corrosion cracking experiments were conducted first on 3 alloys that were characterized using orientation imaging microscopy to determine grain boundary misorientation, and then irradiated to a dose of 5.0 dpa using 2 MeV protons at a temperature of 360°C. Samples were then strained to about 5% plastic strain in two steps in 288°C water with a conductivity of better than 0.2 $\mu\text{S/cm}$. Surface oxides were stripped from the samples to reveal intergranular cracks and surface slip steps. Cracked boundaries were characterized according to the nature of the cracks, their location on the boundary, their angle of the grain boundary trace with respect to the tensile axis, the Schmid and Taylor factors of the bounding grains and the ease of slip transmission across the boundary. Figure 1 shows the two types of cracks formed after 5% strain in 288°C water; localized cracks at the intersection of the dislocation channels and the grain boundary, and IG cracks that extend the lengths of a facet and between triple points.

Cracking behavior exhibits some distinct dependence that can be summarized as follows:

- Cracking is most prevalent on random high angle boundaries (RHAB), less so on low angle boundaries (LAB) and least on coincident site lattice boundaries (CSLB).
- The fraction of cracked boundaries increases with the trace of the grain boundary angle with respect to the tensile axis. Grain boundaries that make an angle of 70-90° to the applied stress direction have a much higher incidence of cracking than those at lower angles, Fig. 2a.

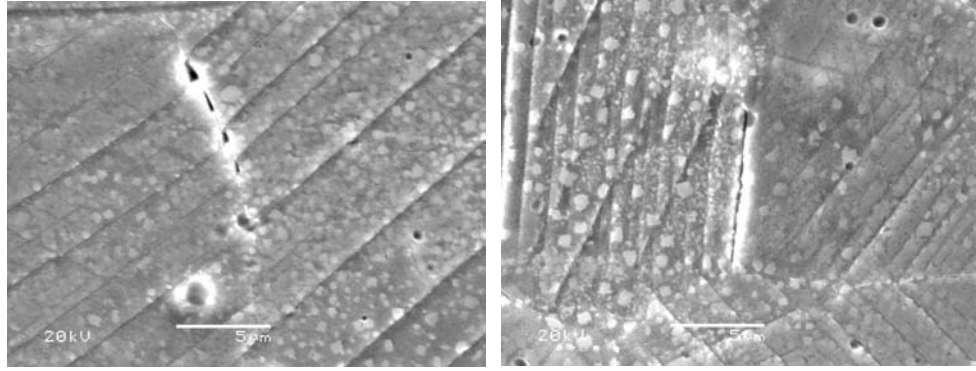


Figure 1. (a) Localized cracks at the intersection of dislocation channels and a grain boundary, and (b) a crack extending the length of a grain boundary facet. Tensile stress is in the horizontal direction.

- Cracking seems to depend on the Taylor factor pair type. If the Taylor factors of grains bordering a cracked grain boundary are divided into categories of low, medium and high, then the cracking propensity of boundaries with at least one grain having a low Taylor factor is significantly lower than the remaining pair types, Fig. 2b.
- There is a dependence of slip continuity on grain boundary angle, with significantly greater slip continuity across boundaries that make smaller angles to the applied tensile stress, Fig 3a.
- If the data is parsed between cracked and uncracked grain boundaries, then slip continuity is greater across boundaries that don't crack vs. ones that do, Fig. 3b.

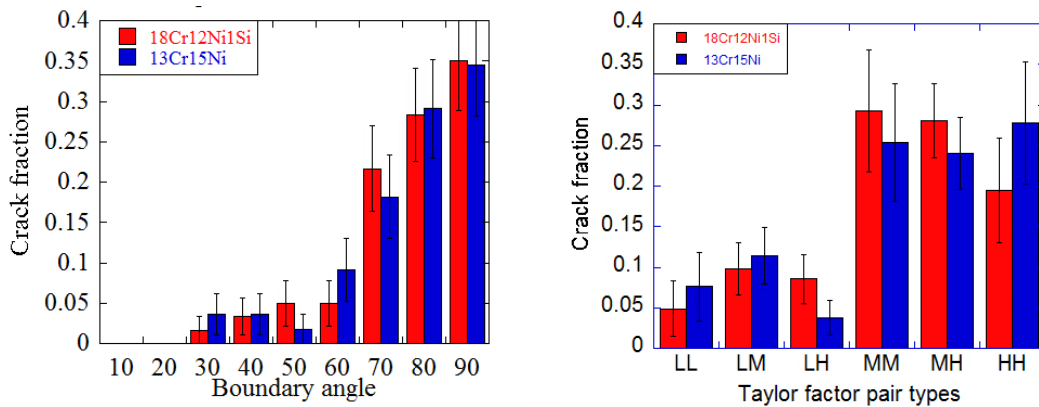


Figure 2. (a) Grain boundary cracking as a function of the angle of the grain boundary trace with respect to the tensile stress, and (b) cracking as a function of Taylor factor pair types.

Molecular dynamics simulations were used in a virtual tensile test, to study the intergranular cracking behavior of model FCC polycrystalline samples. These samples include both columnar grain configurations with random boundaries as well as samples that have a thin-film configuration with grain and grain boundary orientations modeled after distributions determined experimentally. Various characteristics of the boundaries were analyzed; grain boundary energy, type, and Schmid factors of both grains, and boundary orientation with respect to the tensile axis. In agreement with the experimental results, it was found that cracks generally occur in random high angle boundaries that are oriented close to perpendicular to the tensile direction. Within high angle grain boundaries, the orientation of the boundary plane with respect to the tensile axis was the single most important factor that correlated with cracking.

Figure 4 shows an example of cracking along a grain boundary in a sample strained in the horizontal direction.

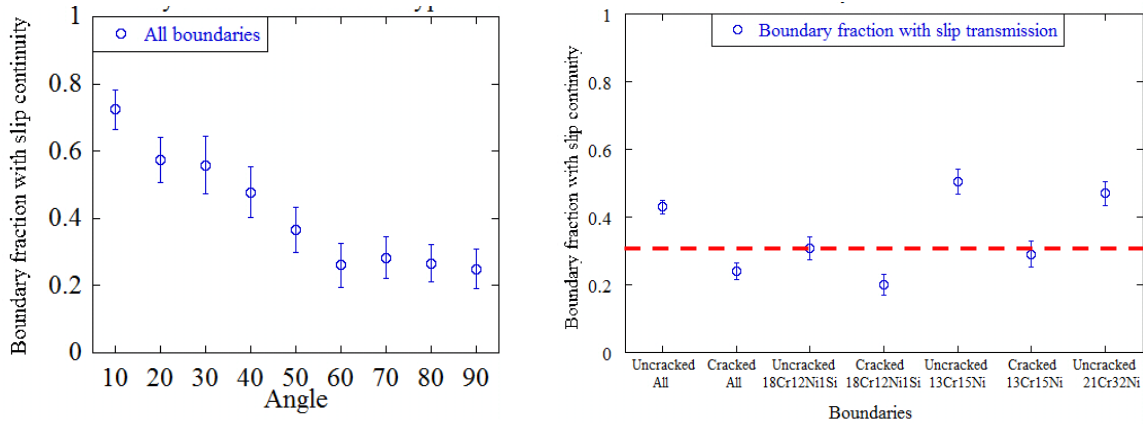


Figure 3. Fraction of boundaries exhibiting slip continuity (a) as a function of the angle of the grain boundary trace with respect to the tensile stress, and (b) as it depends on whether the boundary cracks.

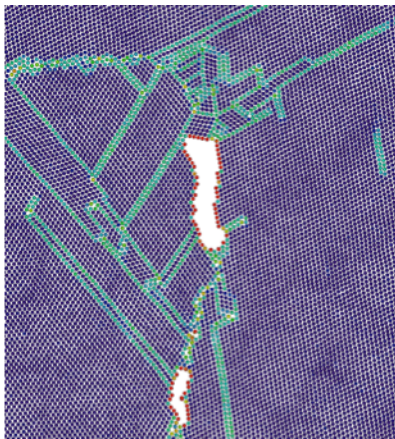


Figure 4. Cracking along a grain boundary lying close to normal to the tensile direction.

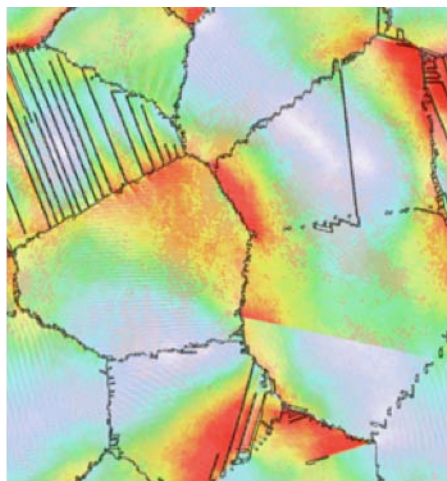


Figure 5: Inhomogeneous nature of strain distribution and dislocation emission in a virtual sample strained 5% in the horizontal direction.

By analyzing the inhomogeneous distribution of strain in the deformed samples, strain localization was studied in the simulations and it was found that strain localization occurs near some of the grain boundaries, contributing to failure. Plastic deformation through dislocation emission also occurred in an inhomogeneous manner, with some grain boundaries emitting more dislocations than others due to the nature

of the boundary and Schmid factor of both grains. Figure 5 shows the inhomogeneous nature of deformation, with color-coding showing the regions of high local strain. The stacking faults left by the emission of Shockley partials are shown in black.

Deformation experiments in-situ in the TEM have been conducted in unirradiated samples as a function of temperature as well as in samples in which the matrix has been hardened by heavy-ion irradiation produced obstacles. The key results from these tests are summarized as follows. The effect of temperature on the interaction of dislocations with grain boundaries is to increase the complexity of the interaction and the final response of the grain boundary to that interaction. This appears as an increase in the number of slip systems activated by the grain boundary to relieve the increase in strain energy density

caused by the dislocation being accommodated in the grain boundary. A more significant difference in the behavior of dislocations is caused by the introduction of a hardened matrix. Irradiation-produced defects were shown unequivocally to arrest mobile dislocations but not to influence significantly the operation of dislocation sources. The obstacle field changed the motion of a dislocation, causing segments of the line dislocation as opposed to the entire dislocation to move in a start-stop manner. This behavior changed as the number of dislocations passing through the obstacle field increased. That is, the effectiveness of the obstacles as barriers decreased with the passage of each dislocation. Consequently, the dislocations moving along a partially cleared channel experienced a resistance that increased with distance travelled from the source. This in turn impacted the dislocation distribution in the cleared channel effectively increasing the equilibrium separation distance between the dislocations. This resulted in two significant effects: First, the spatial arrangement of dislocations against a barrier at least in the early stages evolves more slowly than in the unirradiated case, and this has implications for the local stress generated and, ultimately, for slip transmission. Secondly, at the source end of the channel the dislocations accumulate, and this generates a large back stress on the source that can limit source operation and could cause the grain boundary response to change from slip transmission to crack nucleation. The change in the form of dislocation distribution with the grain boundary as a barrier and as a source is compared in Figure 6.

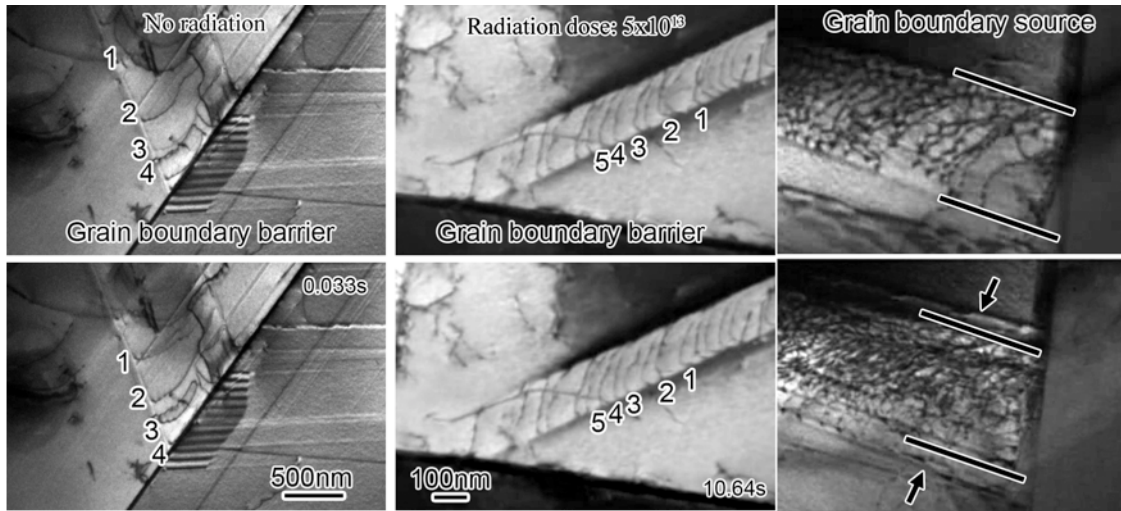


Figure 6. The first two panels compare the build-up of dislocations near a grain boundary in unirradiated and irradiated 304 SS. Note the time difference between the images. The third panel shows the development of the dislocation structure at a grain boundary source. The time difference between the two images is 10 s.

Future Plans

Immediate plans are to continue characterization of cracking and slip transmission in samples strained in either inert environment or in high temperature water and to match simulations to the experiments to understand the features governing slip transmission and cracking as a function of boundary type, stress, grain boundary orientation, etc. We will also continue in-situ deformation experiments on ion irradiated steels as well as commencing in-situ deformation experiments on pre-deformed, proton irradiated steels as a function of temperature. Molecular dynamics simulations will continue to be used to perform virtual tensile tests as a function of temperature and study the influence of stacking fault energy on the deformation behavior.

Investigating Deformation and Failure Mechanisms in Nanoscale Multilayer Metallic Composites

H. M. Zbib, D. F. Bahr
Washington State University, Pullman, WA 99164-2920
zbib@wsu.edu , dbahr@wsu.edu

Extended Abstract

Scope

The goal of this investigation is to advance our fundamental understanding of deformation, strength, damage, and failure mechanisms of NMM composites under various loading and environmental conditions, particularly moderate to high temperature creep-fatigue and irradiation effects with a focus on trimetallic NMM composite systems. Our investigation has involved: 1) Fabricating bimetallic and trimetallic systems based on CuNiNb, 2) experimentally examining their mechanical behavior under monotonic and cyclic loading conditions, and 3) theoretical modeling work based on a multiscale approach which uses a) MD to study dislocation mechanisms and dislocation-interface interactions, and b) MDDP – multiscale dislocation dynamics plasticity- to investigate dislocation mechanisms and dislocation-crack interaction.

Progress

The results of our work are reported in [1-27]. Our studies have suggested that work hardening and the transmission of dislocations between layers in the NMM systems controls the film strength, and that trilayer films may have some unique advantages in terms of overall toughness as well as exhibiting unique dislocation structures. In particular, after the onset of plastic deformation and in the initial strain hardening conditions CuNiNb films appear to be superior to either CuNi or CuNb. The simulations have suggested these effects, and have been coupled with experimental studies to verify and drive new simulations as well as new experiments. Below is a brief description of our main accomplishments.

Experiments- We developed a testing methodology to carry out tests at and near the plastic deformation limit to quantify the onset of plasticity. We fabricated and tested bilayers of CuNb and CuNi as well as trilayer of CuNiNb. Material fabrication was carried out jointly at WSU and at the CINT facility in LANL in collaboration with Dr. Amit Misra. The mechanical properties of the films were measured using bulge testing and nanoindentation. Bulge testing showed that the maximum stress at the onset of yield is significantly lower than the predicted flow stress that would be expected from the hardness data, an important source of this deviation is that the values reported in [1] are for the onset of plasticity; not for uniform deformation over the membrane. The particularly interesting trend is that the hardest samples do not have the highest initial yield stress. This suggests that hardening must have a significant role in the plasticity of the samples at increasing strains. Based on these findings, strain hardening was investigated by both applying a bulge test to approximately 1% strain as well as carrying out indentation tests with Berkovich and Cube Corner Geometries [2], yielding the result shown in Fig. 1a. In moderate strain regions the strain hardening of the films appears to be a significant issue in deformation. The effect of variations in the Nb layer thickness in trilayer systems was also investigated. Based on the MD simulations [12-13], Cu/Ni/Nb thickness between 5/5/4 and 5/5/1 should show properties that exceeded that of a uniform thickness [2]. Figure 1b shows the representative hardness of the trilayer films with variable Nb thickness. While the trend is similar to the MD predictions, the most important aspect of this result is that the scale of the MD predictions is clearly tied to the experimentally measured hardness.

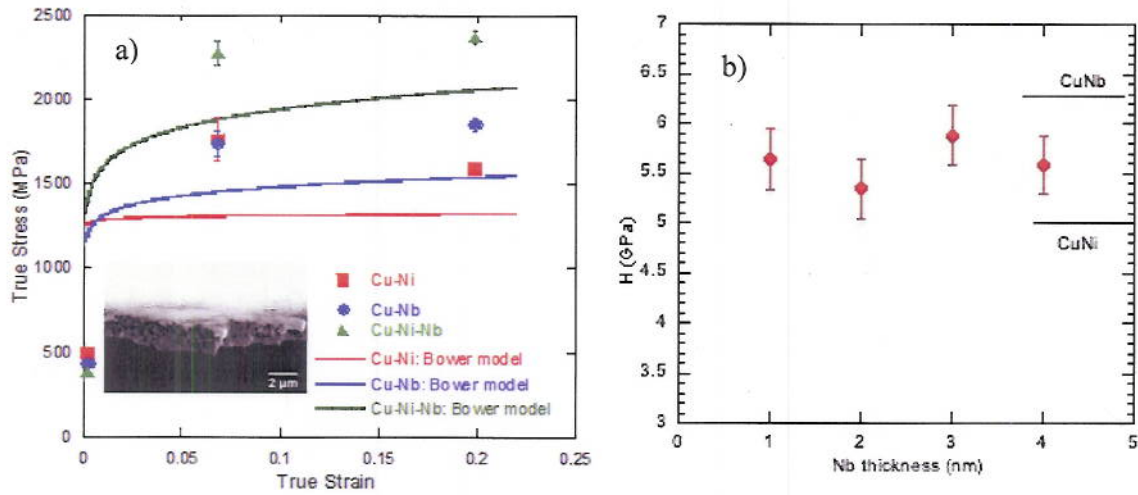


Figure 1. a) Effective strain hardening behavior of multilayer films. The initial yield point (0.2%) was determined via bulge testing, the flow stress at 8% strain was evaluated with a Berkovich indenter tip, and the flow stress at 22% was evaluated with a cube-corner indenter tip. Insert: Cross section of trilayer film after burst failure test; dimples on the fracture surface and evidence of necking (on the order of several %) support the stress-strain results. b) Indentation hardness and initial yield strength of Cu/Ni/Nb films.

MD-Three types of structures were studied using MD simulations: a CuNi fcc/fcc bilayer with coherent interfaces, a CuNb fcc/bcc bilayer with incoherent interfaces and a CuNiNb fcc/fcc/bcc trilayer with both coherent and incoherent interfaces. The structure was loaded biaxially and the dislocation structure and stress-strain curves were obtained and are shown in Fig 2a. The comparison between the deformation behavior of bilayer and trilayer structures revealed that while the bilayer CuNi has higher ductility than the CuNb structure which has higher strength, the trilayer structure possesses the properties of both high strength and ductility [8, 11,14].

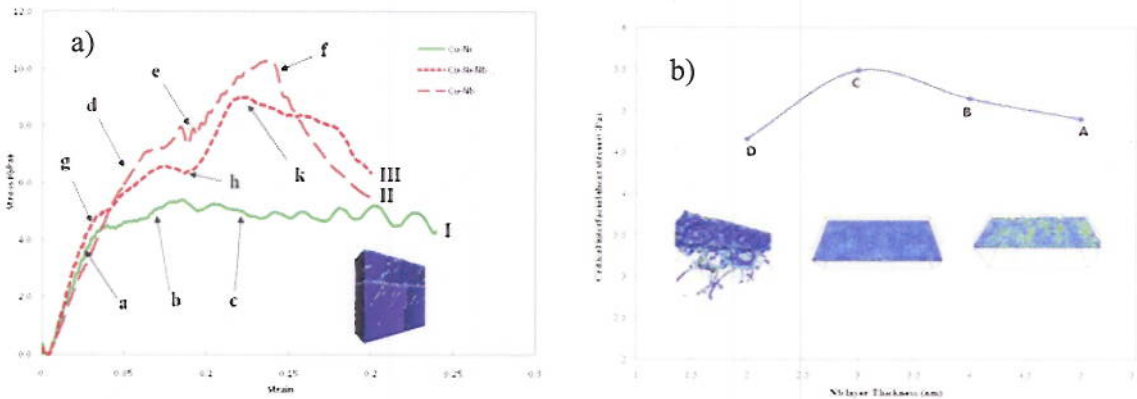


Figure 2. a) Stress-strain curves for three different cases, CuNi, CuNb and CuNiNb. b) The critical stress as function of Nb thickness. Left insert: distribution of residual dislocation. Middle and right inserts: shear strain distribution in the Cu/Nb interface for 5 nm and 2 nm thicknesses, respectively. The atoms are colored according to their shear strain with the brighter colors characterizing higher shear. The thinner Nb layer shows more intense shearing. The average shear strain in the case of 2 nm is 0.3 while in the case of 5 nm it is 0.05.

Also, the Nb layer thickness was varied from 5 nm to 2 nm with constant 5 nm Cu and Ni layers. The results in Figure 2b shows that the strength exhibited by the trilayer depends on the incoherent layer thickness and increases as the layer thickness decreases [12,13]. The comparison with the coherent Cu/Ni structure revealed the importance of the incoherent layer since the presence of a thin Nb layer (up to 3 nm) is enough to strengthen the material considerably. The simulations also showed that when the Nb layer thickness is below 3 nm the strength of the material decreases. This softening behavior is associated with the considerable shearing of the interface, and in the case of the NMM composite with a thin Nb layer the shearing is more intense (inserts in Fig 2b).

MDDP- We developed strength models for dislocations near interfaces and in heterogeneous media. Particularly we have studied the following problems: Koehler force, dislocation-interface interaction, the effect of topology of the interface on strength, and dislocation-crack interaction. The results of this work are reported in [3, 10, 18-22, 25, 26]. Also, atomistic studies unveiled the mechanism by which incoherent interfaces in nanoscale metallic laminates lead to their observed ultra high strength. This effect has been integrated within our dislocation dynamics framework. Our result suggests that the Kurdjumov-Sachs orientation between Cu and Nb can be accomplished in three different ways, each resulting in a different atomic structure of the interface with different energy states and shear properties. Smaller interface hardening and larger elastic modulus lead to greater interactions between the interface and near-by dislocations. Those trends lead to larger plastic shearing of the interface under the same stress field of the dislocation. Nevertheless, the interface hardening has a stronger effect on interface-dislocation interaction. We also studied the effect of Nb thickness on the load carrying capacity of the NMM composite. Some results are shown in Figure 3. With MDDP and the coherent interface model we were able to capture and explain both: a) the increase strength on layer thickness as the layer thickness decreases from 100 nm to 3 nm, and b) the drop in strength as the layer thickness is decreased below 3 nm. Moreover, we identified mechanisms that contribute to hardening and that include, dislocation blocking, intersections and junctions; and dislocation mechanisms that contribute to softening and that includes dislocation crossing the Cu-Ni interface and formation of “super threaders”, and dislocation cross-slip at the Cu-Ni interface as a result of the shearing of the Cu-Nb interface. This last mechanism is very interesting. It occurs even though the macroscopic state of stress is biaxial; an internal shear stress is induced as a result of the shearing of the Cu-Nb interface. This effect becomes large enough to cause cross-slip when the Cu-Ni and Cu-Nb interfaces are close, observed for thickness less than 5 nm.

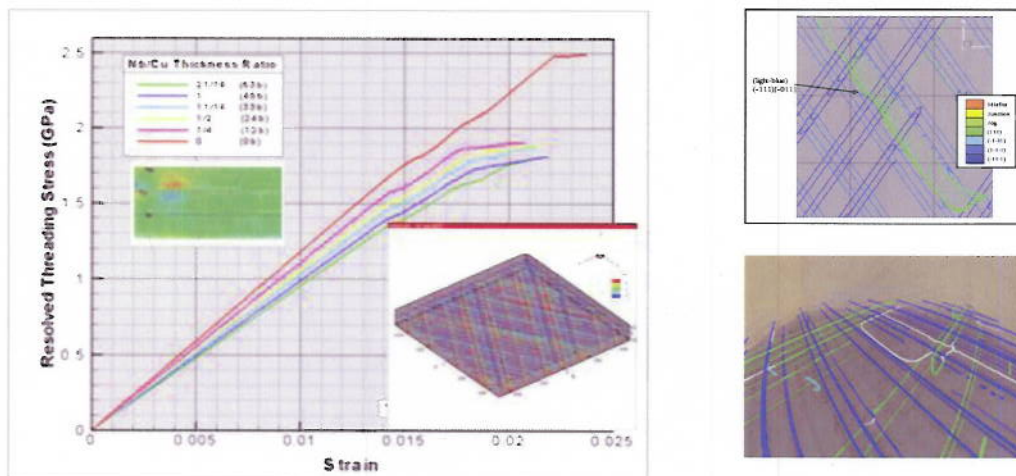


Figure 3. MDDP. a) The stress-strain behavior of a trilayer CuNiNb system with varying Nb thickness; with shearable CuNb and NiNb interfaces; Insert: the contour plot shows the stress distribution within the layers and the underlying dislocation structures. b) and c) Show typical dislocation structures obtained through MDDP.

Future Plans: We intend to focus on the following objectives:

- Investigate, both experimentally and through MD and DD studies, the strength and creep-fatigue behavior of NMM composites under moderate to high temperature, strain rate, and with and without radiation effects.
- Investigate the effect of interface structure, morphology and imperfections on strength and deformation mechanisms of NMM through MD studies.
- Investigate the failure mechanisms of NMM composites through DD analysis enhanced by information from MD of dislocation interaction with interface and interfaces-imperfections.
- Establish general guidelines regarding the tradeoffs between strength, toughness, and fatigue resistance as a function of materials, interfacial properties and layer thicknesses.

List of Publications (Already published, in press, or submitted) in which DOE support is acknowledged.

1. N. Overman, C. Overman, H.M. Zbib, and D.F. Bahr, *Journal of Engineering Materials and Technology*, 131 (4), 0141203-6, 2009.
2. Bellou, A., Misra, A., Zbib, H.M., C. Overman, I. and Bahr, D.F., *Scripta Met*, submitted (2010).
3. Akarapu, S., Zbib, H.M. and Bahr, D.F. *Int. J. Plasticity*, 26, 239-257, 2010.
4. Akarapu, S. and Zbib, H.M., *Phil Mag*, 89, 2149-2166, 2009.
5. S Akarapu, H. M Zbib, and J.P. Hirth, *Scripta Materialia*, 59, 265-267 (2008).
6. Mastorakos I., and Zbib, H.M., *Dislocation, J of Materials*, 60, 59-63, 2008.
7. I.N. Mastorakos, H.M. Zbib and D.F. Bahr, *Appl. Phys. Letters* 94, Issue 17, 173114, 2009.
8. Mastorakos, I.N., Zbib, H.M., Bahr, D.F., Parsons, J and Mased, F. *Appl. Phys. Letters*. 94,4, 043104, 2009.
9. S. N. Medyanik, S. Shao, *Computational Materials Science*, 45, 1129-1133, 2009.
10. H.M. Zbib, C. Overman, F. Akasheh and D. Bahr, under review, *Int. J. Plasticity*, 2010.
11. I.N. Mastorakos, H.M. Zbib, A. Bellou, D. Bahr, *Physical Review B*, submitted, 2010.
12. N. Abdolrahim and H.M. Zbib, *Int. J. Mechanical Science*, 52, 295-302, 2010.
13. N. Abdolrahim, I.N. Mastorakos and H.M. Zbib, *Physical Review B* 81, 054117, 2010.
14. A. Bellou, L. Scudiero, D.F. Bahr, *Journal of Materials Science*, vol. 45, pp. 354-362 (2010) DOI10.1007/s10853-009-3943-4.
15. A. Bellou and D. F. Bahr, *Journal of Materials Science*, in press (2010) DOI 10.1007/s10853-010-4845-1
16. D.F. Bahr, A. Bellou, N. Overman, H.M. Zbib, in *Proceedings of the 12th International Conference on Fracture* 12, Ottawa, Canada, July 17-22 2009
17. F. Akasheh, H. M. Zbib, S. Akarapu, C. Overman, and D. Bahr., *Mater. Res. Soc. Symp. Proc. Vol. 1130*, W13-01, 2009.
18. Zbib, H.M. and Bahr. In: *Microstructure-Property Relations*. Eds. Ghosh, S. and Dimiduk, D., Springer, 2010. In press.
19. Zbib, HM, Akarupa, S, Akasheh, F, Overman, C and Bahr, D. In: *Macro to nano Scale Inelastic behavior of Materials: Plasticity, Fatigue and Fracture*, eds. A. Khan et al, proc. 15th Int. Symp. on Plasticity and Its Current Applications, January 3-9, 2009, St. Thomas, USA, pp. 220-222.
20. Bahr, D, Bellou, A., Overman, N, and Zbib HM, in: *Macro to nano Scale Inelastic behavior of Materials: Plasticity, Fatigue and Fracture*, eds. A. Khan et al, proc 15th Int. Symp. on Plasticity and Its Current Applications, January 3-9, 2009, St. Thomas, USA, pp. 394-396.
21. S. N. Medyanik, S. Shao, *Mater. Res. Soc. Symp. Proc. Vol. 1137*, 1137-EE08-04-W10-04, Materials Research Society, 2009.
22. Zbib, H.M, and Akarapu, S. *Proceedings of the 2nd Int. Sym on Steel Science*, 1-8, in press, Kyoto, Japan, 2009.
23. S. N. Medyanik, S. Shao, *Proceedings of 12th International Conference on Fracture*, Ottawa, July 2009
24. S. Shao, S. N. Medyanik, *ASME Conf. Proc. 2008*, IMECE2008-67523, pp. 1217-1222, 2008
25. C. Overman, MS thesis, 2009, Washington State University, <http://www.cmm.wsu.edu/Publications/Publications.html>
26. N. Overman, MS thesis, 2009, Washington State University, <http://www.cmm.wsu.edu/Publications/Publications.html>
27. S. Akarapu, PhD thesis, 2009, Washington State University <http://www.cmm.wsu.edu/Publications/Publications.html>

Laboratory Projects

Mechanical Properties of Materials: Nature-Inspired Ultrahigh Toughness, Lightweight Structural Materials

Robert O. Ritchie and Antoni P. Tomsia

Materials Sciences Division, Lawrence Berkeley National Laboratory, Berkeley, CA 94720
roritchie@lbl.gov, aptomsia@lbl.gov

Program Scope

The structure of materials invariably defines their mechanical behavior. However, in most materials, specific mechanical properties are controlled by structure at widely differing length scales. Nowhere is this more apparent than with natural materials, which are invariably sophisticated composites whose unique combination of mechanical properties derives from an architectural design that spans nanoscale to macroscopic dimensions with precisely and carefully engineered interfaces. The fracture resistance of such materials originates from toughening mechanisms at almost every one of these dimensions. Few structural engineering materials have such a hierarchy of structure, yet the message from biology is clear – unique mechanical properties can be achieved through the combination of mechanisms acting at multiple length-scales. Nature has successfully used this approach over billions of years, yet despite intense interest by the scientific community, the biomimetic approach has yielded few real technological advances in the design of new synthetic *bulk* structural materials. Unlike engineering composites where properties are invariably governed by the “rule of mixtures”, the mechanical properties of many natural composite materials are generally far greater than their constituent phases. However, progress in this field has been limited because actually making such materials synthetically has proved to be extremely difficult, especially in macroscopic form.

On a fundamental level, our research is focused on experimental and theoretical efforts to probe the mechanics and mechanisms of deformation, fracture and fatigue, *i.e.*, damage-tolerance, at such multiple dimensions in a wide range of structural materials modeled on natural hierarchical designs. However, armed with this knowledge, our objective is to utilize a wide range of material systems, from ceramics and polymers to metals, and to develop feasible processing methods, to create a new suite of hybrid lightweight materials with unprecedented mechanical properties, in particular to achieve damage-tolerance in terms of a combination of the often mutually exclusive properties of ultrahigh toughness and strength.

Recent Progress

Although the notion of mimicking Nature in the development of synthetic materials is hardly new, few successful *bulk* biomimetic materials have ever been made. In our work, we have applied the natural concept of hierarchical design to ceramic/polymer ($\text{Al}_2\text{O}_3/\text{PMMA}$) hybrid materials which we were able to fabricate in bulk form by freeze casting [1]. Using controlled freezing of ceramic-based suspensions in water, we have been able to form large porous ceramic scaffolds (Fig. 1) with architectures that were templated by the ice crystals. Directional freezing is first employed to promote the formation of lamellar ice with prescribed dimensions; this then acts as the “negative” for creation of the layered ceramic scaffolds which were subsequently

infiltrated with the polymeric second phase. In addition to making lamellar structures, nacre-like “brick-and-mortar” structures have also been fabricated, with very high ceramic content, by subsequently hot pressing the scaffolds in the direction perpendicular to the lamellae in order to collapse them followed by a second sintering step to promote densification and the formation of ceramic “bridges” between the “bricks” (Fig. 1D). Using such techniques, we have made complex hierarchical architectures where we can refine the lamellae thickness, control their macroscopic orientation, manipulate the chemistry/roughness of the inter-lamellae interfaces, and generate a given density of inorganic bridges, all over a range of size-scales [1,11].

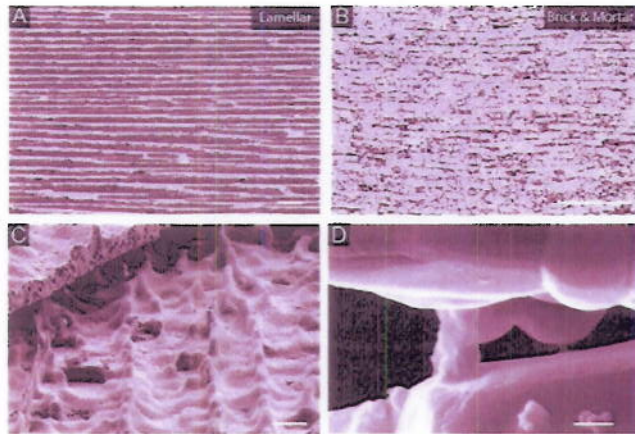


Fig. 1. Structure of ice-templated materials. (A) $\text{Al}_2\text{O}_3/\text{PMMA}$ lamellar composites fabricated using freeze casting of ceramic suspensions followed by polymer infiltration (the lighter phase is the ceramic; the dark phase is the polymer). (B) Brick-and-mortar architectures, prepared by pressing of the lamellar materials and subsequent sintering, have much larger ceramic contents (up to 80 vol%). (C) Using sucrose as an additive to the freeze casting slurry the growing ice crystals develop a characteristic surface topography that translates into a microscopic roughness in the ceramic walls. (D) The process also results in the formation of ceramic bridges between lamellae (due to the trapping of ceramic particles by the growing ice) or bricks (the bridges form during the second sintering steps). By limiting sliding, they provide very effective toughening mechanisms in natural and synthetic materials. The bars are 100 μm in (A) and (B) 10 μm in (C) and 600 nm in (D) [1].

In an attempt to replicate the microstructural design of nacre, we reduced the lamellae thickness to 2-5 μm (this is still ten times thicker than the natural material - we are currently working to further refine this), and used sucrose as an additive to the ceramic slurries (Fig. 1A-B). Sucrose modifies the viscosity and phase diagram of the solvent resulting in the formation of ice crystals with a characteristic microscopic roughness and bridge density akin to nacre (Fig. 1C-D) [11]. Control of the lamellae roughness provides a mechanical means to manipulate adhesion at the inorganic/organic layer interfaces. To achieve a macroscopic alignment of the lamellae similar to nacre, we use a patterning technique; a cold finger where the ice can nucleate is used to generate $\sim 40 \mu\text{m}$ parallel grooves. The highest ceramic contents (now $\sim 80 \text{ vol}\%$) were achieved with brick-and-mortar architectures, prepared through pressing/sintering the lamellar materials. These structures comprised ceramic “bricks”, 2-10 μm wide, 20-100 μm long, separated by thin ($\sim 1\text{-}2 \mu\text{m}$) polymer layers. Using these procedures, we produced a series of $\text{Al}_2\text{O}_3/\text{PMMA}$ hybrid composites (Fig. 1A-B), with hierarchical structures spanning multiple length scales that exhibit distinctive structural and mechanistic features similar to those in nacre.

Resulting mechanical properties have been remarkable. Flexural strengths were high in the direction perpendicular to the lamellae and comparable to that of alumina, with values of 120 to 210 MPa for the lamellae and brick-and-mortar structures, respectively. More importantly, corresponding plane-strain (crack initiation) K_{Ic} fracture toughness values were almost double of that expected from the simple “rule of mixtures” of Al_2O_3 and PMMA. These synthetic composites actually replicated the mechanical behavior of natural materials; they displayed large ($>1\%$) inelastic strains in tension and developed exceptional toughness (Fig. 2). Specifically

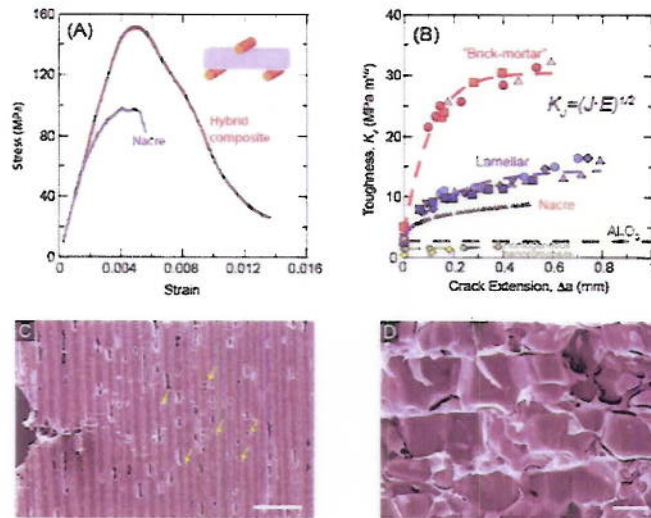


Fig. 2. Toughening mechanisms in synthetic hybrid composites. (A) Bending stress-strain curves for hybrid $\text{Al}_2\text{O}_3/\text{PMMA}$ materials mimic those of nacre, and show >1% inelastic deformation prior to failure. (B) These materials show exceptional toughness for crack growth, akin to natural composites, and display significant rising R-curve behavior. Almost negligible toughening is observed in homogeneous $\text{Al}_2\text{O}_3/\text{PMMA}$ nanocomposites. (C) SEM image taken during an *in situ* R-curve measurement of lamellar structure, showing two of the toughening mechanisms acting at large scales: the wide distribution of damage in the form of contained microcracking within ceramic layers (yellow arrows point to some of these microcracks) and voids in the polymer layers. (D) Fracture surface of a brick-and-mortar structure: controlled sliding contributes to a rise of the crack-growth toughness to values that can be over 300 times higher (in energy terms) than that of Al_2O_3 . In addition to the roughness of the ceramic surfaces and inorganic bridges between ceramic bricks, a principal reason for controlled sliding is the presence of sub-micrometer polymer films between Al_2O_3 blocks. The bars are 250 μm in (C) and 3 μm in (D) [1,11].

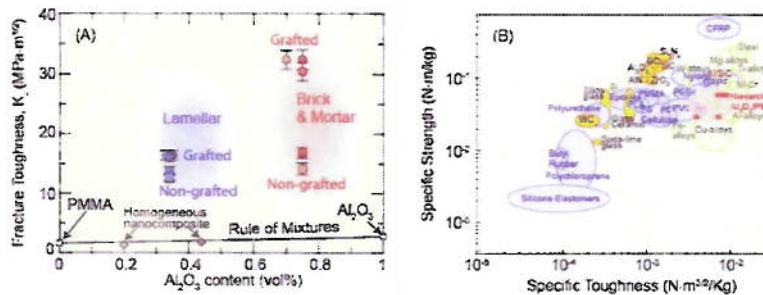


Fig. 3. Specific strength/toughness properties (A) Brick-and-mortar composites display K_{Ic} fracture toughnesses over an order of magnitude larger than their constituent phase Al_2O_3 . (B) Specific strength and toughness (i.e., normalized by density) for a wide range of materials systems, showing that our $\text{Al}_2\text{O}_3/\text{PMMA}$ composites, with ~80 vol% alumina ceramic, have strength/toughness properties comparable with that of metallic aluminum alloys [1,11].

their toughness surpasses that of nacre, the often cited “gold standard” in biomimetic design. Our initial $\text{Al}_2\text{O}_3/\text{PMMA}$ lamellar and brick-and-mortar structures reach (steady-state) fracture toughness K_{Ic} values of 15 $\text{MPa}\sqrt{\text{m}}$ and >30 $\text{MPa}\sqrt{\text{m}}$, respectively (Fig. 3). The latter value is an outstandingly high toughness for a material consisting of 80% alumina with a strength above 200 MPa; indeed, we believe that it is the highest toughness ceramic material ever reported. It is far in excess of the toughness of either constituent, and more than a factor of two higher than any reported values for Si_3N_4 and SiC .

We believe that these results illustrate the importance of the notion of hierarchical design in promoting toughening mechanisms at multiple length scales as a path to create materials with unprecedented combinations of strength and fracture resistance.

Future Plans

These materials derive their ultrahigh toughness through the concept of the “lubricant phase”. The ceramic provides almost entirely for the strength; the polymer has little to no load-bearing role but instead acts like a lubricant to relieve high stress concentrations in the structure, just like dislocations in metals or microcracking in rocks and bone. Accordingly, our current and future plans are focused on the use of metallic “lubricants” in order to enhance the high-temperature capability of our hybrid alloys. We are also attempting (i) to refine our ceramic scaffolds using finer powders and faster cooling rates, (ii) to develop alloys with higher ceramic

contents, (iii) to use improved starting materials in the form of Si₃N₄ and SiC, (iv) to generate more isotropic structures through the use of different forms of cold finger patterning, and (v) to develop a comprehensive theoretical description focused both on MD modeling to enhance our understanding of the control of parameters for optimal processing, and numerical modeling directed to predicting the strength and toughness of two-phase brick-and-mortar ensembles to guide our development of nano/microstructures to achieve optimal structural performance.

DOE-BES Sponsored Publications - 2008-2010 (archival journals only)

1. E Munch, ME Launey, DH Alsem, E Saiz, AP Tomsia, RO Ritchie. Tough bio-inspired hybrid materials. *Science* 2008; 322: 1516.
2. JW Foulk III, GC Johnson, PA Klein, RO Ritchie. On the toughening of brittle materials by grain bridging: Promoting intergranular fracture through grain angle, strength and toughness. *J Mech Phys Solids* 2008; 56: 2381.
3. JJ Kruzic, RL Sadat, MJ Hoffmann, RM Cannon, RO Ritchie. The utility of R-curves for understanding fracture toughness-strength relations in bridging ceramics. *J Am Ceram Soc* 2008; 91: 1986.
4. DH Alsem, CL Muhlstein, EA Stach, RO Ritchie. Further considerations on the high-cycle fatigue of micron-scale polycrystalline silicon. *Scripta Mater* 2008; 59: 931.
5. AM Kueck, DK Kim, Q Ramasse, LC De Jonghe, RO Ritchie. Atomic-resolution imaging of the nanoscale origin of toughness in rare-earth doped SiC ceramics. *Nano Letters* 2008; 8: 2935.
6. DA Alsem, BL Boyce, EA Stach, RO Ritchie. Effect of the post-release sidewall morphology on the fracture and fatigue properties of polycrystalline silicon structural films. *Sens & Actuat A* 2008; 147: 553.
7. SA Sánchez, J Narciso, E Louis, F Rodríguez-Reinoso, E Saiz, AP Tomsia. Wetting and capillarity in the Sn/graphite system. *Mater Sci Engin A* 2008; 495: 187.
8. DH Alsem, MT Dugger, EA Stach, RO Ritchie. Micron-scale friction and sliding wear of polysilicon silicon thin structural films in ambient air. *J MEMS* 2008; 17: 1144.
9. ME Launey, DC Hofmann, WL Johnson, RO Ritchie. Solution to the problem of the poor cyclic fatigue resistance of bulk metallic glasses. *PNAS* 2009; 106: 4986.
10. ME Launey, RO Ritchie. On the fracture toughness of advanced materials. *Advanced Materials*, 2009; 21: 2103.
11. ME Launey, E Munch, DH Alsem, HB Barth, E Saiz, AP Tomsia, RO Ritchie. Designing highly toughened hybrid composites through nature-inspired hierarchical complexity. *Acta Mater* 2009; 57: 2919.
12. ME Launey, DC Hofmann, J-Y Suh, H Kzachkov, WL Johnson, RO Ritchie. Fracture toughness and crack-resistance curve behavior in metallic glass-matrix composites. *Appl Phys Lett* 2009; 94: 241910.
13. S Bechtle, M Kumar, BP Somerday, ME Launey, RO Ritchie. On the use of grain-boundary engineering to enhance resistance to intergranular embrittlement due to hydrogen in metallic materials. *Acta Mater* 2009; 57: 4148.
14. M Benhassine, E Saiz, AP Tomsia, J De Coninck. Nonreactive spreading at high-temperature revisited for metal systems via molecular dynamics. *Langmuir* 2009; 25: 11450.
15. ME Launey, P-Y Chen, J McKittrick, RO Ritchie. Mechanistic aspects of the fracture toughness of elk antler bone. *Acta Biomater* 2010; 6: 1505.
16. AM Kueck, QM Ramasse, LC De Jonghe, RO Ritchie. Atomic-scale imaging and the effect of yttrium on the fracture toughness of silicon carbide ceramics. *Acta Mater* 2010; 58: 2999.
17. CS Lee, JA Lemberg, DG Cho, JY Roh, RO Ritchie. Mechanical properties of Si₃N₄-Al₂O₃ FGM joints with 15 layers for high-temperature applications. *J Eur Ceram Soc* 2010; 30: 1743.
18. ME Launey, E Munch, DH Alsem, E Saiz, AP Tomsia, RO Ritchie. A novel biomimetic approach to the design of high-performance ceramic/metal composites. *J Roy Soc Interface* 2010; 7: 741.
19. DV Wilbrink, M Utz, RO Ritchie, MR Begley. Scaling of strength and ductility in bio-inspired brick and mortar composites. *Appl Phys Lett* 2010 (accepted for publication).
20. DH Alsem, R van der Hulst, EA Stach, MT Dugger, JThM de Hosson, RO Ritchie. Wear mechanisms and friction parameters for sliding wear of micron-scale polysilicon sidewalls. *Sens & Actuat A*. doi: 10.1016/j.sna.2010.06.2010.
21. M Benhassine, E Saiz, AP Tomsia, J De Coninck. The role of the commensurability of the substrate on the nonreactive wetting kinetics of liquid metals. *Acta Mater* 2010; 58: 2068.
22. E Saiz, M Benhassine, J De Coninck, AP Tomsia, Early stages of dissolutive spreading, *Scripta Mater* 2010; 62: 934.

Title

RADIATION DAMAGE EFFECTS IN CERAMICS AND NON-METALS

Principal Investigator

Kurt E. Sickafus

Address

Los Alamos National Laboratory

MS-G755

Los Alamos, NM 87545

e-mail

kurt@lanl.gov

Program Scope

The goal of this program is to understand the radiation damage response of ceramics exposed to neutrons or other energetic particles. Our studies of the damage response of ceramics address two objectives: (1) to predict microstructural evolution in ceramics exposed to radiation; and (2) to identify the physical aspects of ceramics that are effective in promoting radiation resistance. Our ultimate goal is to design new radiation-resistant ceramics. We conduct neutron, ion, and electron irradiation tests on both single and polycrystalline ceramics to evaluate their irradiation damage response. We perform computer simulations of damage evolution in ceramics to assist in our understanding of radiation damage phenomena in these materials. These simulations involve a number of computational techniques. In particular, we apply accelerated molecular dynamics (AMD) to reach experimentally relevant time scales in our simulations. This allows us to assess defect mobility, annihilation and aggregation with the goal of predicting radiation damage in non-metallic model oxides such as MgO and MgAl₂O₄. We have expanded these model oxide studies to examine the effects of impurities, composition and structure on radiation damage tolerance. A new emphasis of our program involves high-temperature irradiations using energetic neutrons, ions, and electrons, over a large range of radiation dose and using a variety of dose rates. We expect radiation resistant ceramics to find application in existing fission reactors, in future fusion reactors, or as ceramic nuclear fuel and waste forms.

Recent Progress

Much of our recent research relates to understanding the influence of atomic disorder on radiation damage evolution in complex oxide ceramics irradiated at low temperature. Our hypothesis is that materials that possess a natural ability to accommodate point defects and the atomic distortions that accompany those defects are the most radiation tolerant materials, in the sense that they are most resistant to radiation-induced amorphization. Amorphization is not the desired response for a material designed for application in a radiation environment because amorphization transformations are typically accompanied by large changes in volume (i.e., macroscopic swelling). Swelling leads to microcracking and thus material failure in application. Below we illustrate one example of the types of experiments we have performed recently.

Recently, we irradiated the following three scandium zirconium oxides (SZO) using 200 keV Ne^+ ions under cryogenic irradiation conditions. The three SZO compounds are: β - $\text{Sc}_2\text{Zr}_7\text{O}_{17}$, γ - $\text{Sc}_2\text{Zr}_5\text{O}_{13}$, and δ - $\text{Sc}_4\text{Zr}_3\text{O}_{12}$. The three oxides, β -, γ -, and δ -SZO, are known to undergo order-to-disorder (O-D) transformations during thermal annealing at temperatures of 630°C, 890°C, and 1763°C, respectively. These O-D transformations are characterized by a change in the atomic structure of the oxygen sublattices. Below the O-D transition temperature, the oxygen sublattices in the β -, γ -, and δ -SZO phases are ordered in the sense that the “vacancies” within each oxygen sublattice form ordered patterns. Above the O-D transition temperature, the vacancies within each oxygen sublattice are randomized and each SZO oxide takes on a crystal structure that is indistinguishable (in a diffraction sense) from the *fluorite* (MO_2) structure (note that the cation sublattices are also disordered). We refer to these high-temperature, disordered structures as “disordered fluorite” phases. Using ion irradiation, we were able to induce O-D transformations in the β -, γ -, and δ -SZO compounds that are apparently equivalent to the thermally-induced O-D transformations described above. We found that the ion dose necessary to induce the O-D transformation in the β and γ phases was lower than in the δ -phase. This is consistent with the thermally-induced disordering tendencies for the β , γ , and δ phases described above. Fig. 1 shows grazing incidence X-ray diffraction (GIXRD) and cross-sectional transmission electron microscopy results indicating that the δ -SZO compound undergoes an O-D transformation that (according to GIXRD) is complete by a Ne ion fluence of $2 \times 10^{16} \text{ Ne/cm}^2$ (~ 7.5 displacements per atom or dpa). It is also important to note that we have not been able to amorphize δ -SZO under cryogenic irradiation conditions to ion doses of nearly 40 dpa.

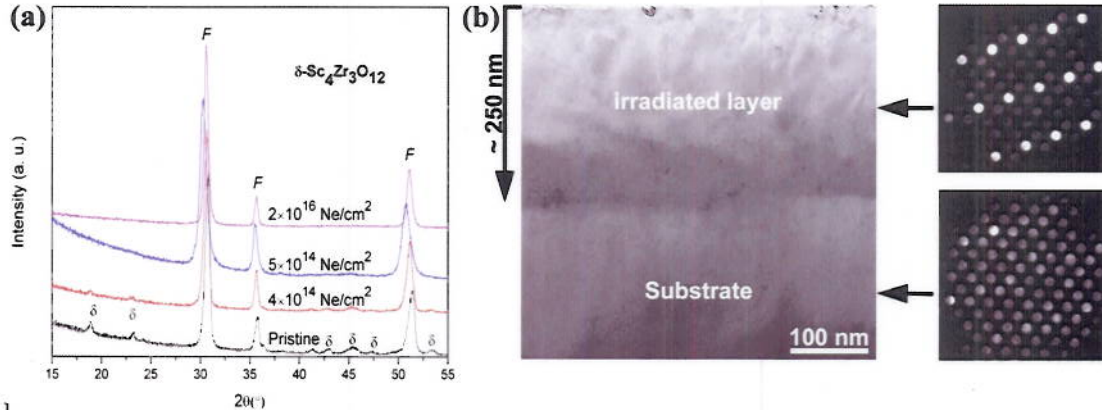


Figure 1. (a) XRD patterns obtained from pristine $\delta\text{-Sc}_4\text{Zr}_3\text{O}_{12}$ and $\delta\text{-Sc}_4\text{Zr}_3\text{O}_{12}$ irradiated with 200 keV Ne^+ ions to various ion fluences; (b) cross-sectional TEM bright-field image obtained from $\delta\text{-Sc}_4\text{Zr}_3\text{O}_{12}$ irradiated with 200 keV Ne^+ to a fluence of $5 \times 10^{14} \text{ Ne/cm}^2$ ($\sim 0.2 \text{ dpa}$). The inset micro-diffraction (μD) patterns show that the irradiated layer structure is partially changed compared to the substrate. The substrate μD pattern indexes as δ -phase, $\vec{H} = [211]_{\delta}$, while the strong reflections in the irradiated region μD pattern are consistent with a cubic fluorite structure with beam direction, $\vec{H} = [211]_f$.

Future Plans

Much of our recent research relates to understanding the influence of atomic disorder on low-temperature, radiation-induced amorphization and concomitant swelling. We have established important guidelines for identifying amorphization-resistant ceramics for use as radiation tolerant materials in extreme environment applications. Our future research will emphasize the development of a fundamental understanding of radiation damage behavior of complex oxides at high temperatures. Under high-temperature irradiation damage conditions, materials are often susceptible to macroscopic swelling due to void nucleation and growth (Fig. 2).

In our future research, we will examine radiation-induced void swelling. Our goal is to identify new materials that are inherently resistant to high-temperature radiation-induced swelling. We will perform high-temperature neutron, ion, and electron irradiations on a variety of simple and complex ceramics. We will complement these experimental studies with computer modeling.

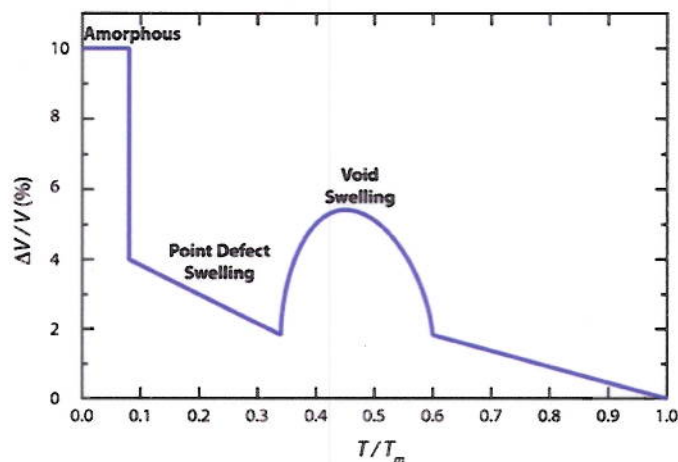


Figure 2. Schematic diagram of macroscopic swelling versus temperature (normalized by the melting temperature, T_m), for a material irradiated with energetic particles.

Selected References

- K. E. Sickafus, M. Ishimaru, Y. Hirotsu, I. O. Usov, J. A. Valdez, P. Hosemann, A.L. Johnson, T. T. Thao, "Compositional analyses of ion-irradiation-induced phases in δ - $\text{Sc}_4\text{Zr}_3\text{O}_{12}$," Nucl. Instr. and Meth. in Phys. Res. B 266 (12) (2008) 2892-2897.
- J. A. Valdez, Z. Chi, and K. E. Sickafus, "Light ion irradiation-induced phase transformations in the monoclinic polymorph of zirconia," J. Nucl. Mater. 381 (2008) 259-266.
- L. Kittiratanawasin, R. Smith, B. P. Uberuaga, K. E. Sickafus, A. R. Cleave, and R. W. Grimes, "Atomistic simulations of radiation induced defect formation in the Er_2O_3 sesquioxide," Nucl. Instr. and Meth. in Phys. Res. B 266 (2008) 2691.
- J. A. Ball, S. T. Murphy, R. W. Grimes, D. Bacorisen, R. Smith, B. P. Uberuaga, and K. E. Sickafus, "Defect processes in MgAl_2O_4 spinel," Solid State Sciences 10 (2008) 717.
- M. Tang, J. A. Valdez, and K. E. Sickafus, "Ion irradiation damage effects in δ -phase $\text{Y}_6\text{W}_1\text{O}_{12}$," J. Nucl. Mater. 376 (2008) 247.
- S. T. Murphy, B. P. Uberuaga, J. B. Ball, A. R. Cleave, K. E. Sickafus, R. Smith, and R. W. Grimes, "Cation diffusion in magnesium aluminate spinel," Sol. St. Ionics 180 (2009) 1-8.
- C. Jiang, C. R. Stanek, K. E. Sickafus, and B. P. Uberuaga, "First-principles prediction of disordering tendencies in pyrochlore oxides," Phys. Rev. B 79 (2009) 104203.
- C. Jiang, C. R. Stanek, N. A. Marks, K. E. Sickafus, and B. P. Uberuaga, "Predicting from first principles the chemical evolution of crystalline compounds due to radioactive decay: The case of the transformation of CsCl to BaCl ," Phys. Rev. B 79 (2009) 132110.
- M. W. Blair, M. R. Levy, R. W. Grimes, B. P. Uberuaga, C. Jiang, J. A. Valdez, J. J. Williams, M. Tang, C. R. Stanek, and K. E. Sickafus, "Charge compensation in an irradiation-induced phase of δ - $\text{Sc}_4\text{Zr}_3\text{O}_{12}$," J. Mater. Sci. 44 (2009) 4754-4757.
- C. R. Stanek, C. Jiang, B. P. Uberuaga, K. E. Sickafus, A. R. Cleave, and R. W. Grimes, "Predicted Structure and Stability of $\text{A}_4\text{B}_3\text{O}_{12}$ δ -phase Compositions," Phys. Rev. B 80 (2009) 174101.
- L. Kittiratanawasin, R. Smith, B. P. Uberuaga and K. E. Sickafus, "Radiation damage and evolution of radiation-induced defects in Er_2O_3 bixbyite," J. Phys.: Condens. Matter 21 (2009) 115403.
- M. Tang, K. S. Holliday, J. A. Valdez, B. P. Uberuaga, P. O. Dickerson, R. M. Dickerson, Y. Q. Wang, K. R. Czerwinski, and K. E. Sickafus, "Radiation damage effects in the uranium-bearing delta-phase oxide $\text{Y}_6\text{U}_1\text{O}_{12}$," J. Nucl. Mater. 389 (2009) 497-499.
- J. Won, J. A. Valdez, M. Naito, M. Ishimaru, and K. E. Sickafus, "Transmission electron microscopy study of an electron-beam-induced phase transformation of niobium nitride," Scripta Mater. 60 (2009) 799-802.
- C. Jiang, B. P. Uberuaga, K. E. Sickafus, F. M. Nortier, J. J. Kitten, N. A. Marks and C. R. Stanek, "Using 'Radioparagenesis' to Design Robust Nuclear Waste Forms," Energy and Environmental Science 3 (2010) 130.
- J. Zhang, Y. Q. Wang, M. Tang, J. Won, J. A. Valdez, and K. E. Sickafus, "Order-to-disorder transformation in δ -phase $\text{Sc}_4\text{Zr}_3\text{O}_{12}$ compounds induced by ion irradiation," J. Mater. Res. 25 (2010) 248.
- M. Tang, M., K. S. Holliday, C. Jiang, J. A. Valdez, B. P. Uberuaga, P. O. Dickerson, R. M. Dickerson, Y. Q. Wang, K. R. Czerwinski, K. E. Sickafus, "Order-to-disorder Phase Transformation in Ion Irradiated Uranium-Bearing Delta-phase Oxides $\text{RE}_6\text{U}_1\text{O}_{12}$ (RE = Y, Gd, Ho, Yb, and Lu)," J. Sol. St. Chem. 183 (2010) 844.
- C. Jiang, C. R. Stanek, N. A. Marks, K. E. Sickafus and B. P. Uberuaga, "Radioparagenesis: The Formation of Novel Crystalline Structures via Radioactive Decay," Phil. Mag. Lett. 90 (6) (2010) 435-446.
- J. Zhang, Y. Q. Wang, M. Tang, J. A. Valdez, and K. E. Sickafus, "Ion irradiation induced order-to-disorder transformations in δ -phase $\text{Sc}_{4-x}\text{Zr}_{3+x}\text{O}_{12+x/2}$," Nucl. Instr. Meth. in Phys. Res. B 268 (2010) 3018-3022.
- B. P. Uberuaga, C. Jiang, C. R. Stanek, K. E. Sickafus, N. A. Marks, D. J. Carter, and A. L. Rohl, "Implications of Transmutation on the Defect Chemistry in Crystalline Waste Forms." Nucl. Instr. Meth. in Phys. Res. B 268 (2010) 3261-3264.

Program title: Deformation Physics of Ultra-fine Scale Materials

PI: Amit Misra

<amisra@lanl.gov>

**Los Alamos National Laboratory, MS K771,
Los Alamos, NM 87545.**

The focus of this research is to integrate cutting-edge experimental techniques and characterization tools with state-of-the-art multi-scale modeling to extend the fundamental knowledge of deformation physics and strength-limiting mechanisms in ultra-fine scale materials, with emphasis on behavior at nanometer length scales. This initiative will focus on developing entirely new levels of understanding of the behavior of materials near their theoretical strength limit, and should catalyze new advances in the applications of such materials. The applicability of this knowledge should impact a broad range of engineering materials, from load-bearing structural components to high-strength electrical conductivity materials to electronic and electro-mechanical systems to structural materials in nuclear power reactors.

This proposal seeks to address a set of questions covering a broad area of deformation physics, and it is therefore appropriate that the program be able to draw upon a broad range of resources and capabilities. The principal investigator is Amit Misra at LANL. Richard G. Hoagland (co-PI until April 2009) is now involved in the program as a LANL Lab Associate, along with John P. Hirth as a consultant. In the modeling area, the program involves Jian Wang (staff scientist, LANL), Tim C. Germann (staff scientist, LANL), X.Y. "Ben" Liu (staff scientist, LANL) and a new hire post-doc (Christian Brandl). On the experimental side, LANL staff include Dhriti Bhattacharyya, Nan Li, Osman Anderoglu (post-doctoral researchers), Arief S. Budiman (Director's postdoctoral Fellow), Pat Dickerson (Electron Microscopy Lab staff), and J. Kevin Baldwin (technologist).

Selected recent accomplishments are summarized as follows:

1) *Dislocation climb at room temperature at interfaces in nanolayered composites*: Scripta Materialia (v. 60 (12) 2009) Journal Cover: Dislocation motion via climb involves diffusive mass transport and hence, this phenomena typically occurs at high homologous temperatures in bulk metals. Using atomistic simulations, we show that dislocations climb efficiently in metallic interfaces, such as Cu-Nb, through absorption and emission of vacancies in the dislocation core and a counter diffusion of Cu atoms in the interfacial plane. The high efficiency of dislocation climb in the interface is ascribed to the high vacancy concentration of 0.05 in the interfacial plane, the low formation energy of 0.12 eV with respect to removal or insertion of Cu atoms, as well as the low kinetic barrier of 0.10 eV for vacancy migration in the interfacial Cu plane. In a parallel study, using *in situ* nanoindentation in a TEM (at CINT core, ABQ), we have performed experiments that show dislocation annihilation via climb at fcc-bcc interfaces. Dislocation climb in the interface facilitates reactions of interfacial dislocations, and enables interfaces to be in the equilibrium state with respect to concentrations of point defects.

2) *De-twinning in nanotwinned Cu*: Using a combination of atomistic modeling and high-resolution TEM and *in situ* straining in a TEM, we have discovered (and understood the mechanisms of) the unusual phenomena of stress-induced migration of incoherent $\Sigma 3$ -{112}

which leads to detwinning (i.e., annihilation) of very thin (< 2 nm thick) growth twins in nanotwinned Cu. Nanotwinning gives rise to unusual combination of properties in metals such as high flow strengths AND high electrical conductivity along with high deformability and high thermal stability. The phenomena of detwinning is crucial in understanding the stability limits of nanotwinned structures and therefore, in design of optimal length scales of twinned structures.

3) *Shear instability in nanolayered composites due to weak interfaces*: Compression tests with Cu-Nb interfaces oriented 45° to compression axis allowed measurement of the shear strength of the interfaces. These experiments validate the earlier atomistic modeling studies in our team that showed the Cu-Nb interfaces are relatively weak in shear. These studies show that the multilayers are weakest when tested such that the applied shear is maximized parallel to the interfaces. These experiments also helped explain the unusual mechanism of shear instability observed for 90° compression tests where the layers were observed to rotate within a shear band such that the interface plane gets inclined to the compression axis. Furthermore, using “tunable” interatomic potentials in an fcc-bcc metal system with Kurdjumov-Sachs orientation, we showed that the variation in heats of mixing has a strong influence on the interfacial shear strength and the active shear plane at the interface. The critical stress for interface shear increases continuously with decreasing positive heat of mixing, but begins to decrease as the heat of mixing becomes negative since the active shear plane at the interface changes from fcc-bcc to fcc-fcc. This shows that the maximum strength in fcc-bcc systems can be tuned by varying the interfacial shear strength.

Spin-off activities

In the last 5 years, this program has led to several spin-off LDRD projects at LANL that have explored the fatigue behavior of nanolayered composites, radiation damage tolerance of nanolayered composites and high strength, high electrical conductivity nanotwinned metals. Most recently, the research from this program provided the basis for an Energy Frontier Research Center titled “*Center for Materials at Irradiation and Mechanical Extremes*” (M. Nastasi, center leader).

Collaborations

We collaborate with BES-user facilities, e.g., Center for Integrated Nanotechnologies at SNL and LANL (N.A. Mara and J.Y. Huang), and Advanced Light Source, Berkeley (N. Tamura).

In addition, significant external interactions are being pursued:

H.M. Zbib and D.F. Bahr (Washington State University): dislocation dynamics simulations and bulge testing of multilayers.

M.J. Demkowicz (MIT): atomic structures of interfaces and radiation damage.

X. Zhang (Texas A&M): nanotwinned fcc metals; radiation damage.

I. M. Robertson (University of Illinois), B. Clarke and K. Hattar (SNL): TEM of dislocation-interface interactions.

M. Uchic (AFRL, Ohio): *in situ* tensile testing in SEM of miniaturized FIB machined samples.

T. Ungar (Budapest, Hungary): XRD measurement of peak broadening in rolled multilayers.

P.M. Anderson (Ohio State University): dislocation models of multilayer strength.

Selected Recent Publications (2009-2010)

D. Bhattacharyya, X.Y. Liu, A. Genc, H.L. Fraser, R.G. Hoagland and A. Misra, *Heterotwin formation during growth of nanolayered Al-TiN composites*, Applied Physics Letters, **96**, 093113 (2010).

D. Bhattacharyya, N. A. Mara, P. Dickerson, R.G. Hoagland, and A. Misra, *A transmission electron microscopy study of the deformation behavior underneath nanoindents in nanoscale Al-TiN multilayered composites*, Philosophical Magazine, **90**:13, 1711 — 1724 (2010).

J. Wang, N. Li, O. Anderoglu, X. Zhang, A. Misra, J.Y. Huang, J.P. Hirth, *Detwinning mechanisms for growth twins in face-centered cubic metals*, Acta Materialia, **58**, iss.6, p.2262-2270, (2010). (ScienceDirect Top 25 Hottest Articles, Materials Science, Acta Materialia, 2010).

O. Anderoglu, J. Wang, J. P. Hirth, R.G. Hoagland, A. Misra, X. Zhang, *Plastic Flow stability of rolled nanotwinned Cu*, International Journal of Plasticity, **26**, iss.6, p.875-886 (2010).

N.A. Mara, D. Bhattacharyya, P. Dickerson, R.G. Hoagland, A. Misra, *Ultra-high strength and ductility of metallic nanolayered composites*, Materials Science Forum, invited overview to a special volume on Ductility of Nanostructured Materials, **633-634**, p. 647-653 (2010).

N. Li, J. Wang, J.Y. Huang, A. Misra and X. Zhang, *In situ TEM observations of room temperature dislocation climb at interfaces in nanolayered Al/Nb composites*, Scripta Materialia, **63**, 363 (2010).

Q. Wei and A. Misra, *Transmission Electron Microscopy Study of Microstructure and Crystallographic Orientation Relationships in V/Ag Multilayers*, Acta Materialia, **58**, 4871 (2010).

X.-Y. Liu, R.G. Hoagland, J. Wang, T.C. Germann, and A. Misra, *The Influence of Dilute Heats of Mixing on the Atomic Structures, Defect Energetics and Mechanical Properties of fcc-bcc Interfaces*, Acta Materialia, **58**, 4549-57 (2010).

N.A. Mara, D. Bhattacharyya, J.P. Hirth, P. Dickerson, and A. Misra, *Mechanism for shear banding in nanolayered composites*, Applied Physics Letters, **97**, 021909 (2010).

J. Wang and A. Misra, *An Overview of Interface-dominated Deformation Mechanisms in Metallic Multilayers*, Current Opinions in Solid State and Materials Science, submitted. (INVITED).

J. Wang, O. Anderoglu, J. P. Hirth, A. Misra, X. Zhang, *Dislocation Structure of $\Sigma 3\{112\}$ Twin Boundaries in Face Centered Cubic Metals*, Applied Physics Letters, **95**, 021098 (2009).

J. Wang, R.G. Hoagland, A. Misra, *Mechanics of nanoscale metallic multilayers: from atomic-scale to micro-scale*, Scripta Materialia, **60**, 1067 (2009). Invited paper in viewpoint set on nanostructured materials. (ScienceDirect Top 25 Hottest Articles, Materials Science, Scripta Materialia, 2009).

J. Wang, R.G. Hoagland, A. Misra, *Room temperature dislocation climb in metallic interfaces*, Applied Physics Letters, 94, 131910 (2009).

D. Bhattacharyya, N.A. Mara, P. Dickerson, R.G. Hoagland, A. Misra, *Transmission electron microscopy study of the deformation behavior of Cu/Nb and Cu/Ni nanoscale multilayers during nano-indentation*, Journal of Materials Research, 24, 1291 (2009).

C. C. Aydiner, J. Almer, D. W. Brown, N. A. Mara, A. Misra, *In situ X-ray investigation of free-standing nanoscale Cu-Nb multilayers under tensile load*, Applied Physics Letters, 94, 031906 (2009).

J.P. Hirth, *The NABARRO Legacy - Perspectives for Advance Materials in the 21st Century - Foreword*, Progress in Materials Science, (2009) Vol.54, iss.6, spec. iss. SI, p. 663-663.

Statistical multi-scale study of twinning in HCP Mg & Zr

C.N. Tomé* (PI), I.J. Beyerlein, J. Wang, R. McCabe

* e-mail: tome@lanl.gov

MST-8, MS G755, Los Alamos National Laboratory, Los Alamos, NM, 87545, USA

Abstract: The focus of this BES Program is to elucidate the fundamental mechanisms of slip and twinning responsible for the plastic deformation of HCP crystals, and to explain the macroscopic response of HCP aggregates via a multi-scale approach that incorporates the elementary mechanisms.

Here we present a statistical experimental characterization and modeling approach for describing twin nucleation and propagation in HCP materials, explain how we incorporate it in polycrystal plasticity models, and show predictions for Mg. This research highlights, for the first time, the role that micro-scale twin nucleation and local stress states play in determining the macro-scale polycrystal response.

Description: Because twin propagation is responsible for the characteristic hardening and texture evolution observed in HCP metals subjected to plastic deformation, most twin analysis are only concerned with propagation. Twin propagation, however, is preceded by twin nucleation. In this work we recognize such subordination, and separate nucleation from propagation effects.

We studied nucleation in hcp metals (Mg, Zn, Zr) using geometrical analysis, molecular static/dynamics (MS/MD), and DFT [J. Wang et al, 2009a,b, 2010a]. The results show that a twin nucleus must consist of at least 6 atomic layers for it to be stable and that a single twinning dislocation cannot glide alone in a perfect HCP crystal, but only on a pre-existing twin boundary plane. The important conclusions from these studies are: 1) *the pole mechanism for twin nucleation proposed time ago by Thompson and Millard [1952] is not feasible for HCP metals;* 2) *twin nucleation is energetically unlikely to occur inside the grain because it involves a zonal dislocation with large Burgers vector.* In addition, experimental observations from EBSD indicate that twins always start at grain boundaries [Capolungo et al, 2009; Beyerlein et al, 2010].

Therefore, we examined the atomic structure of symmetrical tilt grain boundaries (STGBs) using MS, and performed the study of dislocation-GB interactions using MD [Wang et al, 2009b]. We carried this analysis for Mg, for which a reliable interatomic potential is available [Liu et al, 1996]. The important finding of MS is that for tilt angles θ greater than 28° STGBs of Mg can be characterized as a low energy coherent boundary plus an array of grain boundary dislocations (GBDs), which encourages a GB representation using dislocation theory [Wang et al, 2009b] (see Figure 1). The Burgers vectors of these pre-existing GBDs within STGBs are large in comparison to the zonal dislocation, and can potentially react with incoming lattice dislocations or dissociate into partials to produce the defects needed for stable twin nucleus formation. We tested this idea for two STGBs of significantly different tilt angles using MD simulations. For the 17° STGB, the leading dislocation in a pile up reacts with the GB and nucleates a few small ($\bar{1}012$) twin embryos, which coalesce with time to form a sizable and stable twin nucleus (Fig. 1b). For the 68° STGB, we observe migration of the boundary away from the initial boundary plane (Fig. 1c), as the basal dislocations from the pile-up react with the boundary. *This research clearly demonstrates that: 1) twins can nucleate from grain boundaries; 2) the grain boundary misorientation, by way of its atomic structure, has a significant influence on the mechanism for twin nucleation; 3) pile-ups constitute a plausible nucleation triggering mechanism.*

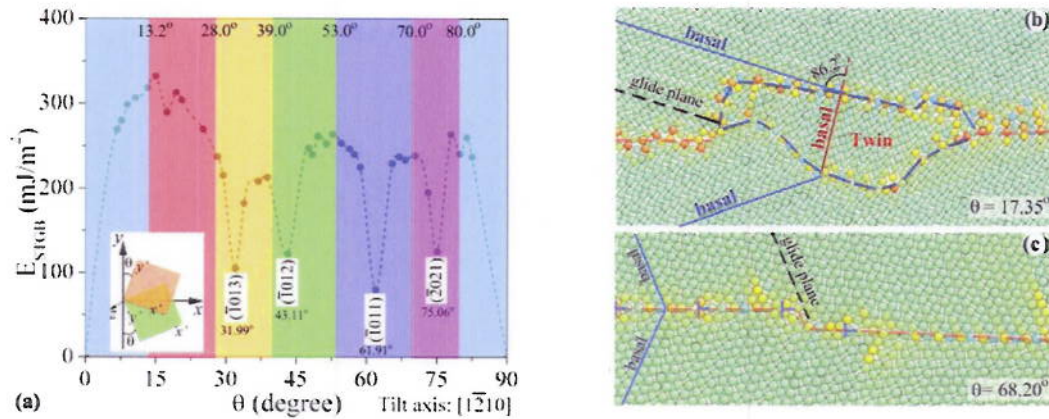


Figure 1: (a) Excess potential energies of grain boundaries as a function of θ . The colored regions mark ranges of θ in which STGBs can be viewed as having similar atomic structure. Blue: arrays of GBDs; red: random configuration STGBs; orange, green, purple: twin boundaries plus GBDs; cyan: $\{-2021\}$ STGB plus GBDs. Interactions of STGBs with a four-dislocation pileup: (b) twin nucleation from a 17.35 STGB; (c) migration of a 68.20 STGB twin boundary.

The atomistic analysis of tilt boundaries described above suggests a plausible twin nucleation mechanism. As a consequence, we undertook making an experimental quantitative statistical analysis of grain boundaries and twins in Mg and Zr. A computer code was developed [Marshall et al, 2010] to derive a large range of twin statistics based on raw EBSD data. The statistics include twinning dependencies (presence of twins, number of twins, twin thickness, twin type, twin variant) on grain parameters such as orientation, size, and neighbor grain parameters. Using the code we analyzed EBSD scans comprising thousands of grains and $\{10-12\}$ tensile twins in Zr deformed 5% and 10% at 76K and Mg deformed 3% at 300K. Twinning statistics for Zr and Mg are reported in [Capolungo et al, 2009c] and [Beyerlein et al, 2010a] and two examples of twin statistics for Mg are shown in Figure 2.

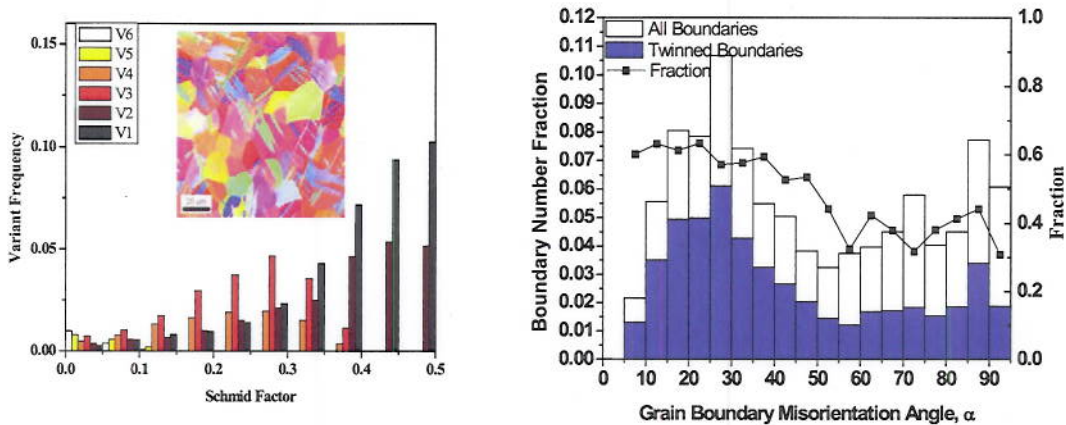


Figure 2: Two examples of twin statistics based on EBSD data for Mg compressed 3%. Left frame: frequency of twins of different variants as a function of Schmid Factor (V1 is the variant with the highest Schmid factor in a grain, and V6 with the lowest). Right frame: probability of twins being observed at a grain boundary based on the misorientation angle across the boundary

The EBSD evidence supports the MD result of dislocation pile ups inducing twin nucleation. Among the important conclusions of this analysis, applicable to Mg and Zr, and probably universal for HCP materials, are: 1) *the twin variant with the highest Schmid factor is not always the one that nucleates*; 2) *twin thickness and twin fraction are independent of grain size, which negates the frequently postulated Hall-Petch effect for twinning*; 3) *low angle grain boundaries exhibit a higher probability of twin nucleation*; 4) *twin nucleation is driven by local (micro) stresses, but twin propagation is driven by the resolved shear associated with grain interactions*.

The constitutive laws used in the literature for describing twinning: 1) do not separate nucleation from propagation; 2) do not acknowledge that nucleation precedes propagation; 3) do not account for the statistical characteristics of deformation twinning. We developed a probabilistic twin nucleation model consistent with the statistical correlations provided by EBSD. Our model dictates when twinning occurs, in which variant, and in which grains [Beyerlein and Tomé, 2010]. Twin nucleation is assumed to be induced by local stresses at grain boundaries, as our MD simulations suggest. The rate of twin nucleation is described by a stochastic Poisson process and increases with the local stress and the grain area. Two other statistical components of the model are: 1) local stress fluctuations at the boundary, associated with the presence of randomly occurring pile ups; 2) a distribution of threshold stresses for nucleation, associated with different local configurations of dislocations at the grain boundary.

This twin nucleation model was combined with a **Composite Grain (CG)** model and with a **Dislocation-Density (DD)** hardening law for slip, both developed within this BES program. In the CG model each grain is treated as a layered structure of twin-matrix domains interacting with each other. The CG model follows the evolution of twin fraction in each individual grain, captures the directionality of twin barriers towards dislocations, and the evolving morphology of twins. The CG model was successfully applied to understand the hardening and texture evolution associated with strain-path changes in Zr and Mg [Tomé & Kaschner, 2005; Proust et al, 2007, 2009]. As for the DD hardening law, it uses dislocation densities on each deformation mode as a state variable, and the activation of the different slip modes is a function of temperature and strain rate [Beyerlein and Tomé, 2008]. The resistance to slip is the result of the storage of forest and substructure dislocations, and their interaction with twins. The predictive capability of the model under temperature and strain path changes has been tested for Zr and Mg [Beyerlein & Tomé, 2008; Capolungo et al., 2009a,b]. *This model is the first of its kind for HCP (and low symmetry) metals, and provides a link with results of Dislocation Dynamic simulations [Capolungo & Beyerlein, 2010], and with experimental determinations of dislocation densities via Diffraction Peak Broadening analysis [Ungar et al, 2010].*

The culmination of this effort consisted in integrating the statistical twin nucleation model, the Composite Grain model and the dislocation density evolution models into a single grain constitutive response model that was implemented inside the polycrystal plasticity code VPSC [Lebensohn & Tomé, 1993]. We applied it to pure Zr and pure Mg, the two HCP materials that were statistically characterized using EBSD. The model captures twin statistics over the grains that are consistent with the EBSD evidence reported in [Beyerlein et al, 2010; Capolungo et al. 2009c], such as the spread in nucleation events along the strain path, the variant selection as a function of grain orientation (shown in Fig 2), and the dispersion in the number of twins per grain. In addition, *we demonstrate that capturing the variability associated with stochastic processes is critical for correctly predicting the strain evolution of flow stress, hardening rate, twin volume fraction, and texture*. Figure 3 compares the measured and predicted stress-strain curves for Zr and Mg as an example [Beyerlein & Tomé, 2010; Beyerlein et al, 2010b].

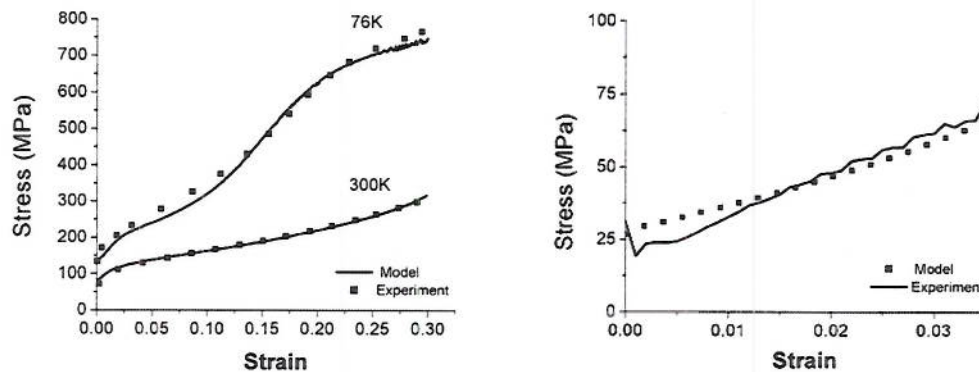


Figure 3. Comparison of the measured (symbols) and predicted (lines) stress-strain curves (a) for Zr at 76K and 300K and (b) for Mg at 300K.

References

- I. J. Beyerlein and C. N. Tomé, "A dislocation-based constitutive law for pure Zr including temperature effects", *International Journal of Plasticity* 24 (2008) 867-895.
- I.J. Beyerlein and C.N. Tomé, "A probabilistic twin nucleation model for HCP polycrystalline metals", *Proc. Royal Soc. of London* 466A (2010) 2517-44
- I.J. Beyerlein, L. Capolungo, P.E. Marshall, R.J. McCabe, C.N. Tomé, "Statistical analyses of deformation twinning in magnesium", *Philos Magazine* 90 (2010a) 2161
- I. J. Beyerlein, R. J. McCabe, C. N. Tomé, "Stochastic processes of (1012) deformation twinning in hcp polycrystalline zirconium and magnesium", *J. of Multiscale Comp. Engng.* (2010b), in press
- L. Capolungo, I.J. Beyerlein and C.N. Tomé, "Slip-assisted twin growth in hexagonal close packed metals", *Scripta Mater.* 60 (2009a) 32-35.
- L. Capolungo, I.J. Beyerlein, G.C. Kaschner and C.N. Tomé, "On the interaction between slip dislocations and twins in HCP Zr", *Mater. Sci. Engng. A* 513-514 (2009b) 42-51.
- L. Capolungo, P.E. Marshall, R.J. McCabe, I.J. Beyerlein and C.N. Tomé, "Nucleation and propagation of twins in Zr: a statistical study", *Acta Mater.* 57 (2009c) 6047-56
- L. Capolungo, I. J. Beyerlein, "The role of elastic anisotropy on plasticity in hcp metals: a 3-dimensional dislocation dynamics study", *Mod. Sim. Mats. Sc. Engng.* (2010) in press
- R.A. Lebensohn and C.N. Tomé, "A self-consistent anisotropic approach for the simulation of plastic deformation and texture development of polycrystals -Application to zirconium alloys", *Acta metall. mater.* 41 (1993) 2611-2624.
- X.Y. Liu, Adams JB, Ercolessi F and Moriarty JA, *Model. Simul. Mater. Sci. Eng.* (1996) 4:293
- P.E. Marshall, G. Proust, J.T Rogers, and R.J. McCabe, "Automatic twin statistics from electron backscattered diffraction data", *J. Microscopy* 238 (2010) 218 .
- G. Proust, C.N. Tomé, and G.C. Kaschner. "Modeling Texture, Twinning, and Hardening Evolution During Deformation of Hexagonal Materials", *Acta Materialia* 55 (2007) 2137-2148.
- G. Proust, C.N. Tomé, A. Jain, S.R. Agnew, "Modeling the effect of twinning and detwinning during strain path changes of Mg alloy AZ31", *Int. J. of Plasticity* 25 (2009) 861-880.
- N. Thompson and D. J. Millard, "Twin formation in cadmium", *Philos. Mag.* 43 (1952) 422-440
- C.N. Tomé and G.C. Kaschner. "Modeling texture, twinning and hardening evolution during deformation of hexagonal materials" *Mats Sc Forum* 495-497 (2005) 1001-1006.
- T. Ungár, G. Ribárik, L. Balogh, A. A. Salem, S. L. Semiatin, *Scripta Mat.*, 63 (2010) 69-72
- J. Wang, J.P. Hirth and C.N. Tomé, "(1012) twinning nucleation mechanisms in hexagonal-close-packed crystals", *Acta Mater.* 57 (2009a) 5521-30
- J. Wang, R.G. Hoagland, J.P. Hirth, L. Capolungo, I.J. Beyerlein and C.N. Tomé, "Nucleation of (1012) twin in hexagonal close packed crystals", *Scripta Mater.* 61 (2009b) 903-906
- J. Wang, I.J. Beyerlein, C.N. Tomé, "An atomic and probabilistic perspective on twin nucleation in Mg", *Scripta Mater.* 63 (2010a) 741-746

SISGR: Evolution of Grain Boundary Networks in Extreme Radiation Environments

Mukul Kumar, James Belak, Joel Bernier, Vasily Bulatov, Thomas Lagrange, Bryan Reed, and Ming Tang
Lawrence Livermore National Laboratory
7000 East Avenue, L-356
Livermore, CA 94550
E-mail: mukul@llnl.gov

Project Definition:

Advanced nuclear energy systems will require materials to perform for extended periods under conditions of elevated temperatures and high radiation exposures. Conventional engineering materials lack the required microstructural stability and exhibit excessive coarsening, hardening, and swelling. It is considered that grain boundaries in nanocrystalline materials can substantially reduce this degradation by acting as highly effective sinks for point defects. Unfortunately, nanocrystalline materials can also be unstable with respect to thermal coarsening, so their long-term efficacy requires the microstructure to be stabilized. Our previous work shows that grain boundary (GB) networks consisting of a high fraction of annealing twins and twin variant boundaries can be stabilized against thermal coarsening [Schwartz, King, and Kumar, *Scripta Mater.*, **54** (2006), 963] and interface-mediated degradation.

We are investigating whether such networks of grain boundaries can also sustain microstructural stability under irradiation. The objective of the project is to develop the basic science needed to address the overarching question: What must a grain boundary network look like if it is to act as an effective point defect sink, not only on initial deployment, but after months or years of severe irradiation? We envision a network in which high free volume, high-energy “random” boundaries act as point defect sinks while the more stable, low energy special boundaries anchor the network, and the entire ensemble is statistically stable over the lifetime of the material. To understand whether this is possible, we are studying (1) the coupled evolution of grain boundary structure and point defects, using simulation, theory, and transmission electron microscopy of irradiated materials, and (2) what this implies about the evolution of the GB network, using spatially-resolved diffraction coupled with mesoscale theory.

In the first year of the project we have initiated inter-related thrusts that represent a tightly coupled combination of theory (crystallography and defect dynamics), computations (molecular dynamics and phase field), and experiment (*in situ* transmission electron microscopy, electron backscatter diffraction, and three-dimensional X-ray diffraction) to explore the basic physics governing the evolution of microstructures under high-dose irradiation. Using a model system (copper), we are exploring the phase space of energy and intrinsic mobilities of interfaces commonly observed in GB engineered microstructures ($\Sigma 3$, $\Sigma 9$, and $\Sigma 27$, and other random, using the notation of the Coincident Site Lattice model) and extending the analysis from perfect structures to vicinal character. These results are informing a crystallographically-sophisticated multiscale model of the interaction between radiation-induced point defects and grain boundaries in the context of a highly coordinated GB network. As a complement to the theory and simulations efforts, the experimental effort in the first year has focused on thermal coarsening of a variety of microstructures in pure copper. A synopsis of this work in progress will be described below.

Recent Progress and Future Plans:

Simulations of Microstructural Evolution

Our previous work (reference above) has shown that GB networks with sufficient special boundary content are substantially more resistant to thermal coarsening than are more random networks. Now we are creating the tools to fully develop this hypothesis in the context of radiation damage. To this end, we have built a suite of GB network analysis and simulation tools, representing both simulated and experimentally derived data with the very same data structures. These structures implement the same kinds of algorithms as are present in standard EBSD packages, but in an explicitly hierarchical class structure that retains high-resolution information and grain-boundary-network-level information side by side.

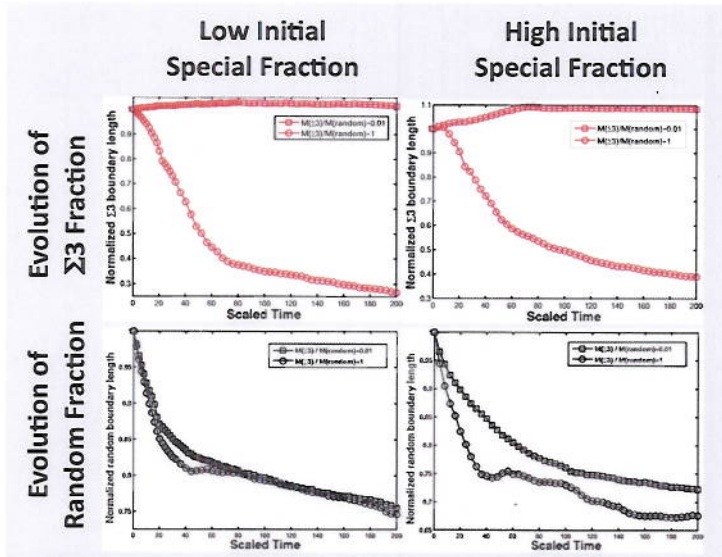


Figure 1. Simulations of coarsening (represented by a change in boundary length per area) in a microstructure typical of normal FCC materials (left) and ones typical of grain boundary engineered materials (right). The upper curve in each case shows the effect of the very low mobility (0.1 of a random boundary) of $\Sigma 3$ boundaries; the lower curve is the same simulation with all anisotropy effects represented through energy alone.

field model in that it discretizes the grain orientation space into a finite number of “representative” orientations and assigns a phase-field variable to each orientation. These representative orientations are chosen by the group-theoretical Monte Carlo code, which by its nature produces an ensemble representative of the microstructures of interest.

Use of this code has shown us that the coarsening of the random boundary network can indeed be slowed by the presence of special boundaries. However, two conditions have to be satisfied: As is shown in Fig. 1, (1) the special boundary fraction must be high; specifically it must be in the range typical of grain-boundary-engineered rather than conventional microstructures, and (2) the special boundaries must have exceptionally low mobility. Low energy alone does not suffice to pin the random boundary network. This result is intuitively reasonable and lends support to the appropriateness and correctness of our modeling approach. Extensions to other microstructural constructs are underway.

The same analysis code is already being extended to three dimensions for analyzing experimental data, specifically in the form of serial-sectioning EBSD data. Using a data set obtained through collaboration with Brigham Young University (Prof. Brent Adams), we have developed robust algorithms for 3-D reconstruction that filters out a wide range of experimental anomalies, including single-pixel noise, nonlinear distortions due to positioning and scanning in the SEM, and finite orientation precision. The reconstruction will be completed in the very near future, providing direct experimental tests of stereological

In particular, the code implements our grain boundary network generation algorithms [Reed and Kumar, *Scripta Mater.*, **54** (2006), 1029] that produce statistically realistic GB networks using a phenomenological group-theory-based variant of the Potts model. This produces GB networks with length fractions, number fractions, and triple junctions distributions (of all relevant boundary disorientation types), as well as cluster metrics matched to those encountered in experimental microstructures; tuning of the parameters of the model allows a significant degree of precision and a statistically realistic starting point for the next, more physics-based, level of modeling.

This has been implemented in a multi-order-parameter phase field model through a collaboration with Dr. Nele Moelans (Catholic University, Leuven, Belgium), using a recently-developed algorithm [Moelans *et al.*, *Phys. Rev. Lett.*, **101** (2008), 025520]. This type of formulation differs from the quaternion-based phase-

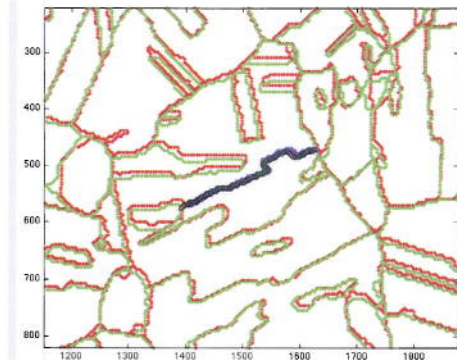


Figure 2. Part of the GUI for checking the alignment and cross-layer identification of grain boundaries, an essential step in the 3D reconstruction. Two neighboring layers (in red and green) are shown, giving a direct visual representation of the distribution of boundary plane tilts, with one layer transformed into the reference frame of the other (with a new algorithm that allows an rms alignment error of less than 2 pixels across a large field of view). Blue and black symbols highlight two boundary traces (one in each layer), which the software has identified as being parts of the same three-dimensional boundary.

methods intended to extract 3D grain boundary populations from 2D cross sections [Reed and Kumar, *Mater. Res. Soc. Symp. Proc.*, **819** (2004)], thus eliminating the exponential cost associated with 3-D sampling.

To take the simulations to the next step, we are developing several improvements in parallel: (1) More realistic, 5-D energy and mobility metrics incorporating GB plane orientation dependence are being derived from molecular dynamics (MD) and crystallographic theory. Work toward enriching this metric by incorporating radiation-induced point defects has also commenced. (2) We have built a fixed, finite ensemble of grain orientations to allow the multi order parameter phase field model to explicitly allow nucleation within a variation on the group-theoretical formulation. (3) Having tested the methods in 2-D, we plan to extend them to 3-D, using phase field methods developed previously for other crystallographic transformations.

To enable physically consistent meso-scale simulations of GB networks under thermal coarsening and irradiation conditions, we have devised a new representation of GB positions in the full 5-dimensional space of macroscopic DOF (mis-orientations + inclinations). The new representation is built on the notion of partially matched bonds inspired by the well-known bond counting arguments from surface sciences. By construction, our metrics obey all crystal symmetries in the 5-D space and satisfy the “no boundary” condition for any two perfectly oriented half-crystals ($\Sigma 1$) regardless of the plane inclination. We are using the new representation to obtain the GB energy as a function of 5 DOF that would provide the best fit to two large sets of boundary energies published recently by Olmsted *et al* for Al and Ni (388 boundaries for each case) [Olmsted, Foiles, and Holm, *Acta Mater.*, **57** (2009) 3694]. Our results so far lead us to believe that a reasonably accurate GB energy function can be defined in the full 5D space of macroscopic DOFs for each distinct crystallography class (FCC, BCC, HCP). Such a function is universal for a given crystallography but contains a handful of material-specific parameters that can be fitted to a few important boundary structures.

The same representation can be used to parameterize the intrinsic boundary mobility as a function of the same five macroscopic DOFs. Given the general confusion about GB mobilities in the literature, we are now performing atomistic simulations of the mobility behavior of boundaries vicinal (in the inclination or the mis-orientation subspace) to the lowest energy $\Sigma 1$ (low-angle) and symmetric and asymmetric $\Sigma 3$ twin boundaries in Cu. This formulation builds upon the ideas of Mott (*Proc. Royal Soc.*, **60(4)** (1949), 309) and Gleiter (*Acta Metall.*, **17** (1969), 853), where the construct considers steps, thus allowing vicinal characteristics more closely representing the observed boundary structures. This is a significant advancement in comparison to reports in the literature that usually consider idealized representations. Bi-layers with such vicinal boundary character were then exercised in a MD simulation. In contrast to idealized representations the observation in this study was that the vicinal nature of these boundaries rendered them mobile. The mechanism enabling this motion is directly related to the response of the steps to the shearing impetus.

Thermal Coarsening Experiments

To understand the thermal evolution and stability of microstructures under particle radiation, we must first examine their thermal stability alone. For this purpose, we have chosen several different microstructural topologies that are observed in copper. Our prior work on conventional and GB engineered microstructures with average grain sizes over a micrometer was repeated in the past year, and will not be discussed further in this report. We have also undertaken thermal coarsening experiments on microstructures with a significantly smaller characteristic length scale. In one case, we aim to repeat the annealing experiments of Simoes *et al* [Simoes, Calinas, *et al.*, *Nanotechnology*, **21** (2010) 145701] with microstructures that contain a significant amount of special boundaries. Our observations suggest that the nanocrystalline Cu foils tend to evolve towards a microstructure with a grain size of ~ 300 nm, when

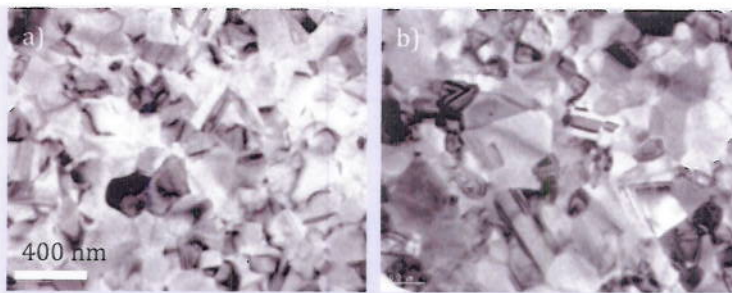


Figure 3. TEM brightfield images of nanocrystalline Cu: a) moderate fraction of twin boundaries before annealing, and b) annealing at 773K for 3hrs *in-situ* in the TEM leads to an increase in grain size and the number of twins.

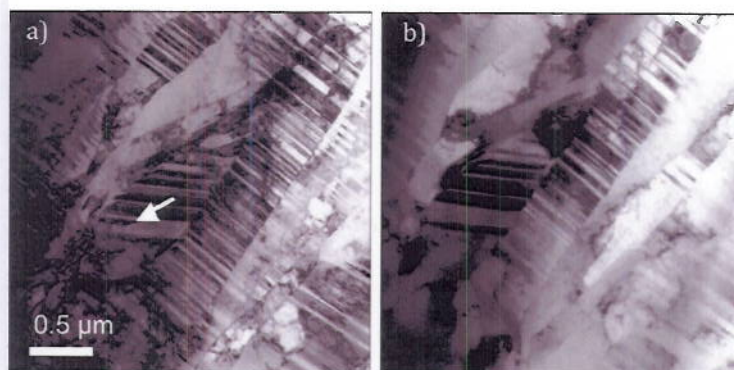


Figure 4. Cross-section TEM images of the unique microstructure in Cu films generated by the pulsed sputter-deposition process. The columnar grains are parallel to the film growth direction and contain a high density of fine twins that are roughly perpendicular to it: a) before annealing, b) annealed sequentially at 573K for 2hrs, 673K for 1hr and 773K for 1hr. With exception to the slight bending of the foil during heating that tilts some the twins out of contrast, the microstructure remains essentially unchanged by the thermal treatment at high temperatures. The arrow indicates an, segmented twin that disappears during annealing.

annealed at 773K for 3 hours, and in addition to a slight increase in grain size also shows a modest bump in the number of annealing twins.

As a contrast, annealing of as-deposited, magnetron-sputtered Cu films with an equiaxed, nanograin microstructure with few special boundaries shows significant grain growth (as much as 4-5X larger than the initial grain diameters (see Fig. 3). The grain growth in these materials was also accompanied by a parabolic increase in the twin boundary area with time. Although the annealing temperatures were moderate (573K-773K), the microstructure was thermally unstable and coarsened quickly. These observations are in accord with those made on more conventional grain sized microstructures, both with an initial low

or high twin and special boundary content.

We have also studied the thermal stability of an exotic microstructure produced by a pulsed, high-power, sputter deposition process (see Fig. 4). The mode of film growth is quite unique under pulsed deposition; large aspect ratio columnar grains grow by a strain relaxation process that generates a high density of fine twins within the grains. Most of the twins are oriented parallel to the substrate in the plan of the film, resulting in a microstructure with a strong $\langle 111 \rangle$ texture. When annealed, no significant change in the microstructure was observed even at temperatures as high as 773K, as evidenced in the *in-situ* TEM experiment from which snapshots are shown in Fig. 4. The thermal stability may stem from the high density of nanometric sized twins that perhaps stabilize and “lock-in” the otherwise mobile random boundaries between the columnar grains. Future experiments will assess the effect of concomitant particle irradiation at high temperature on the stability of this microstructure.

In addition, to better quantify the evolution of the microstructure and change in grain boundary character, we will characterize the evolution in the grain boundary network in the TEM using the newly acquired Nanomegas ASTAR orientation mapping system. This will be complemented by 3-D X-ray diffraction microscopy at APS (Argonne) in collaboration with the Suter group from Carnegie Mellon University. Beam time for these experiments has been allocated in the Fall-Winter cycle of this year. Complementary experiments will be carried out (next spring) at the European Synchrotron Research Facility in collaboration with colleagues at Riso National Laboratory in Denmark, and we also have on-going experiments at the ALS facility (LBNL). The experiments that will map the 3-D GB network will enable us to verify and validate our algorithm for mapping 3-D microstructures from 2-D statistics. Initial exercises in this regard have been reported for the case of isotropic microstructures such as those found in aluminum (from the CMU group), but these data are not readily translatable to the case of copper, which has a broader spectrum of GB energies. In-situ annealing experiments, with and without radiation damage will be a statistical complement to our TEM-based experiments.

Acknowledgments:

This work was performed under the auspices of the U.S. Department of Energy by Lawrence Livermore National Laboratory under Contract DE-AC52-07NA27344, with support from the BES SISGR grant. MT would also like to thank the Lawrence Postdoctoral Fellowship Program at LLNL for support.

Multiscale Mechanical Properties and Alloy Design

Principal Investigators

E. P. George, H. Bei, J. R. Morris, G. M. Pharr

Materials Science and Technology Division, Oak Ridge National Laboratory, 1 Bethel Valley Road, Oak Ridge, TN 37831-6115. Email: georgeep@ornl.gov, beih@ornl.gov, morrisj@ornl.gov, pharrgm@ornl.gov

Principal Collaborators

Y. F. Gao, Department of Materials Science and Engineering, University of Tennessee

Program Scope

This program aims to develop fundamental understanding of mechanical behavior across multiple length scales in metals and alloys. Of special interest are new mechanical phenomena, including size effects on mechanical properties. Interesting size effects occur at several different length scales, but our near-term focus is on small-scale mechanical behavior. Over the long term, our goal is to understand the physical mechanisms of interaction across multiple length scales in multiphase alloy systems. The observed relationships between mechanical properties and microstructural features (controlled, as needed, by innovative processing techniques and characterized by state-of-the-art microanalytical tools) are used to model deformation and fracture processes. This understanding will lead to the formulation of broad scientific principles for the design of advanced metallic materials for use in a variety of next-generation energy conversion and other structural applications.

Recent Progress

Because of space limitations only a few highlights of our recent research progress are provided below. A partial list of publications resulting from this work is provided at the end of this abstract.

Small-scale mechanical behavior: interactions between material and specimen length scales

How a material responds to an increase in dislocation density (ρ) depends on its initial dislocation density [1]. If there are no dislocations in the volume of material tested, yielding requires dislocation nucleation at very high stresses approaching the theoretical strength and, indeed, that is what is observed in whisker tension [e.g., 2], micropillar compression [e.g., 3] and nanoindentation pop-in [e.g., 4] tests. When dislocations are introduced into such pristine volumes, strength is expected to initially *decrease* with increasing dislocation density [1], that is, one expects to see *strain softening* since plastic deformation can occur by the motion of pre-existing dislocations at relatively low stress without the need for dislocation nucleation. With further increases in dislocation density, the trend is expected to eventually reverse course and conventional strain hardening is then expected [1].

To understand size-dependent strength, it is useful to consider two inter-related length scales. One is the average spacing between dislocations (l), which is an intrinsic (material) length scale set by the dislocation density ($l \sim \rho^{-0.5}$). The second length scale is one that is imposed by the size of the specimen, d . For a given ρ , as d decreases, the number of dislocations in the specimen decreases and eventually reaches the dislocation-free limit where yielding can occur only at the theoretical stress. The reverse happens as d increases, eventually reaching the “bulk” or continuum limit in sufficiently large specimens where many dislocations are present. This transition from the bulk to theoretical strength is a manifestation of the “smaller is stronger” size effect and is expected to depend on both length scales l and d .

Following the seminal experiments of Uchic et al. [5], there was a worldwide explosion of research aimed at investigating the effects of d on mechanical behavior. The resulting body of work has shown that strength generally increases with decreasing d [6], and eventually reaches the theoretical strength at micrometer length scales where the specimens are expected to be dislocation-free [3]. We have recently extended these studies to characterize the effects of the second length scale l on mechanical behavior. Our approach utilizes long-aspect-ratio fibrous composites produced by directional solidification of NiAl-Mo eutectic alloys. The composites are compressed along the fiber axes to different levels of pre-strain, followed by etching back of the NiAl matrix to expose the Mo fibers as free-standing micro-pillars [7]. The exposed micro-pillars are then compression tested in a modified nanoindentation system equipped with a flat-tip indenter.

Figure 1 shows stress-strain curves of the $d = 500\text{--}550$ nm micropillars as a function of pre-strain. The as-grown (0% pre-strain) pillars (Fig. 1a) exhibit reproducible stress-strain curves that are initially elastic but, upon reaching the theoretical stress (~ 9.3 GPa), yield with a sudden strain burst and catastrophic plastic collapse. These results are consistent with the notion that yielding in the as-grown pillars is controlled by dislocation nucleation

which happens at approximately the theoretical stress with very little scatter. Similarly reproducible behavior is observed in the case of the 11% pre-strained pillars (Fig. 1d), except that they yield at a much lower stress (~ 1 GPa) and then exhibit stable work hardening without plastic collapse (bulk-like response). These results are consistent with the view that a sufficiently large number of dislocations are present in the 11% pre-strained specimens and their flow behavior is therefore controlled by a “bulk-like” (or continuum) response. Since such a stable response can be obtained in small (sub-micron) pillars it suggests the parameter d by itself is not what controls deformation, but rather the combination of d and l . That is, if l is small, even small pillars will contain many dislocations whereas if l is large then d also has to be large in order to get bulk-like behavior.

In contrast to the deterministic stress-strain behavior seen at these two limiting values of pre-strain, stochastic behavior is seen at the intermediate pre-strains of 4 and 8% (Figs. 1b,c). Some of these pillars exhibit stable flow after yielding, similar to the 11% pre-strained pillars, while others exhibit unstable or stair-step shaped flow curves. The scatter in the flow behavior decreases with increasing amount of pre-strain above 4%. It appears that, when l and d become comparable, yielding is controlled by the probability of finding dislocations in the micro-pillars which in turn leads to a stochastic mechanical response.

Focused ion beam (FIB) milling is the typical way in which micro-pillars are fabricated in the literature. To compare our results on directionally solidified (DS) pillars with those obtained using FIB-milled pillars, we took our DS pillars and FIB milled them down to a smaller diameter. As shown in Fig. 2a, FIB milling has a dramatic softening effect on the DS pillars and lowers their yield strength by almost an order of magnitude [8]. Presumably, the various defects that are introduced during FIB milling (dislocations, interstitials, Ga ions, etc.) cause this softening relative to the pristine, dislocation-free state. Macroscopically, this is similar to what happens when dislocations are initially introduced by pre-straining (Fig. 2b). Microscopically, however, the details of the changes occurring within the FIB milled and pre-strained pillars will determine their respective mechanical responses. It is worth noting that the DS pillars have the distinct advantage that it is easier to vary their internal material length scale (l) by pre-straining than it is in the case of the FIB damaged pillars in which l is ill-defined, especially for small, sub-micron pillars where the FIB damaged region can be a significant fraction of the pillar cross-section.

Given the hypotheses outlined above, a fundamental understanding of small-scale mechanical behavior requires that the two relevant length scales in the micro-pillar problem, l and d , be accurately quantified. The parameter d (diameter in the case of cylindrical FIB-milled pillars and edge length in the case of our approximately square cross-section DS pillars) can be measured in a relatively straightforward way. The parameter l is rather more difficult to measure and requires careful microstructural characterization. Towards this end we have taken some preliminary steps to characterize the defect states of micro-pillars using x-ray micro-diffraction at synchrotron light sources. Figure 3 compares representative Laue peaks obtained from a DS pillar and a single-crystal wafer of Si [9]. Thirteen different pillars were examined and their Mo peak widths in each case were found to be at least as sharp as the Si peak suggesting

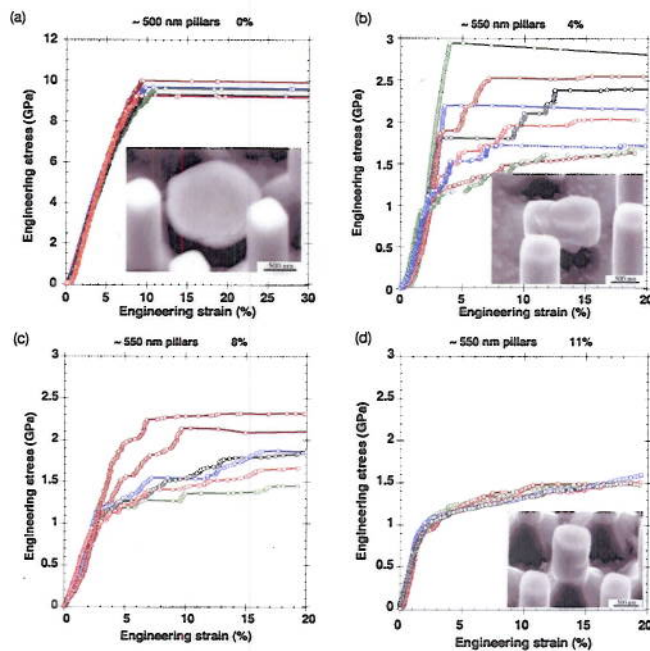


Fig. 1 Stress-strain curves of $d \sim 500$ nm Mo-alloy micropillars as a function of pre-strain. [7].

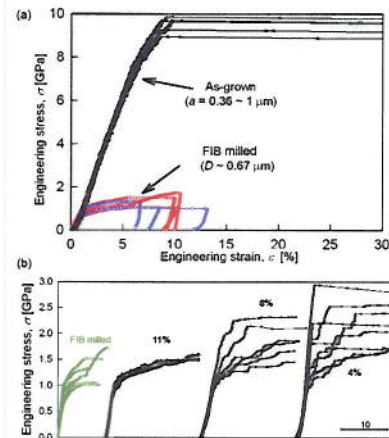


Fig. 2 (a) Effect of FIB milling on stress-strain curves of DS micro-pillars, and (b) comparison of FIB-milled and pre-strained pillars. [8].

that the DS pillars are perfect single crystals. Pre-straining caused the Mo peaks to broaden significantly (Fig. 4). The peak broadening was reasonably isotropic in the 2% pre-strained pillars suggesting the presence of mostly statistically stored dislocations rather than geometrically necessary dislocations in the illuminated volume. The peaks became broader as the pre-strain was increased to 11%. This peak broadening was accompanied by some streaking of the spots but the anisotropy was less than a factor of 2 between the maximum and minimum directions. FIB milling caused peak broadening comparable to that seen in the pre-strained pillars but with significantly more streaking (Fig. 4). The total dislocation density in the Mo pillars was estimated from x-ray peak widths to be $\sim 10^{13} \text{ m}^{-2}$ after both 5 and 11% pre-strain, which is about 2 orders of magnitude higher than similar estimates for the un-strained pillars [10]. These results can be used to rationalize the behavior of the as-grown and pre-strained pillars. In our as-grown pillars the dislocation density ρ is $\sim 10^{11} \text{ m}^{-2}$ which gives a value of $l \sim 3 \text{ }\mu\text{m}$. Since our pillar sizes were in the range $d \sim 0.3\text{-}1.0 \text{ }\mu\text{m}$, they are not expected to contain any dislocations. Yielding therefore has to occur by the nucleation of dislocations at the theoretical stress. After pre-straining, l decreases to about $0.3 \text{ }\mu\text{m}$ which significantly increases the likelihood of finding dislocations in most of our pillars and thus explains the dramatic softening seen after pre-straining (relative to the as-grown pillars). However, these “average” dislocation density estimates cannot explain the significantly different flow behaviors of the 4 and 11% pre-strained pillars (Fig. 1). One possibility is that the distribution of dislocations in the pillars is itself stochastic so that when l and d become comparable in magnitude, the effects of this stochastic distribution start to dominate.

Future Plans

A simple stochastic model of yielding will be developed that incorporates the two important length scales discussed above. Initially, it will be applied to understand size effects in nanoindentation pop-in [11] where the indenter tip radius (r) is the analog of the micro-pillar diameter (d) and the second length scale (l) remains the same as in micro-pillar compression. The advantage of modeling nanoindentation is that experimentally it is much easier to obtain statistically significant data sets that can be rigorously compared with the model predictions. Transmission electron microscopy will be performed to characterize the detailed dislocation distributions in micro-pillars as a function of pre-strain and pillar size. These results will be used to develop more realistic models of pillar microstructures.

References

1. E. T. Lillocooden and W. D. Nix, *Acta Mater.* **54** (2006) 1583-1593.
2. S. S. Brenner, *J. Appl. Phys.* **27** (1956) 1484-1496.
3. H. Bei, S. Shim, E.P. George, M.K. Miller, E.G. Herbert, and G.M. Pharr, *Scr. Mater.* **57** (2007) 397-400.
4. H. Bei, E.P. George, J.L. Hay, and G.M. Pharr, *Phys. Rev. Lett.* **95** (2005) 045501.
5. M.D. Uchic, D.M. Dimiduk, J.N. Florando, and W.D. Nix, *Science* **305** (2004) 986-989.
6. M.D. Uchic, P.A. Shade, and D.M. Dimiduk, *Annu. Rev. Mater. Res.* **39** (2009) 361-386.
7. H. Bei, S. Shim, G.M. Pharr, and E.P. George, *Acta Mater.* **56** (2008) 4762-4770.
8. S. Shim, H. Bei, M.K. Miller, G.M. Pharr, and E.P. George, *Acta Mater.* **57** (2009) 503-510.
9. J. Zimmermann, S. Van Petegem, H. Bei, D. Grolimund, E.P. George, and H. Van Swygenhoven, *Scr. Mater.* **62** (2010) 746-749.
10. R.I. Barabash, H. Bei, Y. Gao, G.E. Ice, and E.P. George, *J. Mater. Res.* **25** (2010) 199-206.
11. S. Shim, H. Bei, E. P. George, and G. M. Pharr, *Scripta Mater.* **59**, 1095-1098 (2008).

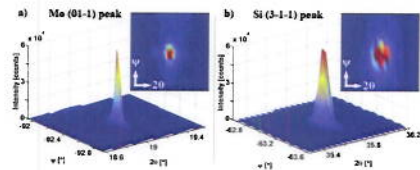


Fig. 3 Laue diffraction peaks from the 0% pre-strained Mo pillars and a single-crystal wafer of Si. [9].

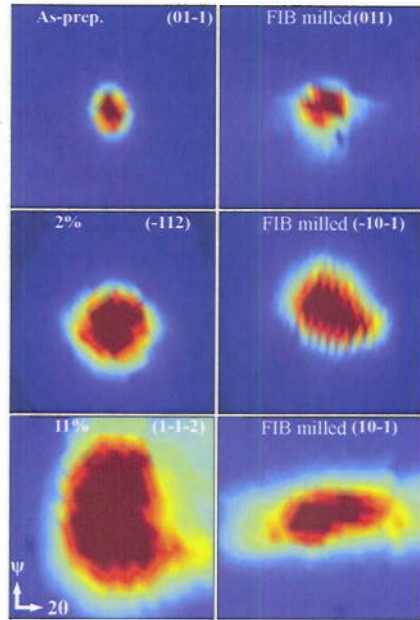


Fig. 4 Change in the size and shape of Laue diffraction peaks as a function of pre-strain and FIB milling. [9].

Partial list of DOE Sponsored Publications in 2008-2010

1. H. Bei, R. I. Barabash, G. E. Ice, W. Liu, J. Tischler, and E. P. George, "Spatially-Resolved Strain Measurements in Mo-Alloy Micro-Pillars by Differential Aperture X-Ray Microscopy," *Appl. Phys. Lett.* **93**, 071904 (2008).
2. H. Bei, Y. F. Gao, S. Shim, E. P. George, and G. M. Pharr, "Strength Differences Arising from Homogeneous Versus Heterogeneous Dislocation Nucleation," *Phys. Rev. B* **77** 060103(R) (2008).
3. M. J. Kramer, M. Xu, Y. Y. Ye, D. J. Sordelet, and J. R. Morris, "Phase Stability and Transformations in the $Zr_2Ni_xCu_{1-x}$ System," *Metall. Trans. A* **39A**, 1847 (2008).
4. Y. Liu, C. T. Liu, L. Heatherly, and E. P. George, "Effects of Alloying Elements on Dendritic Segregation in Iridium Alloys," *J. Alloys Compd.* **459**, 130 (2008).
5. J. R. Morris, R. S. Aga, V. Levashov, and T. Egami, "Many-Body Effects in BCC Metals: An Embedded Atom Model Extension of the Modified Johnson Pair Potential for Iron," *Phys. Rev. B* **77**, 174201-1 (2008).
6. S. Namila, B. Radhakrishnan, and J. R. Morris, "Atomistic Simulation of the Effect of Ga on Crack Tip Opening in Al Bicrystals," *Modeling Simul. Mater. Sci. Eng.* **16**, 075001 (2008).
7. L. J. Peng, J. R. Morris and Y. C. Lo, "Temperature-Dependent Mechanisms of Homogeneous Crystal Nucleation in Quenched Lennard-Jones Liquids," *Phys. Rev. B* **78**, 012201 (2008).
8. H. Bei, E.P. George, G. M. Pharr, "Small-Scale Mechanical Behavior of Intermetallics and their Composites," *Mater. Sci. Eng. A* **483** 218-522 (2008).
9. H. Bei, S. Shim, G. M. Pharr, and E. P. George, "Effects of Pre-Strain on the Compressive Stress-Strain Response of Mo-Alloy Single Crystal Micro-pillars," *Acta Mater.* **56**, 4762-4770 (2008).
10. S. Shim, J. -I. Jang, and G. M. Pharr, "Extraction of Flow Properties of Single-Crystal Silicon Carbide by Nanoindentation and Finite-Element Simulation," *Acta Mater.* **56**, 3824 (2008).
11. E-W. Huang, R. Barabash, N. Jia, Y-D. Wang, G. E. Ice, B. Clausen, J. Horton, and P. K. Liaw, "Slip-System-Related Dislocation Study from In-Situ Neutron Measurements," *Metall. Mater. Trans.* **39A**, 3079-3088 (2008).
12. Z. W. Zhang, G. Chen, H. Bei, F. Ye, G. L. Chen, and C. T. Liu, "Improvement of Magnetic Properties of an Fe-6.5 wt% Si Alloy by Directional Recrystallization," *Appl. Phys. Lett.* **93**, 191908 (2008).
13. R. Barabash, Y.F. Gao, Y. Sun, S. Lee, H. Choo, P.K. Liaw, D.W. Brown, G.E. Ice, "Neutron and x-ray diffraction studies and cohesive interface model of the fatigue crack deformation behavior," *Philos. Mag. Lett.*, **88** (2008) 553-565,
14. A. Gali, H. Bei, and E. P. George, "Thermal Stability of Cr-Cr₃Si Eutectic Microstructures," *Acta Mater.* **57**, 3823-3829 (2009).
15. S. Cheng, A. D. Stoica, X. -L. Wang, Y. Ren, J. Almer, J. A. Horton, C. T. Liu, B. Clausen, D. W. Brown, P. K. Liaw, and L. Zuo, "Deformation Crossover: From Nano- to Mesoscale," *Phys. Rev. Lett.* **103**, 035502 (2009).
16. S. Cheng, J. Xie, A. D. Stoica, X. -L. Wang, J. A. Horton, D. W. Brown, H. Choo, and P. K. Liaw, "Cyclic Deformation of Nanocrystalline and Ultrafine-Grained Nickel," *Acta Mater.* **57**, 1272-1280 (2009).
17. Y. Jiang, C. Deng, Y. He, Y. Zhao, N. Xu, J. Zou, B. Huang, and C. T. Liu, "Reactive Synthesis of Microporous Titanium-Aluminide Membranes," *Mater. Lett.* **63**, 22-24 (2009).
18. L. Li, T. Ungár, Y. D. Wang, G. Tichy, J. R. Morris, J. Lendvai, Y. L. Yang, Y. Ren, H. Choo, and P. K. Liaw, "Microstructure Evolution during Cold Rolling in a Nanocrystalline Ni-Fe Alloy Determined by Synchrotron X-ray Diffraction," *Acta Mater.* **57**, 4988 (2009).
19. T. L. Li, J. H. Lee, Y. F. Gao, G. M. Pharr, M. Huang, and T. Y. Tsui, "Geometric Effects on Dislocation Nucleation in Strained Electronics," *Appl. Phys. Lett.* **94**, 17095 (2009).
20. T. L. Li, J. H. Lee, and Y. F. Gao, "An Approximate Formulation of the Effective Indentation Modulus of Elastically Anisotropic Film-on-Substrate Systems," *Int. J. Appl. Mech.* **1**, 515-525 (2009).
21. H. Saage, M. Krüger, D. Sturm, M. Heilmaier, J. H. Schneibel, E. George, L. Heatherly, Ch. Somsen, G. Eggeler, and Y. Yang, "Ductilization of Mo-Si Solid Solutions Manufactured by Powder Metallurgy," *Acta Mater.* **57**, 3895-3901 (2009).
22. S. Shim, H. Bei, M. K. Miller, G. M. Pharr, and E. P. George, "Effects of Focused Ion Beam Milling on the Compressive Behavior of Directionally Solidified Micropillars and the Nanoindentation Response of an Electropolished Surface," *Acta Mater.* **57**, 503-510 (2009).
23. M. Xu, Y. Y. Ye, J. R. Morris, D. J. Sordelet and M. J. Kramer, "In situ Observation of Thermal Expansion of Tetragonal C11b Phase in $Zr_2Cu_{(1-x)}Pd_x$ Alloys," *Intermetallics* **18**, 8 (2010).
24. A. Gali, H. Bei, and E. P. George, "Effects of Boron on the Microstructure and Thermal Stability of Directionally Solidified NiAl-Mo Eutectic," *Acta Mater.* **58** (2) 421-428 (2010).
25. J. Frenzel, E. P. George, A. Dlouhy, Ch. Somsen, M. F. -X. Wagner, and G. Eggeler, "Influence of Ni on Martensitic Phase Transformations in NiTi Shape Memory Alloys," *Acta Mater.* **58** (9) 3444-3458 (2010).
26. T.-H. Ahn, C.-S. Oh, D. H. Kim, K. H. Oh, H. Bei, E. P. George, and H. N. Ham, "Investigation of Strain-induced Martensitic Transformation in Metastable Austenite Using Nanoindentation," *Scripta Mater.* **63** 540-543 (2010).
27. G.M. Pharr, E.G. Herbert, Y.F. Gao, "The indentation size effect: a critical examination of experimental observations and mechanistic interpretations," *Annu. Rev. Mater. Res.*, **40** 271-292 (2010).
28. R.P. Mulay, J.A. Wollmershauser, M.A. Heisel, H. Bei, A.M. Russell, and S. R. Agnew, "X-ray Diffraction Study of the Phase Purity, Order and Texture of Ductile B2 Intermetallics," *Acta Mater.* **58** 2788-2796 (2010).

Stability of Nanoclusters in Metal Matrices under Extreme Environments

Michael K. Miller	ORNL, Oak Ridge, TN 37831-6136	millermk@ornl.gov
Chong Long Fu	ORNL, Oak Ridge, TN 37831-6114	fucl@ornl.gov
Xun-Li Wang	ORNL, Oak Ridge, TN 37831-6475	wangxl@ornl.gov
Michael J. Mills	The Ohio State University, Columbus, OH 43210	mills.108@osu.edu

Program Objective

The objective of this program is to understand the formation mechanism, stability, and fundamental hardening behavior associated with stable nanoclusters in metallic alloys and to establish a fundamental understanding of the mechanisms that control their response to intense irradiation. Mechanisms will be elucidated through a synergistic approach of ab initio theory, computer simulation and modeling, and atomic level experimental characterization of nanostructured materials before and after neutron and ion irradiation by atom probe tomography (APT), various forms of transmission electron microscopy (TEM), and neutron scattering.

The presence of high number densities of “naturally occurring” 2-4 nm-diameter nanoclusters was observed by APT and by electron microscopy in several (9Cr, MA957, 12YWT and 14YWT) mechanically-alloyed nanostructured ferritic steels. These ultra-fine grained steels were also found to have remarkable stability to high temperature creep and exposure to irradiation and are therefore under consideration for applications in future generations of advanced reactors. In our first-principles studies, we investigated the Fe-O interactions in bcc Fe, mechanisms that explain the high O solubility, and the initial nucleation stage of the observed ultra-stable O-enriched nanoclusters. Vacancies (in the form of oxygen-vacancy pairs) were identified as the most critical alloying element in the formation and stability of these nanoclusters. Our results also suggested that defects and solutes that have high formation energies individually can collectively form a bound state of low energy and high stability. Although O has a very high formation energy (and low solubility) in defect-free Fe, the formation energy of the O-vacancy pairs becomes vanishingly small if the vacancies are present as pre-existing defects in Fe (thus allowing the O concentration to approach that of the vacancies). This O-vacancy mechanism enables the nucleation of O-enriched nanoclusters with structures coherent with the Fe lattice in the presence of solutes with high O affinities.

This basic research is ultimately aimed at developing the understanding needed to enable fundamental discoveries regarding nucleation and defect mechanisms in nanostructured materials. The scientific principles developed with this research are expected to have a broad applicability in the synthesis of new-generation nanostructured materials with high-temperature capability for use in advanced energy production and conversion systems under extreme environments.

Recent progress and future plans

We continue to examine the energetics of additional clusters consisting of oxygen-vacancies pairs, and solutes in Fe. The oxygen binding behavior in the clusters has been studied as a function of cluster size. The results indicate that during the growth stage, a considerable amount of strain energy can develop. The mechanism for this development is the difference in the atomic sizes among Y, Ti, and Fe as well as due to the solute-defect repulsive interactions. In conjunction with the results from first-principles calculations, a theoretical model has been developed by taking into account the strain energy and all possible local binding environments of oxygen-vacancy pairs in the nanoclusters. This model enables us to examine the conditions for growth as well as how local strain energies can limit the size. Our model will also enable predictions of the size, alloy composition and the oxygen concentration in the nanoclusters and comparison with the experimental data. We find that an essential condition for stabilizing these nanoclusters is their exceptionally low interfacial energy in the Fe matrix.

For the interaction between He atoms and defects, first-principles calculations show that the number of He atoms attached to a vacancy can be drastically reduced in the presence of a vacancy-oxygen pair in Fe. The binding energy of a n^{th} He atom attached to a [(n-1)He + vacancy] cluster or a [(n-1)He + oxygen-

vacancy pair] cluster in the Fe matrix as a function of the number of He atoms is shown in Fig. 1. As the binding energy becomes positive, the addition of the n^{th} He atom will be detached from the cluster. Without O, we find that a vacancy can attract up to 8 He atoms. In the presence of oxygen-vacancy pair, however, the number of helium atoms that can be attached to an oxygen-vacancy pair is reduced to 4. Two basic facts can be drawn from these results: (1) vacancy (or vacancy clusters) can attract a large number of He atoms in Fe; and (2) the presence of O drastically limits the growth of He clusters in Fe, due to the unusually strong oxygen-vacancy binding. Both these factors should minimize swelling in high dose neutron irradiated material due to the formation of He bubbles. A series of high dose He ion irradiations have been initiated to quantify the level of He trapping with the nanoclusters and grain boundaries by APT.

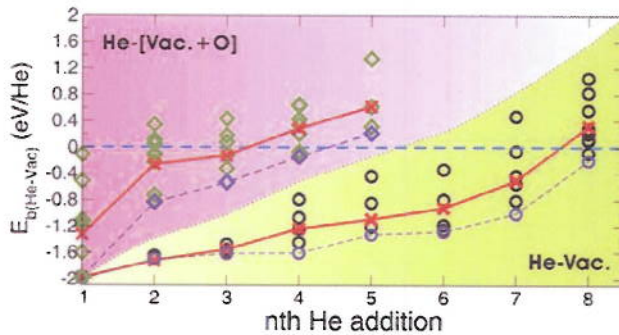


Fig. 1. The binding energy of a n^{th} helium atom (E_b) attached to clusters containing a vacancy and $(n-1)$ He atoms (lower curves) and an oxygen-vacancy pair and $(n-1)$ He atoms (upper curves). The solid and dashed lines represent the averaged and lowest binding energies, respectively, among all atomic configurations being considered.

Strong O-vacancy binding is responsible for the unusual high O solubility and nucleation of stable O-enriched nanoclusters in defect-containing Fe. A magnetism-induced O confinement was identified as a significantly contributing source to this unusually strong O-vacancy binding. The interplay between O-vacancy binding and magnetism will be further studied with magnetic $3d$ transition metal alloying additions.

We are currently examining the effect of alloying additions with strong oxygen affinity (such as V, Cr, Zr, Hf, and La) on the formation and stability of these nanoclusters. Comparison of these alloy systems in Fe allows us to further understand the factors (such as atomic bonding, strain, and magnetism) controlling the alloy compositions, size and growth of nanoclusters. The knowledge base obtained will be applied to other metallic systems containing potentially stable nanoclusters. In particular, we will focus on magnetic systems with the bcc-based structure, such as V-based and B2-ordered intermetallic alloys (FeCo, FeV, and FeCr, etc.)

The formation of the nanoclusters has been investigated through the use of a series of heat treated ball-milled flakes that were isothermally aged between 400 and 850°C (the extrusion temperature). These recent results have indicated that the nanocluster form within 2 min. at 850°C and at temperatures as low as 400°C. We also propose to conduct a SANS annealing study of these samples to examine in-situ the formation of nanoclusters in the 14YWT steel. The goal is to gain insights of the nucleation and growth mechanisms by resolving the kinetics of nanocluster formation upon annealing. These data will be compared to the APT snapshots of the compositions of the nanoclusters at different stages of annealing.

High resolution TEM studies have focused on characterizing the nature of the nanoclusters and other grain boundary precipitates in the 14YWT alloy. The morphological data obtained from the individual low index zones from the nanoclusters suggests a truncated rhombic dodecahedron shape, which is defined by the $\{100\}$ and $\{110\}$ planes in the Fe matrix and consistent with the expected shape of ultrafine precipitates.

Diffraction contrast STEM imaging of deformed substructures has also been used to explore the interaction of dislocations with the nanoclusters. The strong interaction of dislocations with the nanoclusters following constant strain rate deformation at 950°C is clearly shown in the bright field (BF) STEM image of Fig. 2. These observations have inspired the development of a physical deformation

model that appears to have significant promise for describing the high temperature deformation characteristics of this alloy. This model predicts a decreasing stress exponent at low stress, as observed experimentally in creep and constant strain rate testing at 800°C and 950°C. We also propose to conduct an in-situ SANS loading study of the deformation behaviors at ambient and elevated temperatures. Although the study will be preliminary in nature, the results will help us to begin to understand high-temperature deformation behavior and the influence of nanoclusters.



Fig.2 Bright field STEM image of a grain containing dislocations in the 14YWT alloy following deformation at 950°C. The dislocations exhibit numerous cusps along their lengths, and evidence for direct pinning on the nanoclusters. The dislocations appear to be bowed in the same direction, suggesting difficult movement through the dense field of nanoclusters.

The response of these materials to high dose (up to 460 dpa) Au and Pt ion irradiations and low dose (3 dpa) proton and neutron irradiations has been investigated by APT and high angle angular dark field (HAADF)-STEM. Nanoclusters have been observed in the neutron and proton irradiated and all ion irradiations specimens, as shown in Fig. 3. Although the APT results indicate that irradiations did not destroy the nanoclusters by simple ballistic collisions and produce a uniform solid solution, another possibility cannot be completely discounted. It is possible that a cascade impacting a nanocluster, either partially or entirely, could locally disperse the solutes in the nanocluster into the matrix and then the presence of supersaturated vacancies combined with the local temperature increase could enable enhanced diffusion to allow the nanocluster to reform. This self-healing mechanism may be a key feature for the fabrication of highly radiation tolerant microstructures for extreme environments. Detailed characterization of the differences in the atom level solute distributions as a function of dose and irradiation temperature are in progress.

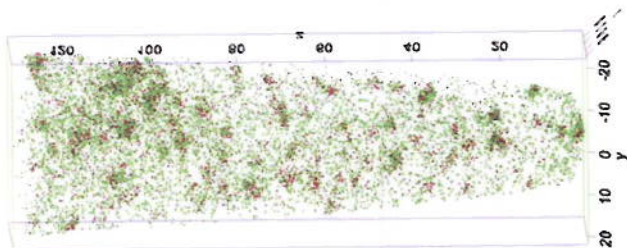


Fig. 3. Atom map of the Ti (green) and Y (red) atom distributions in a 14YWT specimen 10 MeV Au ion irradiated to a dose of ~460 dpa. A high number density of 2-4-nm-diameter nanoclusters is present after the high dose irradiation.

Solute segregation of W, Cr and C to the grain boundaries as well as nanoclusters preferentially located on the grain boundaries were observed by a combination of APT and EFTEM in the thermally annealed and irradiated specimens. An example of the solute segregation in a 14YWT specimen Au ion irradiated to a dose of ~150 dpa is shown in Fig. 4. Similar results were seen in the unirradiated portion of this specimen. The presence of these solutes and nanoclusters (and possibly some coarser grain boundary

precipitates) on the grain boundaries is thought to be the reason for the remarkable creep properties of these materials. More detailed examination of the differences between the irradiated and unirradiated grain boundary character, and EFTEM analysis of the nanocluster population within the grains are in progress.

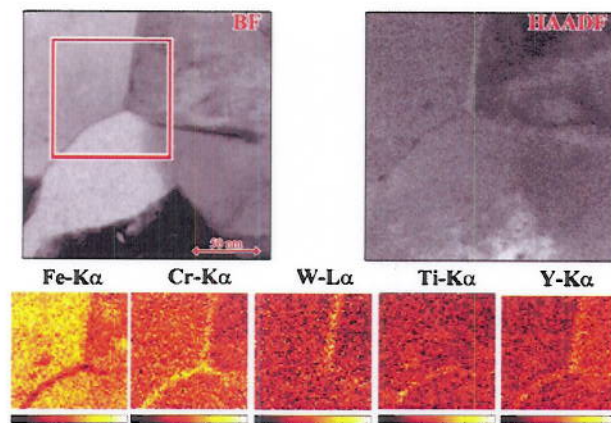


Fig. 4: BF-STEM image, HAADF-STEM image, and X-ray maps of a region that was 10 MeV Au ion irradiated to a dose of ~150 dpa at a temperature of -40°C. Box in BF image denotes mapped area. In both unirradiated and ion irradiated materials, clear Cr segregation is apparent, along with slight W segregation. Slight Ti and Y enrichments are seen and are primarily due to the presence of nanoclusters on the grain boundary. Examination of a large number of boundaries and triple points indicated that Cr segregation is present at most or all boundaries, and W segregation is present but its magnitude is more variable.

Other contributors: C. M. Parish, Y. Zhang, H. Zhao, J. Xu, J. Bentley, D.T. Hoelzer (ORNL), L. Kovarik (OSU), M. Krcmar (GVSU) and others listed in the publications below.

Publications

- M. K. Miller, C. L. Fu, M. Krcmar, D. T. Hoelzer, and C. T. Liu, invited, Vacancies as a constitutive element for the design of nanocluster-strengthened ferritic steels, *Shanghai Metals*, 30 (4) 2008 1-6, in Chinese, *Frontiers of Materials Science in China*, 3(1) (2009) 9-14.
- T. R. Allen, J. Gan and J. I. Cole, M. K. Miller and J. T. Busby, S. Ukai, S. Ohtsuka, S. Shutthanandan and S. Thevuthasan, Radiation Response of a 9 Chromium Oxide Dispersion Strengthened Steel to Heavy Ion Irradiation, *J. Nucl. Mater.*, 375 (2008) 26-37.
- C. Capdevila, M. K. Miller, K. F. Russell, J. Chao and J. L. González-Carrasco, Phase Separation in PM 2000 Fe-Base ODS Alloy: Experimental Study at the Atomic Level, *Mater. Sci. Eng. A*, 490 (2008) 277-299.
- Jun Xu, C. T. Liu, M. K. Miller, and Hongmin Chen, Nanocluster-associated vacancies in nanocluster-strengthened ferritic steel as seen via positron-lifetime spectroscopy, *Phys. Rev. B*, 79, (2009) 020204R.
- S. J. Zinkle, G. E. Ice, M. K. Miller, S. J. Pennycook and X-L. Wang, Advances in Microstructural Characterization, *J. Nucl. Mater.* 386-388 (2009) 8-14.
- J. H. Schneibel, C. T. Liu, M. K. Miller, M. J. Mills, P. Sarosi, M. Heilmaier and D. Sturm, Ultrafine-grained nanocluster-strengthened alloys with unusually high creep strength, *Scripta Mater.*, 61 (2009) 793-796.
- M. K. Miller and R. G. Forbes, invited, Atom Probe Tomography, *Mater. Charact.*, 60 (2009) 461-469
- M. K. Miller, D. T. Hoelzer and K. F. Russell, invited, Towards Radiation Tolerant Nanostructured Ferritic Alloys, *Materials Science Forum*, 654-656 (2010) 23-28.
- M. K. Miller, D. T. Hoelzer and K. F. Russell, Radiation Response of a 12YWT Nanostructured Ferritic Steel, Proc. MRS 2009 Fall Meeting, Symposium V: Materials Research Needs to Advance Nuclear Energy, Boston, MA, Nov. 30-Dec. 3, 2009, eds., G. Baldinozzi, K. L. Smith, K. Yasuda, and Y. Zhang, vol. 1215-V06-02.
- M. K. Miller, K. F. Russell, D. T. Hoelzer, L. Kovarik, M. J. Mills, A. G. Certain, and T. R. Allen, invited, Atom Probe Tomography as a Tool for Characterizing Irradiated Materials, *Microscopy and Microanalysis*, 16 (suppl.2) (2010) 1602-3.
- J. Bentley and D. T. Hoelzer, invited, "In situ ion irradiation of nanostructured ferritic alloys," *Microscopy and Microanalysis*, 16 (suppl 2) (2010) 1610-1.
- A. Certain, K. Field, T. R. Allen, K. Sridharan, M. K. Miller, J. Bentley, and J. T. Busby, Response of nanoclusters in a 9Cr ODS steel to 1 dpa, 525 °C proton irradiation, *J. Nucl. Mater.*, doi: 10.1016/j.jnucmat.2010.07.002.

Interfacial Charge Transfer and the Radiation Response of Nano-Dispersed Ceramics

Ram Devanathan, Fei Gao, Weilin Jiang, Rick Williford, Matt Olszta and Gregory J. Exarhos

Pacific Northwest National Laboratory

MS K2-01, P.O. Box 999, Richland, WA 99352

Email: ram.devanathan@pnl.gov

Phone: 509-371-6487

DOE Program Officer: John Vetrano

1. Program Scope

This research program aims to *integrate synthesis, irradiation, structural characterization, and mechanical property measurement of nanocomposite ceramics with modeling and simulation of radiation-induced defects, charge transfer, electronic excitation, and their effects on mechanical and transport properties*. Bulk composite materials that can withstand intense radiation, elevated temperatures, and harsh chemical environments are promising candidates for advanced reactor and waste form applications. Our ultimate objective is to discover fundamental relationships between structure and properties in oriented three-dimensional (3D) nanoparticle dispersions in ceramic matrices that will enable control of mechanical properties, electron and ion transport, and materials stability in extreme environments. This 3D morphology contrasts with the multilayered nanostructural designs currently under investigation at other laboratories in that collective effects among the oriented nanoparticle structures are expected to strongly influence properties as a result of selecting particle sizes that are comparable to the width of the space charge region. An attractive feature of these ceramic particle hybrid composites is that they can be routinely and inexpensively synthesized in the large quantities necessary for practical applications. The emphasis on understanding charge transfer, electronic excitation and electronic energy loss processes in these materials is a defining feature of our work that will complement related Office of Basic Energy Sciences (BES)-funded studies of structural and elastic strain effects in nanomaterials currently pursued at Pacific Northwest National Laboratory (PNNL) and elsewhere.

2. Recent progress

2.1 Synthesis of dispersed nanoparticles in a host matrix

We have demonstrated the ability to synthesize oriented 3-D nanoparticle dispersions in a host ceramic matrix using a novel surfactant-directed solution self-assembly approach. Recent work in our laboratory showed that metal oxide nanoparticle phase and size homogeneity could be achieved in solution through retardation of the initial stages of hydrolysis in the presence of benzyl alcohol, which acts as a surfactant. This approach is based upon results from a sister BES materials science project at PNNL that demonstrated the efficacy of retarding selected formation reactions in order to drive formation of homogeneous nanoparticles [1]. The 7–8 nm diameter particles produced are readily dispersed in a second ceramic precursor solution and subsequently can either be deposited as very thick films (>100 μm thickness) using an automated fluid dispensing approach or formed as bulk materials. A second method invokes a porous matrix such as a zeolite (< 1 nm diameter pores) or a mineralized bio-template (pore diameter controllable from several to hundreds of nm) through which a ceramic precursor is percolated to fill the pore space [2].

2.2 Characterization of ion irradiation effects in nanomaterials

The radiation response of nanoceramics is driven by interplay of complex mechanisms. Ongoing work by team members has captured contrasting radiation tolerance of nanoceramics in nitride and carbide systems. We have observed AlN nanoparticles in an amorphous AlN matrix to be stable under irradiation with 1 MeV Au⁺ ions at 145 K to cumulative doses of 208 displacements per atom (dpa) [3]. Interstitial diffusion to and annihilation at the crystalline/amorphous interface can explain the stability of the microstructure under irradiation. Similar processes could be active for vacancies. Moreover, irradiation-induced recrystallization and charge transfer effects at the interface cannot be ruled out. Not

all nanomaterials resist amorphization under irradiation. Under 2 MeV Au²⁺ ion irradiation at room temperature, nanostructured high-purity 3C-SiC, composed of 4.6-nm crystallites, was fully amorphized at a dose comparable to the amorphization dose for bulk SiC [4]. The behavior is likely due to local defect accumulation and interaction within the interior of grains, leading to a catastrophic disruption and collapse of the crystal structure.

Our most recent results [5] have revealed that, under identical irradiation conditions with Si⁺ ions at room temperature or 400 K, full amorphization of 3C-SiC with grain sizes ranging from 2.0 – 3.8 nm requires a lower dose than for single crystal 3C-SiC. The average size of the 3C-SiC crystallites, observed from the (111) plane diffraction, decreased nonlinearly from 3.8 nm for an unirradiated sample to 1.5 nm for a fluence of 12 Si⁺/nm² at room temperature, and further decreased until the material was fully amorphized at 0.24 dpa. This effect is shown in Fig. 1 in the form of plots of the decrease in average grain size of nanostructured SiC (blue line) and increasing relative disorder of single crystalline SiC (red line) with increasing dose. We attribute this behavior primarily to the preferential interface amorphization during the ion irradiation, but further work is needed to elucidate the underlying mechanisms.

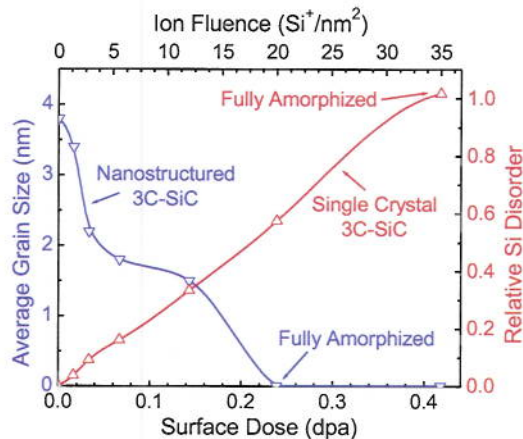


Fig. 1. Relative Si disorder in single crystal 3C-SiC (red line) and average grain size of nanostructured 3C-SiC (blue line) irradiated with 1 MeV Si⁺ ions at room temperature. 3C-SiC crystallites shrink as dose increases.

2.3 Modeling of charge transfer processes in irradiated ceramics

Our experimental studies of radiation effects in nanocrystalline SiC are complemented by systematic modeling of charge transfer effects and damage accumulation starting at the level of density functional theory (DFT) [6, 7]. We have recently applied large-scale *ab initio* molecular dynamics (AIMD) to study atomic dynamics, electronic structure effects on defect generation, charge transfer, and charge-density redistribution in irradiated SiC and GaN [6,7]. We found that defect creation can be affected by charge-transfer processes. Fig. 2 shows charge-density contour plots due to a C primary knock-on atom (PKA) with kinetic energy of 47 eV in SiC. In Fig. 2(a), the C PKA transfers charge to one of its nearest Si neighbors, as indicated by the arrow, but one of the Si atoms, shown on the left of Fig. 2(a), prefers to form a bond with its nearest Si neighbor as the charge begins to accumulate in the bonding regions. Fig. 2(b) shows that the charge is mostly distributed in the region between the C vacancy and its two Si neighbor atoms. This indicates a tendency for pairing of two Si atoms neighboring the C vacancy. As soon as the C PKA passes the energy barrier, further charge transfer from the surrounding atoms to the C vacancy occurs, as indicated by the arrow in Fig. 2(c). This C vacancy is positively charged, which is consistent with experimental observations. The results reveal that charge transfer to and from recoiling atoms can alter the energy barriers for stable defect formation, and illustrate in detail the dynamic processes for charged defect formation.

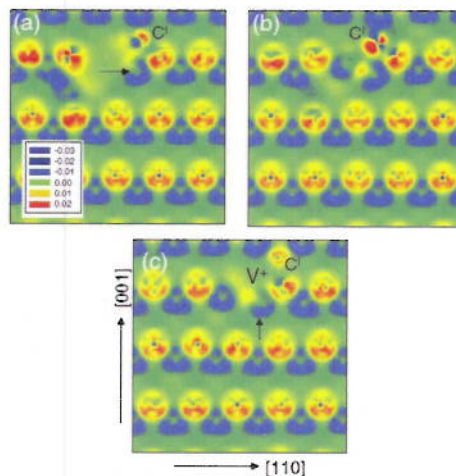


Fig. 2 Charge density contours (a), (b) and (c) in a [110] plane for different atomic configurations due to a C recoil.

2.4 Defect generation in nanocrystalline silicon carbide

Recently, we have employed large-scale molecular-dynamics (MD) simulations [8] to study the primary damage state produced by 10 keV recoils in nanocrystalline (NC) SiC of average grain diameter from 5 to 21 nm. We observed that the local stresses near the grain boundaries (GB) strongly affect the behavior of the PKA and secondary recoil atoms (SRAs), and the GBs act as sinks for deposition of kinetic energy. A striking feature is that the PKA and SRAs preferentially deposit energy along the GBs for grains with average size less than 12 nm, which results in atomic displacements primarily within the GBs. For larger grain sizes, most defects are produced within the grains. The defect production within grains generally increases with increasing grain size, which is manifested in switching from grain boundary damage to grain damage. The most common defects created in NC SiC are antisite defects, following by vacancies and interstitials, in contrast to those produced in single-crystalline SiC, where the dominant defects are Frenkel pairs. It is interesting to note that the defect production efficiency increases with increasing grain size, from about 0.2 for small grains (5 nm) to 0.5 for larger grains.

2.5 Simulation of nanoscale features of swift heavy ion damage in ceramics

We are playing a leading role in implementing the thermal spike model in MD simulations of ceramics in an effort to understand the nanoscale evolution of swift heavy ion damage. Our previous work revealed that interstellar dust grains can be amorphized by cosmic ray bombardment [9]. MD thermal spike simulations have shown radial density changes within the tracks produced by energetic recoils in zircon, which is a candidate ceramic nuclear waste form [10]. Our latest large-scale MD simulations of thermal spikes in the $\text{Gd}_2\text{Zr}_{2-x}\text{Ti}_x\text{O}_7$ system [11] have reproduced the nanoscale fine shell structure observed experimentally in this system by high-resolution transmission electron microscopy (HRTEM). For $\text{Gd}_2\text{Ti}_2\text{O}_7$, as revealed by the HRTEM image in Fig. 6(a) and MD results in Fig. 6(d), the core of the track is amorphous and surrounded by a defect-fluorite structure, with an outermost structure that is highly defective pyrochlore.

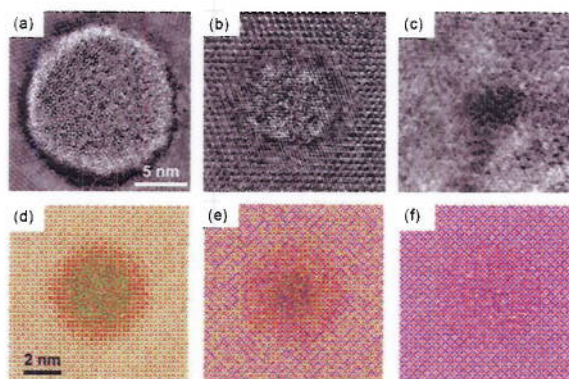


Fig. 3. The nanostructure of individual ion tracks produced by 2.2 GeV Au ions, as revealed by HRTEM, for (a) $\text{Gd}_2\text{Ti}_2\text{O}_7$, (b) $\text{Gd}_2\text{TiZrO}_7$, and (c) $\text{Gd}_2\text{Zr}_2\text{O}_7$ are reproduced by MD thermal spike simulations, for (d) $\text{Gd}_2\text{Ti}_2\text{O}_7$, (e) $\text{Gd}_2\text{TiZrO}_7$, and (f) $\text{Gd}_2\text{Zr}_2\text{O}_7$.

These are the first simulations to show the concentric nature of track structures in complex oxides. For $\text{Gd}_2\text{ZrTiO}_7$, as shown in Fig. 6(b) and 6(e), the amorphous core has decreased in radius, and the relative thickness of the defective crystalline shells has increased. In the case of $\text{Gd}_2\text{Zr}_2\text{O}_7$, as shown in Fig. 6(c) and 6(f), the core does not become amorphous, but has the defect-fluorite structure. These simulations have revealed that the size of the track in pyrochlore does not depend on the extent of a melt zone, but instead on a complex competition among melting, disordering, and recrystallization processes.

Taken collectively, the results discussed above establish a solid scientific foundation for synthesizing novel materials and integrating experiment and computation to study radiation effects and charge transfer processes in nanoceramics.

3. Future Plans

We propose to integrate synthesis, irradiation, structural characterization, and mechanical property measurement of nanocomposite ceramics with modeling and simulation of radiation-induced defect generation and migration, charge transfer, electron excitation, and electronic energy loss processes, and their effects on mechanical and transport properties. The experiments will verify and

validate the models, while the simulations will interpret experiments and help design new experiments to test our hypothesis. Advances in our knowledge of charge transfer will provide underpinning science for developing advanced nuclear reactor materials, improving waste sequestration materials, and improving materials robustness in extreme conditions.

The experimental work will begin with synthesis of three-dimensional (3D) nanoscale ceramic dispersions in a host matrix using surfactant-directed self assembly. We intend to perform irradiation, mechanical property measurements, and materials characterization separately on the matrix phase and the dispersed phase. We will study the material that constitutes the dispersion in the form of large single crystals and as nanoparticles to understand size effects. We plan to grow thin film samples using the facilities at PNNL and also anticipate obtaining samples from collaborators. These studies will serve as benchmarks for subsequent studies of the nanocomposite system. We will examine ion irradiation effects in the individual components and the nanocomposite as a function of particle energy in the keV to GeV range for different temperatures and dose rates, and carry out nanoindentation experiments to study near-surface changes in the mechanical properties of irradiated nanocomposites. Indentation will provide information about the change in particle-matrix interfacial bonding before and after irradiation. These tasks will be supported by unique capabilities currently available or soon to be installed in the Environmental Molecular Sciences Laboratory (EMSL) at PNNL. These include a helium ion microscope, two aberration-corrected transmission electron microscopes, a field emission electron microprobe, the laser-assisted atom probe tomography with 3D chemical imaging facility, a low-temperature scanning probe microscope, a radiological focused ion beam/scanning electron microscope, and a high-resolution spectrometer for ion beam analysis.

We will engage leadership class computing resources in the EMSL at PNNL and NERSC at Lawrence Berkeley National Laboratory to perform hierarchical multiscale modeling studies. Our suite of computational techniques includes *ab initio* molecular dynamics, large-scale tight binding molecular dynamics, embedded cluster approaches, classical molecular dynamics, two-temperature model simulations of swift heavy ion damage, kinetic lattice Monte Carlo simulations, and dislocation dynamics. By performing both simulation and experiment on identical ceramic composite materials systems, we expect to develop fundamental understanding of radiation stability and mechanical toughening that will underpin the design and development of new materials.

References

- [1] C. Yao, Y. Shin, L-Q Wang, C.F. Windisch, Jr., W.D. Samuels, B.W. Arey, C.M. Wang, W.M. Risen Jr., and G.J. Exarhos, *Hydrothermal dehydration of aqueous fructose solutions in a closed system*, Journal of Physical Chemistry C **111** (2007) 15141.
- [2] Y. Shin, and G.J. Exarhos, *Conversion of cellulose materials into nanostructured ceramics by biomineralization*, Cellulose **14** (2007) 269.
- [3] W. Jiang, I.-T. Bae and W. J. Weber, *Disordering and dopant behavior in Au⁺-ion-irradiated-AlN*, Journal of Physics: Condensed Matter **19** (2007) 356207.
- [4] W. Jiang, H. Wang, I. Kim, I.-T. Bae, G. Li, P. Nachimuthu, Z. Zhu, Y. Zhang, and W. J. Weber, *Response of nanocrystalline 3C silicon carbide to heavy-ion irradiation*, Physical Review B **80** (2009) 161301.
- [5] W. Jiang, unpublished results (2010).
- [6] F. Gao and W. J. Weber, *Atomic-level computer simulation of SiC: defect accumulation, mechanical properties and defect recovery*, Philosophical Magazine **85** (2005) 509.
- [7] F. Gao, H. Y. Xiao, X. T. Zu, M. Posselt and W. J. Weber, *Defect-enhanced charge transfer by ion-solid interactions in SiC using large scale ab initio molecular dynamics simulations*, Physical Review Letters **103** (2009) 027405.
- [8] F. Gao, D. Chen, W. Hu and W. J. Weber, *Energy dissipation and defect generation in nanocrystalline silicon carbide*, Physical Review B **81** (2010) 184101.
- [9] R. Devanathan, P. Durham, J. Du, L. R. Corrales and E. M. Bringa, *Molecular dynamics simulation of amorphization in forsterite by cosmic rays*, Nuclear Instruments and Methods B **255** (2007) 172.
- [10] P. A. Moreira, R. Devanathan and W. J. Weber, *Atomistic simulation of track formation by energetic recoils in zircon*, Journal of Physics: Condensed Matter (in press).
- [11] J. Zhang, M. Lang, R. C. Ewing, R. Devanathan, W. J. Weber and M. Toulemonde, *Nanoscale phase-transitions under extreme conditions within an ion track*, Journal of Materials Research **25** (2010) 1344.

Exploring the Radiation Damage Resistance of Nanoscale Interfaces

Principal Investigator: Richard Kurtz
Pacific Northwest National Laboratory
622 Horn Rapids Road, MSIN J4-55
Richland, WA 99354
rj.kurtz@pnl.gov

Co-Principal Investigators: Scott Chambers, Renee Van Ginhoven, Howard Heinisch, Alan Joly, Tiffany Kaspar, Shutta Shutthanandan, Chongmin Wang, Pacific Northwest National Laboratory, and Brian Wirth, University of Tennessee

Program Scope

The objective of this research is to rigorously test the hypothesis that internal interfaces can be manipulated at the nanoscale to enhance recombination of radiation-produced defects to dramatically reduce radiation damage without compromising other physical and mechanical properties. This hypothesis has never been systematically tested and there has never been a fundamental study of radiation damage at interfaces that encompasses the wide range of interface types and structures planned here. In this project we seek to:

- Understand defect absorption at interfaces as a function of interface character and properties.
- Determine interface ability to adsorb and delocalize defects to promote recombination.
- Determine interface stability and evolution under irradiation, including the saturation limit for defect absorption.

The work consists of integrated experiments and modeling of a range of interface types to determine how variation in interface properties can affect defect absorption and recombination. The key scientific objectives of this research are 1) to understand how interface character affects absorption and recombination of radiation-induced defects, 2) to determine the ability of interfaces to delocalize radiation-induced defects to promote recombination, and 3) to determine the stability and evolution of interfaces under irradiation to high doses.

Recent Progress

To understand how interface character affects absorption and recombination of radiation-induced defects, a systematic study of a wide range of interface types is underway to determine how variation in interface properties such as misfit-dislocation density, excess volume, and misorientation affect defect absorption and recombination.

Heteroepitaxial thin films are an ideal model system to fabricate controlled and reproducible interfacial defects for fundamental studies. Epitaxial thin films of metallic Cr, Mo, and their alloys deposited on MgO (001) are a particularly attractive system to probe metal/ceramic interfaces. With a 45° in-plane rotation, both Cr (001) and Mo (001) grow epitaxially on MgO (001); the lattice mismatch for Cr/MgO is -3.3%, while that for Mo/MgO is +5.5%. To accommodate the lattice mismatch, films of sufficient thickness form misfit dislocation arrays at the metal/MgO interface. By controlling the composition of CrMo alloys, the lattice mismatch with MgO can be tuned, allowing a simple mechanism to control the

misfit dislocation array density. We have deposited 100 nm films of Cr, Mo, and alloy compositions on MgO (001) by molecular beam epitaxy at both room temperature and 550°C. The metal fluxes were controlled by atomic absorption spectroscopy, and the lattice spacing during deposition was monitored by reflection high-energy electron diffraction. The resultant crystalline structure and defects are being studied by a combination of x-ray diffraction, transmission electron microscopy, and Rutherford backscattering spectrometry in the channeling geometry. Epitaxial films of Cr on MgO are found to be fully relaxed and of high crystalline quality, in contrast to Mo/MgO, for which the larger lattice mismatch makes epitaxial films more difficult to achieve.

The structure of the unirradiated Cr/MgO interface has been characterized by high-resolution transmission electron microscopy (HRTEM), electron diffraction, and electron energy-loss spectroscopy. Room temperature growth leads to highly oriented columnar Cr grains, while growth at 550°C yields a high quality single crystal Cr film, possessing a 45° rotational relationship between the film and the MgO substrate. For the single crystal film, the interface exhibited coherent regions separated by equally spaced misfit dislocations. When imaged from the MgO [100] || Cr [110] direction, the dislocation spacing is 5.38 nm and 4.64 nm for the films grown at room temperature and 550°C, respectively, which is less than the expected value of 6.25 nm calculated from the differences in lattice spacing based on known lattice constants, Figure 1. The electronic structure of the interface between the film and the substrate was also explored using electron energy-loss spectroscopy.

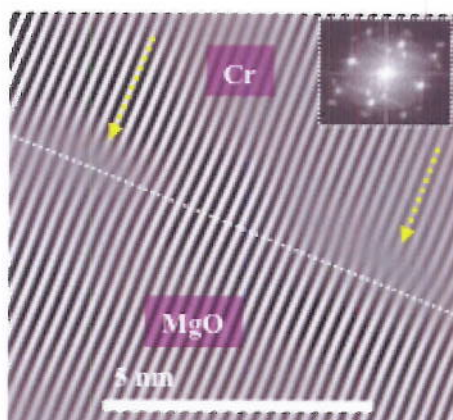


Figure 1. HRTEM micrograph showing the interface structure between the Cr film and the MgO substrate deposited at 550°C. The image has been Fourier filtered to reveal the location of the periodically distributed interface misfit dislocations.

Heavy ion beam irradiations are being used to study the stability of the Cr/MgO interface. Ion irradiation experiments have been performed at room temperature using 1 MeV Au⁺ ions at normal incidence over fluences ranging from 10¹⁶ to 10²¹ ions/m². The experimental conditions were selected in order to produce maximum damage near the interface. The accumulation of damage in both the Cr film and the MgO substrate as well as the depth profiles of implanted Au ions were investigated using Rutherford backscattering spectrometry in channeling geometry with 2 MeV He ions. In general, the degree of disorder in the Cr/MgO interface slightly increases with increasing irradiation damage, but the degree of disorder was far below the random level expected. These results show that the Cr/MgO interface appears to withstand high dose irradiations.

A novel *in situ* optical probing method known as second harmonic generation (SHG) is being developed to monitor interface defect concentrations during and after irradiation. SHG is an interface-specific probe that is sensitive to a variety of defects such as trapped or separated charge carriers, stacking

faults or dislocations, and other types of surface defects. The transparent MgO substrate allows SHG spectroscopy to be used to investigate defect concentrations near an interface in real-time.

Preliminary experimental results utilizing SHG are shown in Figure 2. In this experiment, epitaxially grown Cr films on MgO (001) substrates are irradiated to different doses and the SHG response is compared between damaged and undamaged regions. The SHG experiment measures the changes in output second harmonic photon intensity of a particular polarization (P or S) as a function of input polarization angle. The results clearly indicate that there are significant changes in the intensities and shapes of the resulting SHG angular dependences when samples are irradiated. These experiments, though performed *ex situ*, make it clear that SHG response can be used as an *in situ* probe of radiation-induced damage. Theoretical modeling of induced damage at the interface will be compared with the experimental results leading to greater understanding of the radiation-induced damage at different, well-defined interfaces.

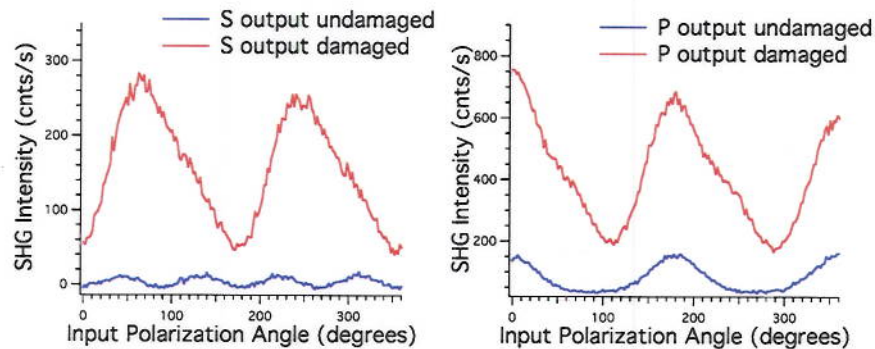


Figure 2. P and S polarized SHG intensities as a function of input polarization angle (P = 0 degrees) for damaged and undamaged regions of a Cr/MgO interface.

The Wirth research group at the University of California, Berkeley and the University of Tennessee is performing *ex situ* positron annihilation spectroscopy. Positrons are sensitive to vacancy concentration and cluster size through measurements of positron lifetime, as well as the local chemical environment through measurements of the Doppler broadening of positron annihilation photons. Preliminary measurements have been performed of pure Cr and MgO, as well as epitaxial Cr films grown on MgO. These measurements have demonstrated that the positrons are sensitive to the MgO in the epitaxial films, and appear to have some sensitivity to the interfacial characteristics. Measurements of the ion-irradiated specimens are planned, and will be reported at the workshop. These measurements will be closely coordinated with the modeling activities to both quantify the vacancy cluster population in the ion irradiated films and hopefully confirm whether structural modifications occur at the interface as a result of irradiation.

To guide and interpret the experimental studies a theory and modeling activity is being carried out. While the focus of this research is primarily on the atomic scale features of interfaces, the experimental information will be obtained over macroscopic time and length scales. Thus, a “multiscale modeling” approach, consisting of *ab initio* and molecular dynamics methods at the atomic scale and stochastic methods at the mesoscale, are being employed to model the evolution of the interfacial regions under irradiation.

Electronic structure calculations are providing critical information for fitting of semi-empirical interatomic potentials and fundamental defect properties for simulations of the Cr-Mo/MgO interface, Figure 3. Such calculations are also being used to explore the localized defect structure of the Cr-

Mo/MgO in detail. Examination of the chemistry and electronic states of local regions with tailored defects in a large interface structure will be carried out via cluster calculations or an embedding method. The detailed information obtained from such calculations will provide insight into the physical, chemical, and electronic properties of the interfacial region, and its response to radiation.

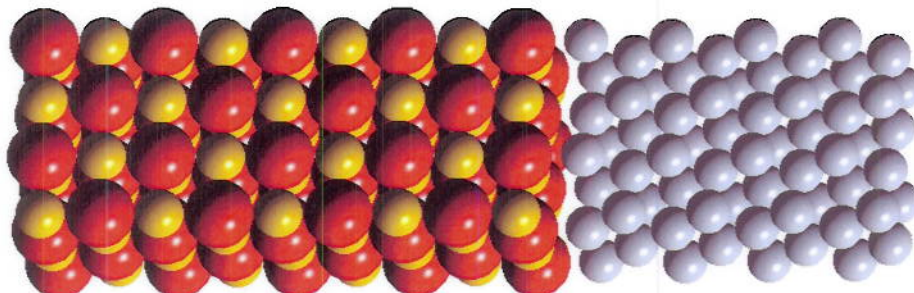


Figure 3. Atomistic depiction of the MgO/Cr interface. Mg is gold, O is red, Cr is blue-grey. The Cr crystal is aligned with the MgO(001) surface such that each Cr is bound to an oxygen atom. *Ab initio* calculations of the binding energy and tensile profile of the interface and near-interface Cr layers provide information for larger scale simulations.

Molecular dynamics (MD) simulations are being used to simulate displacement cascades in the vicinity of grain boundaries. We have used MD to generate fairly low energy (5 keV) cascades in and near a cube-on-cube semi-coherent Cu/Ni interface containing a grid of misfit dislocations, as well as in the same system with a strained coherent interface. The result in both cases is that fewer overall defects are formed than in the bulk pure metals. Some cascade-induced defects tend to cluster at the Cu/Ni interface, especially along the misfit dislocations, while away from the dislocations gliding self-interstitial crowdions freely pass through the interface. MD cascade simulations will provide the defect locations and the number and type of defects produced after the cascade energy dissipates. Long-range diffusion of cascade defects cannot be followed during MD cascade simulations, but Long-Term MD and the Dimer method will be used to determine the migration characteristics of isolated defects as well as defect clusters. The structures and properties of the irradiated interfaces before, during and after irradiation will be characterized and used to develop models of interface evolution under displacement damage conditions.

Future Plans

Future activities will focus on experimental and computational examination of how the radiation damage resistance of the Cr-Mo/MgO interface is affected by the misfit dislocation density. Our future investigations will address fundamental issues of radiation damage in a wider variety of carefully controlled and characterized interfaces. To represent the broad spectrum of interface types found in nuclear energy materials systems we plan to investigate both metal/ceramic and ceramic/ceramic interfaces. Ceramic composites and advanced insulators involve ceramic/ceramic interfaces, while metal/metal and metal/ceramic interfaces are highly relevant to nanolayered and nano-oxide dispersion strengthened ferritic alloys.

Crack-Tip Mechanisms During Environmental Degradation

Stephen M. Bruemmer
Pacific Northwest National Laboratory
P.O. Box 999, Richland, WA 99352
bruemmer@pnl.gov

Kevin M. Rosso, Matthew Olszta, Chongmin Wang and Donald R. Baer
Pacific Northwest National Laboratory

Gary S. Was, University of Michigan
David N. Seidman, Northwestern University

Program Scope

First-of-a-kind, discovery-based research is being conducted to explicate environmental degradation mechanisms through atomistic measurement and modeling of interfacial reactions occurring at buried crack tips. Oxidation at liquid-solid, gas-solid and solid-solid interfaces is being evaluated to establish basic processes leading to grain boundary degradation. This research builds on recent analytical transmission electron microscopy (ATEM) measurements revealing unexpected nanometer-scale crack opening and oxidation reactions driving intergranular (IG) cracking of light-water-reactor structural alloys in service. ATEM measurements have also shown dramatic compositional changes and eventual nanoporosity at the metal grain boundary leading the crack tip. Kinetic development of such features can only be explained by oxidation-induced vacancy injection. Collective evidence and analyses have suggested that IG penetrative degradation can advance in many corrosion-resistant alloys by selective grain-boundary oxidation even at low temperatures. Direct mechanistic links have been made among degradation of corrosion-resistant structural alloys in water, supercritical-water and high-temperature gaseous environments spanning a temperature range from 300 to 1000°C. These measurements and observations are generally inconsistent with continuum mechanics and electrochemical models of environmental degradation and point toward the need for atomic and molecular level understanding of the processes.

Initial Program Activities and Recent Progress

Research activities focus on the ex-situ and in-situ measurement of discrete atomistic, molecular and solid-state reactions integrated with atomistic modeling of chemo-mechanical processes at crack tips. Four primary task areas are being pursued in the first year of the project: (1) quantitative environmental degradation experiments; (2) ex situ atomistic-scale examination of crack tips; (3) in situ studies of selective oxidation and vacancy generation processes, and (4) atomistic modeling to elucidate selective oxidation mechanisms relevant to environment-induced degradation processes at crack tips. A brief description of recent results in all four areas is provided in the following section.

(1) *Quantitative Environmental Degradation Experiments*

Crack-growth-rate experiments are being conducted to produce well-defined crack-tip conditions that will be examined ex situ for structure, composition and chemistry using ATEM and three-dimensional, atom-probe tomography (APT). Two activities have dominated the first phase of the research, construction of a new stress-corrosion test system and casting of binary Ni alloys. The completed system enables the simultaneous testing of three compact-tension samples in high-temperature water with the interactive control of loading/environmental conditions and the in-situ, μm -resolution measurement of crack extension using direct current potential drop. Initial tests are underway on Ni-16%Cr and Ni-30%Cr commercial alloys. Crack-growth response is being mapped as a function of temperature, hydrogen concentration and electrochemical potential assessing behavior in both the Ni-metal and NiO stable regimes as illustrated in Figure 1. Crack-tip stress intensity and environmental conditions will be held constant during the final experimental stage, thereby generating significant crack extension for ex-situ characterizations. Stress-corrosion tests were started on commercial alloys due to delays in the casting of the high-purity binary Ni alloys with controlled alloying additions (including Cr, Fe, Al, Si and Cu) selected based on oxidation characteristics. The high-purity, solution-annealed materials have now been produced and are being cold forged to increase strength, thereby enhancing stress corrosion susceptibility at lower temperatures and minimizing creep-dominated effects at higher temperatures.

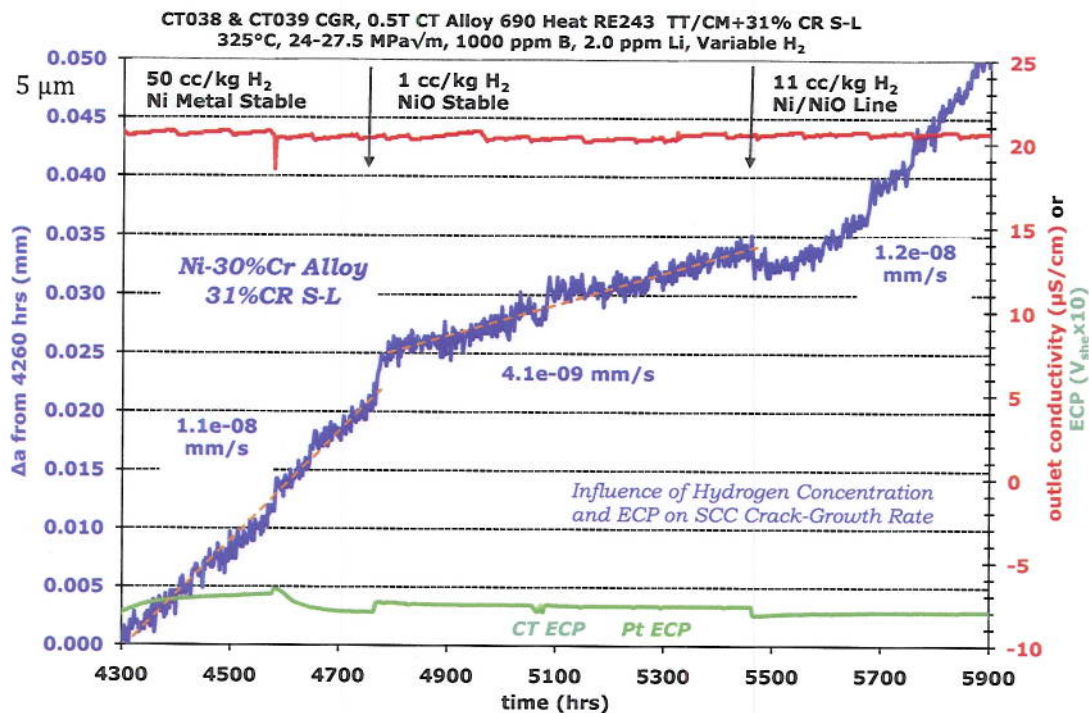


Figure 1. In-situ measurement of stress-corrosion crack growth response as a function of hydrogen concentration in high-temperature water.

(2) Ex Situ Atomistic-Scale Examination of Crack Tips

As noted above, initial stress-corrosion experimentation is being performed on selected commercial Ni-Cr alloys and these materials have also been used for the first crack-tip characterizations. Unexpected solid-state internal oxidation has been discovered at stress-corrosion crack walls in a Ni-30%Cr alloy tested in 360°C hydrogenated water. Selective oxidation of Cr appears to drive this penetrative degradation along dislocations and prevents formation of a protective, Cr-rich passive wall oxide. High-resolution, scanning (SEM) and transmission electron microscopy (TEM) observations are presented in Figure 2 along with APT mapping from a similar wall region. Tunnel-like penetrations are very shallow near the stress-corrosion crack tips, but reach depths of several hundred nm with continued high-temperature water exposure. The unique combination of TEM and APT analyses identified atomistic-scale characteristics and elemental distributions within the oxidation front. This internal oxidation is unexpected, because the higher Cr levels are used in this alloy to stabilize a protective Cr_2O_3 film at surfaces for corrosion and stress corrosion resistance. In addition to the crack wall oxidation studies, intergranular crack tips from Ni-16%Cr stress-corrosion samples (previously characterized by ATEM) are being evaluated by APT for evidence of oxidation in the leading grain boundary.

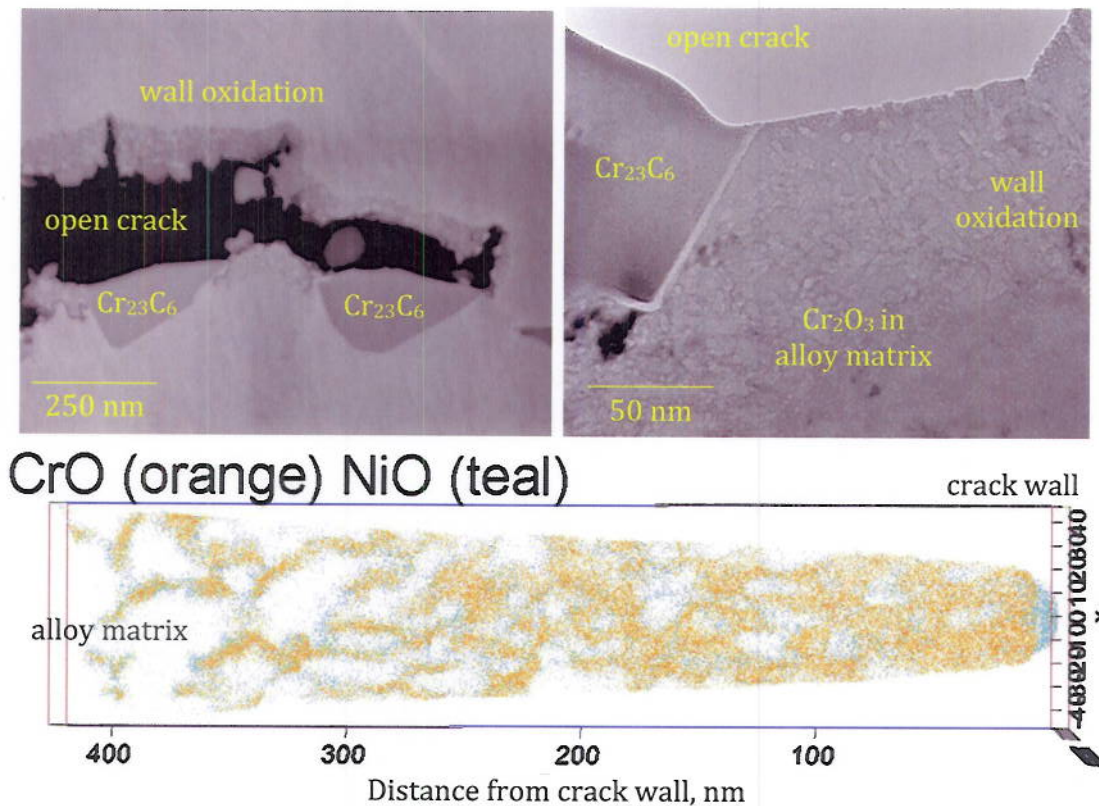


Figure 2. High-resolution characterization of penetrative oxidation off stress corrosion crack walls in a Ni-30% Cr alloy: (a) scanning electron micrograph of crack-tip region and wall oxidation; (b) transmission electron micrograph showing penetrative internal oxidation and Cr_2O_3 particles in alloy matrix; and (c) atom probe tomography map for CrO^+ and NiO^+ ions illustrating tunnel-like oxidation below crack wall into the metal.

(3) In Situ Studies of Selective Oxidation

To gain fundamental information about selective oxidation and vacancy generation processes, nanoparticles with model binary alloy compositions will be characterized by in-situ high-resolution TEM during controlled surface oxidation. Metal composition and environmental conditions will be evaluated that alter vacancy generation at the oxide/metal interface during early stages of oxidation. This can be accomplished by studying the oxide growth and void formation in nanoparticles under different oxidizing environments. The extent of void formation caused by oxidation of simple alloy nanoparticles can provide information about the nature and extent of vacancy formation and migration during oxidation. Initial work has focused on the synthesis of Ni and Ni-Cr nanoparticles by a vacuum-based cluster deposition approach and the examination of their starting structures. Particles greater than ~6 nm in size are observed to have a metal core covered by a NiO-structure oxide surface layer after exposure to ambient air. Smaller particles were completely oxidized to NiO and contain voids suggesting outward metal diffusion during oxidation. Similar nanoparticle characteristics were observed in the Ni-5%Cr solid-solution alloy as for the high-purity Ni. No evidence for significant Cr redistribution during oxidation was detected with both materials forming the NiO-structure oxide on the nanoparticle surfaces.

(4) Atomistic Modeling to Elucidate Selective Oxidation Mechanisms

In order to build an atomistic model for selective oxidation, first-principles and hybrid quantum mechanics/molecular dynamics (QM/MD) computations are being employed to determine rates of elementary electron and ion diffusion processes for parameterization of Kinetic Monte Carlo (KMC) simulations of the collective dynamics. Molecular simulations have started with the simple Ni/NiO model system utilizing concepts of classic analytical oxidation descriptions such as Cabrera-Mott for thin films. Activation energies are being computed for relevant elementary transport processes (cationic/anionic vacancy injection, metal/oxygen vacancies, electrons/holes) from first principles. Initial work has successfully modeled the Ni/NiO interfacial structure and electrostatic potential distribution, and has determined defect migration energies in bulk NiO using density functional theory. These key parameters are being evaluated in the Ni system before expanding complexity into alloying effects.

Future Plans

Stress-corrosion testing in high-temperature water will focus on the Ni-Cr and Ni-Fe binary alloys and selected tests will be initiated in supercritical water and gaseous environments again evaluating crack-growth response under conditions crossing key phase stability regions. Crack-tip characterizations by ATEM and APT will investigate structural and chemical modifications at leading grain boundaries due to oxidation processes. Examinations of crack-wall internal oxidation in the Ni-30%Cr alloy will be completed and linked to new TEM and APT measurements of near-surface oxidation. In-situ TEM oxidation experiments will continue comparing behaviors of Ni and Ni-Cr binary nanoparticles and expand into higher Cr alloys and a Ni-Fe binary. Development of the molecular simulation tool for understanding the dynamics of selective oxidation will move into the Ni-Cr binary. Work on activation energies for transport processes will continue and a Monte Carlo based dynamics code will be developed for coupled collective processes capable of reaching into long length and time scales.

Nanomechanics and Nanometallurgy of Boundaries

B.L. Boyce, B.G. Clark, S.M Foiles, K.M. Hattar, E.A. Holm, J.A. Knapp

Materials Science and Engineering Center
Sandia National Laboratories
PO Box 5800, Mailstop 0889
Albuquerque, NM 87185-0880
e-mail: blboyce@sandia.gov

Program Scope

Nanocrystalline metals have demonstrated exceptional properties including superior strength and fatigue resistance compared to conventional metals. However, these nanocrystalline metals have shown a strong propensity to undergo grain growth, evolving away from the nanocrystalline state. While grain growth in conventional metals only occurs at temperatures $>40\%$ of the melting temperature, nanocrystalline metals have been shown to exhibit grain evolution at $<5\%$ of melting. *Our core hypothesis is that the enhanced properties of nanocrystalline metals are governed in part by the stability (or instability) of the grain boundary structure.*

The Nanomechanics and Nanometallurgy of Boundaries program is an integrated research effort aimed at studying the formation and evolution of defects, nanocrystalline grains, and grain boundaries in metals, and the emergence of often remarkable mechanical and thermal properties as a direct consequence of such defect and grain structure [e.g. Fig. 1]. Through this program, we expect to develop a better understanding of thermal and mechanical grain-boundary processes as well as deformation mechanisms relevant to polycrystalline FCC metals (primarily Ni and Cu) and their alloys, such as Ni-Fe and Ni-W. This program includes elements of material synthesis, physical and structural experimental characterization, and theoretical modeling. The research effort involves three integrated tasks: (1) quantifying the effects of grain boundary instability, (2) theory of microstructures and ensemble-controlled deformation, and (3) observing grain instability and deformation processes using in-situ TEM.

Task 1. Quantifying the Effects of Grain Boundary Instability. Our prior results in this BES program, along with results from LDRD-funded programs at Sandia and in the literature all point to the stability of nanocrystalline alloys as a key factor in understanding their unusual properties. Simply put, nanocrystalline metals with enormous grain boundary content can easily be encouraged to evolve away from their nanocrystalline state through exposure to various thermal or mechanical environments. Many prior studies on nanocrystalline metal properties may have actually been confounded by the evolution away from the initial nanostructure that went undetected. It is not surprising that this evolution has often gone undetected: in some cases, subtle, difficult-to-measure changes in the grain structure of nanocrystalline metals have caused unusual behavior. Nevertheless, nanostructural evolution appears to be prolific. For this reason, Task 1 seeks to develop a more comprehensive, quantitative understanding of the thermal- and mechanical-stability of grain boundaries in nanocrystalline metals as well as linking grain evolution to resulting material properties. The effects of traditional metallurgical stabilizers such as precipitate and solute content will be examined, along with pre-existing deformation substructure and ion-

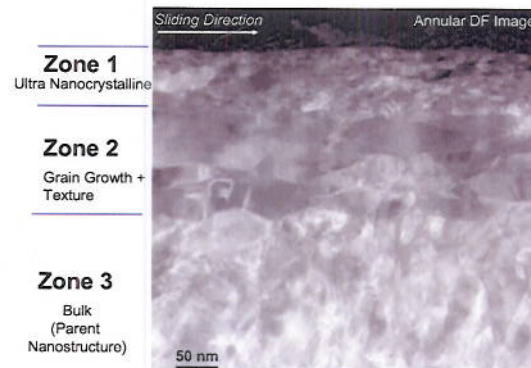


Fig. 1: This wear-induced tribological bilayer in nanocrystalline Ni results in a friction coefficient <0.3 , exceptionally low for an uncoated pure FCC metal.

irradiation damage. To facilitate this discovery and quantification process, we will employ a combination of traditional ex-situ thermal and mechanical testing with post-mortem focused ion beam dissection and characterization along with the development of an in-situ synchrotron transmission x-ray diffraction capability. We envision this effort leading to the formulation of a new style of three-dimensional (stress, temperature, grain size) Ashby deformation mechanism map which establishes the regimes of dominance for several competing thermomechanical grain growth and deformation processes.

Task 2. Theory of Microstructures and Ensemble Controlled Deformation. This modeling task employs molecular dynamics and mesoscale evolution models to explore grain growth behavior under both thermal and mechanical driving forces. Novel algorithms construct and characterize 3D grain boundaries and polycrystals. These structures are input into analysis models to characterize micro- and nanostructural network parameters and properties. Finally, these structures provide input for nanostructural evolution and response simulations on both the atomic and grain scales. These simulations are targeted toward understanding micro- and nanostructural effects in polycrystals with the most realistic structure, crystallography, and boundary properties yet studied. The modeling effort also permits exploration of regimes that are experimentally challenging or inaccessible (e.g. high rates of deformation, ideal microstructures, etc.)

Task 3. Observing Grain Instability and Deformation Processes via In-Situ TEM. This task aims to develop fundamental understandings of mechanisms of deformation and evolution of nanostructured materials, primarily through the use of in-situ thermal and mechanical TEM. This approach provides the ‘seeing-is-believing’ proof of unit evolution processes at the nanoscale. We employ in-house pulsed laser deposition as our primary pathway to produce a wide range of metallurgical scenarios (pure metals, alloyed metals, etc.), although other fabrication methods (electrodeposition, etc.) are also employed where needed. The qualitative nanoscale observations gleaned from these experiments will compliment the quantitative macroscale thermal and mechanical experiments in Task 1, and modeling efforts in Task 2. By developing a thorough understanding of mechanical and thermal behavior of nanostructured materials not only will new knowledge in basic science be revealed, but the full potential of nanostructured materials for advanced applications will be realized.

Recent Progress

- A high-throughput molecular dynamics method was developed to construct minimal-energy bicrystals of 1552 grain boundary types in four FCC Metals: Ni, Al, Cu, and Au. The grain boundary energy and mobility was analyzed through the application of a synthetic driving force [Fig. 2]. A comprehensive examination of the dataset has revealed several fascinating phenomena including: (a) the existence of a thermal roughening transition for all boundaries which substantially affects mobility, (b) a wide range of boundary roughening temperatures, (c) the possibility of dynamical roughening which causes mobility to vary with driving force, (d) the pervasiveness of very fast, shear-coupled boundary motion in over 25% of the bicrystals studied, (e) a decrease in mobility to within the normal range when shear coupled motion is suppressed, (f) the possibility of non-activated grain boundary motion where mobility increases as temperature decreases in about 30% of boundaries studied, (g) the lack of correlation between grain boundary properties and simple boundary parameters such as sigma value or misorientation angle, and (h) the linear relationship between crystallographic distance and boundary mobility.

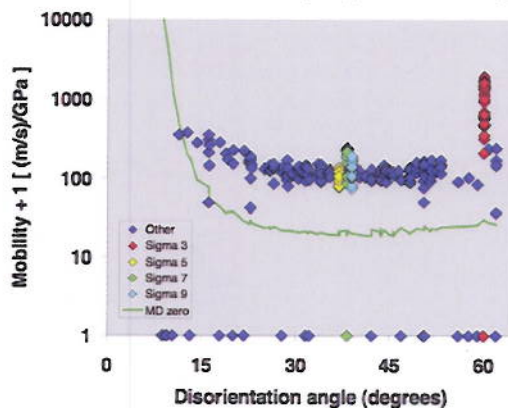


Fig. 2: Boundary mobility of 388 boundary types as a function of disorientation angle.

- The embedded atom method has been used to construct realistic polycrystalline nanostructures with 5×10^6 atoms and ~ 800 nanograins. During thermal annealing simulations, the grain growth process results in the conversion of grain boundary volume into lattice defects including twins, dislocations, vacancies, and stacking fault tetrahedral. All of these defects have been confirmed experimentally through in-situ TEM thermal annealing studies of high-purity Ni.
- Coupled atomistic and mesoscale models have confirmed grain growth stagnation in high-purity metals. These simulations suggest that in the absence of particle or impurity pinning points, grain growth stagnation occurs by the formation of atomically smooth boundaries. (these results were recently published in *Science* vol 328, May 2010)
- Mesoscale grain growth simulations of polycrystals with Zener particles reveal that these particles which impede *normal* grain growth actually serve to induce *abnormal* grain growth.
- Experimental thermal annealing studies of nanocrystalline Ni have revealed the unexpected presence of HCP Ni grains in a matrix of FCC Ni [Fig. 3]. Even more surprising, the HCP grains grow abnormally at the expense of the FCC nanocrystalline matrix. These observations were confirmed through TEM, EBSD, and XRD. While still not understood in its entirety, the growing HCP grains form a nanolamellar defect structure that is very different from the defect structure deposited in abnormally growing FCC grains.
- In-situ TEM fracture testing of nanocrystalline, bimodal, and ultra-fine grained Ni reveal differences in the degree of dislocation activity, twinning, grain agglomeration, localized necking, crack blunting, and crack deflection. All of these energy dissipation processes help explain the enhanced ductility of the bimodal grain structure over the nanocrystalline structure. These in-situ loading experiments have also revealed stress-driven grain growth in PLD Ni for the first time.

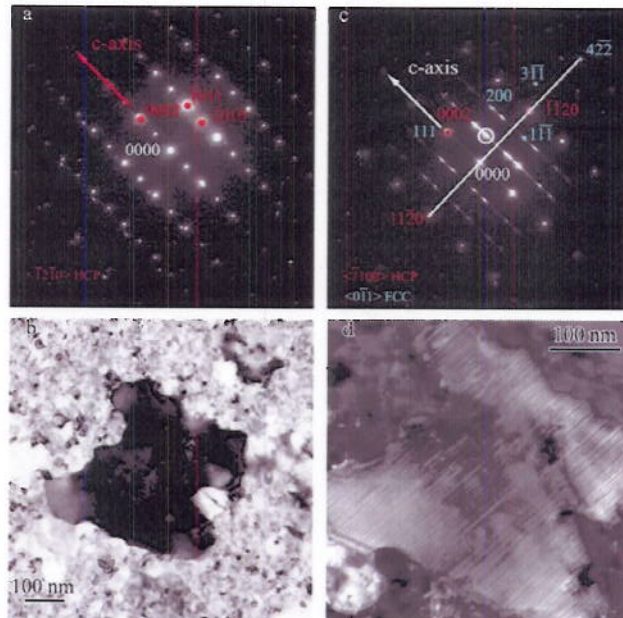


Fig. 3: TEM images and diffraction analysis of a thermally-grown abnormal HCP Ni grain in a matrix of nanocrystalline FCC grains.

Future Plans

- Building on our high-throughput atomistic grain boundary modeling framework, we will investigate interactions between grain boundaries and other microstructural features, including solute particles, second phase particles, nanovoids, and dislocations. This high-throughput method allows exhaustive cataloging of phenomenology rather than one-off observation.
- A simulation-driven comprehensive survey will be constructed for abnormal grain growth mechanisms including persistent growth advantages associated with grain boundary energy, elastic and plastic strain energy, surface energy, and intrinsic and extrinsic boundary mobility.
- A phenomenological understanding of the coupling of mechanical state to microstructural evolution will be developed through both simulation and experimental efforts, including atomistic simulations, mesoscale simulations, in-situ microscopy, and ex-situ thermal+mechanical growth studies.

- An in-situ thermal+mechanical transmission synchrotron x-ray diffraction technique will be developed to investigate grain growth mechanisms in thin film tensile geometries under a wide range of conditions: elastic and plastic, monotonic and cyclic, elevated temperature and ambient.
- Continued investigation of abnormal grain growth and HCP phase growth processes in nanocrystalline Ni using in-situ TEM and XRD techniques.
- Experimental discovery of the interplay between thermal stability and ductility/toughness in nanoparticle-strengthened metals.
- In collaboration with researchers at Los Alamos, apply in-situ TEM methods to investigate confined plasticity processes in strained nanolayer films.
- Investigate cyclic damage processes (fatigue and wear) and the interconnection to cyclically-driven grain growth processes in nanocrystalline metals.
- Employ localized micro-scale and nano-scale ion-irradiation (using μ -ONE and the focused ion nanoimplanter facilities at Sandia's Ion Beam Laboratory) to examine self-ion damage and local alloying effects on deformation and grain growth processes.

Publications 2008-2010

- “How Grain Growth Stops: A Mechanism for Grain-Growth Stagnation in Pure Metals”, E.A. Holm and S.M. Foiles, *Science*, 328 1138 (2010).
- “A Review of Fatigue Behavior in Nanocrystalline Metals”, H.A. Padilla III, and B.L. Boyce, *Experimental Mechanics*, 50 5 (2010).
- “Competitive Abnormal Grain Growth between Allotropic Phases in Nanocrystalline Nickel,” L. N. Brewer, D. M. Follstaedt, J. A. Knapp, M. A. Rodriguez, K. Hattar, and I. M. Robertson, *Advanced Materials*, 22 1161 (2010).
- “Survey of Grain Boundary Properties in FCC Metals: I. Grain Boundary Energy,” D. Olmsted, S. M. Foiles, E. A. Holm, *Acta Materialia*, 57 3694 (2009).
- “Survey of Grain Boundary Properties in FCC Metals: II. Grain Boundary Mobility,” D. Olmsted, E. A. Holm, S. M. Foiles, *Acta Materialia*, 57 3704 (2009).
- “Using Atomistic Simulations to Inform Mesoscale Simulations of Microstructure Evolution,” S. M. Foiles, D. Olmsted, E. A. Holm, Proc. 4th Int. Conf. Multiscale Mater. Model., A. El-Azab (editor) (Florida State University, Tallahassee, FL, 2008, ISBN 978-0-615-24781-6) pp. 362-368.
- “3D Simulation of grain growth in a thermal gradient with non-uniform grain boundary mobility,” A. L. Garcia, V. Tikare, E. A. Holm, *Scripta Materialia*, 59 661 (2008).
- “Defect Structures Produced by Low Temperature Annealing of Pulsed-Laser Deposited Nickel,” K. Hattar, D. M. Follstaedt, J. A. Knapp, and I. M. Robertson, *Acta Mat.* **56**, 794 (2008).
- “Hardening by Bubbles in He-Implanted Ni,” J. A. Knapp, D. M. Follstaedt, and S. M. Myers, *Journal of Applied Physics*, **103**, 013518 (2008).
- “Large Lattice Strain in Individual Grains of Deformed Nanocrystalline Ni,” Z. Shan, J. M. K. Wiezorek, J. A. Knapp, D. M. Follstaedt, E. A. Stach and S. X. Mao, *Applied Physics Letters*, **92**, 091917 (2008).
- “Inter- and Intra-Agglomerate Fracture in Nanocrystalline Nickel,” Z. W. Shan, J. A. Knapp, D. M. Follstaedt, E. A. Stach, J. M. K. Wiezorek, and S. X. Mao, *Physical Review Letters*, **100**, 105502 (2008).
- “Defect Structures Created during Abnormal Grain Growth in Pulsed-Laser Deposited Nickel,” K. Hattar, D. M. Follstaedt, J. A. Knapp, and I. M. Robertson, *Acta Materialia*, **56** 794 (2008).

Author Index

Author Index

Alejandro Strachan,	101	Ian Robertson,.....	125
Alex R. Larzelere,.....	5	Ivar Reimanis,.....	87
Amit Misra,.....	2, 141	Izabela Szlufarska,.....	105
Anter El-Azab,.....	11, 39	J. Lian,.....	43
Antoni P. Tomsia,.....	133	J. R. Morris,.....	153
B.G. Clark,.....	179	J. Wang,.....	145
B.L. Boyce,.....	179	J.A. Knapp,.....	179
Bilge Yildiz,.....	113	James Belak,.....	149
Brian W. Sheldon,.....	100	James C. Williams,.....	59
Bryan Reed,.....	149	James P. Sethna,.....	96
C.N. Tomé,.....	145	James Seal,.....	23
Carl J. Boehlert,.....	23	Jan Schroer,.....	95
Chong Long Fu,.....	157	Jian Gan,.....	11
Chongmin Wang,.....	169	Joel Bernier,.....	149
Christopher Wolverton,.....	35	John Moore,.....	11
Craig Carter,.....	113	K.M. Hattar,.....	179
Cristian Ciobanu,.....	87	Kevin J. Hemker,.....	47
D. F. Bahr,.....	129	Kevin M. Rosso,.....	169
Dallas Trinkle,.....	19	Krystyn Van Vliet,.....	113
David C. Dunand,.....	35	Kurt E. Sickafus,.....	137
David N. Seidman,.....	35, 169	L.-M. Wang,.....	43
Diana Farkas,.....	125	Lumin Wang,	121
Donald R. Baer,.....	175	Marisol Koslowski,.....	51
E. P. George,.....	153	Mark Oliver,	31
E.A. Holm,.....	179	Martin A. Crimp,.....	23
Elisa Riedo,.....	91	Matt Olszta,.....	167
Fei Gao,.....	167	Matthew Olszta,.....	161
G. M. Pharr,	153	Matthew P. Miller,.....	59
G. Malcolm Stocks,.....	9	Michael J. Mills,.....	63, 157
Gary S. Was,.....	125	Michael K. Miller,.....	157
Gregory J.Exarhos,.....	161	Michael Nastasi,.....	2
H. Bei,.....	153	Ming Tang,.....	149
H. M. Zbib,.....	129	Mukul Kumar,.....	159
Harry L. Tuller,.....	113	Nongjian (NJ) Tao,.....	109
Hongmei Li,.....	23	Pascal Bellon,.....	19
I.J. Beyerlein,.....	145	Paul R. Dawson,.....	59
Ian Baker,.....	15	Peter M. Anderson,.....	69

Peter Müllner,.....	67
Qizhen Li,.....	55
R. McCabe,.....	145
Ram Devanathan,.....	161
Reinhold H. Dauskardt,.....	31
Richard Kurtz,.....	165
Rick Williford,.....	161
Rishi Raj,.....	83
Robert Averback,.....	19
Robert O. Ritchie,.....	133
Rodney C. Ewing,.....	43
S.M Foiles,.....	179
Samantha Daly,.....	27
Shen Dillon,.....	19
Sidney Yip,.....	113
Stephen M. Bruemmer,.....	169

T.G. Nieh,.....	71
Taek-Soo Kim,.....	31
Thomas R. Biele,.....	23
Thomas Lagrange.....	159
Todd Allen,.....	1, 11
Ulrich Lienert,.....	59
V. Vitek,.....	117
Vasily Bulatov,.....	149
Wei Lu,.....	121
Weilin Jiang,	167
William A. Curtin,.....	106
William D. Nix,.....	75
William King,.....	19
Xun-Li Wang,.....	157
Yang Shao-Horn,	113
Yanyao Jiang,.....	55
Yet Ming Chiang,	113
Yu Qiao,	79

Participant List

Participant List

Last Name	First Name	Organization	E-mail Address
Allen	Todd	University of Wisconsin-Madison	allen@engr.wisc.edu
Anderson	Peter	The Ohio State University	andersonp@matsceng.ohio-state.edu
Bahr	David	Washington State University	dbahr@wsu.edu
Baker	Ian	Dartmouth College	Ian.Baker@Dartmouth.edu
Belak	James	Lawrence Livermore National Laboratory	belak@llnl.gov
Bellon	Pascal	University of Illinois, Urbana-Champaign	bellon@illinois.edu
Bieler	Thomas	Michigan State University	bieler@egr.msu.edu
Bishop	Sean	Massachusetts Institute of Technology	srbishop@mit.edu
Boyce	Brad	Sandia National Laboratories, Albuquerque	blboyce@sandia.gov
Chen	Yong	Cornell University	yc355@cornell.edu
Clark	Blythe	Sandia National Laboratories, Albuquerque	blyclar@sandia.gov
Crimp	Martin	Michigan State University	crimp@egr.msu.edu
Crockett	Teresa	DOE Basic Energy Sciences	teresa.crockett@science.doe.gov
Daly	Samantha	The University of Michigan	samdaly@umich.edu
Dauskardt	Reinhold	Stanford University	dauskardt@stanford.edu
Devanathan	Ram	Pacific Northwest National Laboratory	ram.devanathan@pnl.gov
Dunand	David	Northwestern University	dunand@northwestern.edu
El-Azab	Anter	Florida State University	aelazab@fsu.edu
George	Easo	Oak Ridge National Laboratory	georgeep@ornl.gov
Hemker	Kevin	Johns Hopkins University	hemker@jhu.edu
Horton	Linda	DOE Basic Energy Sciences	linda.horton@science.doe.gov
Koslowski	Marisol	Purdue University	marisol@purdue.edu
Kumar	Mukul	Lawrence Livermore National Laboratory	mukul@llnl.gov
Lang	Maik	University of Michigan	mklang@umich.edu
Larzelere	Alex	DOE Office of Nuclear Energy	alex.larzelere@nuclear.energy.gov
Li	Qizhen	University of Nevada, Reno	qizhenl@unr.edu
Mailhiot	Christian	Lawrence Livermore National Laboratory	mailhiot1@llnl.gov
Marshall	Frances	Idaho National Laboratory	frances.marshall@inl.gov
Miller	Matthew	Cornell University	mpm4@cornell.edu
Miller	Michael	Oak Ridge National Laboratory	millermk@ornl.gov
Mills	Michael	The Ohio State University	mills.108@osu.edu
Misra	Amit	Los Alamos National Laboratory	amisra@lanl.gov
Müllner	Peter	Boise State University	petermullner@boisestate.edu
Nieh	Taigang (TG)	University of Tennessee	tnieh@utk.edu
Nix	William	Stanford University	nix@stanford.edu
Olszta	Matthew	Pacific Northwest National Laboratory	matthew.olszta@pnl.gov
Papanikolaou	Stefanos	Cornell University	stefan@ccmr.cornell.edu
Pharr	George	Oak Ridge National Laboratory	pharrgm@ornl.gov

Qiao	Yu	University of California, San Diego	yqiao@ucsd.edu
Raj	Rishi	University of Colorado at Boulder	rishi.raj@colorado.edu
Reimanis	Ivar	Colorado School of Mines	reimanis@mines.edu
Riedo	Elisa	Georgia Institute of Technology	elisa.riedo@physics.gatech.edu
Ritchie	Robert	Lawrence Berkeley National Laboratory	roritchie@lbl.gov
Robertson	Ian	University of Illinois, Urbana-Champaign	ianr@illinois.edu
Schroers	Jan	Yale University	jan.schroers@yale.edu
Sethna	James	Cornell University	sethna@lassp.cornell.edu
Sharon	John	Johns Hopkins University	john.sharon@jhu.edu
Sheldon	Brian	Brown University	Brian_Sheldon@brown.edu
Sickafus	Kurt	Los Alamos National Laboratory	kurt@lanl.gov
Stocks	George Malcolm	Oak Ridge National Laboratory	stocksgm@ornl.gov
Strachan	Alejandro	Purdue University	strachan@purdue.edu
Swaminathan	Narasimhan	University of Wisconsin-Madison	swaminathan2@wisc.edu
Szulfarska	Izabela	University of Wisconsin-Madison	izabela@engr.wisc.edu
Talley	Lee-Ann	Oak Ridge Institute for Science and Education	lee-ann.talley@orise.orau.gov
Tao	Nongjian	Arizona State University	njtao@asu.edu
Tome	Carlos	Los Alamos National Laboratory	tome@lanl.gov
Tuller	Harry	Massachusetts Institute of Technology	tuller@mit.edu
Uberuaga	Blas	Los Alamos National Laboratory	blas@lanl.gov
Van Ginhoven	Renee	Pacific Northwest National Laboratory	renee.vanginhoven@pnl.gov
Vetrano	John	DOE Basic Energy Sciences	john.vetrano@science.doe.gov
Vitek	Vaclav	University of Pennsylvania	vitek@seas.upenn.edu
Wang	Jian	Los Alamos National Laboratory	wangj6@lanl.gov
Wang	Lumin	University of Michigan	lmwang@umich.edu
Williams	James	Ohio State University	williams.1726@osu.edu
Woodford	William	Massachusetts Institute of Technology	woodford@mit.edu
Xu	Peng	University of Wisconsin-Madison	pxu8@wisc.edu
Zbib	Hussein	Washington State University	zbib@wsu.edu